HANWEI LIU

CONCEPTUAL DESIGN, STATIC AND DYNAMIC ANALYSIS OF NOVEL CABLE-LOOP-DRIVEN PARALLEL MECHANISMS

Thèse présentée
à la Faculté des études supérieures et postdoctorales de l'Université Laval
dans le cadre du programme de doctorat en génie mécanique
pour l'obtention du grade de Philosophiæ Doctor (Ph.D.)

FACULTÉ DES SCIENCES ET DE GÉNIE
UNIVERSITÉ LAVAL
QUÉBEC

2012

Résumé

Les mécanismes parallèles entraînés par câbles permettent d'obtenir de grands espaces de travail puisque les plages de mouvement des câbles enroulés sur des treuils sont beaucoup plus grandes que celles des mécanismes à barres. De plus, les mécanismes entraînés par câbles possèdent un rapport charge utile sur poids propre avantageux et ils sont capables de produire de grandes vitesses. Toutefois, dans les mécanismes parallèles entraînés par câbles d'architecture classique, les câbles sont enroulés sur des treuils actionnés. Cette approche conduit à des imprécisions puisque le rapport entre la rotation du treuil et l'extension du câble n'est généralement pas constant. Par ailleurs, les mécanismes parallèles entraînés par des câbles sont habituellement actionnés de façon redondante en raison de l'unilatéralité de la force transmise par un câble. Cela conduit à une infinité de solutions au problème statique (ou dynamique) inverse et rend la commande du mécanisme plus compliquée. L'objectif de cette thèse est d'explorer de nouvelles architectures de mécanismes parallèles entraînés par câbles construites à l'aide de boucles de câbles afin d'obtenir une meilleure précision et/ou éviter la redondance.

Tout d'abord, des mécanismes plans à actionnement redondant utilisant des boucles de câbles sont proposés. Dans ces architectures, les câbles forment des boucles fermées fixées à l'effecteur, et dont le mouvement est produit par des actionneurs prismatiques. Un mécanisme plan à deux degrés de liberté est proposé. En remplaçant le système câble-treuil par des boucles de câbles fermées, les difficultés de mesure de l'extension des câbles sont atténuées. Le problème géométrique inverse, les matrices jacobiennes et les équations d'équilibre statique de ces mécanismes sont présentés. En utilisant les matrices jacobiennes, les singularités des mécanismes sont aussi analysées. À partir de l'équation d'équilibre statique, l'ensemble des torseurs applicables à l'effecteur est déterminé. Il est montré que la trajectoire d'un point d'attache d'une boucle de câble sur l'effecteur est une portion d'ellipse. L'intersection des ellipses fournit les modes d'assemblage. Il peut y avoir plus

d'un point d'intersection des ellipses pour une position donnée des actionneurs. Cette caractéristique géométrique est aussi analysée.

Afin d'éliminer la redondance d'actionnement, des ressorts sont introduits dans les mécanismes entraînés par boucles de câbles. Grâce à un arrangement géométrique approprié des ressorts dans les boucles, le mécanisme ne requiert que n actionneurs pour le guidage de n degrés de liberté, éliminant ainsi la redondance d'actionnement. Les mécanismes proposés peuvent être actionnés soit à l'aide d'actionneurs prismatiques ou à l'aide d'actionneurs rotoïdes entraînant une courroie. Le design conceptuel de quelques architectures de mécanismes de ce type est proposé. Une architecture non-symétrique, dans laquelle le ressort est attaché à un seul des côtés des boucles de câbles, est d'abord analysée. Ensuite, une architecture symétrique dans laquelle les deux côtés des boucles de câbles sont atttachés au ressort, est proposée. Une comparaison des architectures est établie pour des mécanismes plans. Puis, l'architecture symétrique est appliquée aux mécanismes spatiaux. Les analyses cinématiques et statiques sont présentées pour ces mécanismes.

À l'aide des équations statiques, l'ensemble des forces disponibles à l'effecteur des mécanismes parallèles entraînés par boucles de câbles incluant des ressorts est déterminé. Pour fins de comparaison, l'ensemble des forces disponibles à l'effecteur de mécanismes plans et spatiaux entraînés par des câbles et des treuils classiques est également déterminé. Une étude dynamique est aussi réalisée afin de déterminer les limites de performance des mécanismes. La méthode de Newton-Euler est utilisée pour l'analyse dynamique et la détermination de la fréquence naturelle de même que des rapports d'amplitude entrée-sortie.

Les mécanismes à boucles de câbles avec ressorts permettent d'éviter la redondance d'actionnement. Les paramètres des ressorts doivent être ajustés correctement afin d'obtenir de bonnes caractéristiques pour ces mécanismes. Toutefois, l'utilisation de ressorts augmente le coût et la complexité des mécanismes. Par conséquent, il est proposé de réaliser la condition d'équilibre des forces sans ressorts. À cet effet, un mécanisme à deux degrés de liberté découplé non redondant à boucles de câbles entraînées par actionneurs prismatiques est proposé. Les actionneurs sont situés sur les arêtes de l'espace de travail. La redondance d'actionnement est éliminée tout en fournissant la condition de fermeture de force (force closure) partout dans l'espace de travail. De plus, l'encombrement du mécanisme est essentiellement égal à son espace atteignable et le mécanisme ne souffre d'aucune singularité. Deux boucles de câble sont utilisées pour chacune des directions de mouvement. Une première boucle agit comme boucle d'actionnement alors que la seconde, qui est passive, est la boucle de contrainte. Grâce à une conception géométrique simple, les équations cinématiques et statiques du mécanisme sont très compactes. Une étude de la raideur effective du mécanisme montre que celle-ci est excellente. Finalement, une analyse dynamique est

proposée en considérant l'élasticité et l'amortissement des câbles.

Abstract

Cable-driven parallel mechanisms have the advantages of large workspace and high speed since the displacement range of cables is much larger than that of links and such mechanisms have higher payload to weight ratio. However, in the conventional cable-driven parallel mechanisms, cables are wound on actuated spools. This approach leads to inaccuracies because the ratio between the rotation of the spool and the extension of the cable is generally not constant. Also, cable-driven parallel mechanisms are usually redundantly actuated due to the unilaterality of the cable force. This leads to infinitely many solutions to the inverse statics or dynamics problem and makes the control of the mechanism more complicated. The objective of this dissertation is to explore new architectures of cable-driven parallel mechanisms using cable loops in order to improve accuracy or/and avoid redundancy.

Firstly, redundantly actuated cable-loop-driven planar mechanism is proposed. The cables form closed loops attached to the end-effector and whose motion is driven by slider actuators. A planar 2-DOF mechanism is proposed. By replacing the cable-spool arrangement with closed cable loops, the difficulties of measuring the extension of the cables are alleviated. The inverse kinematics, the Jacobian matrices and the static equilibrium equations for the mechanism are presented. Using the Jacobian matrices, the singularities of the mechanisms are also analyzed. Based on the static equations, the available wrench set is determined. It is pointed out that the trajectory of the end-point of a given cable loop is a portion of ellipse. The intersection of the ellipses provides the assembly modes. There can be more than one intersection point of the ellipses at a given position of the sliders. Such geometric characteristics are also analyzed.

In order to eliminate the actuation redundancy, springs are introduced in the cable-loop mechanisms. By attaching springs in the cable loops properly, the mechanism only needs n actuators

to control n DOFs and the actuation redundancy can be eliminated. The mechanisms can be actuated using either linear sliders or rotary actuators driving the motion of a cable or belt loop. The conceptual development of the spring-loaded cable-loop architectures is presented. One architecture has a non-symmetric compliance since only one side of the cable loop is attached on the spring. Another architecture has a symmetric compliance since both sides of the cable loop from the actuator are attached on the spring. The architectures are compared by applying them to the planar mechanisms. Then, the symmetric spring-loaded cable-loop architecture is applied to a spatial displacement mechanism. Kinematic and static analyses are presented for the mechanisms.

Based on the static equations, the force capabilities of planar and spatial symmetric compliance spring-loaded cable-loop-driven parallel mechanisms are analyzed using the available force set and the force-closure workspace. The force capabilities of the conventional planar and spatial cable-driven parallel mechanisms which have the same geometry as the spring-loaded cable-loop-driven mechanisms are also derived for comparison purposes. Due to the cable loops in the mechanisms, the cable might become slack when the end-effector moves with a high acceleration. Therefore, it should be verified that the cable forces can be maintained in tension for certain trajectory frequencies. Based on the static force and the Newton-Euler formulation, the natural frequency and the corresponding ratio of the amplitudes for these two types of mechanisms are also found.

Spring-loaded cable-loop-driven parallel mechanisms avoid the actuation redundancy using passive springs. The parameters of the springs must be adjusted properly in order to obtain good characteristics of the mechanisms. The usage of the springs increases the cost and complexity of the mechanisms. Therefore, it is intended to realize the force-closure condition without springs. A 2-DOF decoupled non-redundant cable-loop slider-driven parallel mechanism is proposed in the end. Sliders located on the edges of the workspace are used and actuation redundancy is eliminated while providing force closure everywhere in the workspace. Due to the simple geometric design, the kinematic and static equations of the mechanism are very compact. The stiffness of the mechanism is also analyzed. The dynamics equations including the compliance and the damping of the cables are obtained. It is shown that the proposed mechanism's workspace is essentially equal to its footprint and that there are no singularities.

Foreword

Foremost, I want to thank my supervisor Prof. Clément Gosselin for his invaluable supervision, tremendous support, continuous encouragements over the years. His charming personality, creativity, openness to far out ideas and belief in his students has been a continual source of inspiation. His comprehensive expertise in robotics and mechanisms kept me focused and challenged me to always push to see what else can be accomplished.

I am also grateful to Mr. Thierry Laliberté for his significant help during the various stages of my research. His outstanding comprehension about mechanical is a very important support to complet my research.

Futhermore, I wish to express my gratitude to my thesis defence committee and especially to Prof. Amir Khajepour from University of Waterloo, Prof. Marc J. Richard and Prof. Phillippe Cardou. Their detailed remarks and suggestions are valubale to modify the final version of my thesis.

Special thanks are also due to all the members of the Robotics Laboratory for their help and friendship as well as for their contributious to creating the most pleasing working atmosphere that I ever enjoyed. The help of Alexandre Drouin in the fabrication of the model is also gratefully acknowledged.

Last, but not least, I would like to thank my parents and my husband. The warmth from them encouraged me all these years.

Contents

List of Figures

Chapter 1

Introduction

1.1 Cable-Driven Parallel Mechanisms

1.1.1 Characteristics and Analysis of Cable-Driven Parallel Mechanisms

Cable-driven parallel mechanisms are parallel mechanisms in which a moving platform is driven by a number of cables. Such mechanisms have been studied in the recent literature because of their obvious advantages in terms of small moving mass and large range of motion.

Cables have appeared ten thousands years ago. When human could use the most simple tools, they could entwist out cables with grass and small branches. People used cables to bundle beasts, to tie thatched cottage firmly, to rope grass skirts as belts and other such applications. Cables

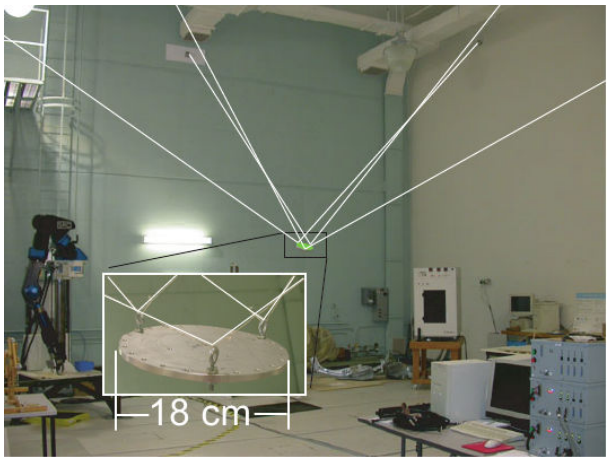

(a)

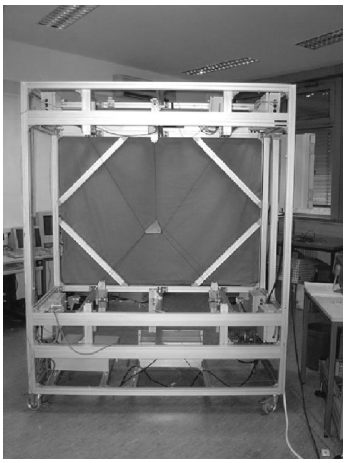

(b)

Figure 1.1: (a) Picture of the experimental setup for the Large Adaptive Reflector taken from [9], (b) SEGESTA manipulator taken from [12].

were also used as a method to keep certain staffs in mind before words were created in ancient China and Peru. In antiquity, more and more simple mechanisms which used cables were invented to serve the human life. For instance, cables were wound on wheels to lift water from the deep wells. Recently, with modern science and technology, the NIST (Nation Institute of Standards and Technology of USA) ROBOCRANE was proposed in the early nineties of the last century [1]. After that, cable-driven parallel mechanisms attracted the attention of researchers all over the world.

Since cables are used to totally or partially replace rigid links in cable-driven parallel mechanisms, this leads to the following special advantages:

- The displacement range of cables is larger than that of links, so the workspace of the cable-driven parallel mechanisms is larger than that of parallel-link mechanisms [1–15] (See for instance the mechanisms shown in Figure 1.1).
- The mass of a cable is smaller than that of a link, so compared with traditional parallel mechanisms, the inertia of cable-driven parallel mechanisms is smaller. This means that such mechanisms have higher payload to weight ratio and that they can move at very high speed [6, 16–20]. (Two of such mechanisms are shown in Figure 1.2.)
- Cables are thinner than links, so cables reduce the probability of interference during motion. Moreover, cables may tangle and the robot may still be functional. The possibility of permitting cable collisions has been analyzed in [99], the experimental platform is shown in Figure 1.3.

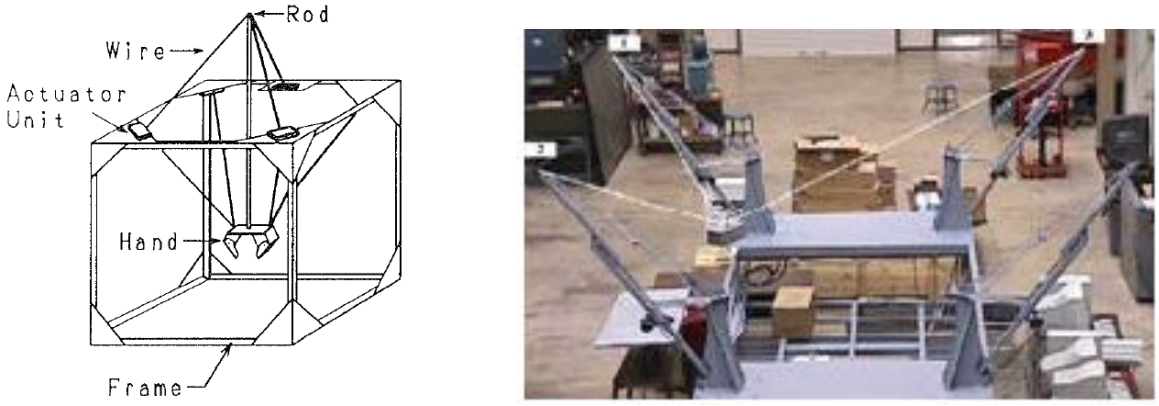

(a) (b)

Figure 1.2: (a) FALCON high-speed parallel manipulator taken from [16], (b)The Cable Array Robot taken from [6].

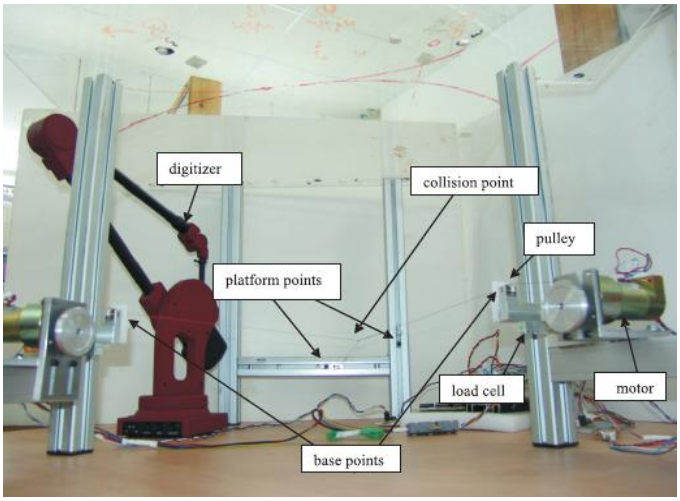

Figure 1.3: The setup used for collision permitting experiment [99].

- Spherical joints can be avoided in these mechanisms, then the limitations on the angular motion range can be partially eliminated.

Because of the potential advantages of cable-driven parallel mechanisms, the research about such mechanisms is very important for many application areas, like manufacturing, processing and assembling, medical treatment, spaceflight, ocean exploration assistive robotics and military robotics.

Several challenging problems arise in the analysis and design of cable-driven parallel mecha-

nisms such as the determination of the workspace, the determination of the wrench capabilities and the computation of the optimal force distribution. Indeed, because cables can only work in tension, cable-driven parallel mechanisms are often redundantly actuated, thereby leading to infinitely many solutions to the inverse statics or dynamics problem.

Basically, the kinematic analysis of cable-driven parallel mechanisms is based on the geometry of the manipulator. If the configuration of the end-effector is given, it is easy to calculate the length of the cables. However, the forward kinematics is much more difficult and usually the results can only be found by numerical methods [21–24, 26–32, 34]. In [100], the elasticity of the cables was also taken into account in the kinematic problem. In this case, inverse kinematics may be solved either by first choosing the wire tensions, the control vector being then a linear function of the tensions or by solving directly a system of nonlinear equations whose unknowns are the components of the control vector.

Workspace is an important issue in cable robots and it has been studied by many researchers. Although it is desirable to obtain the workspace using analytic methods, because of inherent complexity in cable robots, such methods can be used only for planar robots and simple geometries. On the other hand, numerical methods have fewer limitations and are usually used by researchers. One of the disadvantages of numerical methods is that they need an exhaustive and time consuming search in the entire task space [8, 23, 26, 37, 39–46, 48–50]. For the singularity analysis of cable-driven parallel mechanisms, the method can be deduced with the method shown in [51–54], which is analyzed based on the Jacobian matrix of the velocity equations. Considering the special nature of the cables, the singularities of cable-driven parallel mechanisms can be classified as Jacobian singularities and force-closure singularities [55]. Generally speaking, the singularity low is consistent with or is a part of the workspace boundary.

Since cables can only pull and not push on the mobile platform, the forces applied by the cables on the platform have a unidirectional nature. Then, the static analysis and the determination of the available force/wrench set of such mechanisms are different from that of parallel link manipulators. The force closure conditions of the cable-driven parallel mechanisms are usually analyzed based on linear algebra, using, for instance the rank of the wrench matrix or the linear combination of the column vectors of the wrench matrix [56,57,64,66,67]. The available force/wrench set is also a significant indication of the force capabilities of the mechanisms. Since the force space of the end-effector is a zonotope which can be described as the vector sum of a finite number of closed line segments in a certain Euclidean space, the available force/wrench set of the end-effector can

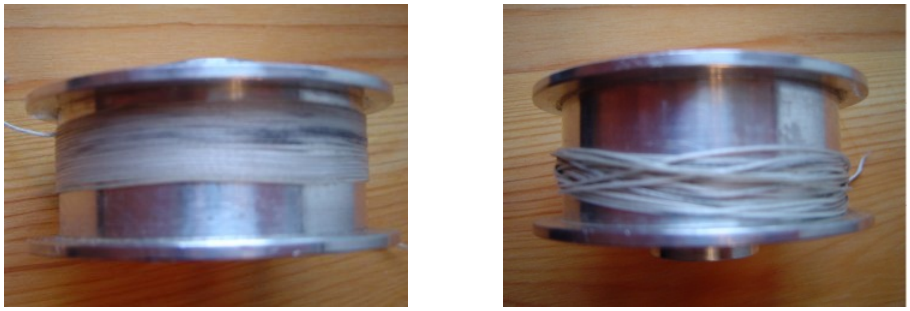

(a) Uniformly wound (b) Non uniformly wound

Figure 1.4: Examples of a cable wound on a spool.

be expressed as a special class of convex polytopes [74, 75]. Interval analysis can also be used since the cable force must lie within a certain range that corresponds to the mechanical properties of the cables [76].

Generally speaking, the dynamic equations for cable-driven parallel mechanisms are simpler than those obtained for link-driven parallel mechanisms if the mass of the cables can be neglected. Dynamic equations of motion can be obtained from the Lagrangian formulation [79] or the Newton-Euler formulation [80, 84, 85]. Usually, it is easier to obtain the dynamic equations of cable-suspended parallel mechanisms using Newton's method. However, the cable mass should be considered for large scale cable-driven parallel mechanisms [93]. Elastic and damping characterics of the cables are also included in the dynamic equations in [88]. Although cable-driven parallel mechanisms can have a sufficient stiffness if the structure of the mechanism is arranged properly [77], the mechanisms might undergo significant vibrations when they are moving with large accelerations. The nonlinear vibrations of the cables are studied in [89] and the vibration of the cable-driven mechanism caused by cable flexibilities in both axial and transversal directions are analyzed in [91]. Natural frequencies and amplitude-frequency relationships are also interesting due to the flexibility of the cables. These problems can be analyzed based on the dynamic equations.

1.1.2 Limitations of Conventional Cable-Driven Parallel Mechanisms

In typical cable-driven parallel mechanisms, the cables are wound on spools. From Figure 1.4, it can be seen that the part of the cable which is wound on a spool might be wound randomly. Such an approach leads to inaccuracies because the ratio between the rotation of the spool and the

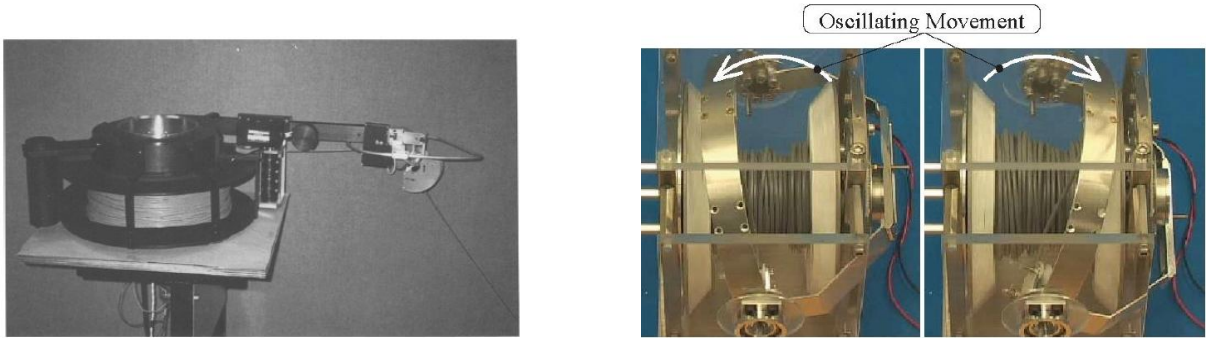

(a) (b)

Figure 1.5: Improved mechanisms to wind a cable uniformly.

extension of the cable varies with time. There are mechanisms which can wind the cable smoothly and neatly [94, 95], as shown in Figure 1.5. Even with the use of such mechanisms in cable-driven parallel mechanisms, the ratio between the rotation of the spool and the extension of the cable is not constant. The ratio is small when the length of the cable which is wound on the spool is short, and the ratio increases with the length of wound cable.

Since cables can only sustain tension forces, cable-driven parallel mechanisms require particular approaches to ensure cable tensions. In order to achieve such condition, suspended cable-driven parallel mechanisms make use of gravity while fully-constrained cable-driven parallel mechanisms are redundantly actuated. Also, some mechanisms use springs to fulfill the unilaterality conditions [106]. Suspended mechanisms have restrictions on their configurations and redundantly actuated mechanisms make the control algorithm more challenging.

Given the above limitations, it can be observed that it wound be of great interest if actuated spools are avoided or/and the actuation redundancy is eliminated in cable-driven parallel mechanisms.

1.1.3 Improvements and Novel Architectures of Cable-Driven Parallel Mechanisms

Actuating a cable-driven mechanism consists in changing the cable lengths between the end-effector and the fixed frame. The approach used to realize the change of length has a significant impact on

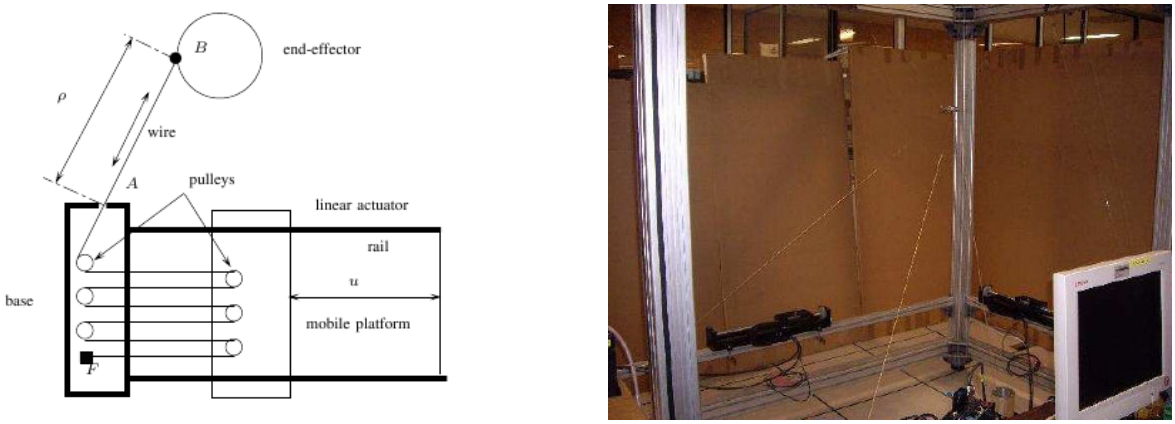

(a) The wire system used to actuate the MARIONET robot

(b) The MARIONET robot

Figure 1.6: Merlet's MARIONET robot taken from [100].

the cable-driven parallel mechanisms since it plays an important role for the workspace, accuracy and force capabilities of the mechanism. In order to avoid the actuated spools and eliminate the actuation redundancy, one idea is to find an innovative mechanism in which there is no cable-spool system. There are many novel cable-driven parallel mechanisms proposed recently, in which the actuating principle is different from that of conventional cable-driven parallel mechanisms.

The wire system (shown in Figure 1.6(a)) used to actuate the MARIONET robot (shown in Figure 1.6(b)) comprises a linear actuator and a pulley system. Such an approach allows a higher modularity of the actuation system and avoids the cable-spool system [100, 101].

The hybrid cable-driven mechanism (shown in Figure 1.7) in which the cable forms one single long loop is introduced in [104]. The Cartesian motion can be realized using only three revolute actuators. There is no actuation redundancy associated with this architecture. However, it needs six long slider guides which introduce significant inertia and the motion in the three directions are coupled.

In [105], several closed-loop cable/belt routings are proposed in order to allow the actuation of Cartesian SCARA-type manipulators from four actuators fixed to the ground and a Cartesian bridge and trolley system. For the closed cable loop, the stabilization of the bridge has to be considered. It is shown that decoupled actuation is possible and leads to great advantages regarding the power needed. Figure 1.8 shows two examples of the proposed routings, which allow the

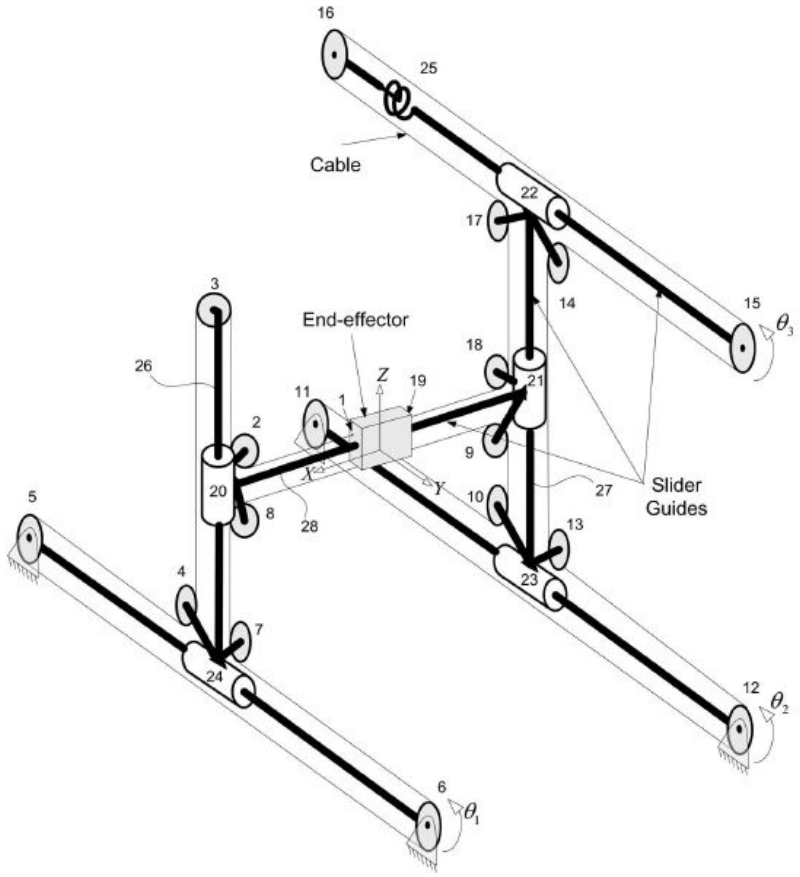

Figure 1.7: Behzadipour's Cartesian cable-loop driven mechanism taken from [104].

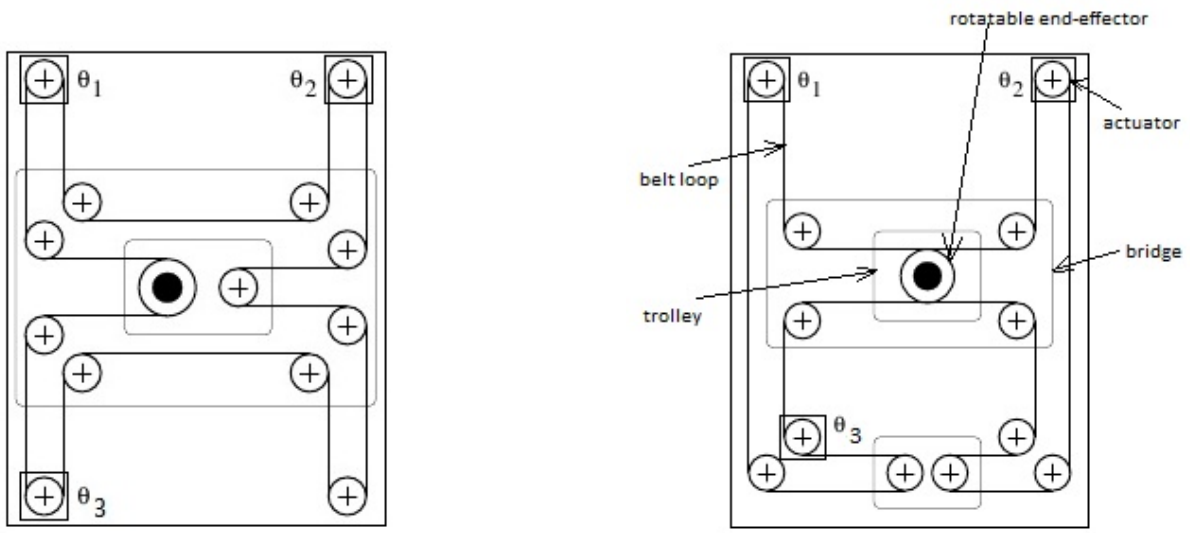

(a) (b)

Figure 1.8: Routings allowing the actuation of planar 3-DOF mechanisms with one cable/belt loop and three actuators, taken form [105].

actuation of planar 3-DOF mechanisms with one cable/belt loop and three actuators.

1.2 Objectives and Contributions of the Thesis

As mentioned above, conventional cable-driven parallel mechanisms have many advantages, but the accuracy is not very good due to the use of cable-spool systems and the actuation redundancy raises control challenges. As a major objective, this thesis aims at exploring new actuation schemes for cable-driven parallel mechanisms in order to lead to improved properties. It is intended to use cable loops instead of the straight cables wound on spools to transfer the movement of the actuator to the end-effector.

When considering new schemes to drive the moving platform, the kinematic problem, static problem, force capabilities and interference of the cables, will be different from these of the traditional cable-driven parallel mechanisms. Therefore, all these problems need to be revisited. The new mechanisms should meet the following conditions:

• The kinematic properties of the proposed mechanisms should be such that they result in a well-conditioned workspace in terms of boundary, singularity and mechanical interference.

• The range of the available wrench set is sufficient to perform the work. The mechanism has the appropriate force capabilities.

• The motion planning and control of the cable-driven parallel mechanisms requires the solution of the inverse kinematic problem. The computational cost of the inverse kinematic problem should be reasonable and not too complicated.

• The vibration should be controlled within the allowed limitation using proper control method even if cables are flexible elements and springs might be introduced in the mechanisms.

In order to have an initial insight of the cable-loop principle, the concept is first introduced in planar mechanisms. As cables provide unidirectional force, the mechanism is redundantly actuated. It only eliminates the cable-spool system and improves the accuracy of the cable-driven mechanisms, which is limited mechanically.

Then, an architecture is proposed in which springs are introduced in the cable-loop mechanisms in order to eliminate the actuation redundancy. There are many methods to introduce the spring compliance in a cable loop. Based on a static model, promising configurations of spring-loaded cable-loop architectures were found for planar mechanisms. Following the application to planar mechanisms, spring-loaded cable-loop architectures are proposed for spatial mechanisms. The force capabilities of planar and spatial spring-loaded cable-loop-driven parallel mechanisms are influenced by the properties of the springs. Since the mechanisms have fewer actuators than the conventional cable-spool mechanisms as they are not redundantly actuated, their force capabilities cannot be expected to be as good as those of conventional cable-spool mechanisms having the same geometry as the spring-loaded cable-loop-driven mechanisms. However, the spring-loaded cable-loop-driven parallel mechanisms can provide very good force capabilities while being more efficient and cost-effective.

The actuation redundancy is converted into passive redundancy which is realized by the springs in the spring-loaded cable-loop-driven parallel mechanisms. In order to have better force capabilities, the springs should be chosen properly. Also, springs increase the cost and complexity of the mechanism. Hence, we intend to find a cable routing which eliminates both the actuation re-

dundancy and the passive redundancy like the cable routings in [102, 104, 105]. Then, the 2-DOF decoupled non-redundant cable-loop slider-driven parallel mechanism is proposed. Due to the simple geometric design, the kinematic and static equations for this mechanism are very compact. And the stiffness of the mechanism is much higher than that of the cables.

1.3 Overview of the Thesis

Our work is presented in six main parts —Chapter 2 to Chapter 7, the most important parts are Chapter 3, 4, 5 and 7. The first part (Chapter 2) starts with an attempt to apply slider-driven cable loops into cable-driven parallel mechanisms. It then continues with the kinematic, static and workspace analyses. The second part (Chapters 3-6) describes the planar and spatial spring-loaded cable-loop-driven parallel mechanisms. Finally, the decoupled 2-DOF non-redundant cable-loop slider-driven parallel mechanism is introduced in the third part (Chapter 7).

In Chapter 2, the concept of cable-loop-driven mechanism is first used in a 3-cable 2-DOF planar mechanism. There are three cable loops in this mechanism. Each cable is controlled by a slider, passes around two fixed pulleys and then attaches to the end-effector. The inverse kinematics, the Jacobian matrices and the static equilibrium equations for the new architecture are given. Using the Jacobian matrices, the singularities of the mechanism are also analyzed. Also, based on the static equations, the available wrench set is determined. It is pointed out that the trajectory of the end-point of a given cable loop is a portion of an ellipse. The intersection of the ellipses provides the assembly modes. There can be more than one intersection point of the ellipses at a given position of the sliders and this geometric characteristic is analyzed.

In Chapter 3, in order to avoid actuation redundancy in cable-driven parallel mechanisms and require only N actuators to control a N-DOF motion, springs are introduced in the cable loops. Some compliance must be introduced in the loops in order to compensate for the change of cable length. Hence, the challenge is to include compliance in the closed loops without introducing compliance between the actuators and the end-effector. Additionally, it is desired to obtain a symmetric layout. The concept is first applied to planar mechanisms. The conceptual development of the 2-DOF spring-loaded cable-loop-driven parallel mechanism is presented at the beginning of this chapter. The spring-loaded cable-loop-driven mechanisms with non-symmetric compliance

and symmetric compliance are proposed. Kinematic and static analyses are presented for the two new architectures. It is verified that the cables and springs can be kept in tension within a certain workspace. It is shown that the spring-loaded mechanism with symmetric compliance has a better available workspace.

In Chapter 4, the spring-loaded cable-loop architecture with symmetric compliance is applied to a spatial displacement mechanism. The inverse kinematics, the static equilibrium equations and the workspace analysis are presented. Because all these equations are obtained based on the cable segment lengths, many square roots appear in the equations. The workspace boundary equations for different arrangements, i.e., preload, non-zero stiffness and external forces, are obtained separately in order to simplify the analysis. The workspace boundary equations of each cable force for any situation can be obtained by combining the equations based on the matrix superposition principle. It is verified that the mechanism has a significantly large workspace within which the cables and the springs can be maintained in tension. It is also shown that the mechanism has a larger workspace with the negative stiffness springs.

Based on the static equations, the force capabilities of planar and spatial spring-loaded cable-loop-driven parallel mechanisms with symmetric compliance are analyzed in Chapter 5. The maximum external force that can be applied from all directions at the end-effector is obtained from the available force set using a geometric method. For comparison purposes, the force capabilities of conventional planar and spatial cable-driven mechanisms which have the same geometry as the spring-loaded cable-loop-driven parallel mechanisms are also derived. Many simulations results are given. The average tolerable external force and the workspace for a certain force are obtained using a numerical method.

In Chapter 6, the dynamic analysis of the symmetric compliance planar and spatial spring-loaded mechanisms are presented. Due to the cable loops in the mechanisms, the cables might become slack when the end-effector moves with a high acceleration. So, it should be verified that the cable forces can be maintained in tension for a certain prescribed trajectories. The required actuating forces are also found. As the dynamic models of the mechanisms are very complex, only the masses of the end-effector and the actuators is considered for the trajectory analysis. Then, the natural frequency and the corresponding ratio of the amplitudes for the mechanisms are obtained based on the static force and the Newton-Euler formulation.

A novel 2-DOF cable-loop slider driven parallel mechanism is introduced in Chapter 7. The two degrees of freedom of the mechanism are decoupled and the mechanism only requires two actuators to control the motion. There are two cable loops for each direction of motion, one acts as the actuating loop while the other is the constraint loop. Due to the creative geometric design, the kinematic and static equations for this mechanism are very simple. Given some reasonable assumptions, the stiffness of the mechanism is analyzed. The dynamic equations of the mechanism, including the compliance and the damping in the cables are obtained. Considering the stiffness and the damping of the cables, though the dynamic equation is complex, the motion of the actuator, the sliders and the connectors and the required actuating force can also be found. The proposed mechanism's workspace is essentiallly equal to its footprint and there are no singularities.

Finally, a summary of the results obtained in this thesis and some discussion as well as directions on future research work are given in Chapter 8.

Chapter 2

Redundantly Actuated Planar Cable-Loop-Driven Mechanism

This chapter introduces a redundantly actuated planar cable-loop slider-driven mechanism. The 2-DOF mechanism has three cable loops: each cable loop is driven by a slider actuator and attached to the end-effector. The inverse kinematics, the static equilibrium equations, the singularity analysis and the available wrench set are given in the following. As the end-effector is driven by cable loops, the position of the end-effector is determined by the intersection point of three ellipses. This geometric characteristic is analyzed at the end of the chapter.

2.1 Introduction

Cable-driven parallel mechanisms attracted the attention of researchers from all over the world since the NIST Robocrane was proposed [1]. Pioneer designs of cable-driven parallel mechanisms also include the Falcon high-speed parallel manipulator [16] and the Skycam [2].

Many challenging problems arise in the analysis and design of cable-driven parallel mechanisms such as the determination of the workspace, the determination of the wrench capabilities and the computation of the optimal force distribution. Since cables can only work in tension, cable-driven parallel mechanisms usually use more actuators than degrees of freedom in order to realize the force-closure condition. This leads to infinitely many solutions to the inverse statics or dynamics problem.

Several practical issues also need to be considered in the design and control of cable-driven parallel mechanisms. In a typical cable-driven parallel mechanism, cables are wound on actuated spools and the extension of the cables is determined using an encoder mounted on the spool. This approach leads to inaccuracies because the ratio between the rotation of the spool and the extension of the cable is generally not constant and depends on how much cable is wound on the spool. Also, it was shown that the tension in the cable at the time of winding may also affect the winding and hence the above mentioned ratio [36].

Given the above limitations, it is proposed here to build a planar cable-driven parallel mechanisms based on closed cable loops. By replacing the cable and spool arrangement with closed cable loops, the difficulties of measuring the extension of the cables are alleviated. Also, the stability of the platform may be improved by increasing the number of cables attached to the platform. This chapter presents the application of this concept to 2-DOF closed-loop cable-driven parallel mechanisms. First, the planar displacement cable-loop slider-driven mechanism is introduced and its mechanical design is described. The inverse kinematic problem is solved and the velocity equations are derived. Two Jacobian matrices are obtained and a singularity analysis is then performed based on the analysis of the Jacobian matrices. The static analysis is presented using the principle of virtual work and the wrench capabilities of the mechanism are discussed. Finally, a geometric analysis is presented in order to support the results of the preceding sections.

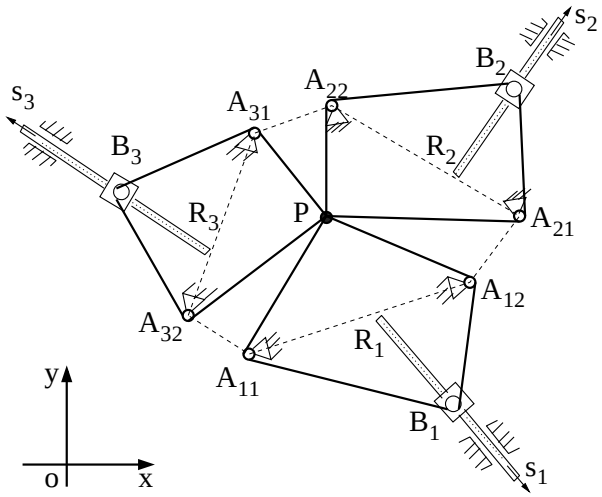

Figure 2.1: Schematic representation of a 3-cable 2-DOF cable-loop slider-driven parallel mechanism.

2.2 Description of the Mechanism

The structure of a 3-cable 2-DOF cable-loop slider-driven parallel mechanism is shown in Figure 2.1. There are three cable loops in this mechanism. Each cable is controlled by a slider, passes around two fixed pulleys and then attaches to the end-effector. The position of the end-effector can be changed by controlling the motion of the sliders.

The fixed pulleys are represented by A_{ij}, $i = 1, 2, 3$, $j = 1, 2$, the sliders are represented by B_i, $i = 1, 2, 3$. The location of point A_{ij}, $i = 1, 2, 3$, $j = 1, 2$ is known and expressed as $\mathbf{r}_{Aij} = [x_{Aij}, y_{Aij}]^T$, $i = 1, 2, 3$, $j = 1, 2$. The respective length of loops $PA_{i1}B_iA_{i2}P$ is L_i, $i = 1, 2, 3$. The direction of motion of the sliders is noted as the unit vector $\mathbf{s}_i = [x_{si}, y_{si}]^T$, $i = 1, 2, 3$. That is to say $\mathbf{s}_i^T\mathbf{s}_i = 1$. And the sliding guides pass through points R_i, $\mathbf{r}_{Ri} = [x_{Ri}, y_{Ri}]^T$, $i = 1, 2, 3$. Then, the position of point B_i, noted $\mathbf{r}_{Bi} = [x_{Bi}, y_{Bi}]^T, i = 1, 2, 3$ can be expressed as

$$\mathbf{r}_{Bi} = \mathbf{r}_{Ri} + \rho_i\mathbf{s}_i, \quad i = 1, 2, 3 \tag{2.1}$$

where ρ_i represents the extension of the ith slider, i.e., the ith actuated joint coordinate.

2.3 Inverse Kinematics

The solution of the inverse kinematic problem consists in determining the actuator coordinates ρ_i for a given position of the end-effector P, given as $\mathbf{r}_p = [x_p, y_p]^T$. From the geometry of the ith cable loop, the total loop length, L_i, can be written as

$$| \mathbf{r}_p - \mathbf{r}_{Ai1} | + | \mathbf{r}_p - \mathbf{r}_{Ai2} | + | \mathbf{r}_{Ai1} - \mathbf{r}_{Bi} | + | \mathbf{r}_{Ai2} - \mathbf{r}_{Bi} | = L_i, \quad i = 1, 2, 3. \tag{2.2}$$

The unknown in the above equation is the extension of the slider. Expanding Eq. (2.2), one has

$$C_{1i}\rho_i^2 + C_{2i}\rho_i + C_{3i} = 0, \quad i = 1, 2, 3, \tag{2.3}$$

where

$$\begin{aligned}
C_{1i} &= 4\left[l_i^2 - \left(\mathbf{r}_{Ai2}^T\mathbf{s}_i - \mathbf{r}_{Ai1}^T\mathbf{s}_i\right)^2\right], \\
C_{2i} &= 4\left[2l_i^2\left(\mathbf{r}_{Ri}^T\mathbf{s}_i - \mathbf{r}_{Ai1}^T\mathbf{s}_i\right) - 4\left(\mathbf{r}_{Ai2}^T\mathbf{s}_i - \mathbf{r}_{Ai1}^T\mathbf{s}_i\right)\left(l_i^2 + \mathbf{r}_{Ai1}^T\mathbf{r}_{Ai1} - \mathbf{r}_{Ai2}^T\mathbf{r}_{Ai2} + 2\mathbf{r}_{Ai2}^T\mathbf{r}_{Ri} - 2\mathbf{r}_{Ai1}^T\mathbf{r}_{Ri}\right)\right], \\
C_{3i} &= 4l_i^2\left(\mathbf{r}_{Ai1}^T\mathbf{r}_{Ai1} + \mathbf{r}_{Ri}^T\mathbf{r}_{Ri} - 2\mathbf{r}_{Ai1}^T\mathbf{r}_{Ri}\right) - l_i^4 - \left(\mathbf{r}_{Ai1}^T\mathbf{r}_{Ai1} - \mathbf{r}_{Ai2}^T\mathbf{r}_{Ai2} + 2\mathbf{r}_{Ai2}^T\mathbf{r}_{Ri} - 2\mathbf{r}_{Ai1}^T\mathbf{r}_{Ri}\right)^2 \\
&\quad -2l_i^2\left(\mathbf{r}_{Ai1}^T\mathbf{r}_{Ai1} - \mathbf{r}_{Ai2}^T\mathbf{r}_{Ai2} + 2\mathbf{r}_{Ai2}^T\mathbf{r}_{Ri} - 2\mathbf{r}_{Ai1}^T\mathbf{r}_{Ri}\right),
\end{aligned}$$

and

$$l_i = L_i - | \mathbf{r}_p - \mathbf{r}_{Ai1} | - | \mathbf{r}_p - \mathbf{r}_{Ai2} | .$$

Therefore, the inverse kinematic problem can be solved by computing the roots of Eq. (2.3). It can be observed that two solutions are obtained for each cable loop which leads to 8 solutions for the complete mechanism. In practice, the correct joint coordinates can be chosen form these solutions according to the geometry of the mechanism.

2.4 Velocity Equations and Jacobian Matrices

In order to find the velocity equations, Eq. (2.2) is differentiated with respect to time. Collecting terms, one obtains

$$\begin{bmatrix} (\mathbf{u}_{11} + \mathbf{u}_{12})^T \\ (\mathbf{u}_{21} + \mathbf{u}_{22})^T \\ (\mathbf{u}_{31} + \mathbf{u}_{32})^T \end{bmatrix} \begin{bmatrix} \dot{x}_p \\ \dot{y}_p \end{bmatrix} = \begin{bmatrix} (\mathbf{v}_{11} + \mathbf{v}_{12})^T \mathbf{s}_1 & 0 & 0 \\ 0 & (\mathbf{v}_{21} + \mathbf{v}_{22})^T \mathbf{s}_2 & 0 \\ 0 & 0 & (\mathbf{v}_{31} + \mathbf{v}_{32})^T \mathbf{s}_3 \end{bmatrix} \begin{bmatrix} \dot{\rho}_1 \\ \dot{\rho}_2 \\ \dot{\rho}_3 \end{bmatrix} \tag{2.4}$$

where

$$\mathbf{u}_{ij} = \frac{\mathbf{r}_p - \mathbf{r}_{Aij}}{\mid \mathbf{r}_p - \mathbf{r}_{Aij} \mid}, \quad i = 1, 2, 3, \quad j = 1, 2,$$
$$\mathbf{v}_{ij} = \frac{\mathbf{r}_{Aij} - \mathbf{r}_{Bi}}{\mid \mathbf{r}_{Aij} - \mathbf{r}_{Bi} \mid}, \quad i = 1, 2, 3, \quad j = 1, 2.$$

Eq.(2.4) can be written in matrix form as

$$\mathbf{J}_x \dot{\mathbf{r}}_p = \mathbf{J}_\rho \dot{\boldsymbol{\rho}} \tag{2.5}$$

where the two Jacobian matrices given in Eq. (2.4) are noted as $\mathbf{J}_x$ and $\mathbf{J}_\rho$ respectively, and $\dot{\boldsymbol{\rho}} = [\dot{\rho}_1, \dot{\rho}_2, \dot{\rho}_3]^T$.

2.5 Singularity Analysis

The configurations of the planar 2-DOF mechanism that lead to the determinant of $\mathbf{J}_\rho$ or $\mathbf{J}_x^T \mathbf{J}_x$ being equal to zero are singular configurations [51, 52].

The first type of singularity occurs when we have

$$\det(\mathbf{J}_\rho) = 0. \tag{2.6}$$

Since the Jacobian matrix $\mathbf{J}_\rho$ is a diagonal matrix, it is easy to see that Eq. (2.6) can be expressed as

$$\mathbf{s}_i^T (\mathbf{v}_{i1} + \mathbf{v}_{i2}) = 0, \quad i = 1 \text{ or } 2 \text{ or } 3. \tag{2.7}$$

From Eq. (2.7), we can find the corresponding value of ρ_i, namely

$$\rho_i = \mathbf{s}_i^T \mathbf{m}_i, \quad i = 1, 2, 3. \tag{2.8}$$

where

$$\mathbf{m}_i = \begin{bmatrix} \dfrac{(x_{Ai1} - x_{Ri}) \mid \mathbf{r}_{Ai2} - \mathbf{r}_{Bi} \mid}{\mid \mathbf{r}_{Ai1} - \mathbf{r}_{Bi} \mid + \mid \mathbf{r}_{Ai2} - \mathbf{r}_{Bi} \mid} + \dfrac{(x_{Ai2} - x_{Ri}) \mid \mathbf{r}_{Ai2} - \mathbf{r}_{Bi} \mid}{\mid \mathbf{r}_{Ai1} - \mathbf{r}_{Bi} \mid + \mid \mathbf{r}_{Ai2} - \mathbf{r}_{Bi} \mid} \\ \dfrac{(y_{Ai1} - y_{Ri}) \mid \mathbf{r}_{Ai2} - \mathbf{r}_{Bi} \mid}{\mid \mathbf{r}_{Ai1} - \mathbf{r}_{Bi} \mid + \mid \mathbf{r}_{Ai2} - \mathbf{r}_{Bi} \mid} + \dfrac{(y_{Ai2} - y_{Ri}) \mid \mathbf{r}_{Ai2} - \mathbf{r}_{Bi} \mid}{\mid \mathbf{r}_{Ai1} - \mathbf{r}_{Bi} \mid + \mid \mathbf{r}_{Ai2} - \mathbf{r}_{Bi} \mid} \end{bmatrix}.$$

By inspection of the above equations, it is clear that if the direction of $\mathbf{s}_i$ is perpendicular to the line $A_{i1}A_{i2}$, i.e., $\mathbf{s}_i \perp \overline{A_{i1}A_{i2}}$, such singularity points are easily avoided.

The second type of singularity can be deduced by the Jacobian matrix $\mathbf{J}_x$. As the mechanism is redundantly actuated, the matrix $\mathbf{J}_x$ is not a square matrix, its dimension is 3×2. Then, this type of singular configurations occurs if

$$\det(\mathbf{J}_x^T \mathbf{J}_x) = 0. \tag{2.9}$$

Since there are many different square roots in the denominators of the components of Jacobian matrix $\mathbf{J}_x$, it is more difficult to obtain a singularity equation from the above expression. However, by inspection of Eq. (2.4) it is clear that this type of singularity occurs when Eqs. (2.10) to (2.12) are all satisfied, i.e.,

$$\det \begin{pmatrix} (\mathbf{u}_{11} + \mathbf{u}_{12})^T \\ (\mathbf{u}_{21} + \mathbf{u}_{22})^T \end{pmatrix} = 0, \tag{2.10}$$

$$\det \begin{pmatrix} (\mathbf{u}_{11} + \mathbf{u}_{12})^T \\ (\mathbf{u}_{31} + \mathbf{u}_{32})^T \end{pmatrix} = 0, \tag{2.11}$$

$$\det \begin{pmatrix} (\mathbf{u}_{21} + \mathbf{u}_{22})^T \\ (\mathbf{u}_{31} + \mathbf{u}_{32})^T \end{pmatrix} = 0. \tag{2.12}$$

Figure 2.2 shows an example of the loci associated with Eqs. (2.10) to (2.12). The solid curve is the solution of each of the equations. It can be observed that the three curves do not have a common intersection point. Actually, in practice, it is easy to design the mechanism such that the singularities corresponding to $\det(\mathbf{J}_x^T \mathbf{J}_x) = 0$ do not exist within the workspace.

2.6 Static Analysis

The forces acting on the sliders and the end-effector of the 3-cable 2-DOF cable-loop slider-driven parallel mechanism are shown in Figure 2.3. The actuator forces are $\mathbf{f}_{Bi}$, $i = 1, 2, 3$. According to the kinematic model mentioned earlier, the directions of the actuating forces are $\mathbf{s}_i$, $i = 1, 2, 3$. The external force at the end-point is $\mathbf{f}_p = [f_x, f_y]^T$. As a whole system, the mechanism should be balanced with the actuating force $\mathbf{f}_{Bi}$, $i = 1, 2, 3$ and the external force $\mathbf{f}_p$. Using the principle of

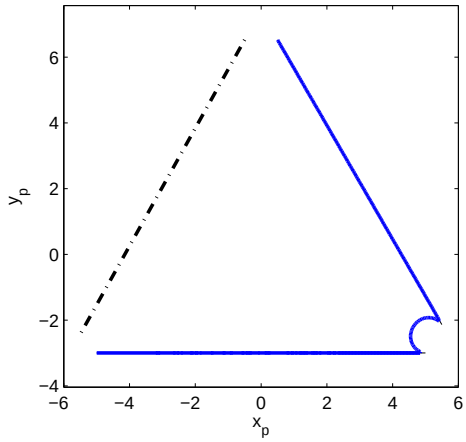

(a) determinant of the matrix formed by 1^{st} and 2^{nd} lines of $\mathbf{J}_x$ equal to 0

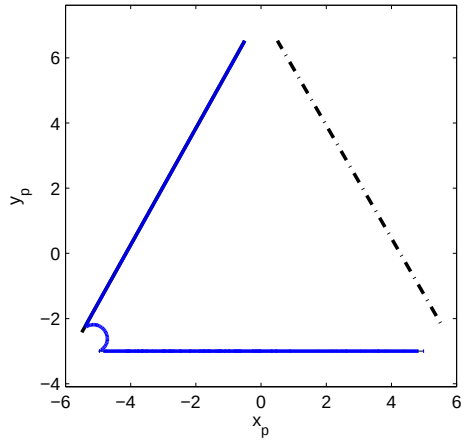

(b) determinant of the matrix formed by 1^{st} and 3^{rd} lines of $\mathbf{J}_x$ equal to 0

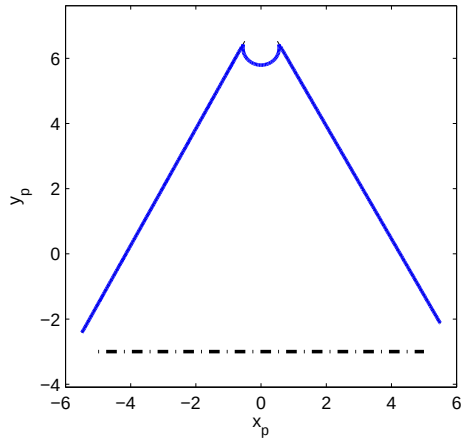

(c) determinant of the matrix formed by 2^{nd} and 3^{rd} lines of $\mathbf{J}_x$ equal to 0

Figure 2.2: Loci corresponding to Eqs.(2.10), (2.11) and (2.12).

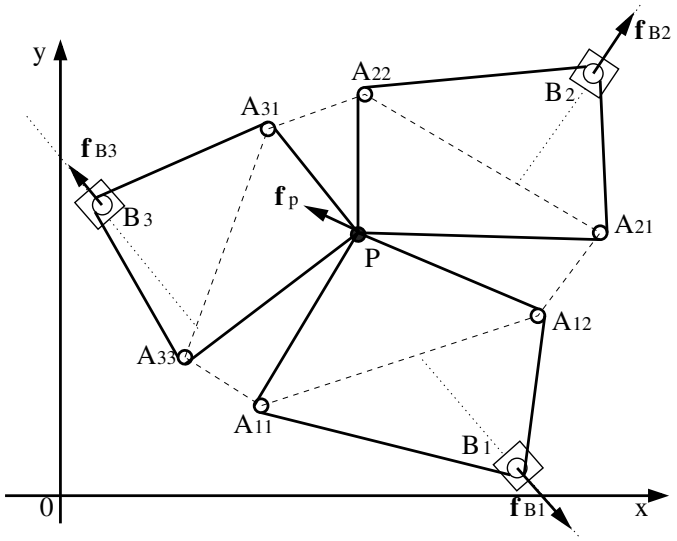

Figure 2.3: Actuation and platform forces for the 3-cable 2-DOF cable-loop slider-driven parallel mechanism.

virtual work, we can get

$$\mathbf{f}_{B1}^T \delta \mathbf{r}_{B1} + \mathbf{f}_{B2}^T \delta \mathbf{r}_{B2} + \mathbf{f}_{B3}^T \delta \mathbf{r}_{B3} + \mathbf{f}_p^T \delta \mathbf{r}_p = 0 \tag{2.13}$$

where the actuating forces are $\mathbf{f}_{Bi} = [f_{bix}, f_{biy}]^T$, $i = 1, 2, 3$.

Substituting Eq.(2.1) into Eq.(2.13), one then obtains

$$\mathbf{f}_{B1}^T \mathbf{s}_1 \delta \rho_1 + \mathbf{f}_{B2}^T \mathbf{s}_2 \delta \rho_2 + \mathbf{f}_{B3}^T \mathbf{s}_3 \delta \rho_3 + \mathbf{f}_p^T \delta \mathbf{r}_p = 0. \tag{2.14}$$

The above equation can be written as

$$-\mathbf{f}_B^T \delta \boldsymbol{\rho} = \mathbf{f}_p^T \delta \mathbf{r}_p, \tag{2.15}$$

where

$$\mathbf{f}_B = \begin{bmatrix} \mathbf{f}_{B1}^T \mathbf{s}_1 & \mathbf{f}_{B2}^T \mathbf{s}_2 & \mathbf{f}_{B3}^T \mathbf{s}_3 \end{bmatrix}^T, \quad \delta \boldsymbol{\rho} = \begin{bmatrix} \delta\rho_1 & \delta\rho_2 & \delta\rho_3 \end{bmatrix}^T$$

in which $\delta \boldsymbol{\rho}$ and $\delta \mathbf{r}_p$ are respectively virtual changes of the positions of the sliders and the virtual generalized displacement of the end-effector.

From Eq.(2.4), it can be obtained that

$$\delta \boldsymbol{\rho} = \mathbf{J}_\rho^{-1} \mathbf{J}_x \delta \mathbf{r}_p$$

and substituting the latter result into Eq.(2.15), we get the static equation as

$$\mathbf{f}_p = -\mathbf{J}_x^T \mathbf{J}_\rho^{-T} \mathbf{f}_B. \tag{2.16}$$

2.7 Force Capabilities of the Mechanism

In this subsection, the force capabilities of the mechanism are investigated using the available force set. The static equation expressing the relationship between the actuator forces and the external force applied at the end-effector can be rewritten as

$$\mathbf{W}\mathbf{f}_B = \mathbf{f}_p \tag{2.17}$$

where

$$\mathbf{W} = -\mathbf{J}_x^T \mathbf{J}_\rho^{-T}.$$

Assuming that the minimum slider force and the maximum slider force are known, then the available force set at the platform can be expressed as

$$A = \left\{ \mathbf{f}_p \in \mathtt{R}^2 \mid \mathbf{f}_p = \mathbf{W}\mathbf{f}_B, \quad \mathbf{f}_{Bmin} \preceq \mathbf{f}_B \preceq \mathbf{f}_{Bmax} \right\}. \tag{2.18}$$

where $\mathbf{f}_{Bmin} = [f_{B1_{min}}, f_{B2_{min}}, f_{B3_{min}},]^T$, $\mathbf{f}_{Bmax} = [f_{B1_{max}}, f_{B2_{max}}, f_{B3_{max}},]^T$ and $\preceq$ denotes the componentwise inequality.

For instance, if the minimum slider force is $\mathbf{f}_{Bmin} = [1, 1, 1]^T$, the maximum slider force is $\mathbf{f}_{Bmax} = [10, 10, 10]^T$, and assuming the geometry of the mechanism is such that the fixed pulleys are located by pairs at points $[-6, 0]^T$, $[6, 0]^T$, $[0, 6\sqrt{3}]^T$, then the available forces are easily determined. They are the convex hull of the extreme forces, as given in Eq.(2.18). Two examples are illustrated for the above parameters in Figure 2.4(a) and Figure 2.4(b).

2.8 Geometric Analysis

Roughly speaking, the end point of this mechanism can reach any point in the polygon formed by vertices $A_{11}A_{12}A_{21}A_{22}A_{31}A_{32}A_{11}$. However, there are some points that can cause the cable loops to

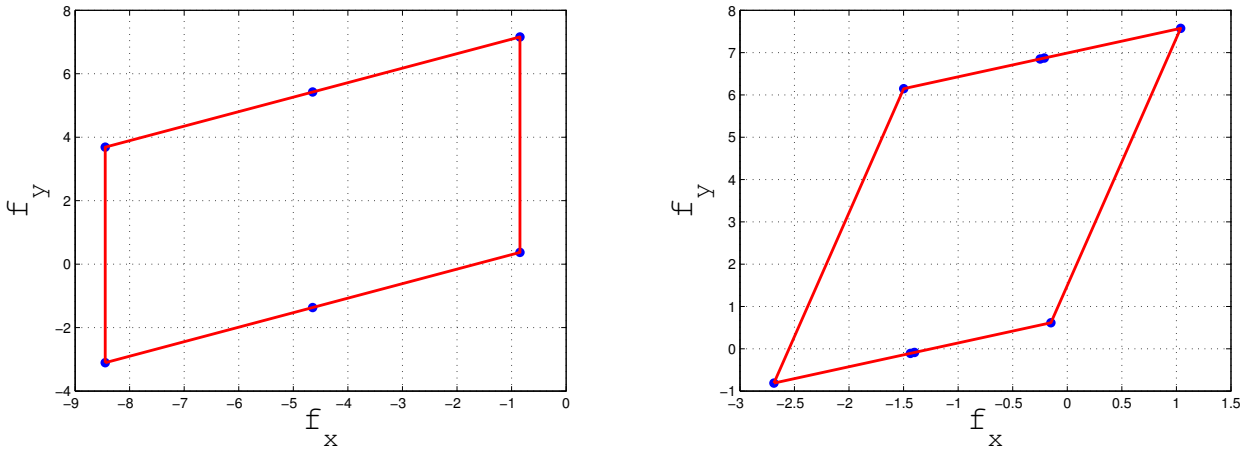

(a) The end-effector is located at $[0, 3\sqrt{3}]^T$ (b) The end effector is located at $[2, 3\sqrt{3}]^T$

Figure 2.4: Examples of the available wrench set.

become slack. Indeed, for a given value of ρ_i, for one cable loop, the two distances between the two fixed pulleys and the slider are determined, then the sum of the cable segments distance from the end-effector and the fixed pulleys are constant. All points of the plane whose distances to two fixed points add to the same constant form an ellipse, so the trajectory of the end-point is a portion of an ellipse. And the intersection of the three ellipses gives the position of the end point. Depending on how the ellipses intersect, some of the cables may become slack. This is illustrated in Figure 2.5.

Two of the ellipses in Figure 2.5(a) are tangent to each other, the third ellipse passes through the tangent point. In Figure 2.5(b), every pair of the three ellipses has two intersection points. One of the two points is the common point consistent with the loci of the end-effector, the other points are outside of the polygon formed by the fixed pulleys. In these two cases, the cables will not become slack. However, if the two intersection points are both within the polygon as shown in Figure 2.5(c), the end-effector of the mechanism can reach the common intersection region which determined by the three ellipses, then the cables will become slack in this situation.

For a given point of the workspace, using the equations of the ellipses we can find out whether the cables will become slack or not. However, it is more meaningful to determine the regions in which the cables cannot become slack using an approach based on geometry.

Since in a given loop the cable can move freely around the pulleys (all pulleys are free to ro-

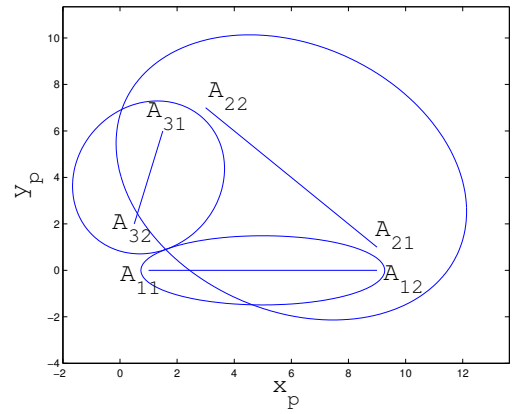

(a) Not slack

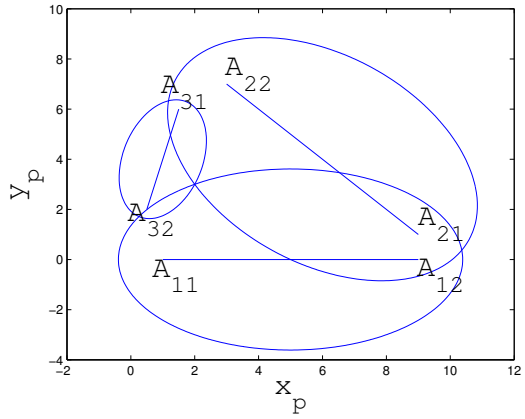

(b) Not slack

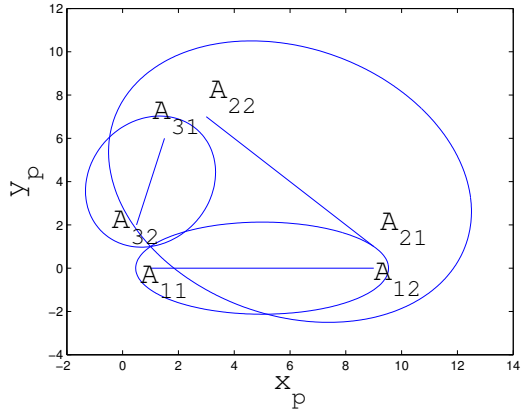

(c) Slack

Figure 2.5: Intersection of the three ellipses associated with the cable loops.

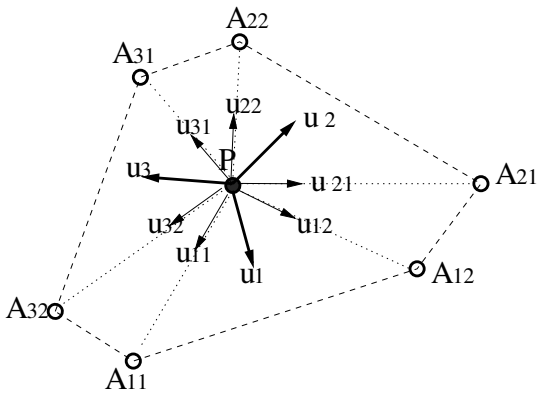

Figure 2.6: Definition of the direction of the force vectors.

tate), the tension in the cable must be the same everywhere (if friction in the pulleys is neglected). Therefore, the tension in each of the two cable ends of a given loop attached to the platform must be the same.

Considering the geometric construction of Figure 2.6, the following vectors are defined as

$$\begin{aligned} \mathbf{u}_1 &= \mathbf{u}_{11} + \mathbf{u}_{12} \\ \mathbf{u}_2 &= \mathbf{u}_{21} + \mathbf{u}_{22} \\ \mathbf{u}_3 &= \mathbf{u}_{31} + \mathbf{u}_{32}. \end{aligned} \tag{2.19}$$

Clearly, the force applied to the platform by the ith cable loop must be in the direction of vector $\mathbf{u}_i$, $i = 1, 2, 3$. To avoid the situation in which one of the cables becomes slack, vectors $\mathbf{u}_i, i = 1, 2, 3$ must be in a force-closed configuration. The boundary of this region is reached when two of the vectors $\mathbf{u}_i, i = 1, 2, 3$ are aligned. Therefore, the equation describing this boundary is the combination of Eq.(2.10), Eq.(2.11) and Eq.(2.12).

The solution of Eqs.(2.10) to (2.12) leads to two possible situations. One situation is that one of the rows is zero, the other situation is that the direction of each row is along the same line. The segment between the pulleys of line $A_{11}A_{12}$, $A_{21}A_{22}$, $A_{31}A_{32}$ corresponds to the first situation. The second situation is the solution of Eq.(2.20).

$$\begin{aligned} &\sqrt{A_{i2}}\sqrt{A_{j2}}\left[(y_{Ai1} - y_{Aj1})x_p + (x_{Aj1} - x_{Ai1})y_p + x_{Ai1}y_{Aj1} - x_{Aj1}y_{Ai1}\right] \\ &+\sqrt{A_{i2}}\sqrt{A_{j1}}\left[(y_{Ai1} - y_{Aj2})x_p + (x_{Aj2} - x_{Ai1})y_p + x_{Ai1}y_{Aj2} - x_{Aj2}y_{Ai1}\right] \\ &+\sqrt{A_{i1}}\sqrt{A_{j2}}\left[(y_{Ai2} - y_{Aj1})x_p + (x_{Aj1} - x_{Ai2})y_p + x_{Ai2}y_{Aj1} - x_{Aj1}y_{Ai2}\right] \\ &+\sqrt{A_{i1}}\sqrt{A_{j1}}\left[(y_{Ai2} - y_{Aj2})x_p + (x_{Aj2} - x_{Ai2})y_p + x_{Ai2}y_{Aj2} - x_{Aj2}y_{Ai2}\right] = 0 \end{aligned} \tag{2.20}$$

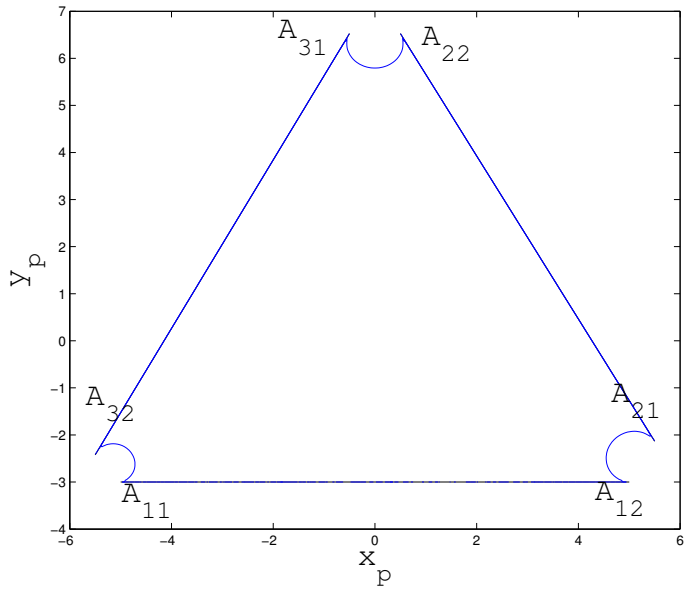

Figure 2.7: Boundary of the force-closed region for the 3-cable 2-dof cable driven parallel mechanism.

where

$$A_{ik} = (x_p - x_{aik})^2 + (y_p - y_{aik})^2, \qquad k = 1, 2.$$

For Eq.(2.10), the i and j of Eq.(2.20) are $i = 1$ and $j = 2$, for Eq.(2.11), the i and j of Eq.(2.20) are $i = 1$ and $j = 3$, and for Eq.(2.12) $i = 2$ and $j = 3$.

One example of the boundary of the force-closed configurations is shown Figure 2.7. Compared with Figure 2.2, it can be seen that the force-closed workspace boundary is the combination of the curves defined by Eqs. (2.10) to (2.12).

2.9 Conclusion

In this chapter, a 3-cable 2-DOF closed-loop cable-driven parallel mechanism is presented. The cables form loops that are free to move around a set of pulleys. The position of the end-effector is controlled using sliders that displace one of the pulleys along an axis. This architecture has the advantage of eliminating the need to wind cables around a spool. The inverse kinematics, the Jacobian matrices and the static equations were determined. The singularities of the mechanism

have been analyzed based on two Jacobian matrices. Also, using the method presented in [74], the set of available forces was obtained from the static equations. The special geometric characteristic of the novel architecture was studied. It was observed that, for a given position of the ith slider, the trajectory of the end-point of the ith cable loop is a portion of ellipse. The intersection of the ellipses gives the position of the end point. Using a geometric reasoning, the boundary of the force-closed workspace was determined.

Chapter 3

Planar Spring-Loaded Cable-Loop-Driven Parallel Mechanism

Two novel architectures of planar spring-loaded cable-loop-driven parallel mechanisms that do not require actuation redundancy are introduced in this chapter. In order to avoid actuation redundancy in the cable-driven parallel mechanisms and require only N actuators to control an N-DOF motion, new spring-loaded cable-loop-driven mechanisms are proposed. By attaching springs to the cable loops, two degrees of freedom can be controlled using only two actuators and spools are also eliminated in these mechanisms. The compliance caused by the spring in the cable loop is acting on one side of the actuator in one of the mechanisms. For the second mechanism, the compliance is symmetrically attached on both sides of the actuator. The mechanisms can be actuated using either linear sliders or rotary actuators driving the motion of a cable or belt loop.

Kinematic and static analyses are presented for the new architectures. It is verified that the cables and springs can be kept in tension within a certain workspace. Results of numerical simulations are also given in order to provide insight into the design issues.

3.1 Introduction

The planar mechanism introduced in the preceding chapter avoids the cable-spool system. However, it is redundantly actuated. Due to the unidirectionality of the cable force, cable-driven parallel mechanisms require the use of certain approaches to realize the force-closure condition. Suspended cable-driven parallel mechanisms make use of the end-effector's weight, while fully-constrained cable-driven parallel mechanisms are redundantly actuated. Also, some cable routings use rigid-link bridge and trolley systems. Here, it is expected to realize the force-closure condition using the compliance provided by springs.

The aim of this work is to avoid cable-spool systems and eliminate actuation redundancy in cable-driven parallel mechanisms using cable loops. Now, it is attempted to use cable loops and springs to reach this goal.

3.2 Conceptual Development of the 2-DOF Spring-Loaded Cable-Loop-Driven Parallel Mechanisms

In this work, it is desired to include a number of actuators equal to the number of degrees of freedom and to eliminate the spools for the cable-driven parallel mechanism. The proposed solution is to include cable loops between the actuators and the end-effector. The cable loops make it possible to avoid the use of spools. Indeed, each of the loops can be driven by a linear actuator (slider) or by a rotary actuator through a timing belt. The main issue with cable loops is that, in general, their length changes when the end-effector is displaced. Therefore, some compliance must be introduced in the loops in order to compensate for this change of length. Here, the challenge is to include compliance in the closed loops without introducing compliance between the actuators and the end-effector. Additionally, it is desired to obtain a symmetric layout.

If the objective is to avoid actuation redundancy and if spools are tolerated, the simple mechanism illustrated in Figure 3.1(a) could be suggested. Suppose $A_1A_2B_1B_2$ is a square with a

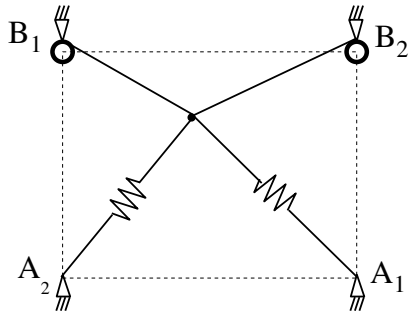

(a) Simple cable mechanism with two actuated spools and two springs.

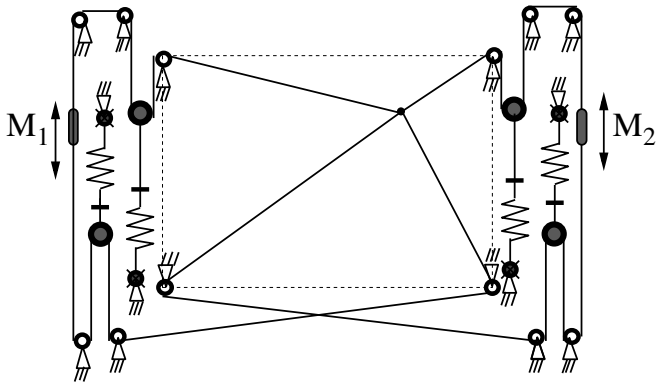

(b) Schematic representation of compliance in the loop on each side of the actuator.

Figure 3.1: Ineffective mechanisms using springs to avoid actuation redundancy.

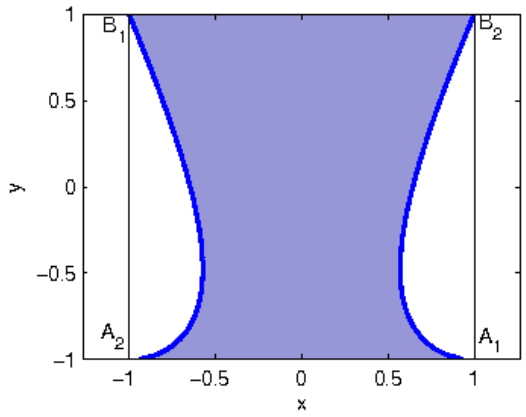

(a) $f_o = 1$ and $k = 0$

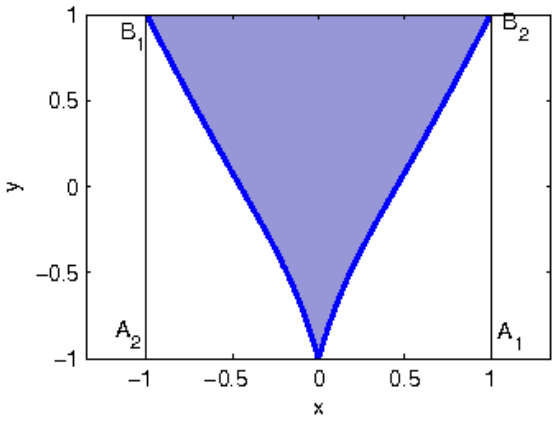

(b) $f_o = 1$ and $k = 1$

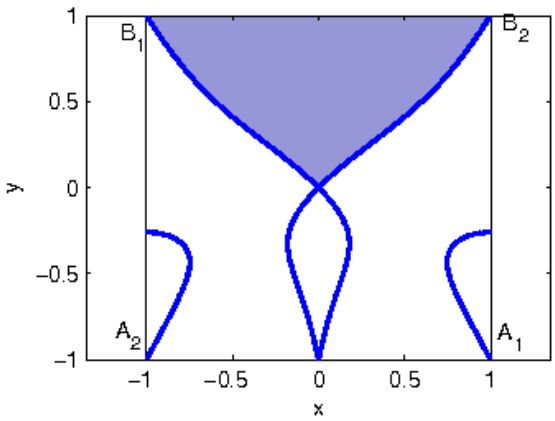

(c) $f_o = 0$ and $k = 1$

Figure 3.2: The workspaces for different spring parameters of the simple cable mechanism. The workspaces are illustrated by the shaded areas.

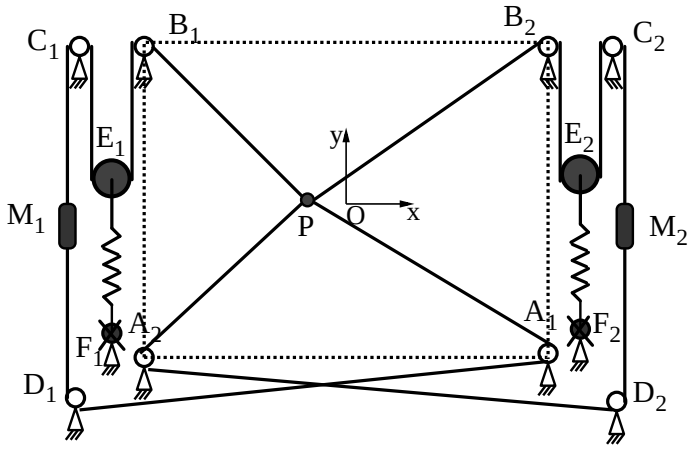

Figure 3.3: Schematic representation of compliance in the loop on one side of the actuator.

unit half side length and the original position of the end-effector is at the centre of the square. The available workspaces for different spring parameters (preload f_o and stiffness k) are shown in Figure 3.2. It can be observed that the workspace obtained is rather limited and not symmetric with respect to a horizontal axis.

One option to eliminate spools is to introduce preloaded compliance in the cables on each side of the actuator, as illustrated in Figure 3.1(b) where M_1 and M_2 represent the actuators. Because there is compliance between the end-effector and the actuators, any external force on the end-effector will cause one of the springs to extend and the other one to retract, which displaces the end-effector even if the actuators are fixed. It can be observed that this mechanism is ineffective.

The first suggested option is to include preloaded compliance on only one side of each loop, as illustrated in Figure 3.3. Then, there is compliance in the loop, but not between the end-effector and the actuator. Indeed, if an external force is applied on the compliant side, the force on the rigid side will decrease accordingly and the length in the compliant side will not change, as long as the external force does not exceed the preload. This arrangement fulfills the design requirements but it is not symmetric.

Another suggested option, illustrated in Figure 3.4, is to include preloaded compliance on each side of the actuator, but to couple these compliances. Figure 3.4(a) illustrates the implementation of the concept using rotary actuators and timing belts while Figure 3.4(b) illustrates the implementation using prismatic actuators (M_1 and M_2) and cables. The resulting mechanism has similarities with the system including compliance on one side of the loop, but it is symmetric. The

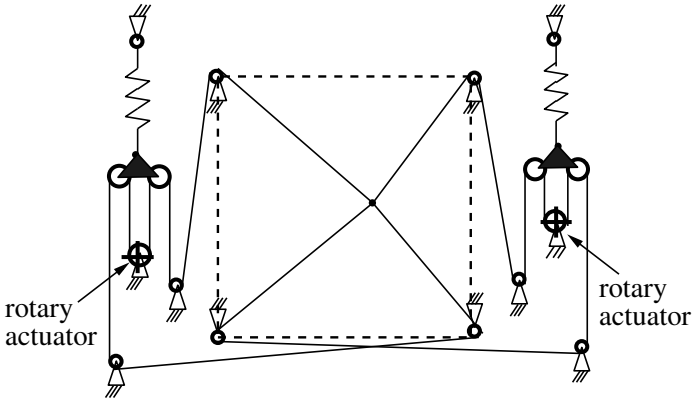

(a) Using rotary actuators

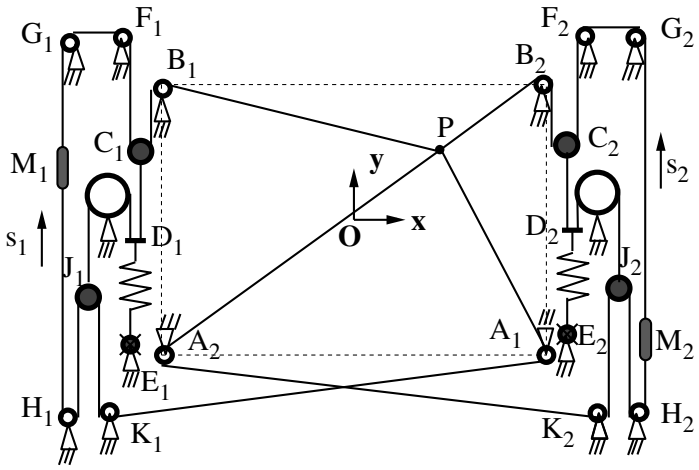

(b) Using prismatic actuators

Figure 3.4: Schematic representation of the 2-DOF spring-loaded cable-loop-driven parallel mechanisms with symmetric compliance.

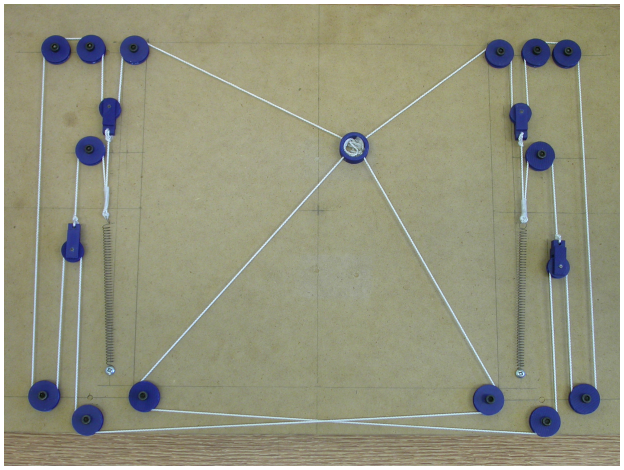

Figure 3.5: Demonstration model of the symmetric 2-DOF spring-loaded cable-loop-driven parallel mechanism.

compliance in the closed loops allows motion of the end-effector, but the transmission between the end-effector and the actuators is ideally rigid, as long as the resulting force on the spring does not exceed its preload. Because of the coupling between the two sides of each loop, if an external force is applied, the additional force on one side of the loop is compensated for by a reduction of the force on the other side of the loop without any effect on the preloaded spring, as long as the external force does not exceed the preload. It is noted that in order to work properly, the two sides of a given loop must be mounted on fixed pulleys that are mounted on opposite corners of the rectangular workspace $A_1A_2B_1B_2$ (Figure 3.4(b)), i.e., the mechanism does not work if the sides of a given loop are mounted on adjacent pulleys.

A demonstration model of the mechanism with symmetric compliance is shown in Figure 3.5. The analysis for the non-symmetric compliance and symmetric compliance spring-loaded cable-loop-driven parallel mechanisms is given in the following.

3.3 Planar Spring-Loaded Cable-Loop-Driven Parallel Mechanism with Non-Symmetric Compliance

3.3.1 Inverse Kinematics

As shown in Figure 3.3, there are two non-symmetric spring-actuator cable-loop systems in the non-symmetric 2-DOF spring-loaded cable-loop-driven mechanism. For the ith, $i = 1, 2$, cable loop, a spring E_iF_i is attached on one side of the actuator and the cable passes around the fixed pulleys A_i, B_i, C_i and D_i to complete the ith loop. The position of the fixed pulleys A_i, B_i, C_i and D_i, $i = 1, 2$, can be expressed by their position vector defined as $\mathbf{a}_i = [x_{ai}, y_{ai}]^T$, $\mathbf{b}_i = [x_{bi}, y_{bi}]^T$, $\mathbf{c}_i = [x_{ci}, y_{ci}]^T$ and $\mathbf{d}_i = [x_{di}, y_{di}]^T$, $i = 1, 2$. The position of the fixed attachment point F_i of the ith spring is defined as $\mathbf{f}_i = [x_{fi}, y_{fi}]^T$, $i = 1, 2$. Suppose the original length of the ith, $i = 1, 2$, spring is l_{oi} and its deformation is δ_i, the position of pulley E_i can be expressed as

$$\mathbf{e}_i = \mathbf{f}_i + (l_{oi} + \delta_i)\mathbf{s}_i = \mathbf{e}_{oi} + \delta_i\mathbf{s}_i, \quad i = 1, 2, \tag{3.1}$$

where $\mathbf{s}_i$ is the moving direction of the ith spring and $\mathbf{e}_{oi}$ is the original position of the spring end E_i, $i = 1, 2$.

The inverse kinematic problem can be stated as follows: given the position of the end-effector $\mathbf{p} = [x, y]^T$, find the position of the actuators M_i, $i = 1, 2$, and the position of the springs' end E_i, $i = 1, 2$, i.e., determine the displacement of the actuators l_{mi}, $i = 1, 2$, and the deformation of the springs δ_i, $i = 1, 2$.

The lengths of the cable segments PA_i and PB_i, $i = 1, 2$, vary according to the position of point P. The variation of cable segment PA_i, $i = 1, 2$, is caused by the displacement of the corresponding actuator; the variation of cable segment PB_i, $i = 1, 2$, is caused by the displacement of the actuator and the deformation of the spring. Assuming the original position of the end-effector is $\mathbf{p}_o = [x_o, y_o]^T$, one has

$$-l_{mi} = |PA_i| - |P_oA_i|, \qquad i = 1, 2, \tag{3.2}$$

$$l_{mi} + 2\delta_i = |PB_i| - |P_oB_i|, \qquad i = 1, 2. \tag{3.3}$$

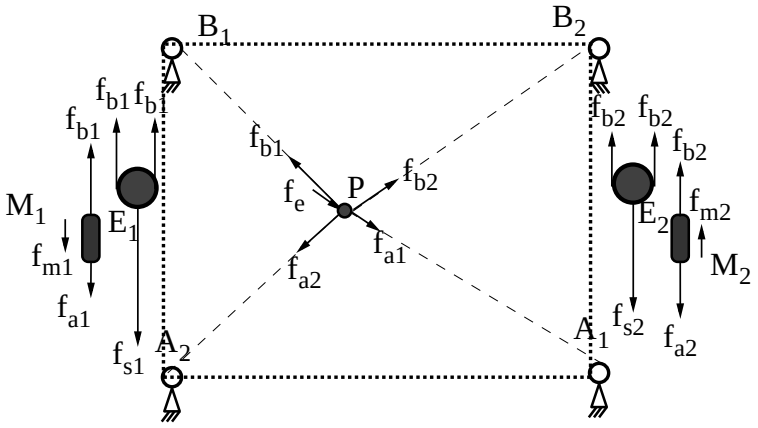

Figure 3.6: Forces acting on the 2-DOF spring-loaded cable-loop-driven parallel mechanism with non-symmetric compliance.

With Eq. (3.2) and Eq. (3.3), l_{mi} and δ_i, $i = 1, 2$, can be found as

$$\delta_i = \frac{n_{ai} + n_{bi}}{2}, \quad i = 1, 2, \tag{3.4}$$

$$l_{mi} = -n_{ai}, \quad i = 1, 2. \tag{3.5}$$

where $n_{ai} = |PA_i| - |P_oA_i|$ and $n_{bi} = |PB_i| - |P_oB_i|$, $i = 1, 2$.

From the above equations, it can be seen that the deformations of the springs and the displacements of the actuators only depend on the position of the end-effector and are independent from the external forces, assuming that the cables are all under tension.

3.3.2 Static Analysis

Neglecting the friction between the cables and pulleys, the forces acting at the end-effector and on the moving fixtures and pulleys are shown in Figure 3.6. The cable forces f_{ai}, f_{bi}, $i = 1, 2$, in the cable segments between the actuators and the end-effector are assumed to be uniform, since all pulleys are free to rotate and friction is neglected. Considering the static equilibrium of the end-effector, we have that

$$f_{a1}\mathbf{s}_{a1} + f_{b1}\mathbf{s}_{b1} + f_{a2}\mathbf{s}_{a2} + f_{b2}\mathbf{s}_{b2} = \mathbf{f}_e, \tag{3.6}$$

where $\mathbf{f}_e = [f_{ex}, f_{ey}]^T$ is the external force applied on the end-effector, $\mathbf{s}_{ai}$, $\mathbf{s}_{bi}$ are the unit vectors in the direction of PA_i and PB_i, $i = 1, 2$, respectively and

$$\mathbf{s}_{ai} = \frac{\mathbf{a}_i - \mathbf{p}}{||\mathbf{a}_i - \mathbf{p}||}, \qquad \mathbf{s}_{bi} = \frac{\mathbf{b}_i - \mathbf{p}}{||\mathbf{b}_i - \mathbf{p}||}, \qquad i = 1, 2. \tag{3.7}$$

The relationship between the ith spring force, f_{si}, and its deformation, δ_i, is assumed to be given by

$$f_{si} = f_{oi} + k_i \delta_i, \qquad i = 1, 2 \tag{3.8}$$

where f_{oi} is the preloading force given for the reference position and k_i is the stiffness of the spring. Also, it can be observed that the forces in the springs are independent from the external forces, assuming that the cables are all under tension, we have

$$f_{si} = 2f_{bi}, \qquad i = 1, 2. \tag{3.9}$$

For a given configuration, the deformation of the spring can be calculated and the cable forces f_{bi} can then be found using the spring parameters as

$$f_{bi} = \frac{1}{2}(f_o + k\delta_i), \quad i = 1, 2. \tag{3.10}$$

Substituting Eq. (3.10) into Eq. (3.6), the cable forces f_{ai}, $i = 1, 2$, are solved as

$$f_{ai} = \frac{\Theta_i}{\Theta}, \quad i = 1, 2, \tag{3.11}$$

where $\Theta = -\mathbf{s}_{a1}^T \mathbf{E} \mathbf{s}_{a2}$, $\Theta_1 = -\mathbf{f}_f^T \mathbf{E} \mathbf{s}_{a2}$, $\Theta_2 = \mathbf{f}_f^T \mathbf{E} \mathbf{s}_{a1}$, $\mathbf{f}_f = \mathbf{f}_e - f_{b1}\mathbf{s}_{b1} - f_{b2}\mathbf{s}_{b2}$ and

$$\mathbf{E} = \begin{bmatrix} 0 & -1 \\ 1 & 0 \end{bmatrix}.$$

The cable force f_{bi}, $i = 1, 2$, can be calculated using Eq. (3.10) for a given position of the end-effector. Then, the cable force f_{ai}, $i = 1, 2$, can be found with Eq. (3.11) for a certain external force.

3.3.3 Workspace Analysis

In order to simplify the analysis and preserve symmetry, the origin of the fixed coordinate frame $O - xy$ is located at the centre of rectangle $A_1A_2B_1B_2$ as shown in Figure 3.3. Moreover, the

modular actuator-spring systems are all assumed to have the same characteristics. That is to say, the preload and the stiffness of the springs are the same in each loop, i.e., $f_{o1} = f_{o2} = f_o$ and $k_1 = k_2 = k$ respectively. Because cables can only pull and not push, it should be verified that the cables and springs can be maintained in tension over the workspace. In other words, the workspace is defined as the set of end-effector positions for which the cables can be maintained in tension.

Assume no external force applied on the end-effector, i.e., $\mathbf{f}_e = \mathbf{0}$. The force in the cables can be obtained from Eq.(3.10) and Eq.(3.11). As mentioned above, the cables and the springs should be maintained in tension if the end-effector is within the workspace.

In the reference configuration, it is expected that there is no deformation of the springs and the spring force equals the preload. That is to say,

$$f_{si} = f_o, \qquad \delta_i = 0, \qquad i = 1, 2.$$

According to their stiffness, springs can be classified as positive stiffness springs, constant force springs and negative stiffness springs (examples of practical implementation of a negative stiffness is presented in [108–110]). In order to maintain the springs in tension, the following relationships should be satisfied

$$f_{si} \begin{cases} \geq f_o, & \text{if} \quad k > 0, \\ = f_o, & \text{if} \quad k = 0, \\ \leq f_o, & \text{if} \quad k < 0, \end{cases} \qquad i = 1, 2. \tag{3.12}$$

Let $\delta_{f_{si}} = f_{si} - f_o$ and from Eq. (3.4) we have

$$\delta_{fsi} = k\delta_i = \frac{k}{2}(n_{ai} + n_{bi}), \tag{3.13}$$

then Eq. (3.12) can be written as

$$n_{ai} + n_{bi} \geq 0, \qquad i = 1, 2. \tag{3.14}$$

The latter condition is equivalent to

$$|A_iP| + |B_iP| \geq c_i, \qquad i = 1, 2, \tag{3.15}$$

where $c_i = |A_iP_0| + |B_iP_0|$, $i = 1, 2$. This means that the reference position of the end-effector should be placed at a point for which the sum of the distances from this point to the pulleys A_i and B_i, $i = 1, 2$, is the shortest distance. Only one point of the workspace satisfies this condition: the intersection of diagonal A_1B_1 and diagonal A_2B_2, namely the centroid of the rectangle formed

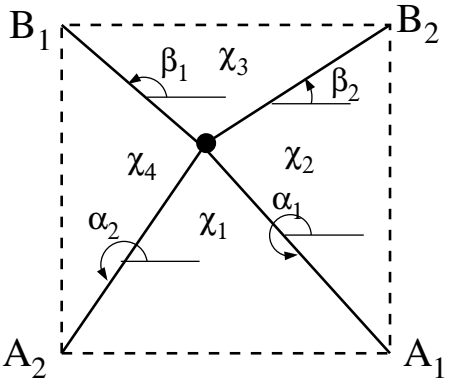

Figure 3.7: Angles made by the cables.

by the four fixed pulleys A_1, A_2, B_1 and B_2.

The cable forces f_{bi}, $i = 1, 2$, are equal to one half of the corresponding springs forces, as shown in Eq. (3.10). Therefore, it suffices needs to investigate the cable forces f_{ai}, $i = 1, 2$, in order to ensure tension in the mechanism.

The maximum potential workspace is assumed to be the rectangle formed by the four fixed pulleys A_1, A_2, B_1, B_2. Within this footprint, the components of vectors $\mathbf{s}_{ai}$, $\mathbf{s}_{bi}$, $i = 1, 2$, can be expressed as the unit vector defined by the angles (defined in Figure 3.7) which are measured between the x-axis and the cables [48]. Because $\Theta = \sin(\alpha_2 - \alpha_1) = -\sin\chi_1 < 0$, the workspace boundary is formed by the curves corresponding to Θ_1 and Θ_2 equal to zero.

Assuming no external force applied on the end-effector, the expressions of Θ_1 and Θ_2 when the springs are constant force springs ($k = 0$) lead to

$$-\frac{a_{22}b_{12}b_{22}}{f_o}\Theta_1 = y_{b2}(x + x_{b2})b_{22} + (y_{b2}x - x_{b2}y)b_{12} \tag{3.16}$$

$$\frac{a_{12}b_{12}b_{22}}{f_o}\Theta_2 = (y_{b2}x + x_{b2}y)b_{22} + y_{b2}(x - x_{b2})b_{12} \tag{3.17}$$

where $a_{i2} = (\mathbf{a}_i - \mathbf{p})^T(\mathbf{a}_i - \mathbf{p})$, $b_{i2} = (\mathbf{b}_i - \mathbf{p})^T(\mathbf{b}_i - \mathbf{p})$, $i = 1, 2$.

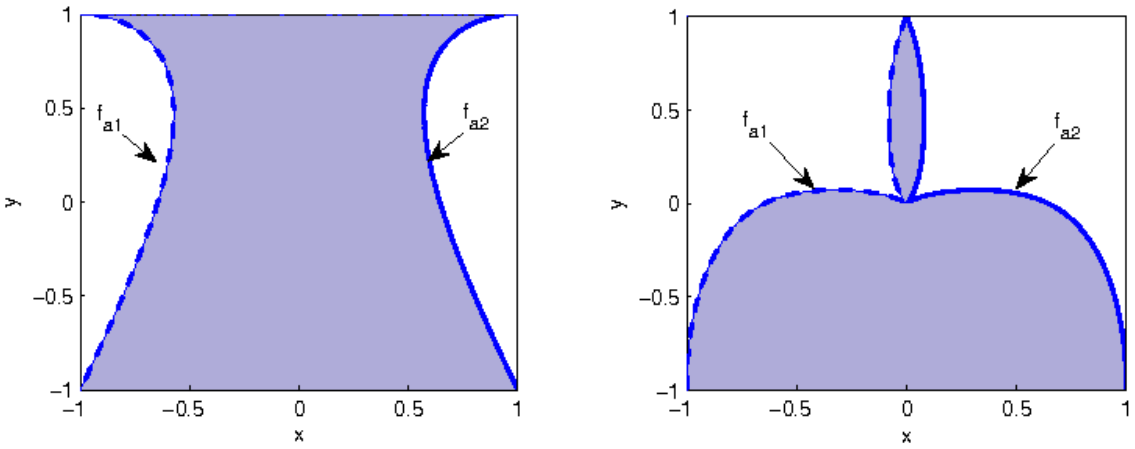

(a) With $k = 0$ (b) With $f_o = 0$

Figure 3.8: Workspace boundary defined by f_{ai}, $i = 1, 2$.

Similarly, if there is no preload in the springs, Θ_i, $i = 1, 2$, can be written as

$$-\frac{2a_{22}b_{12}b_{22}}{k}\Theta_1 = y_{b2}(x + x_{b2})(n_{a1} + n_{b1})b_{22} + (y_{b2}x - x_{b2}y)(n_{a2} + n_{b2})b_{12}, \tag{3.18}$$

$$\frac{2a_{12}b_{12}b_{22}}{k}\Theta_2 = (y_{b2}x + x_{b2}y)(n_{a1} + n_{b1})b_{22} + y_{b2}(x - x_{b2})(n_{a2} + n_{b2})b_{12}. \tag{3.19}$$

Combining Eq. (3.16) with Eq. (3.18) and Eq. (3.17) with Eq. (3.19) respectively, the workspace boundary defined by f_{a1} and f_{a2} for a general spring is obtained. Assuming $y = 0$, and combining Eq. (3.16) with Eq. (3.18), we have

$$\begin{aligned} -a_{22}b_{12}b_{22}\Theta_1 =& y_{b2}\left[(x + x_{b2})\sqrt{(x_{b2} - x)^2 + y_{b2}^2} + x\sqrt{(x_{b2} + x)^2 + y_{b2}^2}\right] \\ & \left[f_o + \frac{k}{2}\left(\sqrt{(x_{b2} - x)^2 + y_{b2}^2} + \sqrt{(x_{b2} + x)^2 + y_{b2}^2} - 2\sqrt{x_{b2}^2 + y_{b2}^2}\right)\right]. \end{aligned} \tag{3.20}$$

From this equation, it can be observed that there exists a certain value for x through which the workspace boundary will pass, regardless of the characteristics of the springs.

Suppose $x_{b2} = y_{b2} = 1$, the curves defined in Eq. (3.16) and Eq. (3.17) are shown in Figure 3.8(a), while the curves defined in Eq. (3.19) and Eq. (3.18) are shown in Figure 3.8(b). The plots for the workspace boundary defined by f_{ai}, $i = 1, 2$, for different values of the non-dimensional parameter $\frac{kr}{f_o}$ are shown in Figure 3.9 and Figure 3.10, where r is the half length of the square side. It can be seen that with negative stiffness springs, the mechanism has a larger workspace.

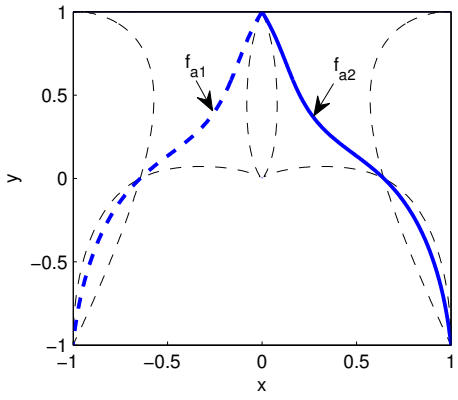

(a) With $\frac{kr}{f_o} = 10$

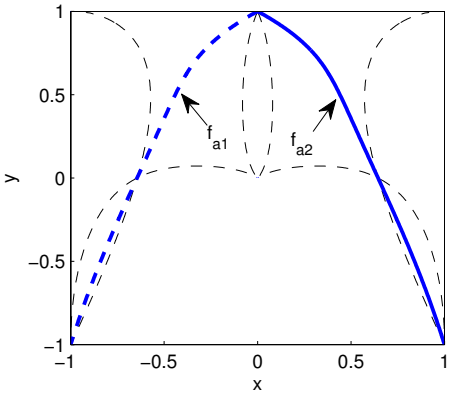

(b) With $\frac{kr}{f_o} = \sqrt{2}$

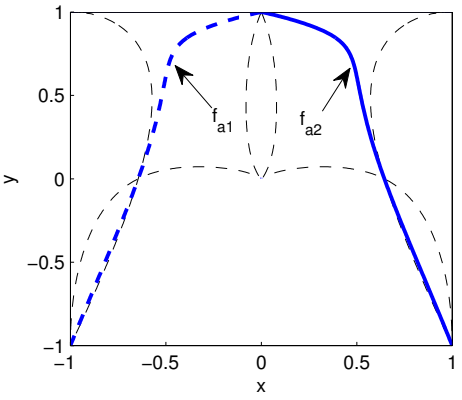

(c) With $\frac{kr}{f_o} = 0.5$

Figure 3.9: Workspace boundaries defined by f_{a1} and f_{a2} for different values of $\frac{kr}{f_o}$.

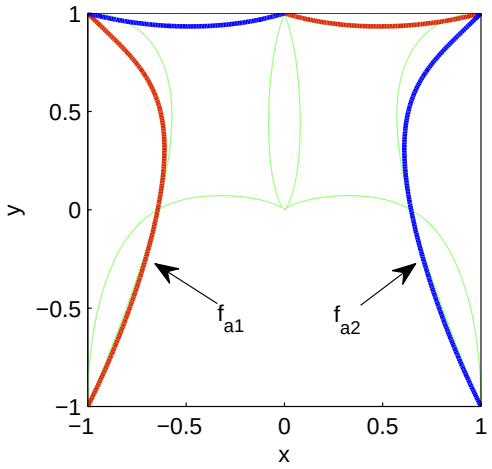

Figure 3.10: Workspace boundaries defined by f_{a1} and f_{a2} with negative stiffness springs, $\frac{kr}{f_o} = -0.5$.

When $y = 0$, the common point on the workspace boundary corresponding to f_{a1} is $[-0.6446, 0]^T$ according to Eq. (3.20). This is consistent with the results of all these figures. It is remarkable that the shapes of Figure 3.2(a) and Figure 3.8(a) are the same, which illustrates that with $k = 0$, both mechanisms have the same workspace.

From the workspace plots, it can be observed that the workspace boundary for the spring-loaded cable-loop-driven parallel mechanism with non-symmetric compliance cannot be the whole rectangle $A_1A_2B_1B_2$ no matter what the ratio $\frac{kr}{f_o}$ is. It is expected that the spring-loaded cable-loop-driven parallel mechanism with symmetric compliance has better characteristics. The analysis for the latter mechanism is performed in the next subsection.

3.4 Planar Spring-Loaded Cable-Loop-Driven Parallel Mechanism with Symmetric Compliance

3.4.1 Inverse Kinematics

In Figure 3.4, there are two schematics of the planar spring-loaded cable-loop-driven parallel mechanisms with symmetric compliance. One uses rotary actuators and while the other uses sliding

actuators. In this section, mechanisms with sliding actuators are analyzed. The mechanisms built with rotary actuators lead to very similar results which are readily obtained by adapting the analysis presented here. The structure of the symmetric 2-DOF spring-loaded cable-loop-driven parallel mechanism with sliding actuators is shown in Figure 3.4(b): there are two spring-actuator cable-loop systems in this mechanism. For the ith, $i = 1, 2$, cable loop, a spring D_iE_i is attached to the base at point E_i. Two pulleys C_i and J_i are connected to the other end of the spring at D_i. Each cable loop passes around these two pulleys and around the fixed pulleys to complete the ith loop, namely $K_iA_iB_iF_iG_iH_iK_i$. Cables are mounted on the slider actuators M_i, $i = 1, 2$. The cable segments between H_iG_i, F_iC_i, C_iB_i, J_iH_i, J_iK_i and the spring D_iE_i are parallel to each other.

The positions of the fixed pulleys A_i, B_i, E_i, F_i, G_i, H_i, K_i, $i = 1, 2$, can be expressed by their position vectors defined as $\mathbf{a}_i = [x_{ai}, y_{ai}]^T$, $\mathbf{b}_i = [x_{bi}, y_{bi}]^T$, $\mathbf{e}_i = [x_{ei}, y_{ei}]^T$, $\mathbf{f}_i = [x_{fi}, y_{fi}]^T$, $\mathbf{g}_i = [x_{gi}, y_{gi}]^T$, $\mathbf{h}_i = [x_{hi}, y_{hi}]^T$ and $\mathbf{k}_i = [x_{ki}, y_{ki}]^T$, $i = 1, 2$. The lengths of the cable segments C_iD_i, J_iD_i, $M_iH_iJ_iK_iA_iP$ and $M_iG_iF_iC_iB_iP$ are constant. For the ith, $i = 1, 2$, loop, when the length of one of the cable segments $H_iJ_iK_iA_iP$ or $G_iF_iC_iB_iP$ decreases, the length of the other increases by the same amount, which corresponds to the actuator motion. The total length of each cable-loop is constant, but the cable length of A_iPB_i, $i = 1, 2$, varies according to the position of point P and this variation is compensated for by the change of length of the spring.

The reference position of points J_i, C_i and D_i are noted $\mathbf{j}_{oi}$, $\mathbf{c}_{oi}$ and $\mathbf{d}_{oi}$, $i = 1, 2$, respectively. Also, the moving direction of the ith spring is represented by unit vector $\mathbf{s}_i$, the undeformed length of the spring is l_{oi}, and its deformation is δ_i. Then, the position of points J_i, C_i and D_i, $i = 1, 2$, with the deformation δ_i can be calculated as

$$\mathbf{d}_i = \mathbf{e}_i + (l_{oi} + \delta_i)\mathbf{s}_i = \mathbf{d}_{oi} + \delta_i\mathbf{s}_i, \qquad i = 1, 2, \tag{3.21}$$

$$\mathbf{j}_i = \mathbf{j}_{oi} - \delta_i\mathbf{s}_i, \qquad i = 1, 2, \tag{3.22}$$

$$\mathbf{c}_i = \mathbf{c}_{oi} + \delta_i\mathbf{s}_i, \qquad i = 1, 2, \tag{3.23}$$

The solution of the inverse kinematics problem consists in finding the position of the actuators M_i, $i = 1, 2$, and the position of D_i, $i = 1, 2$, i.e., determine the displacement of the actuators l_{mi}, $i = 1, 2$, and the deformation of the springs δ_i, $i = 1, 2$ for a given position of the end-effector P, $\mathbf{p} = [x, y]^T$.

The lengths of the cable segments PA_i and PB_i, $i = 1, 2$, vary according to the position of point P and these variations are induced by the displacement of the actuators and the deformation

of the springs. Assuming the reference position of the end-effector to be $\mathbf{p}_o = [x_o, y_o]^T$, we have

$$2\delta_i - l_{mi} = |PA_i| - |P_oA_i|, \quad i = 1, 2, \tag{3.24}$$

$$2\delta_i + l_{mi} = |PB_i| - |P_oB_i|, \quad i = 1, 2. \tag{3.25}$$

With these four equations (Eqn. (3.24) and Eqn. (3.25)), l_{mi} and δ_i, $i = 1, 2$, can be found as

$$\delta_i = \frac{1}{4}(n_{ai} + n_{bi}), \quad i = 1, 2, \tag{3.26}$$

$$l_{mi} = \frac{1}{2}(n_{bi} - n_{ai}), \quad i = 1, 2, \tag{3.27}$$

where $n_{ai} = |PA_i| - |P_oA_i|$, $n_{bi} = |PB_i| - |P_oB_i|$, $i = 1, 2$.

Similarly to the mechanism with the non-symmetric compliance, from Eq. (3.26) and Eq. (3.27), it can be seen that δ_i and l_{mi}, $i = 1, 2$, only depend on the position of the end-effector and are independent from the external forces.

The extension of the spring of a loop occurs when the end-effector is moved away from the diagonal associated with the loop, namely A_iB_i. Also, the maximum elongation of a spring of a loop occurs when the end-effector is at one of the fixed pulleys of the other loop (e.g. A_2 or B_2 for loop 1). Therefore, assuming that the four fixed pulleys $A_1A_2B_1B_2$ are located on the corners of a square, we have

$$n_{ai,max} = n_{bi,max} = (2 - \sqrt{2})r, \tag{3.28}$$

where r is the half length of a side of the square and, from Eqn. (3.26), the maximum elongation of the spring is obtained as

$$\delta_{i,max} = (\frac{2 - \sqrt{2}}{2})r. \tag{3.29}$$

3.4.2 Static Analysis

Neglecting the friction between the cables and pulleys, the forces acting at the end-effector and on the moving fixtures and pulleys are shown in Figure 3.11. The static equilibrium equation for the end-effector is the same as that of the non-symmetric mechanism, that is to say

$$f_{a1}\mathbf{s}_{a1} + f_{b1}\mathbf{s}_{b1} + f_{a2}\mathbf{s}_{a2} + f_{b2}\mathbf{s}_{b2} = \mathbf{f}_e \tag{3.30}$$

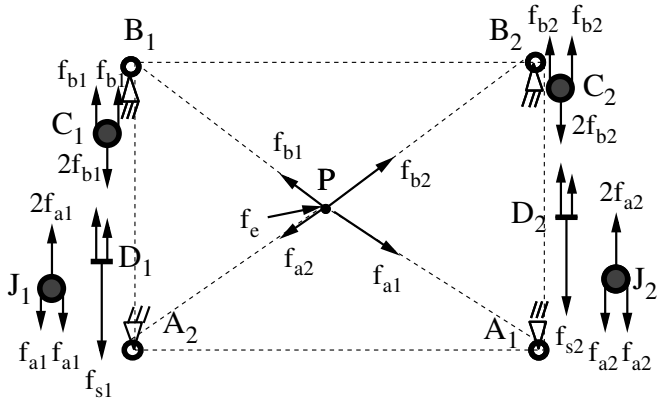

Figure 3.11: Forces acting on the 2-DOF spring-loaded cable-loop-driven parallel mechanism with symmetric compliance.

The relationship between the ith spring force and its deformation is the same as Eq. (3.8). In order to facilitate reading, it is rewritten here in matrix form.

$$\mathbf{f}_s = \mathbf{f}_o + \mathbf{K}\boldsymbol{\delta} \tag{3.31}$$

where $\mathbf{f}_s = [f_{s1}, f_{s2}]^T$, $\mathbf{f}_o = [f_{o1}, f_{o2}]^T$, $\mathbf{K} = \text{diag}[k_1, k_2]$ and $\delta = [\delta_1, \delta_2]^T$. The forces in the springs are also independent from the external forces, assuming that the cables are all under tension. From Figure 3.11, we have

$$f_{si} = 2f_{ai} + 2f_{bi}, \qquad i = 1, 2. \tag{3.32}$$

Equation (3.32) is the result of the coupling between the two sides of a loop, as illustrated in Figure 3.12. Depending on the configuration, the preloaded spring will extend or retract, resulting in a larger or smaller force f_{si}. The line shown in Figure 3.12, representing the locus of points satisfying Eq. (3.32) will move accordingly. Then, for a given configuration, the forces f_{ai} and f_{bi} correspond to a point along the line of the graph of Figure 3.12. The location of the point is dependent on the external forces. If the point is pushed out of the line segment included in the first quadrant, then one of the cables becomes loose and the configuration cannot be maintained. Also, it can be seen that in order to keep the mechanism within its working range, the maximum available force in a cable loop is $f_{si}/2$. Therefore, the cable forces must be such that

$$f_{ai} \in \left[0, \frac{1}{2} f_{si}\right], \qquad f_{bi} \in \left[0, \frac{1}{2} f_{si}\right]. \tag{3.33}$$

It is noted that the maximum sustainable external force will generally be smaller than the latter value especially near the boundary of the workspace. Indeed, at the boundary of the workspace, the sustainable external force vanishes. This issue will be addressed in detail in Chapter 5.

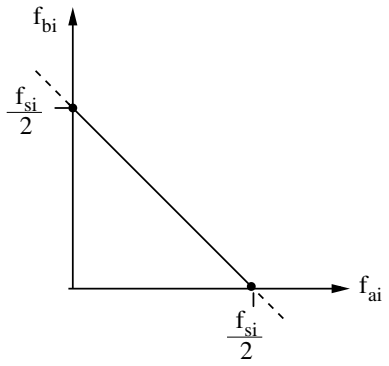

Figure 3.12: Illustration of equation (3.32), for a given configuration.

Rewriting Eq. (3.32) as $f_{ai} = \frac{f_{si}}{2} - f_{bi}$, $i = 1, 2$, and substituting f_{ai} into Eq. (3.30), we then have

$$f_{b1}(\mathbf{s}_{b1} - \mathbf{s}_{a1}) + f_{b2}(\mathbf{s}_{b2} - \mathbf{s}_{a2}) = \mathbf{f}_q \tag{3.34}$$

where

$$\mathbf{f}_q = \mathbf{f}_e - \frac{1}{2}(f_{s1}\mathbf{s}_{a1} + f_{s2}\mathbf{s}_{a2}).$$

Eq. (3.34) can be rewritten in matrix form as

$$\mathbf{M}\mathbf{f}_b = \mathbf{f}_q \tag{3.35}$$

where $\mathbf{f}_b$ is a vector defined as $\mathbf{f}_b = [f_{b1}, f_{b2}]^T$ and $\mathbf{M}$ is a 2×2 matrix given as

$$\mathbf{M} = \begin{bmatrix} (\mathbf{s}_{b1} - \mathbf{s}_{a1}) & (\mathbf{s}_{b2} - \mathbf{s}_{a2}) \end{bmatrix}. \tag{3.36}$$

Equation (3.35) is readily solved for $\mathbf{f}_b$ for a given configuration and external force. Moreover, it can be observed by inspection of Eq. (3.36) that matrix $\mathbf{M}$ cannot become singular inside the footprint of the mechanism (the rectangle defined by $A_1A_2B_1B_2$). Therefore, the above solution is robust and can be used to calculate the cable force anywhere within the workspace.

Once vector $\mathbf{f}_b$ is computed, Eq. (3.32) can be used to compute forces f_{a1} and f_{a2}, namely

$$\mathbf{f}_a = \frac{1}{2}\mathbf{f}_s - \mathbf{f}_b \tag{3.37}$$

where $\mathbf{f}_a = [f_{a1}, f_{a2}]^T$. Upon solving Eq. (3.35) and Eq. (3.37) for $\mathbf{f}_b$ and $\mathbf{f}_a$, it should be verified that all cable tensions are positive.

In fact, Eq. (3.35) is readily solved in closed form, which leads to

$$f_{bi} = \frac{\Delta_i}{\Delta}, \qquad i = 1, 2 \tag{3.38}$$

where

$$\Delta_1 = -\mathbf{f}_q^T \mathbf{E}(\mathbf{s}_{b2} - \mathbf{s}_{a2}), \tag{3.39}$$

$$\Delta_2 = \mathbf{f}_q^T \mathbf{E}(\mathbf{s}_{b1} - \mathbf{s}_{a1}), \tag{3.40}$$

$$\Delta = -(\mathbf{s}_{b1} - \mathbf{s}_{a1})^T \mathbf{E}(\mathbf{s}_{b2} - \mathbf{s}_{a2}), \tag{3.41}$$

and

$$\mathbf{E} = \begin{bmatrix} 0 & -1 \\ 1 & 0 \end{bmatrix}.$$

Hence, closed-form expressions for the cable forces f_{ai}, f_{bi}, $i = 1, 2$, are directly available using Eq. (3.37) and Eq. (3.38).

When the mechanism is in static equilibrium, the actuating force $\mathbf{f}_m$ can be written as

$$\mathbf{f}_m = \mathbf{f}_a - \mathbf{f}_b, \tag{3.42}$$

where $\mathbf{f}_m = [f_{m1}, f_{m2}]^T$. Using Eq. (3.32), the actuating force can be expressed as

$$\mathbf{f}_m = \frac{1}{2}\mathbf{f}_s - 2\mathbf{f}_b. \tag{3.43}$$

Since the cable forces need to satisfy the conditions shown in Eq. (3.33), it follows from interval arithmetics that the required actuating force must be such that $f_{mi} \in \left[-\frac{1}{2}f_{si}, \frac{1}{2}f_{si}\right]$, $i = 1, 2$.

3.4.3 Simplified Preliminary Analysis

In this subsection, a simplified analysis is performed in order to obtain estimates of the design parameters. First, it is assumed that the rectangle $A_1A_2B_1B_2$ is a square whose side is of length $2r$. Similarly to the analysis performed for the non-symmetric mechanism, it can be verified that the reference configuration (springs are without deformations) should be placed at the centre of the square. Therefore, the points of the workspace that lie the furthest from the reference configuration are the four corner points A_1, A_2, B_1 and B_2. If the square is considered as the workspace of the mechanism, these points correspond to the configurations where one of the cable loops reaches its maximum extension with respect to its reference length.

Assuming that the corner points are at the boundary of the workspace, we can set the corresponding cable tension to zero. For instance, if we assume that the end-effector is located at point A_2 and that the latter is at the boundary of the workspace, the critical force will be f_{b2} and the constraint to be satisfied will be

$$f_{b2} \geq 0. \tag{3.44}$$

Assuming that the end-effector is located at point A_2 with zero external force, Eqn. (3.30) and Eqn. (3.32) form a system of four linear equations in f_{ai}, f_{bi}, $i = 1, 2$, which can be readily solved for the latter unknowns. Substituting Eqn. (3.31) and Eqn. (3.29) in the solution then leads to, for f_{b2}:

$$f_{b2} = \left(\frac{2-\sqrt{2}}{4}\right) f_o - \left(\frac{\sqrt{2}-1}{4}\right) kr. \tag{3.45}$$

Substituting Eqn. (3.45) into Inequality (3.44) then leads to

$$\frac{kr}{f_o} \leq \sqrt{2}. \tag{3.46}$$

In other words, Inequality (3.46) provides the maximum ratio of $\frac{kr}{f_o}$ which guarantees that the corners of the square are included in the workspace. Inequality (3.46) can be used as a first estimate in order to determine the proper spring parameters for a given mechanism.

In the above analysis, the following cable forces are obtained when the end-effector is located at point A_2:

$$f_{a1,max} = f_{b1,max} = \frac{1}{2}(f_o + k\delta_{max}) = \frac{f_o}{4} + \left(\frac{2-\sqrt{2}}{8}\right) kr \tag{3.47}$$

$$f_{a2,min} = \frac{1}{2} f_{s,min} = \frac{1}{2} f_o \tag{3.48}$$

where $f_{a1,max}$, $f_{b1,max}$, $f_{a2,min}$ and $f_{s,min}$ are respectively the maximum and minimum values of the forces.

Moreover, the elongation of a spring resulting from the preload is given by

$$\delta_o = \frac{f_o}{k}. \tag{3.49}$$

Then, from Eq. (3.49) and when the preload is set to allow the workspace to reach the corners (Inequality (3.46)), δ_o can be expressed as

$$\delta_o = \frac{\sqrt{2}}{2} r. \tag{3.50}$$

Finally, the maximal total elongation of the spring is given by

$$\delta_{tot} = \delta_{i,max} + \delta_o, \tag{3.51}$$

and when the preload is set to allow the workspace to reach the corners,

$$\delta_{tot} = \frac{2-\sqrt{2}}{2} r + \frac{\sqrt{2}}{2} r = r, \tag{3.52}$$

that is, the maximum total elongation of the spring equals half the side of the square.

3.4.4 Workspace Analysis

The cable forces and the springs should be maintained in tension for the end-effector to remain within the workspace. Similarly to what was done for the non-symmetric mechanism, in order to preserve symmetry, the origin of the fixed coordinate frame $O - xy$ is located at the centre of rectangle $A_1A_2B_1B_2$ as shown in Figure 3.4(b) and the modular actuator-spring systems are all assumed to have the same characteristics.

3.4.4.1 Zero External Forces: Formulation

The mechanism is first assumed to be operated in quasi-static conditions on a horizontal plane without friction and the external force on the end-effector is assumed to be zero, i.e., $\mathbf{f}_e = \mathbf{0}$. The forces in the cables can then be obtained from Eq. (3.37) and Eq. (3.38) where $\mathbf{f}_q$ is simply taken as $\mathbf{f}_q = -\frac{1}{2}(f_{s1}\mathbf{s}_{a1} + f_{s2}\mathbf{s}_{a2})$, $\mathbf{f}_s$ is obtained from Eq. (3.31) and δ_i is obtained from Eq. (3.26).

The springs and the cable forces f_{ai} and f_{bi}, $i = 1, 2$, should be maintained in tension when the position of the end-effector is within the workspace. This condition leads to

$$f_{ai} \geq 0, \qquad i = 1, 2, \tag{3.53}$$

$$f_{bi} \geq 0, \qquad i = 1, 2. \tag{3.54}$$

Or, using Eq. (3.37),

$$0 \leq f_{ai} \leq \frac{1}{2} f_{si}, \qquad 0 \leq f_{bi} \leq \frac{1}{2} f_{si}, \qquad i = 1, 2. \tag{3.55}$$

which is equivalent to Eq. (3.33).

If the original configuration of the end-effector is placed at the centre of the rectangle, the springs will always be maintained in tension no matter what the stiffness is. Therefore, only the conditions of Inequality (3.53) and Inequality (3.54) (or alternatively Inequality (3.55)) need to be considered in order to ensure tension in the mechanism.

As shown in Figure 3.7, the determinant of matrix $\mathbf{M}$ can be written as

$$\Delta = \det\left(\begin{bmatrix} (\cos\beta_1 - \cos\alpha_1) & (\cos\beta_2 - \cos\alpha_2) \\ (\sin\beta_1 - \sin\alpha_1) & (\sin\beta_2 - \sin\alpha_2) \end{bmatrix}\right) = -\sum_{i=1}^{4} \sin\chi_i, \tag{3.56}$$

where $\chi_1 = \alpha_1 - \alpha_2$, $\chi_2 = 2\pi + \beta_2 - \alpha_1$, $\chi_3 = \beta_1 - \beta_2$, $\chi_4 = \alpha_2 - \beta_1$ and $\sum_{i=1}^{4} \chi_i = 2\pi$. Because $0 < \chi_i < \pi$, $i = 1, \ldots, 4$, then it can be seen that the determinant of $\mathbf{M}$ is always negative. Therefore, the numerators appearing in Eq. (3.38) should be negative in order to keep the cables in tension. Equations (3.39) and (3.40) lead to

$$\mathbf{f}_q^T \mathbf{E}(\mathbf{s}_{b2} - \mathbf{s}_{a2}) \geq 0 \tag{3.57}$$

$$-\mathbf{f}_q^T \mathbf{E}(\mathbf{s}_{b1} - \mathbf{s}_{a1}) \geq 0. \tag{3.58}$$

Because rectangle $A_1A_2B_1B_2$ is symmetric and the spring-actuator systems are modular with the same characteristics, then the four cable forces f_{ai}, f_{bi}, $i = 1, 2$, have the same properties. Therefore, it suffices to satisfy any of Inequality (3.57) or Inequality (3.58) in order to verify that the cables can be maintained in tension when the end-effector is within the footprint defined by rectangle $A_1A_2B_1B_2$. Hence, Inequality (3.57) is used in the following analysis.

Two special cases are now analyzed in order to simplify the problem. First, constant-force springs are assumed ($k = 0$). In this case, Inequality (3.57) can be written as

$$\frac{1}{\sqrt{A_{12}}\sqrt{B_{22}}}(a_1x + b_1y + c_1) + \frac{1}{\sqrt{A_{22}}\sqrt{B_{22}}}(a_2x + b_2y + c_2) + \frac{1}{\sqrt{A_{12}}\sqrt{A_{22}}}(a_3x + b_3y + c_3) \geq 0. \tag{3.59}$$

The second special case corresponds to $f_o = 0$, i.e., no preload in the springs. In this case, Inequality (3.57) becomes

$$\begin{aligned} &\frac{1}{\sqrt{B_{22}}}[(a_1 + a_2)x + (b_1 + b_2)y + (c_1 + c_2)] + \frac{1}{\sqrt{A_{22}}}[(a_2 + a_3)x + (b_2 + b_3)y + (c_2 + c_3)] \\ &+ \frac{\sqrt{B_{12}}}{\sqrt{A_{12}}\sqrt{B_{22}}}(a_2x + b_2y + c_2) + \frac{\sqrt{B_{12}}}{\sqrt{A_{12}}\sqrt{A_{22}}}(a_3x + b_3y + c_3) \\ &- \frac{d_{a2} + d_{b2}}{\sqrt{A_{22}}\sqrt{B_{22}}}(a_2x + b_2y + c_2) + \frac{d_{a1} + d_{b1}}{\sqrt{A_{12}}\sqrt{B_{22}}}(a_3x + b_3y + c_3) \\ &+ \frac{d_{a1} + d_{b1}}{\sqrt{A_{12}}\sqrt{A_{22}}}(a_1x + b_1y + c_1) \geq 0. \end{aligned} \tag{3.60}$$

In the above equations, one has

$$
\begin{aligned}
&A_{i2} = (\mathbf{a}_i - \mathbf{p})^T(\mathbf{a}_i - \mathbf{p}), \quad B_{i2} = (\mathbf{b}_i - \mathbf{p})^T(\mathbf{b}_i - \mathbf{p}),\\
&a_1 = y_{b2} - y_{a1}, \quad a_2 = y_{b2} - y_{a2}, \quad a_3 = y_{a1} - y_{a2},\\
&b_1 = x_{a1} - x_{b2}, \quad b_2 = x_{a2} - x_{b2}, \quad b_3 = x_{a2} - x_{a1},\\
&c_1 = -\mathbf{b}_2^T\mathbf{E}\mathbf{a}_1, \quad c_2 = -\mathbf{b}_2^T\mathbf{E}\mathbf{a}_2, \quad c_3 = -\mathbf{a}_1^T\mathbf{E}\mathbf{a}_2,\\
&d_{ai} = |P_oA_i|, \quad d_{bi} = |P_oB_i|, \quad i = 1, 2.
\end{aligned}
$$

First, Inequality (3.59) is analyzed. Because the mechanism is symmetric and the origin of the coordinate system is in the centre of the workspace, the coordinates of the fixed pulleys have the following relationships

$$
\begin{aligned}
&x_{a1} = x_{b2}, \qquad y_{a1} = -y_{b2}, \qquad x_{a2} = -x_{b2},\\
&y_{a2} = -y_{b2}, \qquad x_{b1} = -x_{b2}, \qquad y_{b1} = y_{b2}.
\end{aligned}
$$

Hence, Inequality (3.59) can be simplified to

$$
\begin{aligned}
&y_{b2}(x - x_{b2})\sqrt{(x + x_{b2})^2 + (y + y_{b2})^2} + (y_{b2}x - x_{b2}y)\sqrt{(x - x_{b2})^2 + (y + y_{b2})^2}\\
&- x_{b2}(y + y_{b2})\sqrt{(x - x_{b2})^2 + (y - y_{b2})^2} \leq 0.
\end{aligned}
\tag{3.61}
$$

From the latter equation, the following observations can be made:

1. When $x = x_{b2}$, the left-hand side of Eq. (3.61) becomes 0, so the segment $x = x_{b2}$, $-y_{b2} \leq y \leq y_{b2}$ is a part of the workspace boundary;

2. When $x = -x_{b2}$, the left-hand side of Eq. (3.61) becomes

   $$-(y + y_{b2})\left[2x_{b2}y_{b2} + x_{b2}\sqrt{A_{12}} + x_{b2}\sqrt{B_{22}}\right].$$

   Within the rectangle $A_1A_2B_1B_2$, the value of y is constrained to $-y_{b2} \leq y \leq y_{b2}$, so $-(y + y_{b2}) \leq 0$. Because $\left[2x_{b2}y_{b2} + x_{b2}\sqrt{A_{12}} + x_{b2}\sqrt{B_{22}}\right] > 0$, Eq. (3.61) is satisfied when $x = -x_{b2}$, $-y_{b2} \leq y \leq y_{b2}$ and it becomes identically 0 at point $(-x_{b2}, -y_{b2})$;

3. When $y = y_{b2}$, the left-hand side of Eq. (3.61) becomes

   $$-(x_{b2} - x)\left[y_{b2}\sqrt{A_{22}} + y_{b2}\sqrt{A_{12}} + 2x_{b2}y_{b2}\right].$$

   Within the rectangle $A_1A_2B_1B_2$, the value of x is constrained to $-x_{b2} \leq x \leq x_{b2}$, so $-(x_{b2} - x) \leq 0$. Because $\left[y_{b2}\sqrt{A_{22}} + y_{b2}\sqrt{A_{12}} + 2x_{b2}y_{b2}\right] > 0$, Eq. (3.61) is satisfied when $y = y_{b2}$, $-x_{b2} \leq x \leq x_{b2}$ and it becomes identically 0 at point (x_{b2}, y_{b2});

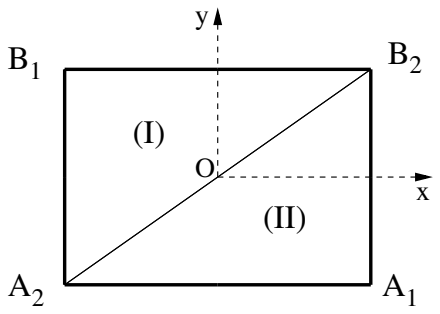

Figure 3.13: Division of the workspace.

4. When $y = -y_{b2}$, the left-hand side of Eq. (3.61) becomes 0, so the segment $y = -y_{b2}$, $-x_{b2} \leq x \leq x_{b2}$ is also a part of the workspace boundary.

Therefore, if there exists any curve corresponding to the equality in Eq. (3.61) within the rectangle $A_1A_2B_1B_2$, the curve must pass through points located on the line segment A_2A_1 or the line segment A_1B_2. However, it turns out that there is no such curve, as will now be shown in the following.

(i) If $y_{b2}x - x_{b2}y \leq 0$ (i.e., in the region noted (I) in Figure 3.13), Eq. (3.61) will always be satisfied, the left-hand side of Eq.(3.61) is negative within this region because $y_{b2}(x - x_{b2}) < 0$ and $-x_{b2}(y + y_{b2}) < 0$, except for point $(-x_{b2}, -y_{b2})$ and point (x_{b2}, y_{b2}).

(ii) If $y_{b2}x - x_{b2}y > 0$ (i.e., in the region noted (II) in Figure 3.13), Eq. (3.61) can be rearranged as

$$\begin{aligned} &y_{b2}(x - x_{b2})\sqrt{(x + x_{b2})^2 + (y + y_{b2})^2} - x_{b2}(y + y_{b2})\sqrt{(x - x_{b2})^2 + (y - y_{b2})^2} \\ &< (x_{b2}y - y_{b2}x)\sqrt{(x - x_{b2})^2 + (y + y_{b2})^2} < 0 \end{aligned} \tag{3.62}$$

Since Eq. (3.61) is equal to 0 when $x = x_{b2}$, $-y_{b2} \leq y \leq y_{b2}$ or $-x_{b2} \leq x \leq x_{b2}$, $y = -y_{b2}$, if there is any curve corresponding to Eq. (3.61) within region (II), the curve should include these two line segments. But it turns out that the left-hand side of Eq. (3.61) is always negative in the area near $x = x_{b2}$, $-y_{b2} \leq y \leq y_{b2}$ or $-x_{b2} \leq x \leq x_{b2}$, $y = -y_{b2}$ within region (II).

Let $-x_{b2} < x < x_{b2}$, $y = -y_{b2} + \varepsilon$, where ε is a small positive quantity. Substituting $y = -y_{b2} + \varepsilon$

into Eq. (3.62), leads to

$$\begin{aligned} 0 &< (y_{b2}x + x_{b2}y_{b2} - x_{b2}\varepsilon)\sqrt{(x - x_{b2})^2 + \varepsilon^2} \\ &< y_{b2}(x_{b2} - x)\sqrt{(x + x_{b2})^2 + \varepsilon^2} + x_{b2}\varepsilon\sqrt{(x - x_{b2})^2 + (2y_{b2} - \varepsilon)^2}. \end{aligned} \tag{3.63}$$

Squaring Eq. (3.63) and simplifying, one has

$$x^2 - x_{b2}^2 - 2y_{b2}\varepsilon + \varepsilon^2 < 0 < \sqrt{(x + x_{b2})^2 + \varepsilon^2}\sqrt{(x - x_{b2})^2 + (2y_{b2} - \varepsilon)^2}. \tag{3.64}$$

Hence, Eq. (3.61) is always negative when $0 < x < x_{b2}$, $y = -y_{b2} + \varepsilon$.

Let $x = x_{b2} - \varepsilon$, $-y_{b2} < y < y_{b2}$, where ε is a small positive quantity. Substituting $x = x_{b2} - \varepsilon$ into Eq. (3.62), leads to

$$\begin{aligned} 0 &< (y_{b2}x_{b2} - y_{b2}\varepsilon - x_{b2}y)\sqrt{\varepsilon^2 + (y + y_{b2})^2} \\ &< y_{b2}\varepsilon\sqrt{(2x_{b2} - \varepsilon)^2 + (y + y_{b2})^2} + x_{b2}(y + y_{b2})\sqrt{\varepsilon^2 + (y - y_{b2})^2}. \end{aligned} \tag{3.65}$$

Squaring Eq. (3.65) and simplifying, one has

$$y^2 - y_{b2}^2 - 2x_{b2}\varepsilon + \varepsilon^2 < 0 < \sqrt{(2x_{b2} - \varepsilon)^2 + (y + y_{b2})^2}\sqrt{\varepsilon^2 + (y - y_{b2})^2}. \tag{3.66}$$

Therefore, Eqn. (3.61) is always negative when $x = x_{b2} - \varepsilon$, $-y_{b2} < y < y_{b2}$.

With Eq. (3.64) and Eq. (3.66), it can be concluded that there is no locus for Eq. (3.61) within region (II). So, the left-hand side of Eq. (3.61) is negative within both region (I) and region (II).

Since the mechanism is symmetric, f_{ai}, f_{bi}, $i = 1, 2$, have the same characteristics, which means that if the springs of the mechanism are constant force springs, the cable forces can be maintained in tension within the workspace defined by the footprint of the mechanism, namely rectangle $A_1A_2B_1B_2$.

The case for which the spring preload is zero but the stiffness is not zero is more difficult to analyze. Indeed, Inequality (3.60) is very complicated and the analysis presented above for Inequality (3.59) cannot be applied. For this case and for the general case for which the stiffness and the preload of the springs are both not zero, one must resort to numerical computations. Examples of results are now presented in order to illustrate how the characteristics of the mechanism can be adjusted by changing the preload and stiffness of the springs.

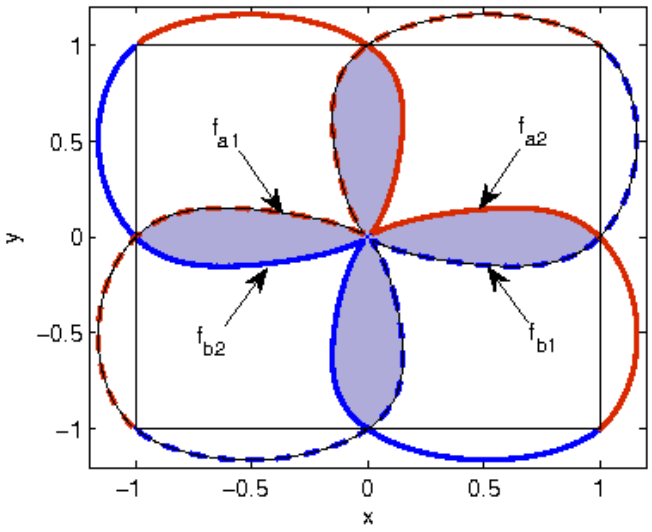

Figure 3.14: Workspace of the mechanism when $f_o = 0$.

For the figures presented in the following, we assume that the workspace $A_1A_2B_1B_2$ is a square and we normalize the square side length as $r = 1$. Also, the original position of the end-effector is placed at $\mathbf{p}_o = [0, 0]^T$. If $f_o = 0$, the boundary curves for $f_{bi} = 0$ and $f_{ai} = 0$, $i = 1, 2$, are shown in Figure 3.14, where the shaded area is the available workspace.

A non-dimensional parameter characterizing the springs' properties with respect to the mechanism's size is then defined as $\frac{kr}{f_o}$. The workspace boundaries defined by $f_{bi} = 0$ and $f_{ai} = 0$, $i = 1, 2$, for different values of $\frac{kr}{f_o}$ are shown in Figure 3.15. The interior of the curves is the available workspace.

It can be observed that there should be preload in the springs because the central configuration $\mathbf{p} = [0, 0]^T$ is at the workspace boundary if $f_o = 0$. Also, the workspace is very small when there is no preload. The mechanism has a smaller workspace if the stiffness of the springs is positive. But if $\frac{kr}{f_o}$ is adjusted properly, a significantly large workspace can be obtained.

It can be seen that the workspace characteristics of the spring-loaded cable-loop-driven mechanism with symmetric compliance is better than that of the non-symmetric spring-loaded cable-loop-driven mechanism.

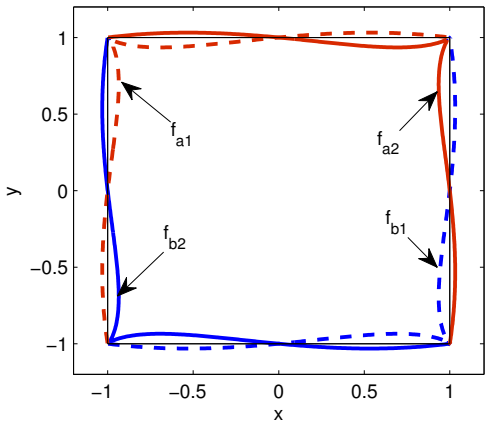

(a) Boundary of the workspace for $\frac{kr}{f_o} = \sqrt{2}$

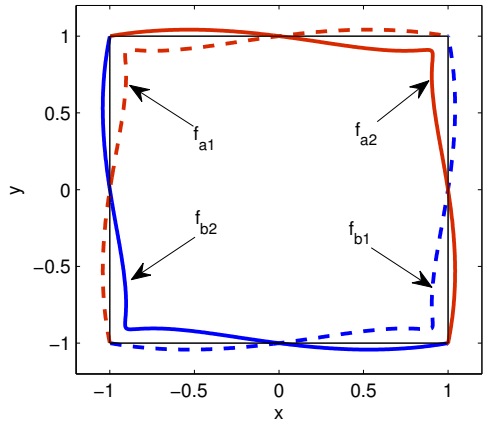

(b) Boundary of the workspace for $\frac{kr}{f_o} = 2$

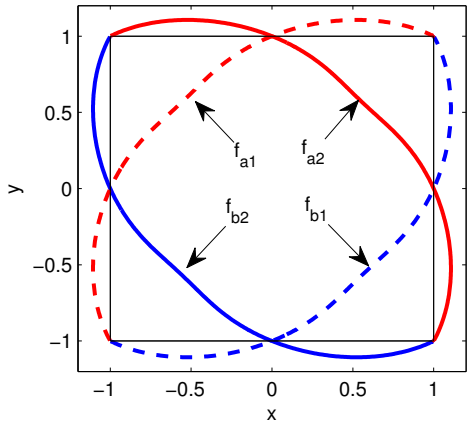

(c) Boundary of the workspace for $\frac{kr}{f_o} = 10$

Figure 3.15: Boundary of the workspace for different values of $\frac{kr}{f_o}$.

3.4.4.2 Nonzero External Forces

If there are external forces applied on the end-effector, the available workspace will be reduced. The effect of the external forces on the workspace boundary is now analyzed. Since the mechanism is symmetric and the four cable forces have the same characteristics, only the analysis for the cable force f_{b1} is given in the following. The analysis for the other cable forces is similar and the results are readily obtained from the analysis shown here. The equations for all the cable forces are given in Appendix A.

(1) Constant force spring

If the springs in the mechanism are constant force springs, modifying Inequality (3.57) we have

$$\left[\mathbf{f}_e - \frac{1}{2} f_o(\mathbf{s}_{a1} + \mathbf{s}_{a2})\right]^T \mathbf{E}(\mathbf{s}_{b2} - \mathbf{s}_{a2}) \geq 0. \tag{3.67}$$

By inspection of the components of the above inequality, it can be observed that the worst condition appears when the x component of $\mathbf{f}_e$ is positive while the y component is negative.

Assuming $f_{ex} = \rho f_o$ and $f_{ey} = -\rho f_o$, where ρ is a positive value, it can be verified that the following inequality should be satisfied:

$$\begin{aligned}&\rho\left[(x+y)\sqrt{A_{12}}(\sqrt{B_{22}} - \sqrt{A_{22}}) + (x_{b2}+y_{b2})\sqrt{A_{12}}(\sqrt{A_{22}} + \sqrt{B_{22}})\right] + y_{b2}(x - x_{b2})\sqrt{A_{22}} \\ &+ (y_{b2}x - x_{b2}y)\sqrt{A_{12}} - x_{b2}(y + y_{b2})\sqrt{B_{22}} \leq 0.\end{aligned} \tag{3.68}$$

From the analysis presented above, we know that the workspace boundary defined by cable force f_{b1} is in range (II) of Figure 3.13. Now, we try to find the boundary point on the diagonal for the situation in which the four fixed pulleys form a square and for the situation in which they form a rectangle.

First, suppose $x_{b2} = y_{b2}$, for the diagonal defined by $y = -x$, let the left-hand side of Inequality (3.68) be equal to zero and simplify it. We have

$$2\sqrt{2}\rho\sqrt{x_{lim}^2 + x_{b2}^2} - \sqrt{x_{lim}^2 + x_{b2}^2} + x_{lim} = 0, \tag{3.69}$$

where x_{lim} stands for the x coordinate of the workspace boundary point on the diagonal. Assuming

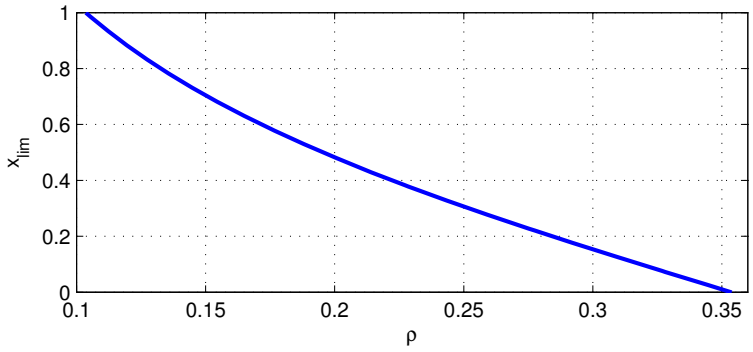

Figure 3.16: Relationship between x_{lim} and ρ for $k = 0$.

$x_{b2} = 1$ and rearranging Eq. (3.69), we obtain

$$\rho = \frac{\sqrt{x_{lim}^2 + 1} - x_{lim}}{2\sqrt{2}\sqrt{x_{lim}^2 + 1}}. \tag{3.70}$$

In order to make sure that the mechanism has a non-vanishing workspace, the boundary defined by the cable force f_{b1} should be in the fourth quadrant which means that x_{lim} should be positive. The largest possible value of ρ is $\frac{\sqrt{2}}{4}$ when $x_{lim} = 0$. The plot representing Eq. (3.70) is shown in Figure 3.16. From this figure, it can be seen that the workspace along the diagonal starts to decrease when $\rho \geq \frac{\sqrt{2}-1}{4}$.

If the quadrilateral formed by the four fixed pulleys is a rectangle, it is assumed that $\gamma = \frac{y_{b2}}{x_{b2}}$ and $x_{b2} = 1$. For the diagonal described by $y = -\gamma x$, letting Inequality (3.68) equal to zero and rearranging it, we have

$$\rho = \frac{\gamma\left[n_2 + n_3 - 2x_{lim}n_1\right]}{n_1\left[(1 + \gamma + x_{lim} - \gamma x_{lim})n_2 + (1 + \gamma - x_{lim} + \gamma x_{lim})n_3\right]}, \tag{3.71}$$

where $n_1 = \sqrt{1 + \gamma^2}$, $n_2 = \sqrt{(x_{lim} - 1)^2 + \gamma^2(x_{lim} + 1)^2}$ and $n_3 = \sqrt{(x_{lim} + 1)^2 + \gamma^2(x_{lim} - 1)^2}$.

If the range of the external force space has the same scale as the rectangle, that is to say $f_{ex} = \rho f_o$ and $f_{ey} = -\gamma\rho f_o$, for f_{b1}, equating the left-hand side of Ineqn. (3.67) to zero leads to:

$$\rho = \frac{n_2 + n_3 - 2x_{lim}n_1}{2n_1\left(n_2 + n_3\right)}. \tag{3.72}$$

The plots of Eq. (3.71) and Eq. (3.72) are shown in Figure 3.17(a) and Figure 3.17(b) respectively. If the required range for the external force applied on the end-effector is the same for all

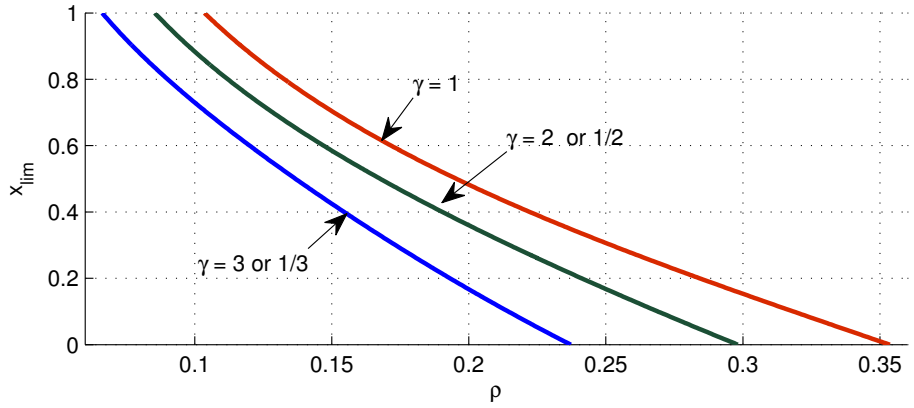

(a) For different shapes of rectangle

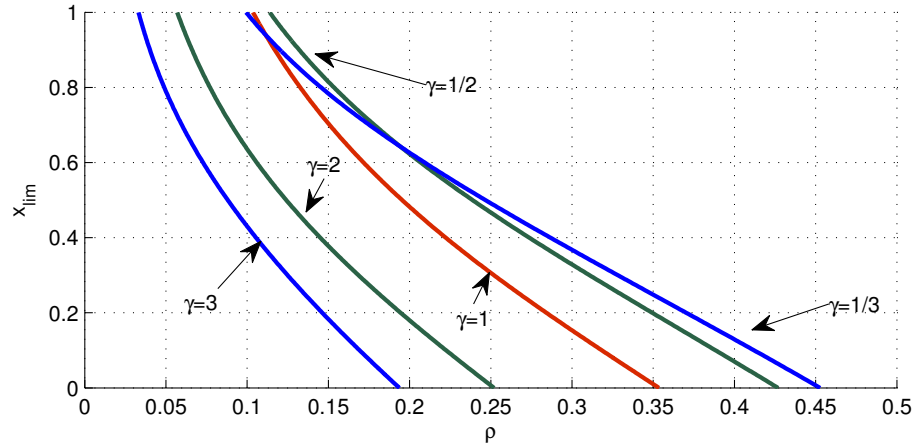

(b) For different shapes of rectangle and corresponding shapes of external force space

Figure 3.17: Relationship between x_{lim} and ρ for $k = 0$.

directions, from Figure 3.17(a), we can see that when $\gamma = 1$, that is to say the four vertices form a square, the workspace is maximized. If the external force has the same direction as the aspect ratio of the rectangle, the smaller γ, the smaller the external force in the y direction is, so the ratio between the external force and the preload is larger for a certain boundary of the workspace.

(2) General Spring

If the springs used in the mechanism have non zero stiffness, the analytical expression for the workspace boundary becomes very complicated. Now, a simplified situation is analyzed. The workspace boundary for general situations can be found numerically using the basic inequalities of Inequality (3.57) and Inequality (3.58).

Similarly to what was done above, we use f_{b1} in the analysis. Assuming that $x_{b2} = y_{b2} = r$, $y = -x$, $f_{ex} = \rho f_o$ and $f_{ey} = -\rho f_o$ and simplifying Inequality (3.57), we obtain the following inequality

$$f_o \left(\frac{-2\sqrt{2}\rho}{\sqrt{x^2 + r^2}} + \frac{1}{\sqrt{x^2 + r^2}} - \frac{x}{x^2 + r^2} \right) - 2\sqrt{2}k \frac{x(\sqrt{x^2 + r^2} - r)}{x^2 + r^2} \leq 0 \tag{3.73}$$

Defining $q = \dfrac{k}{f_o}$, equating the left-hand side of Inequality (3.73) to zero and simplifying it, we obtain

$$q = \frac{(1 - 2\sqrt{2}\rho)\sqrt{x_{lim}^2 + r^2} - x_{lim}}{2\sqrt{2}x_{lim}(\sqrt{x_{lim}^2 + r^2} - r)}. \tag{3.74}$$

Normalizing r as one unit, the plot for Eq. (3.74) is shown in Figure 3.18. It can be observed that the mechanism will have a better workspace if the springs have a proper negative stiffness.

If the external force workspace is defined as $\sqrt{f_{ex}^2 + f_{ey}^2} \leq \sqrt{2}\rho f_o$, by inspection of the components of Inequality (3.67), we know that the worst condition for f_{b1} is $f_{ex} = \rho f_o$ and $f_{ey} = -\rho f_o$. Similarly, it can be shown that the worst condition for f_{b2} is $f_{ex} = -\rho f_o$ and $f_{ey} = -\rho f_o$, for f_{a1} is $f_{ex} = -\rho f_o$ and $f_{ey} = \rho f_o$, for f_{a2} is $f_{ex} = \rho f_o$ and $f_{ey} = \rho f_o$.

Assuming that the rectangle formed by the four fixed pulleys is a square with 2 side length, the half length of the square is $r = 1$. The square length and the characteristics of the spring are normalized as $\frac{kr}{f_o} = \sqrt{2}$. Then, for $\rho = 0.1$ and $\rho = 0.2$, the workspace boundary defined by

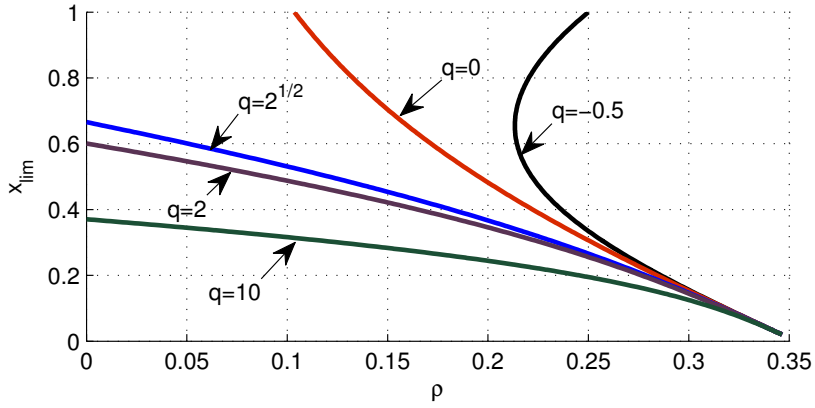

Figure 3.18: Relationship between x_{lim}, ρ and q according to Eqn. (3.74).

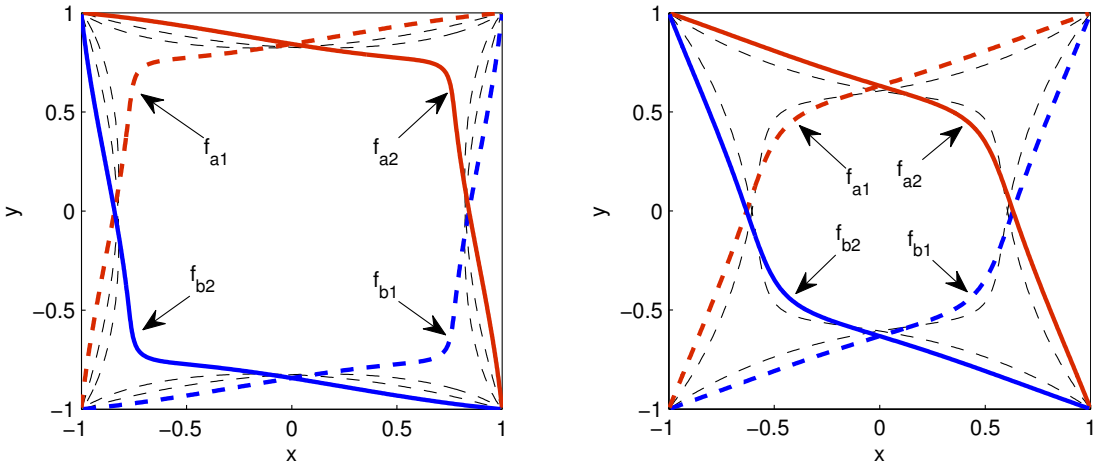

(a) Boundary of the workspace for $\rho = 0.1$

(b) Boundary of the workspace for $\rho = 0.2$

Figure 3.19: Boundary of the workspace for $\frac{kr}{f_o} = \sqrt{2}$.

the four cable forces are shown in Figure 3.19(a) and Figure 3.19(b), respectively. The black thin dashed lines in these figures are the boundaries for $k = 0$.

It can be seen that the workspace is reduced if external forces are applied. However, a large workspace can still be obtained if the springs are sufficiently preloaded, compared to the maximum external forces.

3.5 Conclusion

This chapter presented new spring-loaded cable-loop-driven planar parallel mechanisms. The two degrees of freedom are controlled by two actuators because the cable loops are attached to springs in these mechanisms. The inverse kinematics and statics equations for the non-symmetric and symmetric spring-loaded cable-loop-driven mechanisms are given. The workspace of these two mechanisms is analyzed based on the static equations. It is shown that by coupling the compliance on each side of the actuators, the symmetric mechanism has the best available workspace among the proposed concepts. If constant force springs are used, the workspace covers the whole rectangle formed by the four fixed pulleys directing the cables to the end-effector for a null external force. For the symmetric mechanism, the workspace can also be significantly large provided that the ratio between the stiffness and the preload of the springs is not too large.

Chapter 4

Spatial Spring-Loaded Cable-Loop-Driven Parallel Mechanism

The spring-loaded cable-loop model with symmetric compliance is applied to a spatial mechanism in this chapter. First, the architecture of spatial spring-loaded cable-loop-driven parallel mechanism is introduced. In this mechanism, cable-spool actuating systems and actuation redundancy are avoided. By attaching springs to the cable loops, three degrees of freedom for spatial displacement can be controlled using only three actuators. The inverse kinematics, the static equilibrium equations and the workspace analysis are presented. Because all these equations are obtained based on the cable segment lengths, many square roots appear in the equations. The boundary equations for different arrangements, i.e., preload, non-zero stiffness and external forces, are obtained separately in order to simplify the analysis. The boundary equations of each cable force for any situation can be obtained by combining the equations based on the matrix superposition principle. It is verified that the mechanism has a significantly large workspace within which the cables and the springs can be maintained in tension compared to a standard mechanism actuated with three motors.

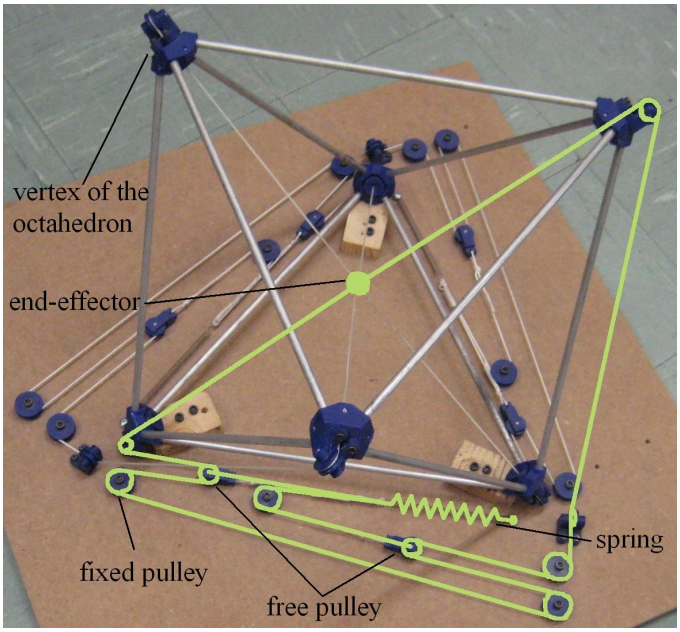

Figure 4.1: Demonstration model of the spatial spring-loaded cable-loop-driven parallel mechanism, one of the loops is highlighted.

4.1 Introduction

In Chapter 3, spring-loaded cable-loops are used to drive a planar mechanism. The suggested option is to include preloaded compliance on each side of the actuators, but to couple these compliances. In such a planar mechanism, the actuators can be rotary actuators or linear actuators. In this chapter, it is intended to apply this model to a spatial mechanism. For a spatial cable-driven mechanism, the end-effector translations without actuation redundancy can be performed using three actuated cables and three springs attached between the end effector and the six vertices of an octahedron. The resulting workspace is a triangular pyramid with its base coincident with one of the faces of the octahedron and its apex at the centroid of the opposite face. The volume of the workspace is approximately one quarter of the volume of the octahedron. In order to improve the size of the workspace, the concept used in the proceeding chapter is applied here.

In this chapter, the concept of spring-loaded cable-loop module is extended to a 3D displacement spatial mechanism and the workspace of this mechanism is analyzed. The demonstration model of this spatial mechanism built in the laboratory is shown in Figure 4.1.

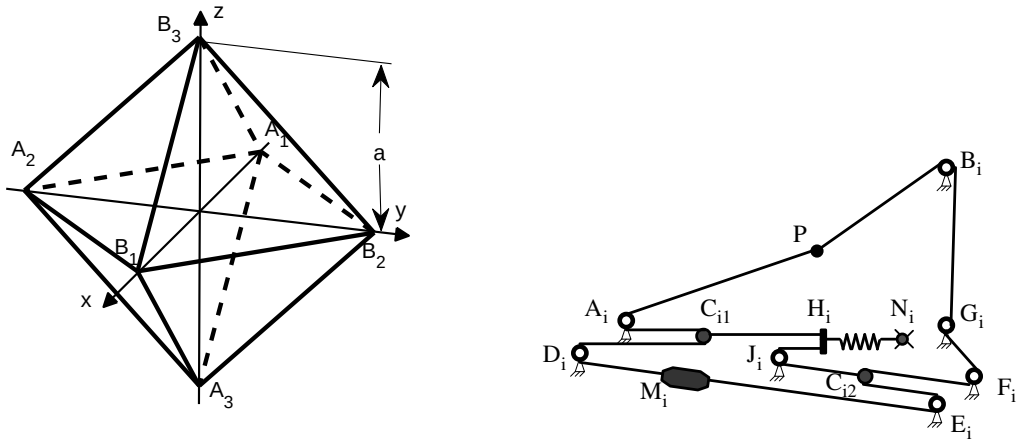

(a) Octahedron formed by the six fixed pulleys

(b) One spring-loaded cable-loop

Figure 4.2: Diagram of a 3-actuator translational spatial spring-loaded cable-loop-driven parallel mechanism.

4.2 Description of the Mechanism

The structure of the translational spatial spring-loaded cable-loop-driven parallel mechanism is illustrated schematically in Figure 4.2. The mechanism includes preloaded compliance on each side of the actuators and these compliances are coupled. The compliance in the closed loop allows motion of the end-effector, but the transmission between the end-effector and the actuators is rigid, as long as the resulting force on the spring does not exceed its preload.

Six fixed pulleys (A_i, B_i, $i = 1, 2, 3$) are mounted on the vertices of a regular octahedron, cables passing on these pulleys are attached to a common end-effector (see in Figure 4.2(a)). Opposing cables are connected by a cable loop. As a result, the cables of the loops are orthogonal to each other when in neutral position. In the practical implementation, one of the faces of the octahedron, as well as the springs and actuators, lie on the ground. Therefore, there are three spring-loaded cable-loop modules (illustrated in Figure 4.2(b)) in this mechanism. For one cable loop, a spring N_iH_i is attached to the ground at point N_i. Two pulleys C_{i1} and C_{i2} are connected to the other end of the spring at H_i. Each cable loop passes around these two pulleys and the fixed pulleys to complete the loop, namely $PA_iC_{i1}D_iE_iC_{i2}F_iG_iB_iP$, $i = 1, 2, 3$. The cable loops are driven by linear actuators M_i, $i = 1, 2, 3$. The cable segments A_iC_{i1}, D_iC_{i1}, $C_{i1}H_i$, J_iH_i and the spring H_iN_i are parallel to each other. The cable segments D_iE_i, $C_{i2}E_i$, J_iC_{i2} and $C_{i2}F_i$ are also parallel to each other. As stated in Chapter 3, rotary actuators also can be used as the drivers if the pulleys

and the routing of the cable are arranged in a different way.

The positions of the fixed pulleys A_i, B_i and the fixed end of the spring N_i can be expressed as $\mathbf{a}_i = [x_{ai}, y_{ai}, z_{ai}]^T$, $\mathbf{b}_i = [x_{bi}, y_{bi}, z_{bi}]^T$ and $\mathbf{n}_i = [x_{ni}, y_{ni}, z_{ni}]^T$, $i = 1, 2, 3$, respectively. The lengths of the cable segments $C_{i1}H_i$, $C_{i2}J_iH_i$, $M_iD_iC_{i1}A_iP$ and $M_iE_iC_{i2}F_iG_iB_iP$ are constant. For the ith, $i = 1, 2, 3$, cable loop, if one length of the cable segments $D_iC_{i1}A_iP$ or $E_iC_{i2}F_iG_iB_iP$ decreases, the other will increase by the same amount as the actuator is moving, because of the closed cable loop.

4.3 Inverse Kinematics

Similarly to the planar symmetric mechanism, the lengths of the cable segments PA_i and PB_i, $i = 1, 2, 3$, vary according to the position of the end-effector. These variations are induced by the displacements of the actuators and the deformations of the springs. Assuming the reference position of the end-effector (centroid of the octahedron) is $\mathbf{p}_o = [x_o, y_o, z_o]^T$, we have

$$2\delta_i + l_{mi} = |PA_i| - |P_0A_i|, \quad i = 1, 2, 3, \tag{4.1}$$

$$2\delta_i - l_{mi} = |PB_i| - |P_0B_i|, \quad i = 1, 2, 3. \tag{4.2}$$

With these six equations (Eq.(4.1) and Eq.(4.2)), l_{mi} and δ_i, $i = 1, 2, 3$, can be found as

$$l_{mi} = \frac{o_{ai} - o_{bi}}{2}, \qquad i = 1, 2, 3, \tag{4.3}$$

$$\delta_i = \frac{o_{ai} + o_{bi}}{4}, \qquad i = 1, 2, 3, \tag{4.4}$$

where o_{ai}, o_{bi} are the length change of cable segments PA_i, PB_i respectively and $o_{ai} = |PA_i| - |P_0A_i|$, $o_{bi} = |PB_i| - |P_0B_i|$, $i = 1, 2, 3$.

It can be seen that l_{mi} and δ_i, $i = 1, 2, 3$, only depend on the position of the end-effector and are independent from the external forces, assuming that the cables are all under tension.

4.4 Static Analysis

Neglecting the friction between the cable and pulleys, the cable forces f_{ai}, f_{bi}, $i = 1, 2, 3$, in the cable segments between the actuators and the end-effector are assumed to be uniform. Considering the static equilibrium of the end-effector, we have that

$$\mathbf{S}_a\mathbf{f}_a + \mathbf{S}_b\mathbf{f}_b = \mathbf{f}_e \tag{4.5}$$

where $\mathbf{f}_a = [f_{a1}, f_{a2}, f_{a3}]^T$ and $\mathbf{f}_b = [f_{b1}, f_{b2}, f_{b3}]^T$ are the forces in the cable segments, $\mathbf{f}_e = [f_{ex}, f_{ey}, f_{ez}]^T$ is the external force applied on the end-effector and $\mathbf{S}_a = [\mathbf{s}_{a1}, \mathbf{s}_{a2}, \mathbf{s}_{a3}]$, $\mathbf{S}_b = [\mathbf{s}_{b1}, \mathbf{s}_{b2}, \mathbf{s}_{b3}]$, where $\mathbf{s}_{ai}$, $\mathbf{s}_{bi}$, $i = 1, 2, 3$, are the unit vectors in the direction of PA_i and PB_i, $i = 1, 2, 3$, respectively. That is to say

$$\mathbf{s}_{ai} = \frac{\mathbf{a}_i - \mathbf{p}}{||\mathbf{a}_i - \mathbf{p}||}, \qquad \mathbf{s}_{bi} = \frac{\mathbf{b}_i - \mathbf{p}}{||\mathbf{b}_i - \mathbf{p}||}, \qquad i = 1, 2, 3.$$

The relationship between the ith spring force, f_{si}, and its deformation, δ_i, is assumed to be given by

$$f_{si} = f_{oi} + k_i\delta_{li}, \qquad i = 1, 2, 3, \tag{4.6}$$

where f_{oi} is the preload and k_i is the stiffness of the ith spring. Also, it can be seen that the forces in the springs are independent from the external forces. They are dependent on the parameters of the springs and the deformation of the spring. If the cables are all under tension, according to the geometry of the mechanism, the spring forces and the cable forces have the following relationship:

$$\mathbf{f}_s = 2\mathbf{f}_a + 2\mathbf{f}_b, \tag{4.7}$$

where $\mathbf{f}_s = [f_{s1}, f_{s2}, f_{s3}]^T$.

Rewriting Eq. (4.7) as $\mathbf{f}_a = \frac{\mathbf{f}_s}{2} - \mathbf{f}_b$ and substituting $\mathbf{f}_a$ into Eq. (4.5), we have

$$\mathbf{M}_b\mathbf{f}_b = \mathbf{f}_{be} \tag{4.8}$$

where $\mathbf{M}_b = \mathbf{S}_b - \mathbf{S}_a$ and $\mathbf{f}_{be} = \mathbf{f}_e - \frac{1}{2}\mathbf{S}_a\mathbf{f}_s$.

If the end-effector is not in a singular configuration, with Eq. (4.8), f_{b1}, f_{b2} and f_{b3} can be solved as

$$f_{bi} = \frac{\det(\mathbf{B}_i)}{\det(\mathbf{M}_b)}, \qquad i = 1, 2, 3, \tag{4.9}$$

where

$$\mathbf{B}_1 = \begin{bmatrix} \mathbf{f}_{be} & (\mathbf{s}_{b2} - \mathbf{s}_{a2}) & (\mathbf{s}_{b3} - \mathbf{s}_{a3}) \end{bmatrix},$$
$$\mathbf{B}_2 = \begin{bmatrix} (\mathbf{s}_{b1} - \mathbf{s}_{a1}) & \mathbf{f}_{be} & (\mathbf{s}_{b3} - \mathbf{s}_{a3}) \end{bmatrix},$$
$$\mathbf{B}_3 = \begin{bmatrix} (\mathbf{s}_{b1} - \mathbf{s}_{a1}) & (\mathbf{s}_{b2} - \mathbf{s}_{a2}) & \mathbf{f}_{be} \end{bmatrix}.$$

Using the same method we can find the equations to calculate the cable forces f_{ai}, $i = 1, 2, 3$. Combining the equations for f_{ai} and f_{bi}, $i = 1, 2, 3$, we have

$$\mathbf{M}\mathbf{f} = \mathbf{f}_f \tag{4.10}$$

where

$$\mathbf{M} = \begin{bmatrix} -\mathbf{M}_b & \mathbf{0} \\ \mathbf{0} & \mathbf{M}_b \end{bmatrix}, \quad \mathbf{f} = \begin{bmatrix} \mathbf{f}_a \\ \mathbf{f}_b \end{bmatrix}, \quad \mathbf{f}_f = \begin{bmatrix} \mathbf{f}_{ae} \\ \mathbf{f}_{be} \end{bmatrix},$$

and $\mathbf{f}_{ae} = \mathbf{f}_e - \frac{1}{2}\mathbf{S}_b\mathbf{f}_s$.

Because the deformations of the springs are determined when the position of the end-effector is given. The sum for the cable forces f_{ai} and f_{bi} is equal to one half of the spring force f_{si}, $i = 1, 2, 3$, according to Eq. (4.7). But the cable forces f_{ai} and f_{bi}, $i = 1, 2, 3$, vary for different external forces.

For the actuator of the mechanism, we have

$$\mathbf{f}_m = \mathbf{f}_a - \mathbf{f}_b \tag{4.11}$$

where $\mathbf{f}_m = [f_{m1}, f_{m2}, f_{m3}]^T$ is the actuator force vector. Substituting $\mathbf{f}_a = \frac{\mathbf{f}_s}{2} - \mathbf{f}_b$ into Eqn. (4.11), it can be found that

$$\mathbf{f}_m = \frac{\mathbf{f}_s}{2} - 2\mathbf{f}_b \tag{4.12}$$

Like in the planar mechanism, the required actuating force range is $f_{mi} \in \left[-\frac{1}{2}f_{si}, \frac{1}{2}f_{si}\right]$, $i = 1, 2, 3$.

4.5 Workspace Analysis

In order to preserve symmetry, the octahedron formed by the six pulleys A_i, B_i, $i = 1, 2, 3$, is a regular octahedron and the radius of the circumsphere for this octahedron is noted a, as shown in

Figure 4.2(a). The coordinates for the six pulleys are

$$\mathbf{a}_1 = \begin{bmatrix} -a & 0 & 0 \end{bmatrix}^T, \quad \mathbf{a}_2 = \begin{bmatrix} 0 & -a & 0 \end{bmatrix}^T, \quad \mathbf{a}_3 = \begin{bmatrix} 0 & 0 & -a \end{bmatrix}^T,$$
$$\mathbf{b}_1 = \begin{bmatrix} a & 0 & 0 \end{bmatrix}^T, \quad \mathbf{b}_2 = \begin{bmatrix} 0 & a & 0 \end{bmatrix}^T, \quad \mathbf{b}_3 = \begin{bmatrix} 0 & 0 & a \end{bmatrix}^T.$$

Moreover, the modular actuator-spring systems are all assumed to have the same characteristics. Let the preload and the stiffness of the springs be $f_{oi} = f_o$ and $k_i = k$, $i = 1, 2, 3$. Because cables can only pull and not push, it should be verified that there is a certain workspace within which the cables and the springs can be maintained in tension.

When the position of the end-effector is within the range of the workspace, the cable extension forces should satisfy all the following conditions:

$$\mathbf{f}_a \succeq \mathbf{0}, \qquad \mathbf{f}_b \succeq \mathbf{0}. \tag{4.13}$$

Or, using Eq. (4.7),

$$\mathbf{0} \preceq \mathbf{f}_b \preceq \frac{1}{2}\mathbf{f}_s. \tag{4.14}$$

where $\succeq$ and $\preceq$ denote the componentwise inequality.

In the reference configuration, it is expected that there is no deformation of the springs and the spring force is equal to the preload. That is to say,

$$f_{si} = f_o, \quad \delta_i = 0, \quad i = 1, 2, 3. \tag{4.15}$$

According to their stiffness, springs can be classified as positive stiffness springs, constant force springs and negative stiffness springs. In order to maintain the springs in tension, the following relationships should be satisfied

$$f_{si} \begin{cases} \geq f_o, & \text{if} \quad k > 0, \\ = f_o, & \text{if} \quad k = 0, \\ \leq f_o, & \text{if} \quad k < 0, \end{cases} \qquad i = 1, 2, 3. \tag{4.16}$$

Let $\delta_{f_{si}} = f_{si} - f_o$ and from Eq. (4.4) we have

$$\delta_{fsi} = k\delta_i = \frac{k}{4}(o_{ai} + o_{bi}), \tag{4.17}$$

then Eq. (4.16) can be written as

$$o_{ai} + o_{bi} \geq 0, \qquad i = 1, 2, 3. \tag{4.18}$$

The latter condition is equivalent to

$$|A_iP| + |B_iP| \geq c_i, \qquad i = 1, 2, 3 \tag{4.19}$$

where $c_i = |A_iP_0| + |B_iP_0|$. This means that the reference position of the end-effector should be placed at a point for which the sum of the distances from this point to the pulleys A_i and B_i, $i = 1, 2, 3$, is the shortest distance. Only one point of the workspace satisfies this condition: the intersection of line A_1B_1, line A_2B_2 and line A_3B_3, namely the centroid of the octahedron. Then, only the conditions of Eq. (4.13) or alternatively Eq. (4.14) need to be considered in order to ensure tension in the mechanism.

For a given configuration of the mechanism, the position of the end-effector is $\mathbf{p} = [x, y, z]^T$. The unit vectors for the direction of the end-effector to the six pulleys are

$$\mathbf{s}_{a1} = \frac{1}{X_a}\begin{bmatrix} -a-x \\ -y \\ -z \end{bmatrix}, \qquad \mathbf{s}_{a2} = \frac{1}{Y_a}\begin{bmatrix} -x \\ -a-y \\ -z \end{bmatrix}, \qquad \mathbf{s}_{a3} = \frac{1}{Z_a}\begin{bmatrix} -x \\ -y \\ -a-z \end{bmatrix},$$

$$\mathbf{s}_{b1} = \frac{1}{X_b}\begin{bmatrix} a-x \\ -y \\ -z \end{bmatrix}, \qquad \mathbf{s}_{b2} = \frac{1}{Y_b}\begin{bmatrix} -x \\ a-y \\ -z \end{bmatrix}, \qquad \mathbf{s}_{b3} = \frac{1}{Z_b}\begin{bmatrix} -x \\ -y \\ a-z \end{bmatrix},$$

where

$$X_a = |PA_1|, \quad Y_a = |PA_2|, \quad Z_a = |PA_3|, \quad X_b = |PB_1|, \quad Y_b = |PB_2|, \quad Z_b = |PB_3|.$$

From Eq. (4.10), it can be seen that the cable forces f_{ai} and f_{bi}, $i = 1, 2, 3$, are the ratios of the determinants of matrices $\mathbf{A}_i$ or $\mathbf{B}_i$ over the determinant of matrix $\mathbf{M}_b$ (where matrix $\mathbf{A}_i$ is similar to matrix $\mathbf{B}_i$). Matrix $\mathbf{M}_b$ can be written explicitly using the expressions of the unit vectors and its determinant can be expanded and written as

$$\begin{aligned} \det(\mathbf{M}_b) = & \frac{a^2}{X_aX_bY_aY_bZ_aZ_b}\,[a(X_a + X_b)(Y_a + Y_b)(Z_a + Z_b) \\ & - x(X_a - X_b)(Y_a + Y_b)(Z_a + Z_b) - y(X_a + X_b)(Y_a - Y_b)(Z_a + Z_b) \\ & - z(X_a + X_b)(Y_a + Y_b)(Z_a - Z_b)]\,. \end{aligned} \tag{4.20}$$

It can seen from Eq. (4.20) that the determinant of $\mathbf{M}_b$ vanishes at the six vertices, and that it is always positive within the octahedron. Then, in order to find the boundary of the workspace, it suffices to find the combinations of the surfaces for which $\det(\mathbf{B}_i) = 0$ and $\det(\mathbf{A}_i) = 0$ (where

matrix $\mathbf{A}_i$ is similar to matrix $\mathbf{B}_i$), $i = 1, 2, 3$. Because the mechanism is symmetric and the spring-actuator systems are modular with identical characteristics, the six cable extension forces f_{bi} and f_{ai}, $i = 1, 2, 3$, have similar properties. Therefore, in what follows only the expression of the determinant of $\mathbf{B}_1$ is analyzed, the analysis of the determinants of $\mathbf{B}_i$ and $\mathbf{A}_i$, $i = 1, 2, 3$, being similar.

From the expression of matrix $\mathbf{B}_1$, we can see that the determinant of this matrix depends on the springs' characteristics (the preload f_o, the stiffness k) and the external force $\mathbf{f}_e$ as well as the position of the end-effector. We will now describe the workspace boundaries associated with these parameters separately in the following. The boundary equations of each cable force for any general situation can then be obtained by combining these equations based on the matrix superposition principle. The expressions for the determinants of $\mathbf{B}_i$ and $\mathbf{A}_i$, $i = 1, 2, 3$, for these parameters are shown in Appendix B.

4.5.1 Zero External Forces

First, in order to find the influence of the springs' characteristic for the workspace, we assume that there is no external forces applying on the mechanism. The springs' preload and the springs' stiffness are analyzed seperately, then they are combined to analyze.

4.5.1.1 Let $f_o \neq 0$, $k = 0$ and $\mathbf{f}_e = \mathbf{0}$

When the spring is constant force spring and there is no external force applied at the end-effector, $\mathbf{f}_{be}$ can be expressed as

$$\mathbf{f}_{be} = \frac{1}{2} f_o \begin{bmatrix} \dfrac{a+x}{X_a} + \dfrac{x}{Y_a} + \dfrac{x}{Z_a} \\ \dfrac{y}{X_a} + \dfrac{a+y}{Y_a} + \dfrac{y}{Z_a} \\ \dfrac{z}{X_a} + \dfrac{z}{Y_a} + \dfrac{a+z}{Z_a} \end{bmatrix}. \tag{4.21}$$

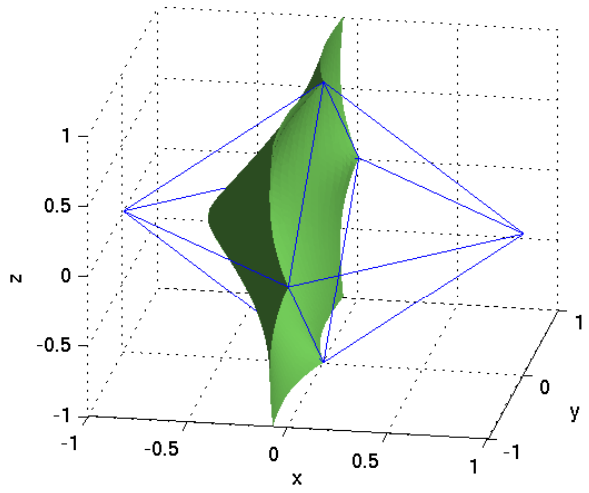

Figure 4.3: Plot of $\det(\mathbf{B}_1)_{f_o} = 0$ when $f_o \neq 0$, $k = 0$ and $\mathbf{f}_e = \mathbf{0}$.

Substituting $\mathbf{f}_{be}$ into $\mathbf{B}_1$ and calculating the determinant of this matrix, we have

$$\begin{aligned}\det(\mathbf{B}_1)_{f_o} =& \frac{f_o a^2}{2X_a Y_a Y_b Z_a Z_b}\left[(x+a)(Y_a+Y_b)(Z_a+Z_b) - y(Y_a-Y_b)(Z_a+Z_b)\right. \\ & \left. - z(Y_a+Y_b)(Z_a-Z_b) + 2xX_a(Y_a+Y_b+Z_a+Z_b)\right].\end{aligned} \tag{4.22}$$

Assuming $a = 1$, the surface for $\det(\mathbf{B}_1)_{f_o} = 0$ is shown in Figure 4.3. With a similar method, the expression for the determinant of matrices $\mathbf{A}_i$ and $\mathbf{B}_i$ can be found. The plot for the whole workspace of the mechanism is shown in Figure 4.4. We can see that the workspace of the mechanism is like a ball with six bumps on it when the springs in the mechanism are constant force springs and there is no external force.

In order to get further insight, the following cases are considered.

(1) When the end-effector is at the centre of the octahedron, that is to say $\mathbf{p} = [0, 0, 0]^T$, we have

$$\mathbf{f}_{be} = \frac{1}{2} f_o \begin{bmatrix} 1 & 1 & 1 \end{bmatrix}^T, \quad \mathbf{M}_b = \operatorname{diag}\left(\begin{bmatrix} 2 & 2 & 2 \end{bmatrix}\right).$$

Then, the value of the cable force f_{b1} can be found as

$$f_{b1} = \frac{\det(\mathbf{B}_1)_{f_o}}{\det(\mathbf{M}_b)} = \frac{f_o}{4}.$$

Because the deformations of the springs are zero in this reference configuration, we can see that all the cable forces are a quarter of the springs' preload.

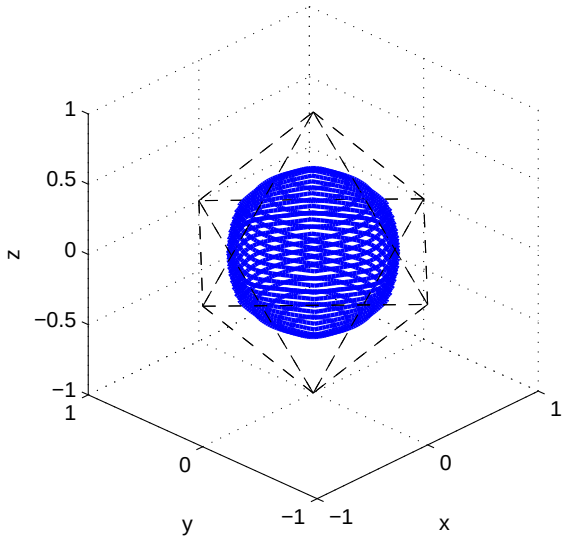

Figure 4.4: Plot of the whole workspace when $f_o \neq 0$, $k = 0$ and $\mathbf{f}_e = \mathbf{0}$.

(2) When the end-effector is on the x axis, which means $y = 0$ and $z = 0$, that is one of the diagonals of the octahedron, then we have

$$\det(\mathbf{B}_1)_{f_o} = \frac{2f_o a^2}{(x^2+a^2)^{3/2}}\left(\sqrt{x^2+a^2}+2x\right). \tag{4.23}$$

By making Eq. (4.23) equal to zero, the boundary of the workspace on the x axis is obtained as $x_{lim} = -\frac{\sqrt{3}}{3}a$ and x_{lim} stands for the boundary of the workspace on the x axis. Because the mechanism is symmetric, we can see that the workspace boundary at the axes is at the distance of $\frac{\sqrt{3}}{3}a$ from the centre of the octahedron. It is consistent with the inscribed sphere of the octahedron.

(3) When the end-effector is on a line perpendicular to the opposite planes of the octahedron, for example in the direction of $x = y = z$, Eq. (4.22) can be simplified as

$$\det(\mathbf{B}_1)_{f_o} = \frac{(3x+a)f_o a^2}{(9x^4+2a^2x^2+a^4)\sqrt{3x^2-2ax+a^2}}\left(3x^2+a^2+\sqrt{3x^2+2ax+a^2}\right). \tag{4.24}$$

It can be seen that $\det(\mathbf{B}_1)_{f_o}$ equals zero when $x = -\frac{1}{3}a$, and the distance from the centre of the octahetron to the workspace boundary point in this direction is $r = \sqrt{3x^2} = \frac{\sqrt{3}}{3}a$ which is also consistent with the inscribed sphere of the octahedron.

(4) When the end-effector is on the plane given by $x = 0$, the determinant of $\mathbf{B}_1$ can be simplified as

$$\det(\mathbf{B}_1)_{f_o} = \frac{f_o a}{2X_a}\left(\frac{a+y}{Y_a}-\frac{y-a}{Y_b}\right)\left(\frac{a+z}{Z_a}-\frac{z-a}{Z_b}\right). \tag{4.25}$$

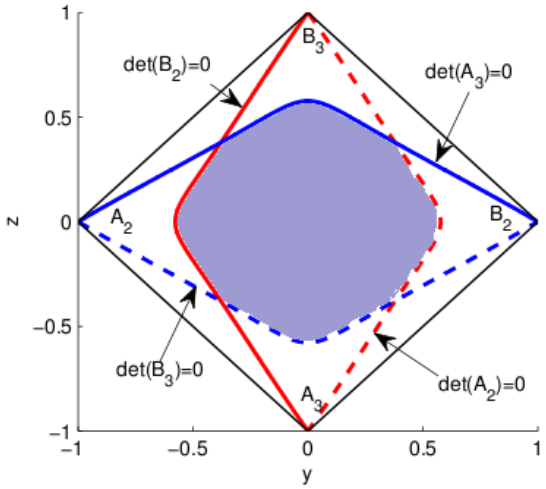

Figure 4.5: Plots of the $\det(\mathbf{A}_i) = 0$ and $\det(\mathbf{B}_i) = 0$, $i = 2, 3$, on the plane defined by $x = 0$.

Within the square formed be the four pulleys $A_2A_3B_2B_3$, there is no configuration which makes Eq. (4.25) equal to zero.

When the end-effector is on the plane given by $y = 0$, the determinant of $\mathbf{B}_1$ is

$$\det(\mathbf{B}_1)_{f_o} = \frac{f_o a^2}{Y_a}\left(\frac{x+z+a}{X_a Z_a} + \frac{x-z+a}{X_a Z_b} + \frac{x}{Y_a Z_a} + \frac{x}{Y_b Z_b} + \frac{2x}{Z_a Z_b}\right). \tag{4.26}$$

Because the mechanism is symmetric, the expressions for the determinant of $\mathbf{B}_i$, $\mathbf{A}_i$, $i = 1, 2, 3$, in the planes defined by $x = 0$, $y = 0$ or $z = 0$ are all similar. With $a = 1$, the workspace boundaries in the plane defined by $x = 0$ formed by these determinants are shown in Figure 4.5. It can be seen that the boundary point on the axes is consistent with the result of the above case (2).

4.5.1.2 Let $f_o = 0$, $k \neq 0$ and $\mathbf{f}_e = \mathbf{0}$

Now, it is assumed that the springs just have stiffness without preload and no external force applied at the end-effector. In order to be concise, $\mathbf{f}_{be}$ can be written as

$$\mathbf{f}_{be} = \frac{k}{8}\begin{bmatrix} a + 3x + \frac{a+x}{X_a}(X_b - 2a) + \frac{x}{Y_a}(Y_b - 2a) + \frac{x}{Z_a}(Z_b - 2a) \\ a + 3y + \frac{y}{X_a}(X_b - 2a) + \frac{a+y}{Y_a}(Y_b - 2a) + \frac{y}{Z_a}(Z_b - 2a) \\ a + 3z + \frac{z}{X_a}(X_b - 2a) + \frac{z}{Y_a}(Y_b - 2a) + \frac{a+z}{Z_a}(Z_b - 2a) \end{bmatrix}. \tag{4.27}$$

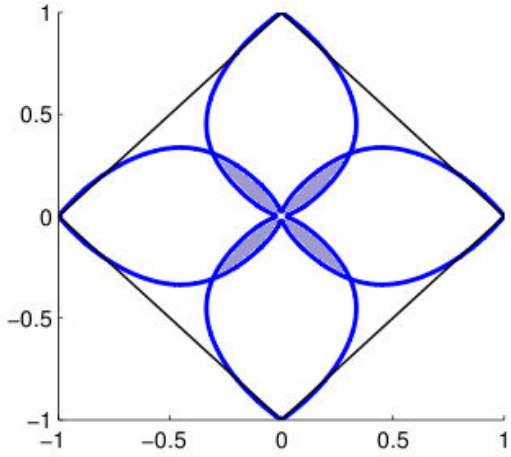

Figure 4.6: General aspect of the curves for $\det(\mathbf{A}_i)_k = 0$ and $\det(\mathbf{B}_i)_k = 0$ on the planes defined by $x = 0$, $y = 0$ or $z = 0$.

The determinant of $\mathbf{B}_1$ in this case, $\det(\mathbf{B}_1)_k$, can be calculated as

$$\begin{aligned}\det(\mathbf{B}_1)_k = \frac{ka^2}{8X_aY_aY_bZ_aZ_b}\,[&a(X_a+X_b)(Y_a+Y_b)(Z_a+Z_b) + x(5X_a+X_b)(Y_a+Y_b)\\ &(Z_a+Z_b) - y(X_a+X_b)(Y_a-Y_b)(Z_a+Z_b) - z(X_a+X_b)(Y_a+Y_b)(Z_a-Z_b)\\ &- 2a(x+a)(Y_a+Y_b)(Z_a+Z_b) + 2ay(Y_a-Y_b)(Z_a+Z_b)\\ &+ 2az(Y_a+Y_b)(Z_a-Z_b) - 4axX_a(Y_a+Y_b+Z_a+Z_b)]\,.\end{aligned} \tag{4.28}$$

When the end-effector is at the centre of the octahedron, there is no deformation in the springs, then $\mathbf{f}_{be} = \mathbf{f}_{ae} = \mathbf{0}$. Therefore, all the determinants of matrices $\mathbf{B}_i$ and $\mathbf{A}_i$, $i = 1, 2, 3$, are equal to zero. This means that the cable forces are zero and the centre of the octahedron is on the workspace boundary. Since the centre of the octahedron is an important configuration which has to be included in the workspace, the springs of the mechanism must have a preload.

Similarly to the case which only considers the preload of the springs, the curves in planes $x = 0$, $y = 0$ and $z = 0$ for $\det(\mathbf{B}_i)_k = 0$ and $\det(\mathbf{A_i})_k = 0$ in this case have the same shape. Assuming $a = 1$, Figure 4.6 shows the general aspect of the curves in these three planes. The workspace is quite small in this situation.

However, it should be noticed that for the direction orthogonal to the opposite planes, which

is the direction of $x = y = z$, the expression of $\det(\mathbf{B}_1)_k$ can be rewritten as

$$\det(\mathbf{B}_1)_k = \frac{-ka^2(a+3x)}{2X_a^2X_b^3}\left[(3x^2+a^2)(a-X_a-X_b)+ax(X_a-X_b)+aX_aX_b\right]. \tag{4.29}$$

Let $\det(\mathbf{B}_1)_k$ be equal to zero, the solutions of the x coordinate are 0 and $-\frac{1}{3}a$. Considering the analysis stated above, the solution $x_{lim} = 0$ is the solution for the situation for which the springs have no preload. But $r = \frac{\sqrt{3}}{3}a$ still is a solution for Eq. (4.29).

4.5.1.3 Let $f_o \neq 0$, $k \neq 0$ and $\mathbf{f}_e = \mathbf{0}$

According to their stiffness, springs can be classified as constant force springs, positive stiffness springs and negative stiffness springs. If the preload and the stiffness of the springs in the mechanism are adjusted properly, the workspace boundary should be larger. The ratio between the preload and the stiffness is defined as $q_s = \frac{k}{f_o}$. Then the influence of this ratio on the workspace boundary on the axes is analyzed in the following.

Since the global effect is a linear combination of the effects of the preload, the spring stiffness and the external force, the determinant of matrix $\mathbf{B}_1$ equals the sum of $\det(\mathbf{B}_1)_{f_o}$, $\det(\mathbf{B}_1)_k$ and $\det(\mathbf{B}_1)_{\mathbf{f}_e}$. Here, we only consider the situation for which $\mathbf{f}_e = \mathbf{0}$, and hence we have

$$\det(\mathbf{B}_1) = \det(\mathbf{B}_1)_{f_o} + \det(\mathbf{B}_1)_k. \tag{4.30}$$

As both of Eq. (4.22) and Eq. (4.28) have a solution at $x = -\frac{1}{3}a$ for the direction of the lines orthogonal to two opposite planes, the workspace boundary in these directions is always at a distance of $\frac{\sqrt{3}}{3}a$ from the centre of the octahedron. These three directions are similar to the two line segments between the opposite centre points of the square sides of the spring-loaded planar mechanism, which are always included in the static workspace no matter what the spring parameters are.

However, the effect of the preload and the stiffness of the springs on the determinant of $\mathbf{B}_1$ should now be assessed. Suppose $a = 1$, on the x axis we can get the expression of $\det(\mathbf{B}_1)$ as

$$\det(\mathbf{B}_1) = 2(x^2+1)^{-3/2}\left[f_o(\sqrt{x^2+1}+2x)+kx(\sqrt{x^2+1}-1)\right]. \tag{4.31}$$

Making Eq. (4.31) equal to zero, then we have

$$q_s = \frac{\sqrt{x_{lim}^2+1}+2x_{lim}}{x_{lim}(1-\sqrt{x_{lim}^2+1})}. \tag{4.32}$$

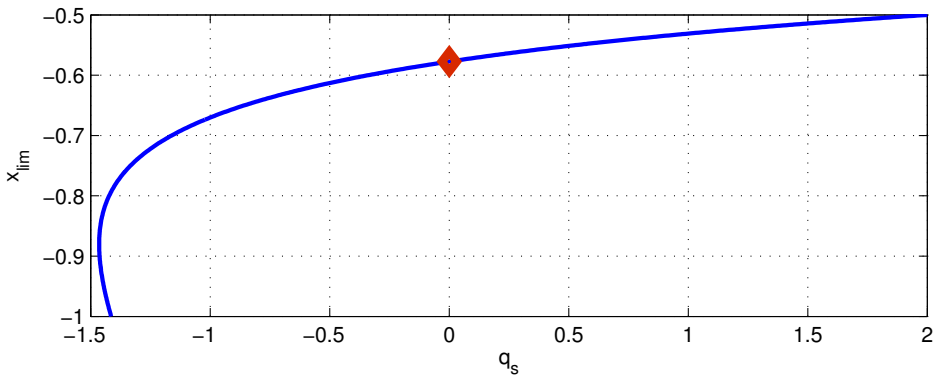

Figure 4.7: Position x_{lim} of the workspace boundary on the negative x semi-axis for different values of q_s.

According to the mechanism geometry, the mechanism will have a certain workspace only when the boundary on the axes defined by the determinant of matrices $\mathbf{B}_1$, $\mathbf{A}_1$, $\mathbf{B}_2$, $\mathbf{A}_2$, $\mathbf{B}_3$ and $\mathbf{A}_3$ are respectively on the negative side of the x axis, the positive side of the x axis, the negative side of the y axis, the positive side of the y axis, the negative side of the z axis and the positive side of the z axis. The relationship between the workspace boundary in the negative part of the x axis and the value of q_s is shown in Figure 4.7. The red point in this figure means $x_{lim} = -\frac{\sqrt{3}}{3}$ when the springs' stiffness is zero. We can see from this figure that the workspace becomes smaller when the stiffness is positive, the workspace can be broadened with negative stiffness springs. Moreover, whatever the value of q_s, the workspace of this mechanism cannot be the whole octahedron. Suppose $q_s = -2$, the whole workspace of the mechanism is shown in Figure 4.8. Compared with Figure 4.4, it can be seen that the workspace is larger especially on the diagonals. Also, it is consistent with Figure 4.7 which shows that the workspace includes the whole diagonal of the octahedron when q_s is smaller than -1.5.

4.5.2 Nonzero External Forces

The purpose of designing a mechanism is to use such a mechanism to realize an application. So, the mechanism should successfully carry out its job. This means, the end-effector has to be subjected to certain external forces. We now consider the influence of the external force on the determinant of $\mathbf{B}_1$. $\det(\mathbf{B}_1)_{\mathbf{f}_e}$ can be expressed as

$$\begin{aligned}\det(\mathbf{B}_1)_{\mathbf{f}_e} =& \frac{a}{Y_a Y_b Z_a Z_b}\left[f_{ex}a(Y_a+Y_b)(Z_a+Z_b) + (f_{ey}x - f_{ex}y)(Y_a-Y_b)(Z_a+Z_b)\right.\\ &\left.+(f_{ez}x - f_{ex}z)(Y_a+Y_b)(Z_a-Z_b)\right].\end{aligned} \tag{4.33}$$

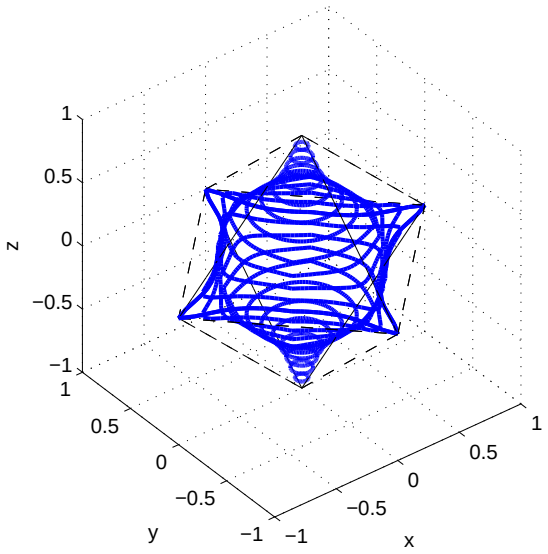

Figure 4.8: Plot of the whole workspace boundary when $q_s = -2$.

As mentioned above, the determinant of $\mathbf{B}_1$ is the sum of Eqs. (4.22), (4.28) and (4.33). That is to say

$$\det(\mathbf{B}_1) = \det(\mathbf{B}_1)_{f_o} + \det(\mathbf{B}_1)_k + \det(\mathbf{B}_1)_{\mathbf{f}_e}. \tag{4.34}$$

The workspace boundary, the external force space, the characteric of the springs are combined with each other. Now, their relationships should be analyzed.

From the above analysis, it is known that the springs should have a certain preload in order to get a proper workspace. In practice, we can use constant force springs or springs with nonzero stiffness. So the two situations should be analyzed in the following.

4.5.2.1 Let $f_o \neq 0$, $k = 0$ and $\mathbf{f}_e \neq \mathbf{0}$

If the springs in the mechanism are constant force springs, using the distributive law, the determinant of $\mathbf{B}_1$ is expressed in Eq. (4.35).

$$\begin{aligned}\det(\mathbf{B}_1) =& \frac{a}{Y_a Y_b Z_a Z_b}\left\{ f_o a x(Y_a + Y_b + Z_a + Z_b) + \left[a f_{ex} + \frac{f_o a}{2X_a}(x + a)\right](Y_a + Y_b)(Z_a + Z_b)\right. \\ &+ \left(f_{ey}x - f_{ex}y - \frac{f_o a}{2X_a}y\right)(Y_a - Y_b)(Z_a + Z_b) \\ &\left.+ \left(f_{ez}x - f_{ex}z - \frac{f_o a}{2X_a}z\right)(Y_a + Y_b)(Z_a - Z_b)\right\}.\end{aligned} \tag{4.35}$$

This equation is rather complex. In order to get some intuitive relationships between the preload, the affordable external force and the workspace of the mechanism, this equation will be simplified by assuming that the end-effector is located at the centre of the octahedron or on the axes of the coordinate system.

When the end-effector is at the centre of the octahedron, we have

$$\det(\mathbf{B}_1) = 4\left(f_{ex} + \frac{f_o}{2}\right) \geq 0. \tag{4.36}$$

From Eq. (4.36), we can see that f_{ex} should satisfy $-\frac{f_o}{2} \leq f_{ex}$. And it can be verified that f_{ex} should smaller than $\frac{f_o}{2}$ by considering the determinant of $\mathbf{A}_1$.

Assume the external force space of this mechanism is

$$|f_{ex}| \leq q_f f_o; \quad |f_{ey}| \leq q_f f_o; \quad |f_{ez}| \leq q_f f_o, \tag{4.37}$$

where q_f is the ratio between the external force and the preload of the springs. Because the workspace of the mechanism should include the centre of the octahedron and the mechanism has a good symmetric property, then, from the above analysis we can see that q_f should satisfy

$$0 < q_f < \frac{1}{2}.$$

This conclusion is reasonable: the actuating force is about one half of the spring preload as stated above and the affordable external force cannot be larger than the actuating force.

When the end-effector is on the x axis, which means $y = 0$ and $z = 0$, we have

$$\det(\mathbf{B}_1) = 4a^2(x^2 + a^2)^{-3/2}\left[\left(f_{ex} + \frac{f_o}{2}\right)\sqrt{x^2 + a^2} + f_o x\right]. \tag{4.38}$$

From Eq. (4.38), it can be seen that the worst condition for $\det(\mathbf{B}_1)$ is when $f_{ex} < 0$, then assume $f_{ex} = -q_f f_o$. If there is any workspace of this mechanism, the workspace boundary on the x axis determined by $\det(\mathbf{B}_1)$ should be in the negative semi-axis. Suppose $a = 1$ and the workspace boundary on the negative x axis is x_{lim}, letting $\det(\mathbf{B}_1)$ be equal to zero, we can get the following relationship:

$$q_f = \frac{x_{lim}}{\sqrt{x_{lim}^2 + 1}} + \frac{1}{2}. \tag{4.39}$$

Because x_{lim} is negative, the square root is positive, it is known that q_f will always be smaller than $\frac{1}{2}$. The plot of Eq. (4.39) is shown in Figure 4.9.

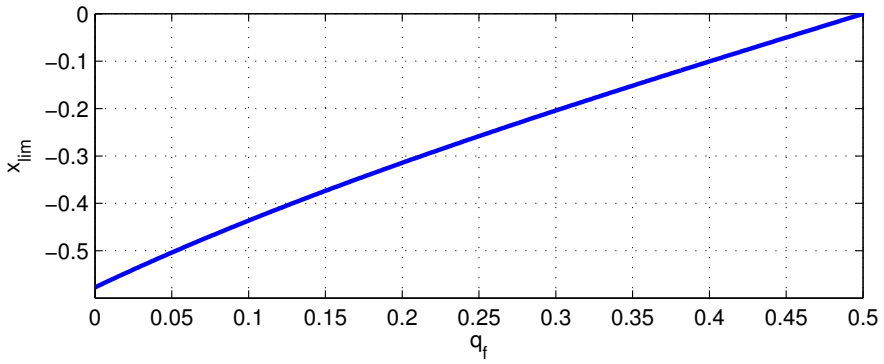

Figure 4.9: Plot of the relationship between the workspace boundary on the x axis and the external force coefficient q_f.

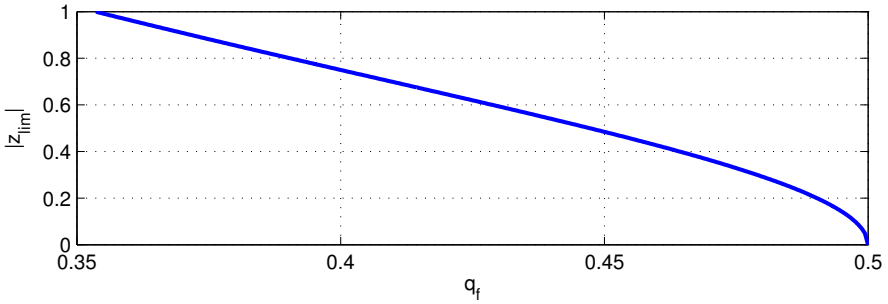

Figure 4.10: Plot of the relationship between the workspace boundary on the z axis and the external force coffercience q_f.

When the end-effector is on the z axis, that is to say $x = y = 0$, simplifing Eq. (4.35) we have

$$\det(\mathbf{B}_1) = \frac{4a}{\sqrt{a^2 + z^2}} \left(f_{ex} + \frac{f_o a}{2\sqrt{a^2 + z^2}} \right). \tag{4.40}$$

Equating Eq. (4.40) to zero, we get

$$q_f = -\frac{a}{2\sqrt{a^2 + z_{lim}^2}} \quad \text{or} \quad |z_{lim}| = a\sqrt{\frac{1}{4q_f^2} - 1}. \tag{4.41}$$

where z_{lim} stands for the boundary of the workspace on the z axis. Normalizing with $a = 1$, the plot for Eq. (4.41) is shown in Figure 4.10.

This result is consistent with the practical observation that the larger the worspace is, the smaller the external force it can afford as shown in Figure 4.9 and Figure 4.10. Comparing these plots, it can be seen that the workspace boundary determined by the cable force f_{b1} is much more constraining on the negative x axis. The workspace boundary curves on the xy plane are shown in Figure 4.11 respectively for $q_f = 0.1$ and $q_f = 0.2$ (the curves on the xy plane and yz plane

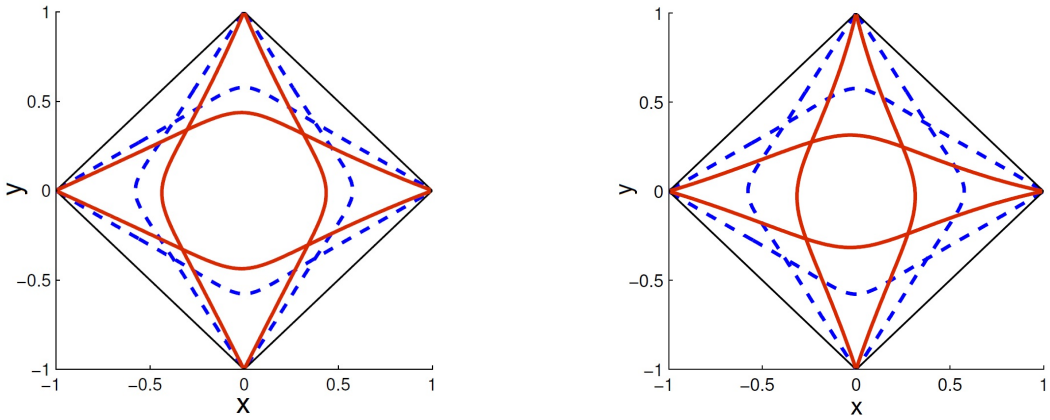

(a) For $q_f = 0.1$ (b) For $q_f = 0.2$

Figure 4.11: Plots of the workspace boundary for different coefficient q_f.

are same with these shown in Figure 4.11). In these figures, the dashed curves are the workspace boundary when $q_f = 0$. It can be observed that in order to get a proper workspace, the external force space is small compared with the preload or the actuating forces.

4.5.2.2 Let $f_o \neq 0$, $k \neq 0$ and $\mathbf{f}_e \neq \mathbf{0}$

Now, the general situation of the mechanism is analyzed. Due to the matrix superposition principle and the distributive law of matrix determinants, for the most general situation, the determinant of $\mathbf{B}_1$ is

$$\det(\mathbf{B}_1) = \det(\mathbf{B}_1)_{f_o} + \det(\mathbf{B}_1)_k + \det(\mathbf{B}_1)_{\mathbf{f}_e}. \tag{4.42}$$

From the above analysis, it is known that the workspace boundary point on the negative x semi-axis is determined by the determinant of $\mathbf{B}_1$. Suppose the end-effector is on the x axis, i.e. $y = 0$ and $z = 0$, based on Eq. (4.42) we get

$$\det(\mathbf{B}_1) = \frac{4a}{(x^2+a^2)^{\frac{3}{2}}}\left[ax\left(f_o - \frac{ka}{2}\right) + \sqrt{x^2+a^2}\left(\frac{f_o a}{2} + \frac{kax}{2} + f_{ex}a\right)\right]. \tag{4.43}$$

Normalizing with $a = 1$ and assuming $f_{ex} = -q_f f_o$, letting $\det(\mathbf{B}_1)$ equal zero, then Eq. (4.43) can be simplified as

$$\left(\frac{1}{2} + \frac{1}{2}x_{lim}q_s - q_f\right)\sqrt{x_{lim}^2+1} = x_{lim}\left(\frac{1}{2}q_s - 1\right) \tag{4.44}$$

where $-\frac{\sqrt{3}}{3} < x_{lim} < 0$ and $0 < q_f < \frac{1}{2}$.

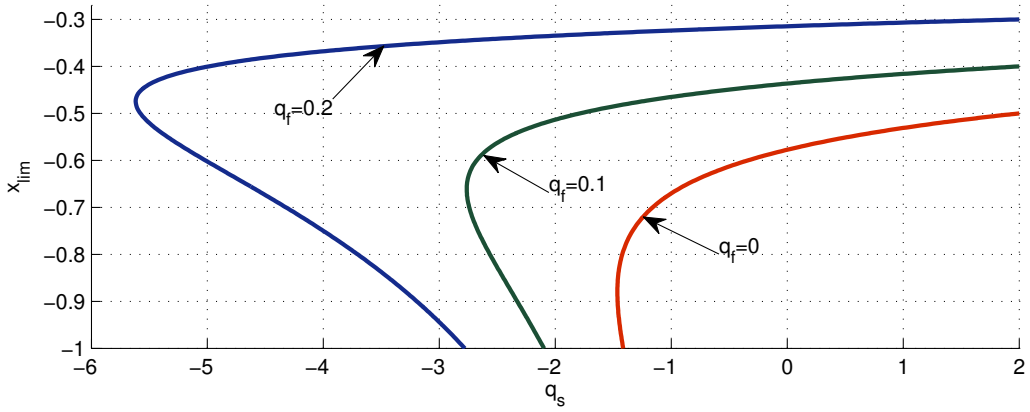

Figure 4.12: The relationship between the workspace boundary on the negative x semi-axis and parameters q and k_{fe}.

Rearranging Eq. (4.44), we have

$$q_s = \frac{(1-2q_f)\sqrt{x_{lim}^2+1}+2x_{lim}}{x_{lim}(1-\sqrt{x_{lim}^2+1})} \tag{4.45}$$

For different values of q_f ($q_f = 0$, $q_f = 0.1$, $q_f = 0.2$), the relationship between the ratio of the springs' stiffness and springs' preload q_s and the workspace boundary on the negative x semi-axis x_{lim} are shown in Figure 4.12. From this figure, it can be seen that it is better to choose a negative stiffness spring. Such a spring can also avoid large cable forces in the mechanism. Optimizing the characteristics of the spring, the mechanism can get a proper large workspace with a certain external force space. Based on this figure, suppose $q_s = -2$, $q_f = 0.1$, the whole workspace boundary for this mechanism is shown in Figure 4.13, the slender curves are the workspace boundary when $q_s = 0$, $q_f = 0$, the thick curves are the workspace boundary when $q_s = -2$, $q_f = 0.1$.

4.6 Conclusion

This chapter has applied the symmetric compliance spring-loaded cable-loop model to a spatial mechanism. The three degrees of freedom of the mechanism can be controlled by three actuators because the cable-loops are attached to springs. The solutions for the inverse kinematic and static problems were given. The workspace analysis for this mechanism was presented. It was shown that if constant force springs are used, the reachable workspace is like a ball and is slightly smaller than the sphere inscribed in the octahedron. In fact, the workspace reaches this sphere along the axes and at the centre of the faces of the octahedron. In practice, the workspace can also be

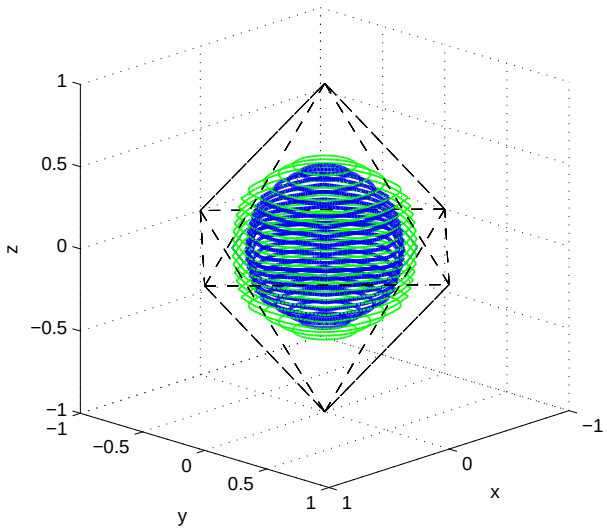

Figure 4.13: Plot of the whole workspace when $a = 1$, $q_s = -2$ and $q_f = 0.1$.

significantly large with non zero stiffness springs provided that the stiffness and the preload of the springs are properly adjusted. If external forces are applied on the end-effector, the available workspace becomes smaller as the applied external force is enlarged. The largest external force should be less than half of the spring's preload, that is to say the maximum actuating force. In practice, in order to keep an acceptable workspace, the largest external force should be significantly smaller than the actuating force.

Chapter 5

Force Capabilities of the Planar and Spatial Spring-Loaded Cable-loop-driven Parallel Mechanisms

In order to avoid actuation redundancy in cable-driven parallel mechanisms and eliminate cable spool drive systems which cause inaccuracies, spring-loaded cable-loop-driven parallel mechanisms were proposed in Chapter 3 and 4. In this chapter, the force capabilities of the symmetric planar and spatial spring-loaded cable-loop-driven parallel mechanisms are analyzed using the available force set and the force-closure workspace based on the static equations. The force capabilities of conventional planar and spatial cable-driven mechanisms based on spools are also derived for comparison purposes. The comparison of the results obtained for the two types of mechanisms provides insight into the force characteristics of spring-loaded cable-loop-driven parallel mechanisms.

5.1 Introduction

Since cables can only work in tension, the study and determination of the available wrench set for given poses is an important issue for parallel cable-driven mechanisms. The available wrench set is the set of wrenches that the mechanism can generate [62,74,75]. This set depends on the architecture of the mechanism, the pose and the minimum and maximum acceptable tension in the cables. An approach for the determination of the available wrench set based on the geometric concept of zonotope was proposed in [74]. Based on the fact that the available wrench set is a zonotope in a given configuration, [75] dealt with the characterization of the facet-defining hyperplanes of the available wrench set. The latter approach leads to the representation of the available wrench set as the set of solutions of a system of linear inequalities. Using convex analysis, a sufficient and necessary tension-closure condition is also proposed in [67].

A pose is a wrench-closure pose if the corresponding available wrench set satisfies certain conditions. A review of these characteristics of a force-closure pose was proposed in the form of theorems in [72]. The wrench-closure workspace is the set of poses in which any wrench can be generated at the end-effector assuming no limit on the cable tensions. The wrench-closure workspace is therefore a purely geometric property. Wrench-closed poses can also be referred to as fully constrained poses. The shape and size of the wrench-closure workspace (the force-closure workspace for a point end-effector) — whose name derives from an analogy with force-closure grasps of robotic hands [60] — depends on the geometry of the mechanism and the routing of the cables. Reference [61] analyzed the force-feasible workspace of planar and spatial mechanisms with a point-mass end-effector. A detailed study of the wrench-closure workspace of planar cable-driven mechanisms is provided in [70] while [64] deals with the wrench-closure workspace of 6-DOF parallel cable-driven mechanisms. Finally, an approach based on interval analysis for the determination of the wrench-feasible workspace of n-DOF parallel mechanisms driven by n or more than n cables was proposed in [76]. The wrench-feasible workspace is defined as the set of poses in which a prescribed set of external wrenches can be produced at the end-effector. As opposed to the wrench-closure workspace, the wrench-feasible workspace is not a purely geometric property since it is also dependent on the minimum and maximum forces that can be supported by the cables.

In this chapter, the force capabilities of planar and spatial spring-loaded cable-loop-driven parallel mechanisms are analyzed mainly based on the approach proposed in [74]. Since these mechanisms have point end-effectors, the terms available force set and force-feasible workspace

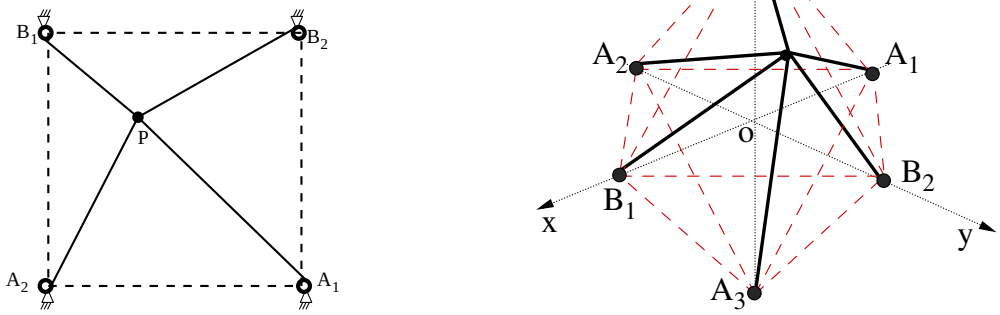

(a) Planar cable-spool mechanism

(b) Spatial cable-spool mechanism

Figure 5.1: Cable-spool mechanisms having the same geometry as the spring-loaded cable-loop-driven mechanisms. The planar mechanism uses four spools while the spatial mechanism uses six spools.

are used in the following. The boundaries of the force-feasible workspace can be determined by considering the limit poses in which the prescribed force set can no longer be produced.

5.2 Analysis of the Force Capabilities

In conventional cable-driven mechanisms using spools, the actuators can apply torques only in one direction since the cables must remain in tension. In spring-loaded cable-loop-driven parallel mechanisms, however, both directions can be used, as shown in the preceding chapters. In this regard, spring-loaded cable-loop-driven parallel mechanisms can be viewed as more efficient since the capabilities of the actuators are better exploited. However, spring-loaded mechanisms have fewer actuators than cable-spool mechanisms and cannot be expected to have the same force capabilities because there is no actuation redundancy.

The force capabilities of the planar and spatial spring-loaded cable-loop-driven parallel mechanism with symmetric compliance are now investigated. For comparison purposes, the force capabilities of conventional planar and spatial cable-spool-driven parallel mechanisms (shown in Figure 5.1(a) and Figure 5.1(b)) are also analyzed in the following.

Because the mechanisms are symmetric, it is assumed that the different cable loops have the same characteristics. This means that the springs of the cable loops have the same stiffness ($k_i = k$) and the same preload ($f_{oi} = f_o$). Moreover, the actuators have the same maximum actuating force $f_{mi,max} = f_{m,max}$. In order to keep the cables in tension, the spring preload should be equal to at least twice the maximum actuating force. Also, a minimum force, f_{min}, should be applied in the cables in order to guarantee that they do not become slack. The maximum cable force might be determined by the cable capabilities, safety issues, or the maximum actuating force. If the cables and actuators are designed accordingly, the cable forces can reach the maximum force that the spring can provide and then the maximum cable force is given by

$$f_{max} = \frac{f_{si}}{2} - f_{min}. \tag{5.1}$$

It should be noted that since the spring force is configuration dependent, the maximum cable force given by Eq.(5.1) is not constant within the workspace. In other words, although the line shown in Figure 3.12 always has the same slope, it is located closer or further away from the origin depending on the configuration, thereby changing the force capabilities of the mechanism.

5.2.1 Planar Mechanisms

5.2.1.1 Spring-loaded Cable-Loop-Driven Parallel Mechanism with Symmetric Compliance

Based on the static equilibrium of the end-effector — Eq. (3.30) — the available force set of the cable-loop-driven planar mechanism in a given configuration can be expressed as

$$\mathcal{A} = \left\{ \mathbf{f} \in \Re^2 \mid \mathbf{f} = \sum_{i=1}^{2} \left[f_{ai}\mathbf{s}_{ai} + (\frac{1}{2}f_{si} - f_{ai})\mathbf{s}_{bi} \right], \quad f_{ai} \in (f_{min}, f_{max}), \quad i = 1, 2 \right\}, \tag{5.2}$$

where f_{max} is given by Eq.(5.1). The above set, $\mathcal{A}$, represents the set of available forces at the end-effector in the given configuration. Since vectors $\mathbf{s}_{ai}$ and $\mathbf{s}_{bi}$ are constant in a given configuration and that $\mathcal{A}$ is defined as a linear combination of these vectors, it is clear that the available force set has four vertices. The vertices can be defined as

- $\mathbf{f}_1 = [x_{f1}, y_{f1}]^T$ for $f_{a1} = f_{min}$, $f_{a2} = f_{min}$,
- $\mathbf{f}_2 = [x_{f2}, y_{f2}]^T$ for $f_{a1} = f_{max}$, $f_{a2} = f_{min}$,
- $\mathbf{f}_3 = [x_{f3}, y_{f3}]^T$ for $f_{a1} = f_{max}$, $f_{a2} = f_{max}$,

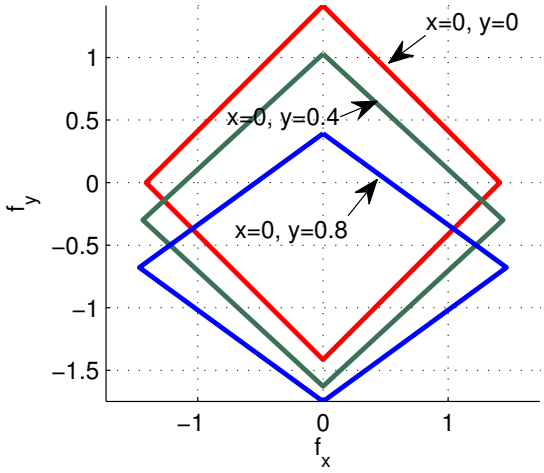

Figure 5.2: Examples of available force sets for different configurations (obtained with $r = 1$, $f_o = 2$, $k = 0$, $f_{min} = 0$ and $f_{max} = \frac{1}{2} f_o = 1$, where r is one half of the distance between A_1 and A_2).

- $\mathbf{f}_4 = [x_{f4}, y_{f4}]^T$ for $f_{a1} = f_{min}$, $f_{a2} = f_{max}$.

Substituting the above conditions into Eq.(5.2) and subtracting the equations corresponding to neighboring vertices, one then obtains

$$\mathbf{f}_2 - \mathbf{f}_1 = (f_{min} + f_{max})(\mathbf{s}_{a1} - \mathbf{s}_{b1}), \tag{5.3}$$
$$\mathbf{f}_3 - \mathbf{f}_2 = (f_{min} + f_{max})(\mathbf{s}_{a2} - \mathbf{s}_{b2}), \tag{5.4}$$
$$\mathbf{f}_4 - \mathbf{f}_3 = (f_{min} + f_{max})(\mathbf{s}_{b1} - \mathbf{s}_{a1}), \tag{5.5}$$
$$\mathbf{f}_1 - \mathbf{f}_4 = (f_{min} + f_{max})(\mathbf{s}_{b2} - \mathbf{s}_{a2}). \tag{5.6}$$

It can be seen that $\mathbf{f}_2 - \mathbf{f}_1 = \mathbf{f}_3 - \mathbf{f}_4$ and $\mathbf{f}_3 - \mathbf{f}_2 = \mathbf{f}_4 - \mathbf{f}_1$, which means that the quadrilateral of the available force set is a parallelogram and that the available force set is defined by a zonotope.

Examples of available force sets for different configurations are shown in Figure 5.2. From this figure, it can be observed that the force capabilities can vary significantly from one configuration to another. One useful measure of the force capability is the maximum force that can be provided by the mechanism in all directions. This concept is illustrated schematically in Figure 5.3 where the radius of the shaded disk, noted r_f, is the maximum force that can be applied in all directions. This value is easily determined once the force parallelogram has been established.

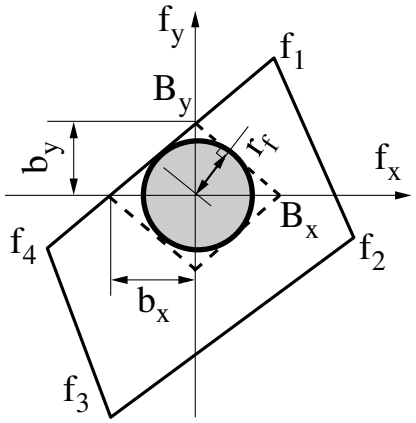

Figure 5.3: Available force set and the maximum force that can be applied in all directions.

The equations of the lines $\mathbf{f}_1\mathbf{f}_2$, $\mathbf{f}_2\mathbf{f}_3$, $\mathbf{f}_3\mathbf{f}_4$, $\mathbf{f}_4\mathbf{f}_1$ and the intercepts on the f_x and f_y axes for these four straight lines, noted b_{xi} and b_{yi}, can be found after forces $\mathbf{f}_i$ have been calculated, $i = 1, \ldots, 4$. The smallest absolute value of the intercept on the f_x and f_y axes, noted b_x and b_y, can then be found. For instance, if the spring in the cable loop is a constant force spring (zero stiffness) and if the minimum cable force is equal to zero ($f_{min} = 0$), one has

$$b_x = \begin{cases} b_{x1}, & \text{if} \quad \rho_x \geq 0, \quad \rho_y \leq 0 \\ b_{x2}, & \text{if} \quad \rho_x \geq 0, \quad \rho_y \geq 0 \\ -b_{x3}, & \text{if} \quad \rho_x \leq 0, \quad \rho_y \geq 0 \\ -b_{x4}, & \text{if} \quad \rho_x \leq 0, \quad \rho_y \leq 0 \end{cases} \tag{5.7}$$

$$b_y = \begin{cases} b_{y1}, & \text{if} \quad \rho_x \geq 0, \quad \rho_y \leq 0 \\ -b_{y2}, & \text{if} \quad \rho_x \geq 0, \quad \rho_y \geq 0 \\ -b_{y3}, & \text{if} \quad \rho_x \leq 0, \quad \rho_y \geq 0 \\ b_{y4}, & \text{if} \quad \rho_x \leq 0, \quad \rho_y \leq 0 \end{cases} \tag{5.8}$$

where the position of point P (the end-effector) is noted

$$\mathbf{p} = [\rho_x r, \rho_y r]^T, \qquad -1 \leq \rho_x, \rho_y \leq 1, \tag{5.9}$$

in which r is equal to one half of the distance between A_1 and A_2, i.e., one half of the side of the square defining the footprint of the mechanism. It should also be verified that the force capability parallelogram includes the origin. Then, the equations for line B_xB_y (B_x $[b_x, 0]^T$, B_y $[0, b_y]^T$) and for the line which is orthogonal to line B_xB_y and passes through the origin can be obtained. The coordinate for the intersection point of these two lines can be calculated as

$$\left(\frac{b_x b_y^2}{b_x^2 + b_y^2}, \quad \frac{b_x^2 b_y}{b_x^2 + b_y^2} \right) \tag{5.10}$$

and the radius r_f can be written as

$$r_f = \frac{b_x b_y}{\sqrt{b_x^2 + b_y^2}}. \tag{5.11}$$

The force-feasible workspace corresponding to a prescribed force value f_p can be defined as the set of all configurations of the mechanism for which $r_f > f_p$.

5.2.1.2 Four-Actuator Cable-Spool Mechanism

The available force set of the mechanism shown in Figure 5.1(a) can be expressed as

$$\mathcal{B} = \left\{ \mathbf{f} \in \Re^2 \mid \mathbf{f} = \sum_{i=1}^{2} \left[f_{ai}\mathbf{s}_{ai} + f_{bi}\mathbf{s}_{bi} \right], \quad f_{ai}, f_{bi} \in (f_{min}, f_{max}), \quad i = 1, 2 \right\}. \tag{5.12}$$

It can be observed that the definition of sets $\mathcal{A}$ and $\mathcal{B}$ is similar. However, in $\mathcal{B}$, the cable forces f_{ai} and f_{bi} can vary independently, whereas they are coupled in $\mathcal{A}$ (f_{bi} is replaced with $(\frac{1}{2}f_{si} - f_{ai})$ in the latter). Therefore, the available force set of the cable-spool mechanism may have up to 16 vertices, corresponding to the combinations obtained when f_{a1}, f_{a2}, f_{b1} and f_{b2} take the values f_{min} or f_{max}. This force set is also a zonotope in the (f_x, f_y) space.

Using the same parameters as for the cable-loop-driven mechanism, namely $r = 1$, $f_{max} = 1$ and $f_{min} = 0$, the available-force sets obtained for a few configurations are shown in Figure 5.4. In the latter plots, the dashed lines correspond to the available-force sets of the cable-loop-driven mechanism. From these figures, it can be observed that the force capabilities in the centre configuration is the same for the two mechanisms while the force capabilities of the four-actuator cable-spool mechanism are better when the end-effector moves away from the centre configuration.

The approach proposed above to find the value of r_f can easily be extended to the four-actuator cable-spool mechanism.

5.2.2 Spatial Mechanisms

The approach presented above for the analysis of the force capabilities of planar mechanisms is now extended to spatial mechanisms.

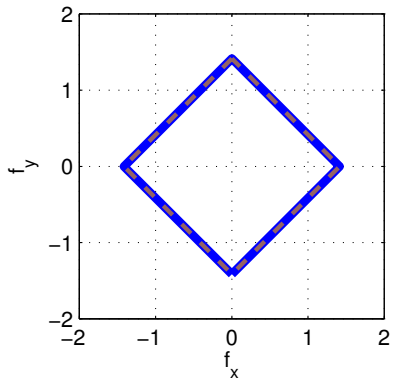

(a) $\mathbf{p} = [0, 0]^T$

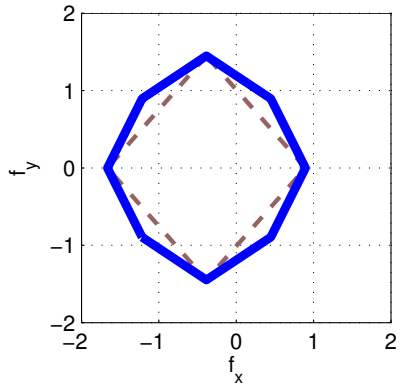

(b) $\mathbf{p} = [0.5, 0]^T$

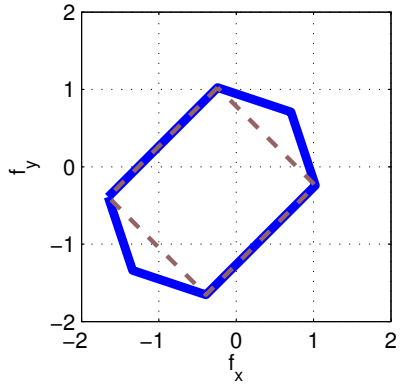

(c) $\mathbf{p} = [0.5, 0.5]^T$

Figure 5.4: Comparison of the available force set of the four-actuator cable-spool mechanism (solid line) and the available force set of the cable-loop-driven mechanism (dashed line) for three different configurations.

5.2.2.1 Spring-Loaded Cable-Loop-Driven Mechanism

The available force set of the spatial spring-loaded cable-loop-driven mechanism can be expressed as

$$\mathcal{C} = \left\{ \mathbf{f} \in \Re^3 \mid \mathbf{f} = \sum_{i=1}^{3} \left[f_{ai}\mathbf{s}_{ai} + (\frac{1}{2}f_{si} - f_{ai})\mathbf{s}_{bi} \right], \quad f_{ai} \in (f_{min}, f_{max}), \quad i = 1, 2, 3. \right\}. \tag{5.13}$$

The available force set $\mathcal{C}$ is embedded in a three-dimensional space and may have up to 8 vertices, corresponding to the combinations of minimum and maximum cable forces. For a given configuration of the mechanism, assume that the 8 vertices of the available force set are defined as $\mathbf{f}_i$, $i = 1, 2, \ldots, 8$. These vertices form an hexahedron. Vectors normal to the faces of the hexahedron are readily obtained and the distance from the origin of the force space to the faces can be calculated.

For instance, consider the face defined by $\mathbf{f}_1\mathbf{f}_2\mathbf{f}_3\mathbf{f}_4$. A vector normal to this face can be obtained as

$$\mathbf{n}_1 = (\mathbf{f}_2 - \mathbf{f}_1) \times (\mathbf{f}_3 - \mathbf{f}_2), \tag{5.14}$$

where $\times$ is the cross product of the vectors. Then, the distance from the origin of the force space to the face can be written as

$$r_{f1} = \frac{|\mathbf{f}_1^T \mathbf{n}_1|}{||\mathbf{n}_1||}. \tag{5.15}$$

After all the six distances r_{fi}, $i = 1, \ldots, 6$, to the faces are calculated, the maximum force that can be applied in all directions is found as the minimum value of $r_{fi}, i = 1, \ldots, 6$.

Assuming that the length of a diagonal of the octahedron is $2a = 2$ and that $k = 0$, $f_o = 2$, $f_{min} = 0$ and $f_{max} = \frac{1}{2}f_o = 1$, plots of the available force set are shown for three different configurations in Figure 5.5.

5.2.2.2 Six-Actuator Cable-Spool Mechanism

If the end-effector of the mechanism is driven by six actuated spools located on the vertices of an octahedron as shown in Figure 5.1(b), the available force set for a given configuration is defined as

$$\mathcal{D} = \left\{ \mathbf{f} \in \Re^3 \mid \mathbf{f} = \sum_{i=1}^{3} \left[f_{ai}\mathbf{s}_{ai} + f_{bi}\mathbf{s}_{bi} \right], \quad f_{ai}, f_{bi} \in (f_{min}, f_{max}), \quad i = 1, 2, 3. \right\}. \tag{5.16}$$

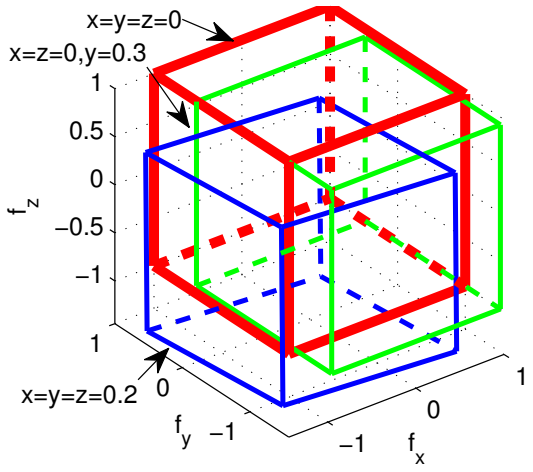

Figure 5.5: The available force set of the spatial spring-loaded cable-loop-driven mechanism for different configurations. ($2a = 2$, $k = 0$, $f_0 = 2$, $f_{min} = 0$ and $f_{max} = 1$)

The available force set $\mathcal{D}$ is embedded in a three-dimensional space and may have up to $2^6 = 64$ vertices. For a given configuration, the maximum force that can be applied in all directions can be found using the following steps:

1. Obtain the vertices of the available force set of the end-effector, which form a polyhedron (zonotope);

2. Find vectors normal to the faces of the polyhedron;

3. Calculate the distance from the origin of the force space to the planes of the convex polyhedron;

4. Find the smallest distance.

Using the same parameters as for the cable-loop-driven mechanism, namely $a = 1$ and $f_{max} = 1$, $f_{min} = 0$, the available force sets of this mechanism for different configurations are shown in Figure 5.6. Comparing Figure 5.6 with Figure 5.5, it can be observed that the available-force set of the two mechanisms is the same in the centre configuration and that the six-actuator mechanism has a better available force set when the end-effector moves away from the centre configuration. This result is similar to what was obtained for the planar mechanisms.

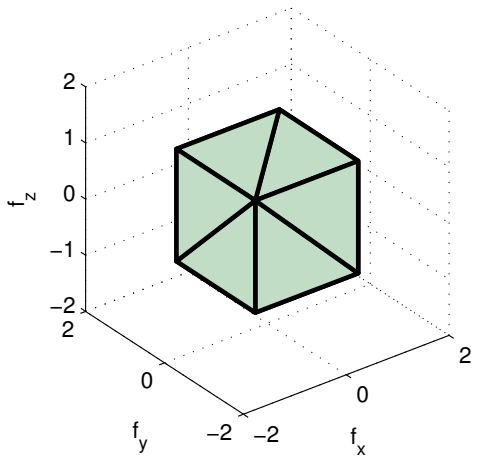

(a) $\mathbf{p} = [0, 0, 0]$

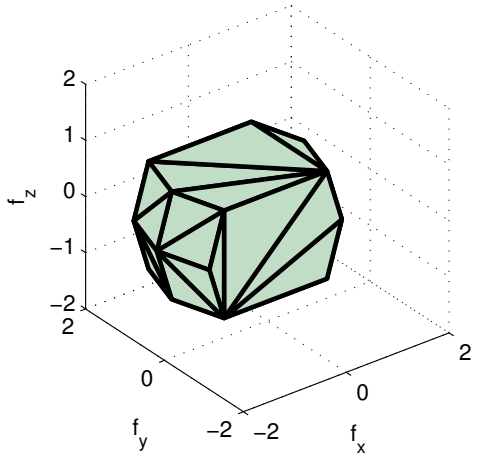

(b) $\mathbf{p} = [0.3, 0, 0]$

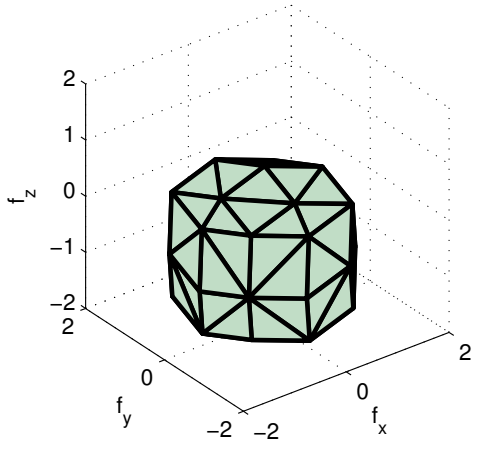

(c) $\mathbf{p} = [0.2, 0.2, 0.2]$

Figure 5.6: The available-force set of the six-actuator cable-spool mechanism. ($a = 1$, $f_{max} = 1$, $f_{min} = 0$)

5.3 Simulation Results

The average value of index r_f over a given workspace as well as the workspace within which r_f is larger than a prescribed value are now used in order to obtain a more global comparison of the force capabilities of spring-loaded cable-loop-driven parallel mechanisms and cable-spool parallel mechanisms.

5.3.1 Planar Mechanisms

Consider a workspace defined as a disk bounded by a circle which can be defined as $x^2+y^2 = (\rho r)^2$, where $0 < \rho < 1$. Also, assume $r = 1$, $f_{min} = 0.1$ and $f_{m,max} = 1$. For the four-actuator cable-spool mechanism, the average value of r_f over the workspace is $\bar{r}_f = 0.6660$ when $\rho = 0.9$ and $\bar{r}_f = 0.7144$ when $\rho = 0.8$. With the same minimum and maximum cable force, the average value of r_f for the spring-loaded cable-loop-driven mechanism is $\bar{r}_f = 0.4749$ when $\rho = 0.9$ and $\bar{r}_f = 0.5168$ when $\rho = 0.8$. As expected, the four-actuator mechanism has better force capabilities than the two-actuator mechanism. However, the spring-loaded mechanism still has acceptable force capabilities.

For the spring-loaded cable-loop-driven mechanisms, the preload of the springs should be approximately equal to twice the maximum actuating force, $f_o = 2f_{m,max} = 2$, considering the coupled compliance on each side of the actuator. In order to assess the effect of the springs' stiffness and preload on the force capabilities, assume that the cable force can be zero and that the cable can bear the maximum force generated by the springs. The average value of r_f is plotted for $\frac{kr}{f_o} \in [-\sqrt{2}, \sqrt{2}]$ in Figure 5.7 for two different workspaces. It can be noted that the spring-loaded mechanism has better force capabilities when the springs have a negative stiffness.

The workspace boundaries within which a value of $r_f > 0.6$ can be maintained are now shown for different minimum cable forces. Figure 5.8 shows the plots for the four-actuator mechanism with a force range $[0, 1]$ and the spring-loaded mechanism with spring characteristics of $f_o = 2$, $k = -1$. The plots are repeated with different values of f_{min}. It can be observed that the minimum cable force has a more significant effect on the spring-loaded mechanism.

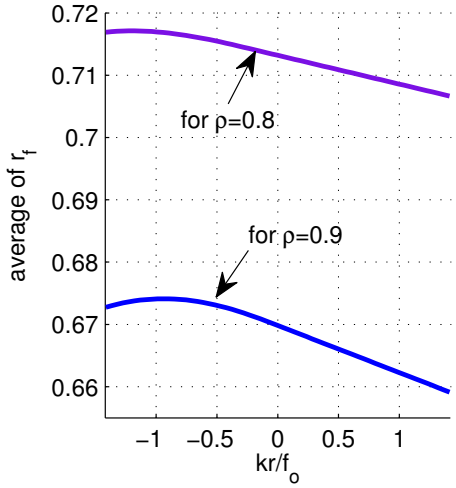

Figure 5.7: The average value of r_f as a function of the spring parameters.

5.3.2 Spatial Mechanisms

Similarly to what was shown for planar mechanisms, the workspace within which one has $r_f > 0.4$ is now plotted for the two types of spatial mechanisms. Figure 5.9 shows the result obtained for the spring-loaded cable-loop-driven mechanism while Figure 5.10 presents the workspace for the six-actuator cable-spool mechanism. It is obvious that the volume of the workspace for the cable-spool mechanism is larger than that of the spring-loaded mechanism.

5.4 Conclusion

The force capabilities of planar and spatial spring-loaded cable-loop-driven parallel mechanisms are investigated in this chapter. The concept of available force set is used to obtain a clear representation of the capabilities of the mechanisms. Based on this concept, indices are defined that provide some insight into the characteristics of the mechanisms. Also, the force capabilities of spring-loaded cable-loop-driven parallel mechanisms are compared with those of more conventional redundantly actuated cable-driven mechanisms. As expected, simulation results show that the redundantly actuated mechanisms have better force capabilities. However, it is also shown that spring-loaded cable-loop-driven parallel mechanisms can provide very good force capabilities while being more efficient and cost-effective. Based on the simulation results, it is also found that the minimum cable force has a significant impact on the spring-loaded mechanisms due to

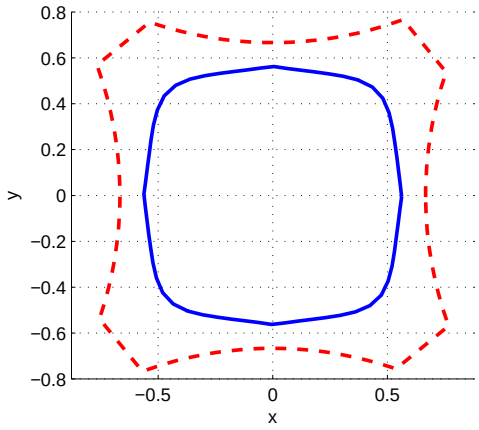

(a) minimum cable force is zero

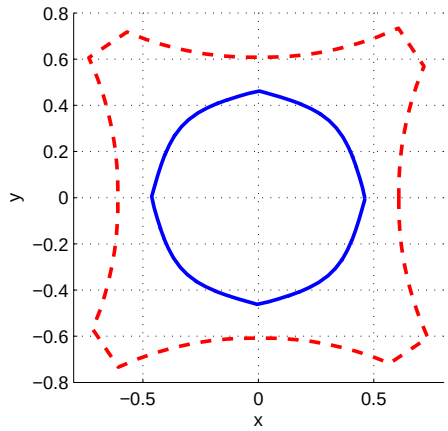

(b) minimum cable force is 0.05

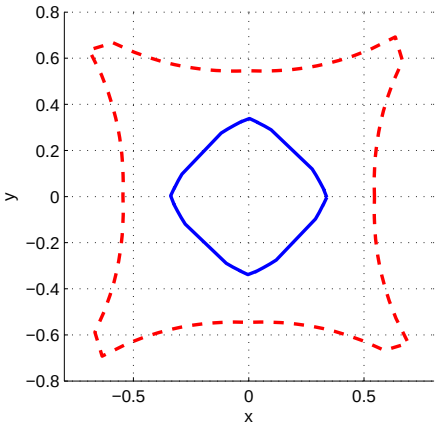

(c) minimum cable force is 0.1

Figure 5.8: The workspace boundary within which one has $r_f > 0.6$ for the spring-loaded mechanism (solid line) and the cable-spool mechanism (dashed line) for different value of f_{min}. ($f_o = 2, k = -1, f_{max} = 1$).

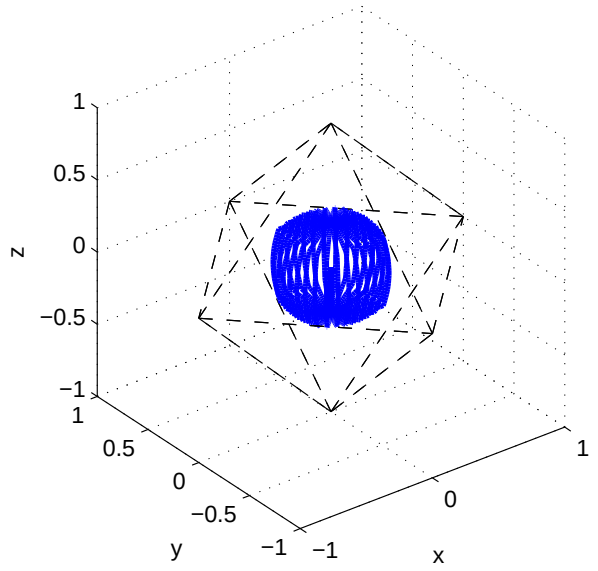

Figure 5.9: The workspace within which one has $r_f > 0.4$ for the spring-loaded mechanism ($f_o = 2$, $k = 0$, $f_{min} = 0$, $f_{max} = \frac{1}{2} f_o = 1$).

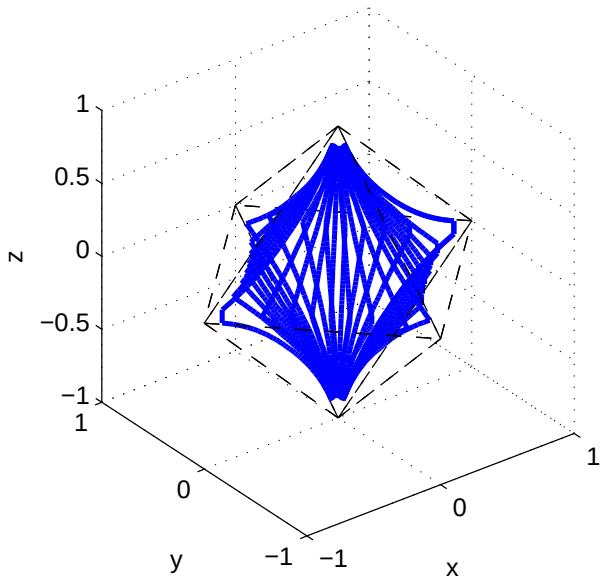

Figure 5.10: The workspace within which one has $r_f > 0.4$ for the cable-spool mechanism ($f_{min} = 0$, $f_{max} = 1$).

the coupled compliance on each side of the actuators. Therefore, friction should be minimized in a practical design so that the minimum force can be kept low. Finally, it is shown that the performance of the mechanisms can be improved if the ratio between the stiffness and the preload of the springs is adjusted properly and if negative stiffness springs are used.

Chapter 6

Dynamic Modelling and Mechanical Bandwidth of Planar and Spatial Spring-Loaded Cable-Loop-Driven Parallel Mechanisms

The dynamic analysis of the novel architectures of planar and spatial spring-loaded cable-loop-driven parallel mechanisms is introduced in this chapter. The cable forces are obtained for the dynamic operation of the mechanisms. Due to the cable loops in the mechanisms, the cables might become slack when the end-effector moves with high accelerations. Therefore, it should be verified that the cable forces can be maintained in tension for a certain range of the trajectory frequencies. The required actuating forces are found. Based on the static force and the Newton-Euler formulation, the natural frequency and the corresponding ratio of the amplitudes for these two mechanisms are also found.

6.1 Introduction

For conventional cable-driven parallel mechanisms, one end of the cables is wound on an actuated drum while the other end attaches to the end-effector directly. In this approach, the cables can be maintained in tension if the end-effector is not in a singular configuration no matter how large the acceleration is. Because the mass of the cables can be neglected and the actuators are fixed, the dynamic model of the conventional cable-driven parallel mechanisms is quite simple compared to that of the link-driven parallel mechanisms. For such mechanisms, more attention is payed to the workspace within which the cables always maintain in tension.

However, in cable-loop-driven mechanisms, a spring is attached in each cable loop. When the mechanisms are moving with high accelerations, vibrations might occur and the cables might become slack. Therefore, it is important to investigate the dynamic characteristics of these mechanisms and find the acceleration range within which the cables can be maintained in tension. The natural frequencies and the corresponding ratio of the amplitudes should also be found.

6.2 Velocity and Acceleration of the Mechanisms

The inverse kinematic equations for the planar and spatial mechanisms have be found in Chapters 3 and 4. For convenience, the equations are repeated in the following. One has

$$\delta_i = \frac{1}{4}(n_{ai} + n_{bi}), \tag{6.1}$$

$$l_{mi} = \frac{1}{2}(n_{bi} - n_{si}), \tag{6.2}$$

where $n_{ai} = |PA_i| - |P_oA_i|$, $n_{bi} = |PB_i| - |P_oB_i|$. And $i = 1, 2$ for the planar mechanism, $i = 1, 2, 3$ for the spatial mechanism.

Differentiating the expressions of δ_i and l_{mi}, for the planer mechanism, one has

$$\begin{bmatrix} \dot{\delta}_i \\ \dot{l}_{mi} \end{bmatrix} = \begin{bmatrix} \frac{1}{4}\left(\frac{x - x_{ai}}{|PA_i|} + \frac{x - x_{bi}}{|PB_i|}\right) & \frac{1}{4}\left(\frac{y - y_{ai}}{|PA_i|} + \frac{y - y_{bi}}{|PB_i|}\right) \\ \frac{1}{2}\left(\frac{x - x_{bi}}{|PB_i|} - \frac{x - x_{ai}}{|PA_i|}\right) & \frac{1}{2}\left(\frac{y - y_{bi}}{|PB_i|} - \frac{y - y_{ai}}{|PA_i|}\right) \end{bmatrix} \begin{bmatrix} \dot{x} \\ \dot{y} \end{bmatrix}$$

and

$$\begin{bmatrix} \ddot{\delta}_i \\ \ddot{l}_{mi} \end{bmatrix} = \begin{bmatrix} \frac{1}{4}\left(\frac{x-x_{ai}}{|PA_i|}+\frac{x-x_{bi}}{|PB_i|}\right) & \frac{1}{4}\left(\frac{y-y_{ai}}{|PA_i|}+\frac{y-y_{bi}}{|PB_i|}\right) \\ \frac{1}{2}\left(\frac{x-x_{bi}}{|PB_i|}-\frac{x-x_{ai}}{|PA_i|}\right) & \frac{1}{2}\left(\frac{y-y_{bi}}{|PB_i|}-\frac{y-y_{ai}}{|PA_i|}\right) \end{bmatrix} \begin{bmatrix} \ddot{x} \\ \ddot{y} \end{bmatrix}$$
$$+ \begin{bmatrix} \frac{(y-y_{ai})^2}{4|PA_i|^3}+\frac{(y-y_{bi})^2}{4|PB_i|^3} & -\frac{(x-x_{ai})(y-y_{ai})}{2|PA_i|^3}-\frac{(x-x_{bi})(y-y_{bi})}{2|PB_i|^3} & \frac{(x-x_{ai})^2}{4|PA_i|^3}+\frac{(x-x_{bi})^2}{4|PB_i|^3} \\ \frac{(y-y_{bi})^2}{2|PB_i|^3}-\frac{(y-y_{ai})^2}{2|PA_i|^3} & \frac{(x-x_{ai})(y-y_{ai})}{|PA_i|^3}-\frac{(x-x_{bi})(y-y_{bi})}{|PB_i|^3} & \frac{(x-x_{bi})^2}{2|PB_i|^3}-\frac{(x-x_{ai})^2}{2|PA_i|^3} \end{bmatrix} \begin{bmatrix} \dot{x}^2 \\ \dot{x}\dot{y} \\ \dot{y}^2 \end{bmatrix}$$

For the spatial spring-loaded mechanism, the velocity and acceleration of the spring deformations and the displacements of the actuators can be obtained as

$$\dot{\delta} = \mathbf{J}_\delta \dot{\mathbf{p}}, \tag{6.3}$$
$$\dot{\mathbf{l}}_m = \mathbf{J}_m \dot{\mathbf{p}}, \tag{6.4}$$

where $\delta = [\dot{\delta}_1, \dot{\delta}_2, \dot{\delta}_3]^T$, $\dot{\mathbf{l}}_m = [\dot{l}_{m1}, \dot{l}_{m2}, \dot{l}_{m3}]^T$ and

$$\mathbf{J}_\delta = \frac{1}{4}\begin{bmatrix} \frac{x+a}{|PA_1|}+\frac{x-a}{|PB_1|} & \frac{y}{|PA_1|}+\frac{y}{|PB_1|} & \frac{z}{|PA_1|}+\frac{z}{|PB_1|} \\ \frac{x}{|PA_2|}+\frac{x}{|PB_2|} & \frac{y+a}{|PA_2|}+\frac{y-a}{|PB_2|} & \frac{z}{|PA_2|}+\frac{z}{|PB_2|} \\ \frac{x}{|PA_3|}+\frac{x}{|PB_3|} & \frac{y}{|PA_3|}+\frac{y}{|PB_3|} & \frac{z+a}{|PA_3|}+\frac{z-a}{|PB_3|} \end{bmatrix}$$

$$\mathbf{J}_m = \frac{1}{2}\begin{bmatrix} \frac{x+a}{|PA_1|}-\frac{x-a}{|PB_1|} & \frac{y}{|PA_1|}-\frac{y}{|PB_1|} & \frac{z}{|PA_1|}-\frac{z}{|PB_1|} \\ \frac{x}{|PA_2|}-\frac{x}{|PB_2|} & \frac{y+a}{|PA_2|}-\frac{y-a}{|PB_2|} & \frac{z}{|PA_2|}-\frac{z}{|PB_2|} \\ \frac{x}{|PA_3|}-\frac{x}{|PB_3|} & \frac{y}{|PA_3|}-\frac{y}{|PB_3|} & \frac{z+a}{|PA_3|}-\frac{z-a}{|PB_3|} \end{bmatrix}$$

and

$$\ddot{\delta} = \mathbf{J}_\delta \ddot{\mathbf{p}} + \mathbf{K}_\delta \dot{\mathbf{p}}, \tag{6.5}$$
$$\ddot{\mathbf{l}}_m = \mathbf{J}_m \ddot{\mathbf{p}} + \mathbf{K}_m \dot{\mathbf{p}}, \tag{6.6}$$

where

$$\mathbf{K}_\delta(1,1) = \frac{1}{4}\left[\frac{(y^2+z^2)\dot{x}-(x+a)y\dot{y}-(x+a)z\dot{z}}{|PA_1|^3}+\frac{(y^2+z^2)\dot{x}-(x-a)y\dot{y}-(x-a)z\dot{z}}{|PB_1|^3}\right],$$

$$\mathbf{K}_\delta(1,2) = \frac{1}{4}\left\{\frac{-(x+a)y\dot{x} + [(x+a)^2+z^2]\dot{y} - yz\dot{z}}{|PA_1|^3} + \frac{-(x-a)y\dot{x} + [(x-a)^2+z^2]\dot{y} - yz\dot{z}}{|PB_1|^3}\right\},$$

$$\mathbf{K}_\delta(1,3) = \frac{1}{4}\left\{\frac{-(x+a)z\dot{x} - yz\dot{y} + [(x+a)^2+y^2]\dot{z}}{|PA_1|^3} + \frac{-(x-a)z\dot{x} - yz\dot{y} + [(x-a)^2+y^2]\dot{z}}{|PB_1|^3}\right\},$$

$$\mathbf{K}_\delta(2,1) = \frac{1}{4}\left\{\frac{[(y+a)^2+z^2]\dot{x} - x(y+a)\dot{y} - xz\dot{z}}{|PA_2|^3} + \frac{[(y-a)^2+z^2]\dot{x} - x(y-a)\dot{y} - xz\dot{z}}{|PB_2|^3}\right\},$$

$$\mathbf{K}_\delta(2,2) = \frac{1}{4}\left[\frac{-x(y+a)\dot{x} + (x^2+z^2)\dot{y} - (y+a)z\dot{z}}{|PA_2|^3} + \frac{-x(y-a)\dot{x} + (x^2+z^2)\dot{y} - (y-a)z\dot{z}}{|PB_2|^3}\right],$$

$$\mathbf{K}_\delta(2,3) = \frac{1}{4}\left\{\frac{-xz\dot{x} - (y+a)z\dot{y} + [x^2+(y+a)^2]\dot{z}}{|PA_2|^3} + \frac{-xz\dot{x} - (y-a)z\dot{y} + [x^2+(y-a)^2]\dot{z}}{|PB_2|^3}\right\},$$

$$\mathbf{K}_\delta(3,1) = \frac{1}{4}\left\{\frac{[y^2+(z+a)^2]\dot{x} - xy\dot{y} - x(z+a)\dot{z}}{|PA_3|^3} + \frac{[y^2+(z-a)^2]\dot{x} - xy\dot{y} - x(z-a)\dot{z}}{|PB_3|^3}\right\},$$

$$\mathbf{K}_\delta(3,2) = \frac{1}{4}\left\{\frac{-xy\dot{x} + [x^2+(z+a)^2]\dot{y} - y(z+a)\dot{z}}{|PA_3|^3} + \frac{-xy\dot{x} + [x^2+(z-a)^2]\dot{y} - y(z-a)\dot{z}}{|PB_3|^3}\right\},$$

$$\mathbf{K}_\delta(3,3) = \frac{1}{4}\left[\frac{-x(z+a)\dot{x} - y(z+a)\dot{y} + (x^2+y^2)\dot{z}}{|PA_3|^3} + \frac{-x(z-a)\dot{x} - y(z-a)\dot{y} + (x^2+y^2)\dot{z}}{|PB_3|^3}\right].$$

$$\mathbf{K}_m(1,1) = \frac{1}{2}\left[\frac{(y^2+z^2)\dot{x} - (x+a)y\dot{y} - (x+a)z\dot{z}}{|PA_1|^3} - \frac{(y^2+z^2)\dot{x} - (x-a)y\dot{y} - (x-a)z\dot{z}}{|PB_1|^3}\right],$$

$$\mathbf{K}_m(1,2) = \frac{1}{2}\left\{\frac{-(x+a)y\dot{x} + [(x+a)^2+z^2]\dot{y} - yz\dot{z}}{|PA_1|^3} - \frac{-(x-a)y\dot{x} + [(x-a)^2+z^2]\dot{y} - yz\dot{z}}{|PB_1|^3}\right\},$$

$$\mathbf{K}_m(1,3) = \frac{1}{2}\left\{\frac{-(x+a)z\dot{x} - yz\dot{y} + [(x+a)^2+y^2]\dot{z}}{|PA_1|^3} - \frac{-(x-a)z\dot{x} - yz\dot{y} + [(x-a)^2+y^2]\dot{z}}{|PB_1|^3}\right\},$$

$$\mathbf{K}_m(2,1) = \frac{1}{2}\left\{\frac{[(y+a)^2+z^2]\dot{x} - x(y+a)\dot{y} - xz\dot{z}}{|PA_2|^3} - \frac{[(y-a)^2+z^2]\dot{x} - x(y-a)\dot{y} - xz\dot{z}}{|PB_2|^3}\right\},$$

$$\mathbf{K}_m(2,2) = \frac{1}{2}\left[\frac{-x(y+a)\dot{x} + (x^2+z^2)\dot{y} - (y+a)z\dot{z}}{|PA_2|^3} - \frac{-x(y-a)\dot{x} + (x^2+z^2)\dot{y} - (y-a)z\dot{z}}{|PB_2|^3}\right],$$

$$\mathbf{K}_m(2,3) = \frac{1}{2}\left\{\frac{-xz\dot{x} - (y+a)z\dot{y} + [x^2+(y+a)^2]\dot{z}}{|PA_2|^3} - \frac{-xz\dot{x} - (y-a)z\dot{y} + [x^2+(y-a)^2]\dot{z}}{|PB_2|^3}\right\},$$

$$\mathbf{K}_m(3,1) = \frac{1}{2}\left\{\frac{[y^2+(z+a)^2]\dot{x} - xy\dot{y} - x(z+a)\dot{z}}{|PA_3|^3} - \frac{[y^2+(z-a)^2]\dot{x} - xy\dot{y} - x(z-a)\dot{z}}{|PB_3|^3}\right\},$$

$$\mathbf{K}_m(3,2) = \frac{1}{2}\left\{\frac{-xy\dot{x} + [x^2+(z+a)^2]\dot{y} - y(z+a)\dot{z}}{|PA_3|^3} - \frac{-xy\dot{x} + [x^2+(z-a)^2]\dot{y} - y(z-a)\dot{z}}{|PB_3|^3}\right\},$$

$$\mathbf{K}_m(3,3) = \frac{1}{2}\left[\frac{-x(z+a)\dot{x} - y(z+a)\dot{y} + (x^2+y^2)\dot{z}}{|PA_3|^3} - \frac{-x(z-a)\dot{x} - y(z-a)\dot{y} + (x^2+y^2)\dot{z}}{|PB_3|^3}\right].$$

Observing the previous expressions, it can be seen that the velocity and acceleration equations of the springs deformations and the displacements of the actuators for both of the planar and spatial mechanisms can be expressed as

$$\dot{\boldsymbol{\delta}} = \mathbf{J}_\delta \dot{\mathbf{p}}, \tag{6.7}$$

$$\dot{\mathbf{l}}_m = \mathbf{J}_l \dot{\mathbf{p}}, \tag{6.8}$$

$$\ddot{\boldsymbol{\delta}} = \mathbf{J}_\delta \ddot{\mathbf{p}} + \mathbf{K}_\delta \dot{\mathbf{p}}, \tag{6.9}$$

$$\ddot{\mathbf{l}}_m = \mathbf{J}_l \ddot{\mathbf{p}} + \mathbf{K}_l \dot{\mathbf{p}}, \tag{6.10}$$

where

$$\mathbf{J}_\delta = -\frac{1}{4}(\mathbf{S}_b + \mathbf{S}_a)^T, \quad \mathbf{J}_l = -\frac{1}{2}(\mathbf{S}_b - \mathbf{S}_a)^T,$$

$$\mathbf{K}_\delta = -\frac{1}{4}\left[\begin{array}{cc} \dfrac{\partial(\mathbf{S}_b + \mathbf{S}_a)^T}{\partial x}\dot{\mathbf{p}} & \dfrac{\partial(\mathbf{S}_b + \mathbf{S}_a)^T}{\partial y}\dot{\mathbf{p}} \end{array} \right],$$

$$\mathbf{K}_l = -\frac{1}{2}\left[\begin{array}{cc} \dfrac{\partial(\mathbf{S}_b - \mathbf{S}_a)^T}{\partial x}\dot{\mathbf{p}} & \dfrac{\partial(\mathbf{S}_b - \mathbf{S}_a)^T}{\partial y}\dot{\mathbf{p}} \end{array} \right].$$

and $\mathbf{S}_a = [\mathbf{s}_{a1}, \ldots, \mathbf{s}_{aj}]$, $\mathbf{S}_b = [\mathbf{s}_{b1}, \ldots, \mathbf{s}_{bj}]$. $j = 2$ for the planar mechanism and $j = 3$ for the spatial mechanism. $\mathbf{s}_{ai}$, $\mathbf{s}_{bi}$ are the unit vectors for the direction of the cable segments from the end-effector to the fixed pulleys in which the cables pass first, namely

$$\mathbf{s}_{ai} = \frac{\mathbf{a}_i - \mathbf{p}}{||\mathbf{a}_i - \mathbf{p}||}, \qquad \mathbf{s}_{bi} = \frac{\mathbf{b}_i - \mathbf{p}}{||\mathbf{b}_i - \mathbf{p}||}.$$

Then, the inverse kinematics equations for the position, velocity and acceleration relationships are found as Eq. (6.2), Eq. (6.8) and Eq. (6.10) respectively. From the above equations, it can be observed that the inverse kinematic equations only depend on the position, velocity and acceleration of the end-effector and are independent from the external forces, assuming that the cables are all under tension.

6.3 Dynamic Model

The dynamic equations of the mechanism provide the relationships between actuation and external forces acting on the mechanism and the acceleration and motion trajectories that result.

Usually, cable-driven parallel mechanisms have simpler dynamic models than link-driven parallel mechanisms because the mass of the cables can be neglected. The dynamic equations of motion can be obtained from the Lagrangian formulation or the Newton-Euler formulation. Here, the Newton-Euler formulation is used to obtain the dynamic equations of the planar and spatial spring-loaded cable-loop-driven parallel mechanisms.

Assume that the masses of the springs and the free pulleys are small enough to be neglected. Neglecting the friction between the cables and pulleys and considering only the mass of the end-effector m_p and the mass of the actuators m_m, the forces acting at the end-effector and on the moving fixtures and pulleys f_{ai}, f_{bi} are assumed to be uniform. The dynamic equations for the end-effector and the actuators can be found as

$$\mathbf{M}_m \ddot{\mathbf{l}}_m = \mathbf{f}_b - \mathbf{f}_a + \mathbf{f}_m, \tag{6.11}$$

$$\mathbf{M}_p \ddot{\mathbf{p}} = \mathbf{S}_a \mathbf{f}_a + \mathbf{S}_b \mathbf{f}_b. \tag{6.12}$$

where $\mathbf{M}_m$ and $\mathbf{M}_p$ are the mass matrices for the actuator and the end-effector, respectively, namely $\mathbf{M}_m = \text{diag}\left[\ m_{m1},\ \ m_{m2}\ \right]$, $\mathbf{M}_p = \text{diag}\left[\ m_p,\ \ m_p\ \right]$ for the planar mechanism, $\mathbf{M}_m = \text{diag}\left[\ m_{m1},\ \ m_{m2},\ \ m_{m3}\ \right]$, $\mathbf{M}_p = \text{diag}\left[\ m_p,\ \ m_p,\ \ m_p\ \right]$ for the spatial mechanism.

From Eq. (6.12) and Eq. (3.32) or (4.7) which expresses the relationship between the spring force and the two cable forces, the cable forces $\mathbf{f}_a$, $\mathbf{f}_b$ in a dynamic situation can be found as

$$\begin{bmatrix} \mathbf{f}_a \\ \mathbf{f}_b \end{bmatrix} = \begin{bmatrix} \mathbf{I} + \mathbf{S}_{ba}^{-1}\mathbf{S}_a & -\mathbf{S}_{ba}^{-1} \\ -\mathbf{S}_{ba}^{-1}\mathbf{S}_a & \mathbf{S}_{ba}^{-1} \end{bmatrix} \begin{bmatrix} \frac{1}{2}\mathbf{f}_s \\ \mathbf{M}_p \ddot{\mathbf{p}} \end{bmatrix} \tag{6.13}$$

where $\mathbf{I}$ is an 2×2 or 3×3 identity matrix. Moreover, matrix $\mathbf{S}_{ba} = \mathbf{S}_b - \mathbf{S}_a$ is always invertible within the square or the octahedron which is formed by the fixed pulleys A_i and B_i. When the cable forces $\mathbf{f}_a$ and $\mathbf{f}_b$ are known, the actuating force $\mathbf{f}_m$ can be found using the dynamic equations for the actuators Eq. (6.11) as

$$\mathbf{f}_m = \frac{1}{2}(\mathbf{S}_b - \mathbf{S}_a)^{-1}(\mathbf{S}_a + \mathbf{S}_b)\mathbf{f}_s - 2(\mathbf{S}_b - \mathbf{S}_a)^{-1}\mathbf{M}_p \ddot{\mathbf{p}} + \mathbf{M}_m(\mathbf{J}_l \ddot{\mathbf{p}} + \mathbf{K}_l \dot{\mathbf{p}}). \tag{6.14}$$

Moreover, the modular actuator-spring systems are all assumed to have the same characteristics, that is to say $f_o = f_{oi}$, $k = k_i$ and $m_m = m_{mi}$. Then, the cable extension forces f_{ai} and f_{bi} have the same properties for each mechanism. Because the cables can only pull and not push, it should be verified that the cable forces $\mathbf{f}_a$ and $\mathbf{f}_b$ can be maintained in tension for a certain set of trajectories of the end-effector. Then, the frequency limitation for the mechanisms can be found.

In order to preserve symmetry, the origin of the fixed coordinate frame $O-xy$ is located at the centre of the rectangle $A_1A_2B_1B_2$ for the planar mechanism. Similarly, the origin of the fixed coordinate frame for the spatial mechanism is also located at the centre of the octahedron as shown in Figure 4.2(a). The expression of Eq. (6.13) are very complicated, in order to get some basic dynamic characteristics of the mechanisms, assume that the quadrilateral of the planar mechanism is a square with $2r$ side length and the octahedron of the spatial mechanism has $2a$ diagonal length.

For the planar mechanism, Eq. (6.13) can be modified as

$$\begin{bmatrix} \mathbf{f}_a \\ \mathbf{f}_b \end{bmatrix} = \frac{1}{\Omega} \begin{bmatrix} \mathbf{W}_{p1,1} & \mathbf{W}_{p1,2} \\ \mathbf{W}_{p2,1} & \mathbf{W}_{p2,2} \end{bmatrix} \begin{bmatrix} \frac{1}{2}\mathbf{f}_s \\ \mathbf{M}_p\ddot{\mathbf{p}} \end{bmatrix} \tag{6.15}$$

where $\Omega = 2r[(a_2b_1 - a_1b_2)x + (a_1a_2 - b_1b_2)y - (a_1+b_1)(a_2+b_2)r]$,

$$\begin{aligned} a_1 &= \sqrt{(r-x)^2+(r+y)^2}, \qquad & a_2 &= \sqrt{(r+x)^2+(r+y)^2}, \\ b_1 &= \sqrt{(r+x)^2+(r-y)^2}, \qquad & b_2 &= \sqrt{(r-x)^2+(r-y)^2}, \end{aligned}$$

$$\begin{aligned} \mathbf{W}_{p1,1} &= \begin{bmatrix} 2ra_1[a_2(y-r)-b_2(x+r)] & -2ra_1b_1(x-y) \\ 2ra_2b_2(x+y) & 2ra_2[a_1(y-r)+b_1(x-r)] \end{bmatrix}, \\ \mathbf{W}_{p2,1} &= \begin{bmatrix} 2rb_1[a_2(x-r)-b_2(y+r)] & 2ra_1b_1(x-y) \\ -2ra_2b_2(x+y) & -2rb_2[a_1(x+r)+b_1(y+r)] \end{bmatrix}, \\ -\mathbf{W}_{p1,2} &= \mathbf{W}_{p2,2} = \begin{bmatrix} \mathbf{w}_1 & \mathbf{w}_2 \end{bmatrix}, \end{aligned}$$

and

$$\mathbf{w}_1 = \begin{bmatrix} a_1b_1[(b_2-a_2)y + (a_2+b_2)r] \\ a_2b_2[(a_1-b_1)y - (a_1+b_1)r] \end{bmatrix}, \quad \mathbf{w}_2 = \begin{bmatrix} a_1b_1[(a_2-b_2)x - (a_2+b_2)r] \\ a_2b_2[(b_1-a_1)x - (a_1+b_1)r] \end{bmatrix}.$$

For the spatial mechanism, Eq. (6.13) can be modified as

$$\begin{bmatrix} \mathbf{f}_a \\ \mathbf{f}_b \end{bmatrix} = \frac{1}{\Theta} \begin{bmatrix} \mathbf{w}_{s1} & \mathbf{w}_{s2} & \mathbf{w}_{s3} & \mathbf{w}_{s4} & \mathbf{w}_{s5} & \mathbf{w}_{s6} \end{bmatrix} \begin{bmatrix} \frac{1}{2}\mathbf{f}_s \\ \mathbf{M}_p\ddot{\mathbf{p}} \end{bmatrix} \tag{6.16}$$

where

$$\begin{aligned} \Theta =& a[(a_1+b_1)(a_2+b_2)(a_3+b_3)a - (a_1-b_1)(a_2+b_2)(a_3+b_3)x \\ & - (a_1+b_1)(a_2-b_2)(a_3+b_3)y - (a_1+b_1)(a_2+b_2)(a_3-b_3)z], \end{aligned}$$

and a_i, b_i, $i = 1, 2, 3$, are the distances between the end-effector and the fixed pulleys

$$\begin{aligned} a_1 &= \sqrt{(a+x)^2 + y^2 + z^2}, & b_1 &= \sqrt{(a-x)^2 + y^2 + z^2}, \\ a_2 &= \sqrt{x^2 + (a+y)^2 + z^2}, & b_2 &= \sqrt{x^2 + (a-y)^2 + z^2}, \\ a_3 &= \sqrt{x^2 + y^2 + (a+z)^2}, & b_3 &= \sqrt{x^2 + y^2 + (a-z)^2}. \end{aligned}$$

with also

$$\mathbf{w}_{s1} = a \begin{bmatrix} x_{1,1} \\ -2a_2b_2(a_3+b_3)y \\ -2a_3b_3(a_2+b_2)z \\ z_{1,1} \\ 2a_2b_2(a_3+b_3)y \\ 2a_3b_3(a_2+b_2)z \end{bmatrix}, \quad \mathbf{w}_{s2} = a \begin{bmatrix} -2a_1b_1(a_3+b_3)x \\ x_{2,2} \\ -2a_2b_3(a_1+b_1)z \\ 2a_1b_1(a_3+b_3)x \\ z_{2,2} \\ 2a_3b_3(a_1+b_1)z \end{bmatrix}, \quad \mathbf{w}_{s3} = a \begin{bmatrix} -2a_1b_1(a_2+b_2)x \\ -2a_2b_2(a_1+b_1)y \\ x_{3,3} \\ 2a_1b_1(a_2+b_2)x \\ 2a_2b_2(a_1+b_1)y \\ z_{3,3} \end{bmatrix},$$

$$\mathbf{w}_{s4} = \begin{bmatrix} -\mathbf{v}_4 \\ \mathbf{v}_4 \end{bmatrix}, \quad \mathbf{v}_4 = \begin{bmatrix} y_{1,1} \\ a_2b_2(a_1-b_1)(a_3+b_3)y \\ a_3b_3(a_1-b_1)(a_2+b_2)z \end{bmatrix},$$

$$\mathbf{w}_{s5} = \begin{bmatrix} -\mathbf{v}_5 \\ \mathbf{v}_5 \end{bmatrix}, \quad \mathbf{v}_5 = \begin{bmatrix} a_1b_1(a_2-b_2)(a_3+b_3)x \\ y_{2,2} \\ a_3b_3(a_1+b_1)(a_2-b_2)z \end{bmatrix},$$

$$\mathbf{w}_{s6} = \begin{bmatrix} -\mathbf{v}_6 \\ \mathbf{v}_6 \end{bmatrix}, \quad \mathbf{v}_6 = \begin{bmatrix} a_1b_1(a_2+b_2)(a_3-b_3)x \\ a_2b_2(a_1+b_1)(a_3-b_3)y \\ y_{3,3} \end{bmatrix}.$$

and

$$\begin{aligned} x_{1,1} =& a_1[(a_2+b_2)(a_3+b_3)(a-x) - (a_2-b_2)(a_3+b_3)y - (a_2+b_2)(a_3-b_3)z], \\ x_{2,2} =& a_2[(a_1+b_1)(a_3+b_3)(a-y) - (a_1-b_1)(a_3+b_3)x - (a_1+b_1)(a_3-b_3)z], \\ x_{3,3} =& a_3[(a_1+b_1)(a_2+b_2)(a-z) - (a_1-b_1)(a_2+b_2)x - (a_1+b_1)(a_2-b_2)y], \end{aligned}$$

$$\begin{aligned} y_{1,1} =& a_1b_1[(a_2+b_2)(a_3+b_3)a - (a_2-b_2)(a_3+b_3)y - (a_2+b_2)(a_3-b_3)z], \\ y_{2,2} =& a_2b_2[(a_1+b_1)(a_3+b_3)a - (a_1-b_1)(a_3+b_3)x - (a_1+b_1)(a_3-b_3)z], \\ y_{3,3} =& a_3b_3[(a_1+b_1)(a_2+b_2)a - (a_1-b_1)(a_2+b_2)x - (a_1+b_1)(a_2-b_2)y], \end{aligned}$$

$$\begin{aligned} z_{1,1} =& b_1[(a_2+b_2)(a_3+b_3)(a+x) - (a_2-b_2)(a_3+b_3)y - (a_2+b_2)(a_3-b_3)z], \\ z_{2,2} =& b_2[(a_1+b_1)(a_3+b_3)(a+y) - (a_1-b_1)(a_3+b_3)x - (a_1+b_1)(a_3-b_3)z], \\ z_{3,3} =& b_3[(a_1+b_1)(a_2+b_2)(a+z) - (a_1-b_1)(a_2+b_2)x - (a_1+b_1)(a_2-b_2)y]. \end{aligned}$$

The static workspace of the planar mechanism always includes the line segments between the corresponding centre points of the four sides of the square. And if the ratio between the stiffness and the preload of the springs changes, the direction in which the workspace changes the most is the diagonals of the square. For the spatial mechanism, the static workspace is similar to a ball with six bumps which point to the six pulleys on the diagonal directions. From the numerical results, it can be seen that the largest variation of the workspace boundary caused by the parameters of the springs is the diagonal directions of the octahedron. Along the line orthogonal to two opposite planes of the octahedron, the diameter of the inscribed sphere of the octahedron is always included in the workspace boundary.

Because the mechanism is symmetric, the cable forces have the same characteristics when the end-effector is moving along the lines orthogonal to the faces or moving along the diagonals. Therefore, in the following sections, we will analyze the trajectories in one of these directions for the two mechanisms separately. For the planar mechanism, the line orthogonal to an edge is analyzed using the x axis direction and the diagonal trajectory using $x = y$ direction. For the spatial mechanism, the direction along $x = y = z$ is used for the line orthogonal to a face and the x axis is used for the diagonal trajectory.

6.4 Mechanical Bandwidth and Actuating Force

In this section, the frequency limitations for a periodic sinusoidal trajectory for the two special directions will be obtained for both the planar and the spatial mechanisms. The corresponding required actuating forces will be found.

6.4.1 Planar Mechanism

6.4.1.1 Direction Orthogonal to an Edge

For the planar mechanism, the x axis direction is used to analyze the cable force characteristics in a direction orthogonal to an edge. When the end-effector is on the x axis, the cable forces can

be simplified to as

$$f_{b1} = f_{a2} = \frac{a_2(a_1+a_2)}{2\Upsilon}\left\{a_1 m_p \ddot{x} + (x-r)\left[f_o + \frac{k}{4}(a_1+a_2-2\sqrt{2}r)\right]\right\}, \tag{6.17}$$

$$f_{b2} = f_{a1} = -\frac{a_1(a_1+a_2)}{2\Upsilon}\left\{a_2 m_p \ddot{x} + (x+r)\left[f_o + \frac{k}{4}(a_1+a_2-2\sqrt{2}r)\right]\right\}, \tag{6.18}$$

where $\Upsilon = 2rx^2 - 4r^3 - 2r\sqrt{4r^4+x^4}$, $a_1 = \sqrt{(r-x)^2+r^2}$, $a_2 = \sqrt{(r+x)^2+r^2}$. It can be observed that Υ is always negative when the end-effector is moving along the x axis and $x \in [-r, r]$.

Suppose the trajectory and the acceleration of the end-effector are

$$\mathbf{p} = \begin{bmatrix} r\sin(\omega t) \\ 0 \end{bmatrix}, \qquad \ddot{\mathbf{p}} = \begin{bmatrix} -r\omega^2\sin(\omega t) \\ 0 \end{bmatrix}.$$

Because cables can only works in tension, there will exist a maximum frequency which ensures that $\frac{2\Upsilon f_{b1}}{a_2(a_1+a_2)}$ is negative and $-\frac{2\Upsilon f_{b2}}{a_1(a_1+a_2)}$ is positive. This frequency will be determined. Then, the conditions which ensure that the cable forces are positive for different kinds of springs are analyzed.

(1) If the springs used in the mechanism are constant force springs, substituting $\mathbf{p}$ and $\ddot{\mathbf{p}}$ into Eq. (6.17) and Eq. (6.18), then the condition which ensure that the cable forces are positive are

$$q = \frac{f_o}{m_p r\omega^2} \geq \frac{-s_{\omega t}\sqrt{2-2s_{\omega t}+s_{\omega t}^2}}{1-s_{\omega t}} \tag{6.19}$$

$$q = \frac{f_o}{m_p r\omega^2} \geq \frac{s_{\omega t}\sqrt{2+2s_{\omega t}+s_{\omega t}^2}}{1+s_{\omega t}} \tag{6.20}$$

where $s_{\omega t} = \sin(\omega t)$. If $s_{\omega t}$ is considered as the variable argument of the functions defined by the right-hand side of Eq. (6.19) and Eq. (6.20), the derivative of the function defined by the right-hand side of Eq. (6.19) is always negative as $s_{\omega t}$ belongs to the interval $[-1, 1]$. Therefore, it is a decreasing function, the largest value of function shown in Eq. (6.19) appears when $s_{\omega t} = -1$. Similarly, the significant value for q appears when $s_{\omega t} = 1$ according to Eq. (6.20). From Eq. (6.19) and Eq. (6.20), we get the same condition which can maintain the cable forces in tension. That is

$$q \geq \frac{\sqrt{5}}{2}. \tag{6.21}$$

Then, the maximum frequency is

$$\omega_{max} = \sqrt{\frac{2f_o}{\sqrt{5}m_p r}}. \tag{6.22}$$

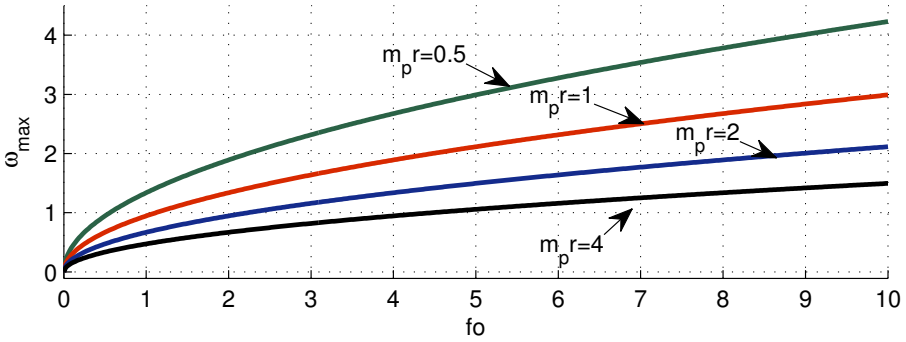

Figure 6.1: Plots of maximum frequency of the planar mechanism along the direction orthogonal to an edge for different values of $m_p r$.

For different values of $m_p r$, the plot for Eq. (6.22) is shown in Figure 6.1.

(2) If the springs used in the mechanism have a nonzero stiffness, the mechanism has a large enough workspace if the ratio of $\frac{kr}{f_o}$ is properly adjusted.

The end-effector can reach the four fixed pulleys only when the factor $\frac{kr}{f_o}$ is smaller than $\sqrt{2}$ but no matter what is the amount of factor $\frac{kr}{f_o}$ the workspace always includes the line segments within the square along the x and y axes. So when the preloaded springs have the stiffness, based on Eq. (6.17) and Eq. (6.18) the condition that maintains the cable forces in tension can be modified as

$$q = \frac{f_o}{m_p r\omega^2} \geq \frac{-s_{\omega t} a_{s_{\omega t}1}}{[1 - s_{\omega t}]\left\{1 + \frac{d}{4}\left[a_{s_{\omega t}1} + a_{s_{\omega t}2} - 2\sqrt{2}\right]\right\}} \tag{6.23}$$

$$q = \frac{f_o}{m_p r\omega^2} \geq \frac{s_{\omega t} a_{s_{\omega t}2}}{[1 + s_{\omega t}]\left\{1 + \frac{d}{4}\left[a_{s_{\omega t}1} + a_{s_{\omega t}2} - 2\sqrt{2}\right]\right\}} \tag{6.24}$$

where $a_{s_{\omega t}1} = \sqrt{2 - 2s_{\omega t} + s_{\omega t}^2}$, $a_{s_{\omega t}2} = \sqrt{2 + 2s_{\omega t} + s_{\omega t}^2}$ and $d = \frac{kr}{f_o}$.

Considering the physical meaning of factor q which has to be positive and using a method similar to the one applied for the constant force springs mechanism, it can be found that the significant value of q appears when $s_{\omega t} = -1$ for Eq. (6.23) and $s_{\omega t} = 1$ for Eq. (6.24). Then we get the same condition which can guarantee that the cables are not slack, i.e.,

$$q \geq \frac{\sqrt{5}}{2 + \frac{d}{2}(1 + \sqrt{5} - 2\sqrt{2})}. \tag{6.25}$$

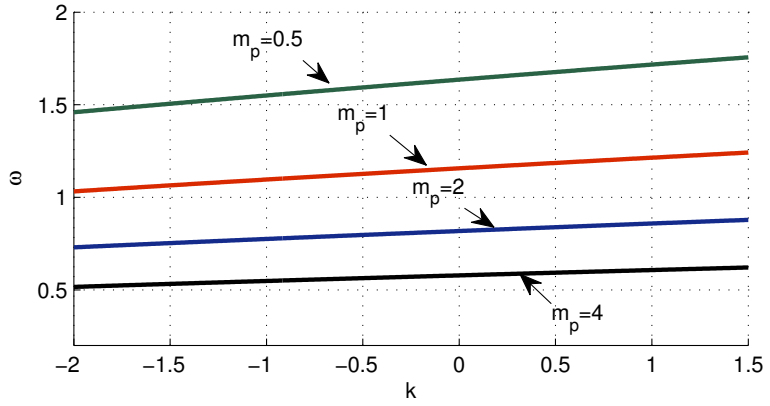

Figure 6.2: Trajectory frequency limit along a direction orthogonal to an edge for different end-effector masses.

Then, the maximum frequency for this trajectory is

$$\omega_{max} = \sqrt{\frac{f_o}{m_p r}} \frac{\sqrt{2 + \frac{d}{2}(1 + \sqrt{5} - 2\sqrt{2})}}{\sqrt[4]{5}}. \tag{6.26}$$

Suppose the frequency of the trajectory is the above ω_{max}, the actuating forces can be modified as

$$f_{m1} = -f_{m2} = f_o f_{ab} + \frac{m_m f_o}{m_p} f_{m_m l_m}, \tag{6.27}$$

where

$$\begin{aligned} f_{ab} = &- \frac{[4 + d(1 + \sqrt{5} - 2\sqrt{2})] s_{\omega t} a_{s_{\omega t}1} a_{s_{\omega t}2}}{4\sqrt{5}[(1 + s_{\omega t}) a_{s_{\omega t}1} + (1 - s_{\omega t}) a_{s_{\omega t}2}]} + \frac{(1 + s_{\omega t}) a_{s_{\omega t}1} - (1 - s_{\omega t}) a_{s_{\omega t}2}}{2[(1 + s_{\omega t}) a_{s_{\omega t}1} + (1 - s_{\omega t}) a_{s_{\omega t}2}]} \\ &\left[1 + \frac{d}{4}\left(a_{s_{\omega t}1} + a_{s_{\omega t}2} - 2\sqrt{2}\right)\right], \\ f_{m_m l_m} = &\frac{4 + d(1 + \sqrt{5} - 2\sqrt{2})}{2\sqrt{5}} \left[\frac{s_{\omega t}(s_{\omega t} - 1)}{a_{s_{\omega t}1}} - \frac{a(a+1)}{a_{s_{\omega t}2}} + \frac{1 - s_{\omega t}^2}{2a_{s_{\omega t}1}^3} - \frac{1 - s_{\omega t}^2}{2a_{s_{\omega t}2}^3}\right]. \end{aligned}$$

When $s_{\omega t} = \pm 1$, the actuating force has the maximum absolute value

$$f_{m,max} = \frac{4 + d(1 + \sqrt{5} - 2\sqrt{2})}{5} \frac{m_m f_o}{m_p}. \tag{6.28}$$

Normalizing the ratio between the half side length of the footprint square and the springs' preload as a unit, the plot of the Eq. (6.26) is shown in Figure 6.2 for different values of m_p.

Normalizing the mass of the end-effector and the square length as $m_p = 1$, $r = 1$, $\omega = 1$. Let $q = \frac{\sqrt{5}}{2 + \frac{d}{2}(1 + \sqrt{5} - 2\sqrt{2})}$ and $f_o = q m_p r \omega^2$, the plots for the cable forces f_{bi}, f_{ai}, $i = 1, 2$, for $d = 0$,

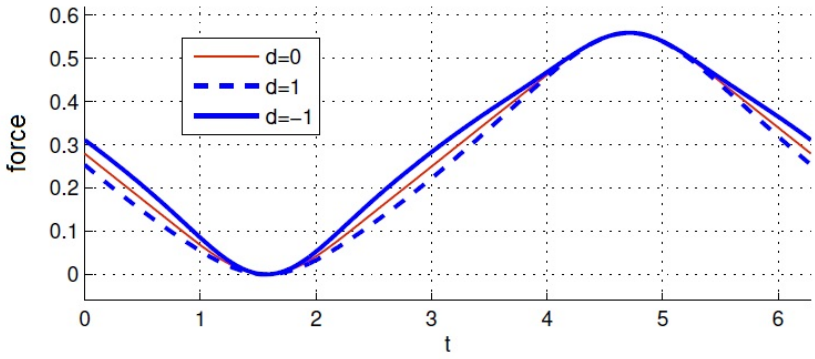

(a) f_{a1} and f_{b2}

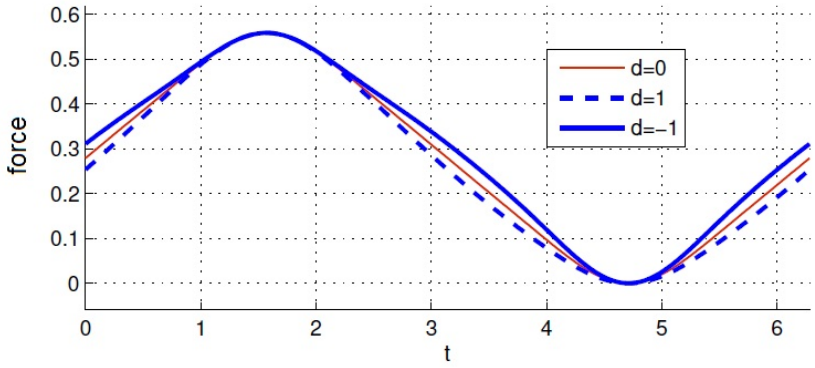

(b) f_{a2} and f_{b1}

Figure 6.3: Plots of the cable forces for $d = 0$, $d = 1$ and $d = -1$.

$d = 1$ and $d = -1$ are shown in Figure 6.3.

Since the mechanism is symmetric, the results of Eq. (6.22) and Eq. (6.26) can be obtained for such a trajectory in the y direction.

6.4.1.2 Diagonal Direction

It was shown in Chapters 3 and 4 that the workspace boundary of the mechanism will retract to the centre of the square formed by the four fixed pulley $A_1A_2B_1B_2$ if the ratio between the stiffness and the preload of the springs is increased. Moreover, the main directions in which the workspace boundary contracts significantly are along the two diagonals. Therefore, the moving trajectory along the diagonals should be analyzed. As the mechanism is symmetric, the positive diagonal will be used in the following analysis. When $x = y$, the cable forces expressed in Eq. (6.15) can be expressed as

$$f_{a1} = f_{b1} = \frac{1}{4}f_{s1} = \frac{1}{4}f_o + \frac{\sqrt{2}k}{8}\left(\sqrt{r^2+x^2} - r\right), \tag{6.29}$$

$$f_{a2} = \frac{f_o}{4} - \frac{x}{2\sqrt{x^2+r^2}}\left[\frac{f_o}{2} + \frac{\sqrt{2}k}{4}\left(\sqrt{r^2+x^2} - r\right)\right] - \frac{\sqrt{2}}{2}m_p\ddot{x}, \tag{6.30}$$

$$f_{b2} = \frac{f_o}{4} + \frac{x}{2\sqrt{x^2+r^2}}\left[\frac{f_o}{2} + \frac{\sqrt{2}k}{4}\left(\sqrt{r^2+x^2} - r\right)\right] + \frac{\sqrt{2}}{2}m_p\ddot{x}. \tag{6.31}$$

The end-effector certainly cannot reach the four fixed pulleys in practice. Here, it is supposed that the amplitude of the movement is the same as that of the analyzed trajectory in the x direction. That is to say, the trajectory and the acceleration of the end-effector are

$$\mathbf{p} = \begin{bmatrix} \frac{\sqrt{2}}{2}r\sin(\omega t) \\ \frac{\sqrt{2}}{2}r\sin(\omega t) \end{bmatrix}, \quad \ddot{\mathbf{p}} = \begin{bmatrix} -\frac{\sqrt{2}}{2}r\omega^2\sin(\omega t) \\ -\frac{\sqrt{2}}{2}r\omega^2\sin(\omega t) \end{bmatrix}.$$

Substituting $\mathbf{p}$ in Eq. (6.29), Eq. (6.30) and Eq. (6.31), the cable forces can be expressed as

$$f_{a1} = f_{b1} = \frac{1}{4}f_o + \frac{kr}{8}(a_{s_{\omega t}} - \sqrt{2}), \tag{6.32}$$

$$f_{a2} = \frac{1}{4}f_o(1 - \frac{s_{\omega t}}{a_{s_{\omega t}}}) + \frac{kr}{8}(\frac{\sqrt{2}s_{\omega t}}{a_{s_{\omega t}}} - s_{\omega t}) + \frac{1}{2}m_p r\omega^2 s_{\omega t}, \tag{6.33}$$

$$f_{b2} = \frac{1}{4}f_o(1 + \frac{s_{\omega t}}{a_{s_{\omega t}}}) - \frac{kr}{8}(\frac{\sqrt{2}s_{\omega t}}{a_{s_{\omega t}}} - s_{\omega t}) - \frac{1}{2}m_p r\omega^2 s_{\omega t}. \tag{6.34}$$

where $a_{s_{\omega t}} = \sqrt{2 + s_{\omega t}^2}$.

In order to get a significantly large workspace, the ratio d needs to be within a certain range if the springs have stiffness, no matter whether it is negative or positive. For the sake of maintaining the cable forces f_{a1} and f_{b1} in tension, the following inequality should be satisfied:

$$d = \frac{kr}{f_o} \geqslant \frac{2}{\sqrt{2} - \sqrt{2 + s_{\omega t}^2}}.$$

When $s_{\omega t}$ equals 1 or -1, we get the minimal value of d, that is $-2(\sqrt{2} + \sqrt{3})$.

Substituting $d = \frac{kr}{f_o}$ into Eq. (6.33) and Eq.(6.34), the coefficients of $\frac{1}{4} f_o$ for these two equations are

$$f_{fo1} = (1 - \frac{s_{\omega t}}{a_{s_{\omega t}}}) + \frac{d}{2}(\frac{\sqrt{2} s_{\omega t}}{a_{s_{\omega t}}} - s_{\omega t}),$$
$$f_{fo2} = (1 + \frac{s_{\omega t}}{a_{s_{\omega t}}}) - \frac{d}{2}(\frac{\sqrt{2} s_{\omega t}}{a_{s_{\omega t}}} - s_{\omega t}).$$

It can be found that both f_{fo1} and f_{fo2} are positive when $\frac{\sqrt{3}+1}{\sqrt{2}-\sqrt{3}} < \frac{d}{2} < \frac{\sqrt{3}-1}{\sqrt{3}-\sqrt{2}}$. Actually, the chosen d should always be within this range. Then, in order to maintain the cable forces f_{a2} and f_{b2} in tension, from Eq. (6.33) and Eq. (6.34), we get

$$q = \frac{f_o}{m_p r \omega^2} \geqslant \frac{-2 s_{\omega t} a_{s_{\omega t}}}{(a_{s_{\omega t}} - s_{\omega t}) + \frac{d}{2}(\sqrt{2} s_{\omega t} - s_{\omega t} a_{s_{\omega t}})},$$
$$q = \frac{f_o}{m_p r \omega^2} \geqslant \frac{2 s_{\omega t} a_{s_{\omega t}}}{(a_{s_{\omega t}} + s_{\omega t}) - \frac{d}{2}(\sqrt{2} s_{\omega t} - s_{\omega t} a_{s_{\omega t}})}.$$

The above relationship can be reduced to

$$q \geqslant \frac{2\sqrt{3}}{(\sqrt{3} + 1) + \frac{d}{2}(\sqrt{3} - \sqrt{2})}. \tag{6.35}$$

Then, the affordable maximum trajectory frequency is

$$\omega_{max} = \sqrt{\frac{f_o}{m_p r} \left[\left(\frac{1}{2} + \frac{1}{2\sqrt{3}} \right) + \frac{1}{4} d \left(1 - \sqrt{\frac{2}{3}} \right) \right]}. \tag{6.36}$$

Since f_{a1} and f_{b1} are equal to each other, the required actuating force of M_1 is zero, that is to say $f_{m1} = 0$. If the end-effector is moving with the largest frequency, f_{m2} can be expressed as

$$f_{m2} = \frac{f_o s_{\omega t}}{2} \left[1 + \frac{\sqrt{3}}{3} - \frac{2}{a_{s_{\omega t}}} + \frac{d}{2} \left(\frac{\sqrt{2}}{a_{s_{\omega t}}} - \sqrt{\frac{2}{3}} \right) \right] + \frac{m_m f_o s_{\omega t}}{m_p} \left[\frac{1}{2} + \frac{1}{2\sqrt{3}} + d \left(\frac{1}{4} - \frac{\sqrt{2}}{4\sqrt{3}} \right) \right]. \tag{6.37}$$

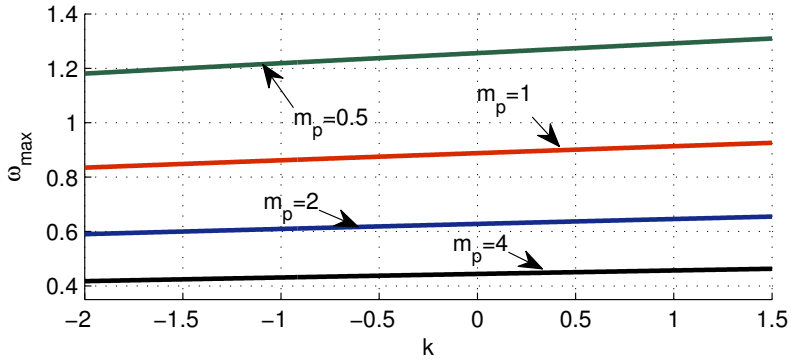

Figure 6.4: Plot of the maximum trajectory frequency for the diagonal direction and for different values of m_p.

When $s_{\omega t} = \pm 1$, the actuating force f_{m2} has the maximum absolute value as

$$f_{m2,max} = f_o(1 - \frac{\sqrt{3}}{3}) + \frac{m_m f_o}{m_p}\left[(\frac{1}{2} + \frac{1}{2\sqrt{3}}) + d(\frac{1}{4} - \frac{\sqrt{2}}{4\sqrt{3}})\right].$$

Normalizing the ratio between the half square side length and the preload of the springs as a unit $\frac{f_o}{r} = 1$, the plot of the maximum frequency for different values of m_p is shown in Figure 6.4.

Assuming the mass of the end-effector and the half square side length as $m_p = 1$ and $r = 1$ and assuming that the preload of the springs is $f_o = 1$, let $q = \frac{4\sqrt{3}}{2(\sqrt{3}+1)+d(\sqrt{3}-\sqrt{2})}$, then the maximum frequency of the trajectory should be $\omega = \sqrt{\frac{f_o}{m_p r q}}$. The plots of the cable forces for $k = 0$ and $k = -1.5$ are shown in Figure 6.5.

6.4.2 Spatial Mechanism

6.4.2.1 Motion along a Direction Orthogonal to a Face

When $x = y = z$, the cable force equations can be simplified as

$$f_{ai} = \frac{a_1}{d_3}\left\{(a - 3x)[\frac{f_o}{2} + \frac{k}{8}(a_1 + b_1 - 2a)] - m_p \ddot{x} b_1\right\}, \tag{6.38}$$

$$f_{bi} = \frac{b_1}{d_3}\left\{(a + 3x)[\frac{f_o}{2} + \frac{k}{8}(a_1 + b_1 - 2a)] + m_p \ddot{x} a_1\right\}, \tag{6.39}$$

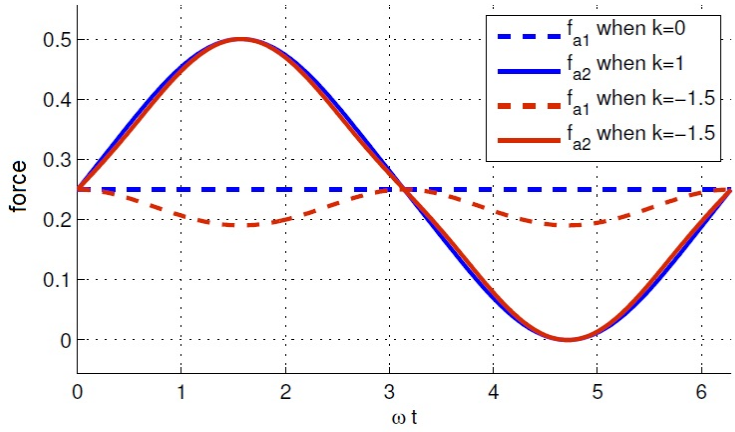

(a) f_{a1} and f_{a2}

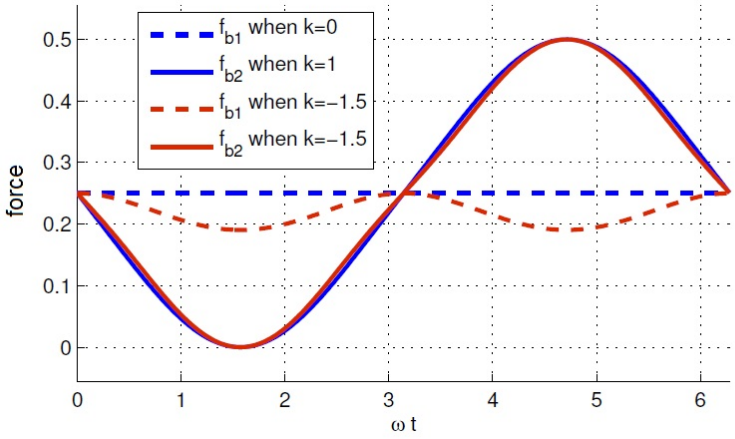

(b) f_{b1} and f_{b2}

Figure 6.5: Plots of the cable forces when the end-effector move in the diagonal direction for $k = 0$ and $k = -1.5$.

where $a_1 = \sqrt{3x^2 + 2ax + a^2}$, $b_1 = \sqrt{3x^2 - 2ax + a^2}$, $d_3 = a(a_1 + b_1) - 3x(a_1 - b_1)$ and $i = 1, 2, 3$. Because $\frac{a_1}{d_3}$ and $\frac{b_1}{d_3}$ are always positive, the conditions which guarantee that the cable forces are positive are

$$(a - 3x)[\tfrac{f_o}{2} + \tfrac{k}{8}(a_1 + b_1 - 2a)] - m_p\ddot{x}b_1 \geq 0 \tag{6.40}$$

$$(a + 3x)[\tfrac{f_o}{2} + \tfrac{k}{8}(a_1 + b_1 - 2a)] + m_p\ddot{x}a_1 \geq 0 \tag{6.41}$$

Since the static workspace boundary in this direction is at a distance of $\frac{\sqrt{3}}{3}$ from the centre of the octahedron, the trajectory can be defined as

$$\mathbf{p} = \frac{1}{3}a\sin(\omega t)\begin{bmatrix} 1 & 1 & 1 \end{bmatrix}^T.$$

For this trajectory, Eq. (6.40) and Eq. (6.41) can be written as

$$f_o(1 - s_{\omega t})\left[\tfrac{1}{2} + \tfrac{\rho}{8}\left(a_{xyz} + b_{xyz} - 2\right)\right] + \tfrac{1}{3}m_p a\omega^2 s_{\omega t} b_{xyz} \geq 0,$$
$$f_o(1 + s_{\omega t})\left[\tfrac{1}{2} + \tfrac{\rho}{8}\left(a_{xyz} + b_{xyz} - 2\right)\right] - \tfrac{1}{3}m_p a\omega^2 s_{\omega t} a_{xyz} \geq 0,$$

where $\rho = \frac{ka}{f_o}$, $a_{xyz} = \sqrt{\frac{1}{3}s_{\omega t}^2 + \frac{2}{3}s_{\omega t} + 1}$ and $b_{xyz} = \sqrt{\frac{1}{3}s_{\omega t}^2 - \frac{2}{3}s_{\omega t} + 1}$. It can be observed that the coefficients of the preload f_o are always positive. The condition which ensures that the cable forces are positive expressed as a function of the ratio of the mechanism parameters and the trajectory frequency can be obtained as

$$\frac{f_o}{m_p a\omega^2} \geq \frac{\sqrt{2}}{3 + \frac{\rho}{4}(3\sqrt{2} + \sqrt{6} - 6)} \tag{6.42}$$

The maximum trajectory frequency for a certain workspace boundary is then

$$\omega_{max} = \sqrt{\frac{f_o}{m_p a}[\frac{3\sqrt{2}}{2} + \frac{\rho}{4}(3 + \sqrt{3} - 3\sqrt{2})]}. \tag{6.43}$$

If the springs are constant force springs, $\rho = 0$, then the maximum trajectory frequency can be found as $\sqrt{\frac{3\sqrt{2}f_o}{2m_p a}}$.

When the end-effector moves in the direction defined as $x = y = z$, the actuating forces are

$$f_{mi} = f_{f_o i} f_o + f_{m_p i} m_p a\omega^2 + f_{m_m i} m_m a\omega^2, \tag{6.44}$$

where

$$f_{f_o i} = \frac{(s_{\omega t} - 1)a_{xyz} + (1 + s_{\omega t})b_{xyz}}{(1 - s_{\omega t})a_{xyz} + (1 + s_{\omega t})b_{xyz}}\left[\frac{1}{2} + \frac{\rho}{8}(a_{xyz} + b_{xyz} - 2)\right],$$
$$f_{m_p i} = -\frac{2}{3}\frac{s_{\omega t} a_{xyz} b_{xyz}}{(1 - s_{\omega t})a_{xyz} + (1 + s_{\omega t})b_{xyz}},$$
$$f_{m_m i} = -\frac{s_{\omega t}}{6}\left(\frac{1 + s_{\omega t}}{a_{xyz}} + \frac{1 - s_{\omega t}}{b_{xyz}}\right) + \frac{1 - s_{\omega t}^2}{18}\left(\frac{1}{a_{xyz}^3} - \frac{1}{b_{xyz}^3}\right).$$

Suppose that the trajectory has the maximum frequency shown in Eq. (6.43), the maximum actuating force is

$$f_{mi,max} = \frac{f_o}{2}(1 + \frac{m_m}{m_p})[1 + \frac{\rho}{4}(\sqrt{2} + \frac{\sqrt{6}}{3} - 2)].$$

6.4.2.2 Diagonal Direction

If the end-effector is moving along the x-axis, Eq. (6.16) can be simplified to

$$f_{a1} = \frac{1}{4}f_o - \frac{x}{\sqrt{a^2+x^2}}\left[\frac{1}{2}f_o + \frac{k}{4}\left(\sqrt{a^2+x^2} - a\right)\right] - \frac{1}{2}m_p\ddot{x}, \tag{6.45}$$

$$f_{b1} = \frac{1}{4}f_o + \frac{x}{\sqrt{a^2+x^2}}\left[\frac{1}{2}f_o + \frac{k}{4}\left(\sqrt{a^2+x^2} - a\right)\right] + \frac{1}{2}m_p\ddot{x}, \tag{6.46}$$

$$f_{ai} = f_{bi} = \frac{1}{4}f_o + \frac{k}{8}\left(\sqrt{a^2+x^2} - a\right), \qquad i = 2, 3. \tag{6.47}$$

It can be observed that the cable forces f_{ai} and f_{bi}, $i = 2, 3$, are always positive if $\frac{ka}{f_o} > \frac{2}{1-\sqrt{1+(\frac{x}{a})^2}}$. It is verified that the workspace boundary point on this direction is larger than $\frac{\sqrt{3}}{3}a$ from the centre of the octahedron if the springs are negative stiffness springs. Substituting $\frac{\sqrt{3}}{3}a$, the minimum value of $\frac{ka}{f_o}$ is about -13. In practice, the springs' stiffness cannot be so small. Hence, we can say that the cable forces f_{ai} and f_{bi}, $i = 2, 3$, are always positive.

Assume the trajectory of the end-effector to be

$$\mathbf{p} = \lambda a \sin(\omega t)\mathbf{e}, \tag{6.48}$$

where $\mathbf{e} = [1, 0, 0]^T$ and $\lambda > 0$. Eq. (6.45) and Eq. (6.46) can be simplified as

$$f_{a1} = \frac{1}{4}f_o - \frac{\lambda_{\omega t}}{a_{diag}}\left[\frac{1}{2}f_o + \frac{ka}{4}\left(a_{diag} - 1\right)\right] + \frac{1}{2}m_p a\omega^2\lambda_{\omega t}, \tag{6.49}$$

$$f_{b1} = \frac{1}{4}f_o + \frac{\lambda_{\omega t}}{a_{diag}}\left[\frac{1}{2}f_o + \frac{ka}{4}\left(a_{diag} - 1\right)\right] - \frac{1}{2}m_p a\omega^2\lambda_{\omega t}, \tag{6.50}$$

where $\lambda_{\omega t} = \lambda \sin(\omega t)$ and $a_{diag} = \sqrt{1 + \lambda_{\omega t}^2}$.

In order to maintain f_{a1} and f_{b1} be positive, the following relationships should be satisfied

$$f_o\left[\frac{1}{2} - \frac{\lambda_{\omega t}}{a_{diag}} - \frac{\rho\lambda_{\omega t}}{2}\left(1 - \frac{1}{a_{diag}}\right)\right] \geq -m_p a\omega^2\lambda_{\omega t}, \tag{6.51}$$

$$f_o\left[\frac{1}{2} + \frac{\lambda_{\omega t}}{a_{diag}} + \frac{\rho\lambda_{\omega t}}{2}\left(1 - \frac{1}{a_{diag}}\right)\right] \geq m_p a\omega^2\lambda_{\omega t}. \tag{6.52}$$

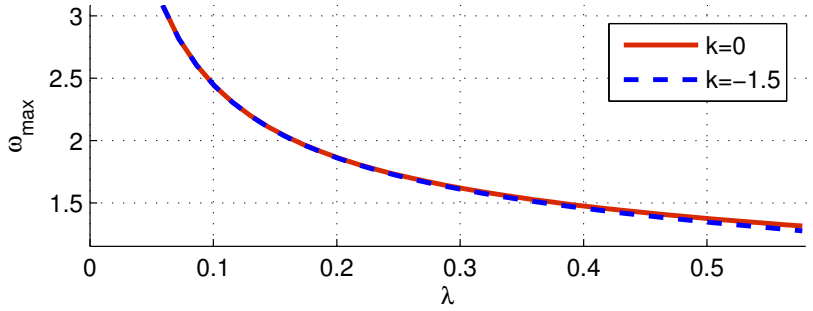

Figure 6.6: The relationship between λ and ω_{max}.

In Chapter 4, it was shown that the mechanism has a better workspace with negative stiffness springs. When $\rho < 0$ and $\lambda \in [0, \frac{\sqrt{3}}{3}]$, the coefficients of f_o in Eq. (6.51) and Eq. (6.52) are always positive. The condition which can ensure that the cable forces f_{a1} and f_{b1} are positive can be found as

$$\frac{f_o}{m_p a\omega^2} \geq \frac{2\lambda\sqrt{1+\lambda^2}}{\sqrt{1+\lambda^2}+2\lambda+\rho\lambda(\sqrt{1+\lambda^2}-1)}. \tag{6.53}$$

Then, the maximum trajectory frequency can be determined as

$$\begin{aligned} &\omega_{max} = \sqrt{\frac{f_o}{m_p a}}\sqrt{\frac{\sqrt{1+\lambda^2}+2\lambda+\rho\lambda(\sqrt{1+\lambda^2}-1)}{2\lambda\sqrt{1+\lambda^2}}}, \\ &s.t. \quad \lambda \in (0, \frac{\sqrt{3}}{3}), \qquad \rho < 0. \end{aligned} \tag{6.54}$$

Similarly to the diagonal direction of motion of the planar mechanism, the cable forces which are not in this direction are equal to each other, $f_{ai} = f_{bi}$, $i = 2, 3$. Then, the actuating force of the corresponding actuators is equal to zero. If the end-effector moving at the trajectory frequency, the maximum actuating force $f_{m1,max}$ is

$$f_{m1,max} = (\frac{1}{2} + \frac{m_m}{2m_p})f_o + \frac{m_m\lambda}{m_p\sqrt{1+\lambda^2}}f_o\left[1+\frac{\rho}{2}(\sqrt{1+\lambda^2}-1)\right].$$

Normalizing the parameters of the mechanism, the half of the diagonal is $a = 1$, the mass of the end-effector is $m_p = 1$ and the preload of the springs is $f_o = 1$. Based on Eq. (6.54), the relationships between the workspace boundary point on the diagonal of the octahedron λ and the maximum frequency of the trajectory ω_{max} for different values of springs stiffness are shown in Figure 6.6. It can be seen that the maximum frequency is smaller when the larger the workspace is desired.

The periodic sinusoidal trajectories on the two special directions were used to obtain the basic requirements of the mechanism's parameters. But there are many kinds of trajectories, and the above analysis is not sufficient to get the overall behaviour of the mechanism. In the following section, the natural frequency of the mechanisms will be analyzed.

6.5 Natural Frequency

The natural frequency of the mechanisms will be obtained based on the Newton-Euler formulation and the ratio of the amplitudes of motion of the actuators and the end-effector will be found.

6.5.1 Planar Mechanism

The dynamic equation for the end-effector Eq. (6.12) can be rewritten as

$$g_1(x,y) = f_{a1}x_{sa1} + f_{b1}x_{sb1} + f_{a2}x_{sa2} + f_{b2}x_{sb2} = m_p\ddot{x},$$
$$g_2(x,y) = f_{a1}y_{sa1} + f_{b1}y_{sb1} + f_{a2}y_{sa2} + f_{b2}y_{sb2} = m_p\ddot{y},$$

where x_{ai}, y_{ai}, x_{bi} and y_{bi} are the x and y components of the unit vectors $\mathbf{s}_{ai}$ and $\mathbf{s}_{bi}$, respectively. In static situation, f_{ai} and f_{bi}, $i = 1, 2$, can be obtained using Eq. (4.10) for a given configuration. Assuming f_{ai} and f_{bi}, $i = 1, 2$, are constant and substituting them in the initial end-effector dynamic equation, then the above dynamic equations can be written as

$$\begin{bmatrix} m_p & 0 \\ 0 & m_p \end{bmatrix} \begin{bmatrix} \ddot{x} \\ \ddot{y} \end{bmatrix} + \begin{bmatrix} \dfrac{\partial g_1}{\partial x} & \dfrac{\partial g_1}{\partial y} \\ \dfrac{\partial g_2}{\partial x} & \dfrac{\partial g_2}{\partial y} \end{bmatrix} \begin{bmatrix} \dot{x} \\ \dot{y} \end{bmatrix} = \begin{bmatrix} 0 \\ 0 \end{bmatrix} \tag{6.55}$$

Let $x = x_o e^{st}$ and $y = y_o e^{st}$, and substituting them into Eq. (6.55), we get

$$\begin{bmatrix} m_p s + \dfrac{\partial g_1}{\partial x} & \dfrac{\partial g_1}{\partial y} \\ \dfrac{\partial g_2}{\partial x} & m_p s + \dfrac{\partial g_2}{\partial y} \end{bmatrix} \begin{bmatrix} x_o \\ y_o \end{bmatrix} = \begin{bmatrix} 0 \\ 0 \end{bmatrix} \tag{6.56}$$

where

$$\frac{\partial g_1}{\partial x} = f_{a1}\frac{-(y_{a1}-y)^2}{[(x_{a1}-x)^2+(y_{a1}-y)^2]^{\frac{3}{2}}} + f_{b1}\frac{-(y_{b1}-y)^2}{[(x_{b1}-x)^2+(y_{b1}-y)^2]^{\frac{3}{2}}} + f_{a2}\frac{-(y_{a2}-y)^2}{[(x_{a2}-x)^2+(y_{a2}-y)^2]^{\frac{3}{2}}} + f_{b2}\frac{-(y_{b2}-y)^2}{[(x_{b2}-x)^2+(y_{b2}-y)^2]^{\frac{3}{2}}},$$

$$\frac{\partial g_1}{\partial y} = \frac{\partial g_2}{\partial x} = f_{a1}\frac{(x_{a1}-x)(y_{a1}-y)}{[(x_{a1}-x)^2+(y_{a1}-y)^2]^{\frac{3}{2}}} + f_{b1}\frac{(x_{b1}-x)(y_{b1}-y)}{[(x_{b1}-x)^2+(y_{b1}-y)^2]^{\frac{3}{2}}} + f_{a2}\frac{(x_{a2}-x)(y_{a2}-y)}{[(x_{a2}-x)^2+(y_{a2}-y)^2]^{\frac{3}{2}}} + f_{b2}\frac{(x_{b2}-x)(y_{b2}-y)}{[(x_{b2}-x)^2+(y_{b2}-y)^2]^{\frac{3}{2}}},$$

$$\frac{\partial g_2}{\partial y} = f_{a1}\frac{-(x_{a1}-x)^2}{[(x_{a1}-x)^2+(y_{a1}-y)^2]^{\frac{3}{2}}} + f_{b1}\frac{-(x_{b1}-x)^2}{[(x_{b1}-x)^2+(y_{b1}-y)^2]^{\frac{3}{2}}} + f_{a2}\frac{-(x_{a2}-x)^2}{[(x_{a2}-x)^2+(y_{a2}-y)^2]^{\frac{3}{2}}} + f_{b2}\frac{-(x_{b2}-x)^2}{[(x_{b2}-x)^2+(y_{b2}-y)^2]^{\frac{3}{2}}}.$$

This equation is satisfied for any x_o and y_o if the determinant of the matrix in the above equation is zero. That is to say

$$m_p^2 s^2 + m_p(\frac{\partial g_1}{\partial x} + \frac{\partial g_2}{\partial y})s + \frac{\partial g_1}{\partial x}\frac{\partial g_2}{\partial y} - \frac{\partial g_1}{\partial y}\frac{\partial g_2}{\partial x} = 0 \tag{6.57}$$

Then, the two natural frequencies can be calculated using the latter equation.

Suppose the rectangle formed by the four fixed pulleys is a square and the side length is $2r$, at the reference configuration ($x = 0$ and $y = 0$), for the static situation, we have

$$f_{s1} = f_{s2} = f_o, \quad f_{a1} = f_{a2} = f_{b1} = f_{b2} = \frac{f_o}{4}.$$

Then, using Eq. (6.57), the natural frequency can be found as

$$s_{o_{1,2}} = \frac{f_o}{2\sqrt{2}m_p r}. \tag{6.58}$$

From Eq. (6.56), two expressions for the ratio of the amplitudes are found:

$$\frac{x_o}{y_o} = -\frac{\frac{\partial g_1}{\partial y}}{m_p s + \frac{\partial g_1}{\partial x}}, \quad or \quad \frac{x_o}{y_o} = -\frac{m_p s + \frac{\partial g_2}{\partial y}}{\frac{\partial g_2}{\partial x}}. \tag{6.59}$$

The substitution of the natural frequencies in either of these equations leads to the ratio of the amplitudes.

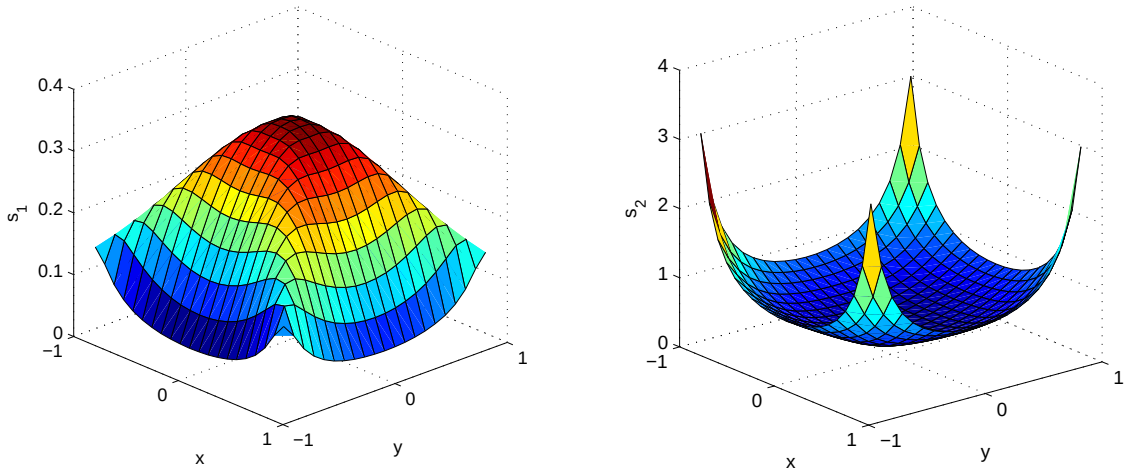

(a) Plot of s_1

(b) Plot of s_2

Figure 6.7: Plots of the natural frequency when $k = 0$ for the planar mechanism.

Normalizing the parameters for the mechanism as $x_{b2} = y_{b2} = 1$, $m_p = 1$, $f_o = 1$, suppose the springs used in the mechanism are constant force springs, then the natural frequencies s_1 and s_2 are shown in Figure 6.7. The corresponding ratio of the amplitudes for these two natural frequencies are shown in Figure 6.8. In these figures, the small black dots represent the position of the end-effector and the small line segments represent the direction associated with the corresponding ratio of the amplitudes. The plots of the two natural frequencies and ratio of the amplitude are symmetric since the mechanism is symmetric. It can be noticed that the directions of the two ratio of amplitude are perpendicular to each other.

If the springs have non-zero stiffness, the shape of surfaces for the two natural frequencies are similar to the surfaces shown in Figure 6.7. Moreover, the natural frequency will increase when the stiffness of the springs is increased. The working frequency of the mechanism should be below the natural frequency s_1 in order to avoid undesired vibration.

6.5.2 Spatial Mechanism

For the spatial mechanism, the dynamic equation of the end-effector is

$$\mathbf{g} = \mathbf{S}_a\mathbf{f}_a + \mathbf{S}_b\mathbf{f}_b = \mathbf{M}_p\ddot{\mathbf{p}} \tag{6.60}$$

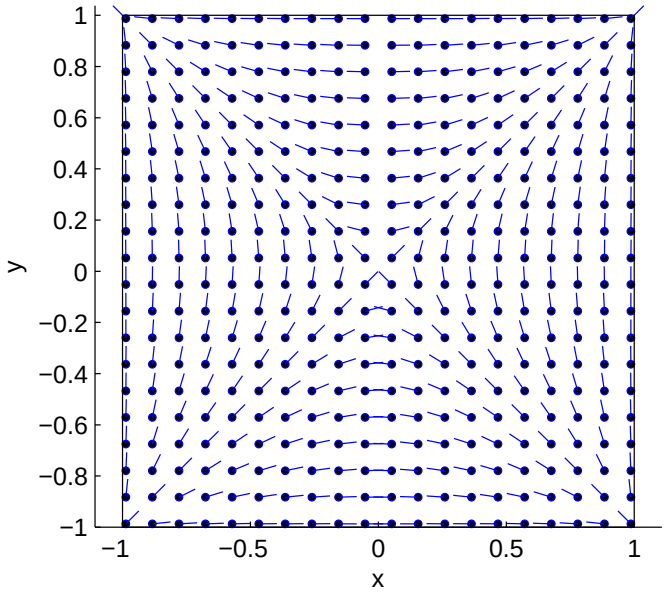

(a) ratio of the amplitudes for s_1

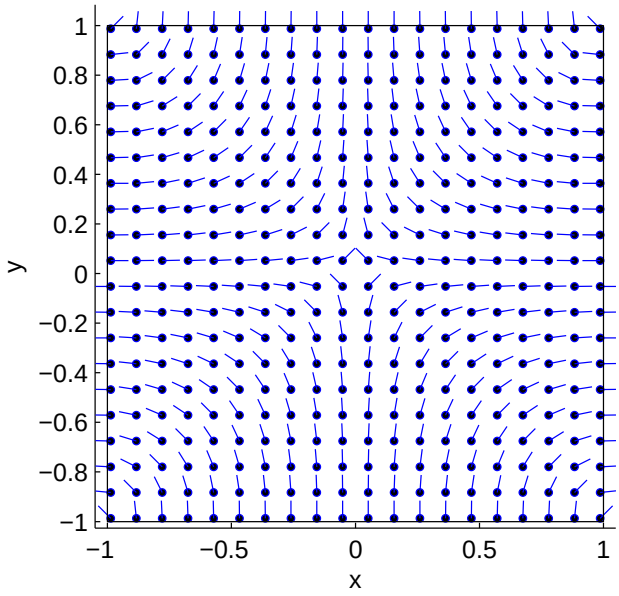

(b) ratio of the amplitudes for s_2

Figure 6.8: Ratio of the amplitudes for the planar mechanism.

where $\mathbf{g}(x,y,z) = [g_1(x,y,z), g_2(x,y,z), g_3(x,y,z)]^T$. In a static situation, the cable forces can be obtained using Eq. (4.10) for a given configuration $\mathbf{p}_p = [x_p, y_p, z_p]^T$. Assuming the cable forces $\mathbf{f}_a$ and $\mathbf{f}_b$ are constant and substituting them in the initial end-effector dynamic equation, then Eq. (6.60) can be rewritten as:

$$\mathbf{M}_p\ddot{\mathbf{p}} + \mathbf{G}\dot{\mathbf{p}} = \mathbf{0} \tag{6.61}$$

where

$$\mathbf{G} = \begin{bmatrix} \dfrac{\partial g_1}{\partial x} & \dfrac{\partial g_1}{\partial y} & \dfrac{\partial g_1}{\partial z} \\ \dfrac{\partial g_2}{\partial x} & \dfrac{\partial g_2}{\partial y} & \dfrac{\partial g_2}{\partial z} \\ \dfrac{\partial g_3}{\partial x} & \dfrac{\partial g_3}{\partial y} & \dfrac{\partial g_3}{\partial z} \end{bmatrix}.$$

and

$$\begin{aligned}
\frac{\partial g_1}{\partial x} =& f_{a1}\frac{-y^2-z^2}{[(x+a)^2+y^2+z^2]^{\frac{3}{2}}} + f_{a2}\frac{-(y+a)^2-z^2}{[x^2+(y+a)^2+z^2]^{\frac{3}{2}}} + f_{a3}\frac{-y^2-(z+a)^2}{[x^2+y^2+(z+a)^2]^{\frac{3}{2}}} \\
&+ f_{b1}\frac{-y^2-z^2}{[(x-a)^2+y^2+z^2]^{\frac{3}{2}}} + f_{b2}\frac{-(y-a)^2-z^2}{[x^2+(y-a)^2+z^2]^{\frac{3}{2}}} + f_{b3}\frac{-y^2-(z-a)^2}{[x^2+y^2+(z-a)^2]^{\frac{3}{2}}},
\end{aligned}$$

$$\begin{aligned}
\frac{\partial g_1}{\partial y} = \frac{\partial g_2}{\partial x} =& f_{a1}\frac{(x+a)y}{[(x+a)^2+y^2+z^2]^{\frac{3}{2}}} + f_{a2}\frac{x(y+a)}{[x^2+(y+a)^2+z^2]^{\frac{3}{2}}} + f_{a3}\frac{xy}{[x^2+y^2+(z+a)^2]^{\frac{3}{2}}} \\
&+ f_{b1}\frac{(x-a)y}{[(x-a)^2+y^2+z^2]^{\frac{3}{2}}} + f_{b2}\frac{x(y-a)}{[x^2+(y-a)^2+z^2]^{\frac{3}{2}}} + f_{b3}\frac{xy}{[x^2+y^2+(z-a)^2]^{\frac{3}{2}}},
\end{aligned}$$

$$\begin{aligned}
\frac{\partial g_1}{\partial z} = \frac{\partial g_3}{\partial x} =& f_{a1}\frac{(x+a)z}{[(x+a)^2+y^2+z^2]^{\frac{3}{2}}} + f_{a2}\frac{xz}{[x^2+(y+a)^2+z^2]^{\frac{3}{2}}} + f_{a3}\frac{x(z+a)}{[x^2+y^2+(z+a)^2]^{\frac{3}{2}}} \\
&+ f_{b1}\frac{(x-a)z}{[(x-a)^2+y^2+z^2]^{\frac{3}{2}}} + f_{b2}\frac{xz}{[x^2+(y-a)^2+z^2]^{\frac{3}{2}}} + f_{b3}\frac{x(z-a)}{[x^2+y^2+(z-a)^2]^{\frac{3}{2}}},
\end{aligned}$$

$$\begin{aligned}
\frac{\partial g_2}{\partial y} =& f_{a1}\frac{-(x+a)^2-z^2}{[(x+a)^2+y^2+z^2]^{\frac{3}{2}}} + f_{a2}\frac{-x^2-z^2}{[x^2+(y+a)^2+z^2]^{\frac{3}{2}}} + f_{a3}\frac{-x^2-(z+a)^2}{[x^2+y^2+(z+a)^2]^{\frac{3}{2}}} \\
&+ f_{b1}\frac{-(x-a)^2-z^2}{[(x-a)^2+y^2+z^2]^{\frac{3}{2}}} + f_{b2}\frac{-x^2-z^2}{[x^2+(y-a)^2+z^2]^{\frac{3}{2}}} + f_{b3}\frac{-x^2-(z-a)^2}{[x^2+y^2+(z-a)^2]^{\frac{3}{2}}},
\end{aligned}$$

$$\begin{aligned}
\frac{\partial g_2}{\partial z} = \frac{\partial g_3}{\partial y} =& f_{a1}\frac{yz}{[(x+a)^2+y^2+z^2]^{\frac{3}{2}}} + f_{a2}\frac{(y+a)z}{[x^2+(y+a)^2+z^2]^{\frac{3}{2}}} + f_{a3}\frac{y(z+a)}{[x^2+y^2+(z+a)^2]^{\frac{3}{2}}} \\
&+ f_{b1}\frac{yz}{[(x-a)^2+y^2+z^2]^{\frac{3}{2}}} + f_{b2}\frac{(y-a)z}{[x^2+(y-a)^2+z^2]^{\frac{3}{2}}} + f_{b3}\frac{y(z-a)}{[x^2+y^2+(z-a)^2]^{\frac{3}{2}}},
\end{aligned}$$

$$\begin{aligned}
\frac{\partial g_3}{\partial z} =& f_{a1}\frac{-(x+a)^2-y^2}{[(x+a)^2+y^2+z^2]^{\frac{3}{2}}} + f_{a2}\frac{-x^2-(y+a)^2}{[x^2+(y+a)^2+z^2]^{\frac{3}{2}}} + f_{a3}\frac{-x^2-y^2}{[x^2+y^2+(z+a)^2]^{\frac{3}{2}}} \\
&+ f_{b1}\frac{-(x-a)^2-y^2}{[(x-a)^2+y^2+z^2]^{\frac{3}{2}}} + f_{b2}\frac{-x^2-(y-a)^2}{[x^2+(y-a)^2+z^2]^{\frac{3}{2}}} + f_{b3}\frac{-x^2-y^2}{[x^2+y^2+(z-a)^2]^{\frac{3}{2}}}.
\end{aligned}$$

Assuming $\mathbf{p}_p = [x_p e^{st}, y_p e^{st}, z_p e^{st}]^T$ and substituting it into the above equation, we get

$$(s\mathbf{M}_p + \mathbf{G})\mathbf{p}_p = \mathbf{0} \tag{6.62}$$

This equation is satisfied for any $\mathbf{p}_p$ if the determinant of the matrix $s\mathbf{M}_p + \mathbf{G}$ equals zero, that is to say

$$m_p^3 s^3 + S_1 m_p^2 s^2 + S_2 m_p s + S_3 = 0 \tag{6.63}$$

where

$$\begin{aligned}
S_1 &= \frac{\partial g_1}{\partial x} + \frac{\partial g_2}{\partial y} + \frac{\partial g_3}{\partial z}, \\
S_2 &= \frac{\partial g_1}{\partial x}\frac{\partial g_2}{\partial y} + \frac{\partial g_2}{\partial y}\frac{\partial g_3}{\partial z} + \frac{\partial g_3}{\partial z}\frac{\partial g_1}{\partial x} - \left(\frac{\partial g_1}{\partial y}\right)^2 - \left(\frac{\partial g_1}{\partial z}\right)^2 - \left(\frac{\partial g_2}{\partial z}\right)^2, \\
S_3 &= \frac{\partial g_1}{\partial x}\frac{\partial g_2}{\partial y}\frac{\partial g_3}{\partial z} + 2\frac{\partial g_1}{\partial y}\frac{\partial g_1}{\partial z}\frac{\partial g_2}{\partial z} - \frac{\partial g_1}{\partial x}\left(\frac{\partial g_2}{\partial z}\right)^2 - \left(\frac{\partial g_1}{\partial y}\right)^2\frac{\partial g_3}{\partial z} - \left(\frac{\partial g_1}{\partial z}\right)^2\frac{\partial g_2}{\partial y}.
\end{aligned}$$

Using Eq. (6.63), the three natural frequencies can be found. The eigenvectors, which can be considered as the ratio of the amplitude, can be obtained as

$$\mathbf{v}_1 = \begin{bmatrix} 1 \\ \dfrac{-\frac{\partial g_1}{\partial y}m_p s - \frac{\partial g_1}{\partial y}\frac{\partial g_3}{\partial z} + \frac{\partial g_1}{\partial z}\frac{\partial g_2}{\partial z}}{m_p^2 s^2 + (\frac{\partial g_2}{\partial y} + \frac{\partial g_3}{\partial z})m_p s + \frac{\partial g_2}{\partial y}\frac{\partial g_3}{\partial z} - (\frac{\partial g_2}{\partial z})^2} \\ \dfrac{-\frac{\partial g_1}{\partial z}m_p s - \frac{\partial g_2}{\partial y}\frac{\partial g_1}{\partial z} + \frac{\partial g_1}{\partial y}\frac{\partial g_2}{\partial z}}{m_p^2 s^2 + (\frac{\partial g_2}{\partial y} + \frac{\partial g_3}{\partial z})m_p s + \frac{\partial g_2}{\partial y}\frac{\partial g_3}{\partial z} - (\frac{\partial g_2}{\partial z})^2} \end{bmatrix}, \tag{6.64}$$

$$\mathbf{v}_2 = \begin{bmatrix} \dfrac{-\frac{\partial g_1}{\partial y}m_p s - \frac{\partial g_1}{\partial y}\frac{\partial g_3}{\partial z} + \frac{\partial g_1}{\partial z}\frac{\partial g_2}{\partial z}}{m_p^2 s^2 + (\frac{\partial g_1}{\partial x} + \frac{\partial g_3}{\partial z})m_p s + \frac{\partial g_1}{\partial x}\frac{\partial g_3}{\partial z} - (\frac{\partial g_1}{\partial z})^2} \\ 1 \\ \dfrac{-\frac{\partial g_2}{\partial z}m_p s - \frac{\partial g_1}{\partial x}\frac{\partial g_2}{\partial z} + \frac{\partial g_1}{\partial y}\frac{\partial g_1}{\partial z}}{m_p^2 s^2 + (\frac{\partial g_1}{\partial x} + \frac{\partial g_3}{\partial z})m_p s + \frac{\partial g_1}{\partial x}\frac{\partial g_3}{\partial z} - (\frac{\partial g_1}{\partial z})^2} \end{bmatrix}, \tag{6.65}$$

$$\mathbf{v}_3 = \begin{bmatrix} \dfrac{-\frac{\partial g_1}{\partial z}m_p s - \frac{\partial g_1}{\partial z}\frac{\partial g_2}{\partial y} + \frac{\partial g_1}{\partial y}\frac{\partial g_2}{\partial z}}{m_p^2 s^2 + (\frac{\partial g_1}{\partial x} + \frac{\partial g_2}{\partial y})m_p s + \frac{\partial g_1}{\partial x}\frac{\partial g_2}{\partial y} - (\frac{\partial g_1}{\partial y})^2} \\ \dfrac{-\frac{\partial g_2}{\partial z}m_p s - \frac{\partial g_1}{\partial x}\frac{\partial g_2}{\partial z} + \frac{\partial g_1}{\partial y}\frac{\partial g_1}{\partial z}}{m_p^2 s^2 + (\frac{\partial g_1}{\partial x} + \frac{\partial g_2}{\partial y})m_p s + \frac{\partial g_1}{\partial x}\frac{\partial g_2}{\partial y} - (\frac{\partial g_1}{\partial y})^2} \\ 1 \end{bmatrix}. \tag{6.66}$$

At the original configuration, the spring forces are $f_{si} = f_o$, the cable forces are $f_{ai} = f_{bi} = \frac{f_o}{4}$, $i = 1, 2, 3$, and $\mathbf{G} = -af_o\mathbf{I}$ ($\mathbf{I}$ is a 3×3 identity matrix). Then, Eq. (6.63) becomes

$$(M_p s - af_o)^3 = 0 \tag{6.67}$$

It can be seen that the natural frequencies in the original configuration are

$$s_{io} = \frac{af_o}{m_p}, \quad i = 1, 2, 3.$$

Using Eq. (6.64) to Eq. (6.66), the three ratios of the amplitude eigenvectors can be found as

$$\mathbf{v}_{1o} = \begin{bmatrix} 1 \\ 0 \\ 0 \end{bmatrix}, \qquad \mathbf{v}_{2o} = \begin{bmatrix} 0 \\ 1 \\ 0 \end{bmatrix}, \qquad \mathbf{v}_{3o} = \begin{bmatrix} 0 \\ 0 \\ 1 \end{bmatrix}.$$

Normalizing the parameters of the mechanism as $a = 1$ and $m_p = 1$, suppose the springs in the mechanism are constant force springs and $f_o = 1$. The natural frequencies for $z = 0$, $z = \pm 0.2$, $z = \pm 0.4$ are shown in Figure 6.9.

It can be seen that the three natural frequencies have little differences near the centre of the octahedron, the farther the distance from the centre of the octahedron the bigger differences the three natural frequencies have. It has been verified that the reference position of the end-effector should be placed in the centroid of the octahedron in order to keep the springs in tension. Hence, the most important natural frequency is the smallest one s_1. In order to avoid significant vibrations, the mechanisms should work below the smallest natural frequency in most situations.

6.6 Conclusions

In this chapter, the dynamic characteristics of planar and spatial spring-loaded cable-loop-driven parallel mechanisms are analyzed. The velocity and acceleration equations for the inverse kinematics are deduced based on the displacement equations. The dynamic equations which only consider the mass of the actuators and the end-effector are obtained. The frequency limitations of the sine trajectories in the two special directions for both of the two spring-loaded mechanisms have been found based on the dynamic equations. The natural frequencies and the ratio of the amplitudes of both mechanisms have been found using a Newton-Euler formulation and the static cable forces. With these results, undesired vibration can be avoided for the mechanisms.

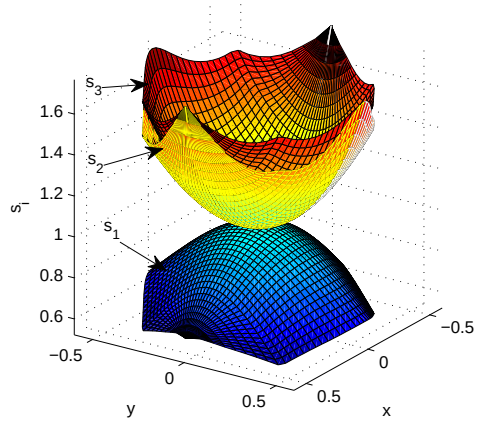

(a) $z = 0$

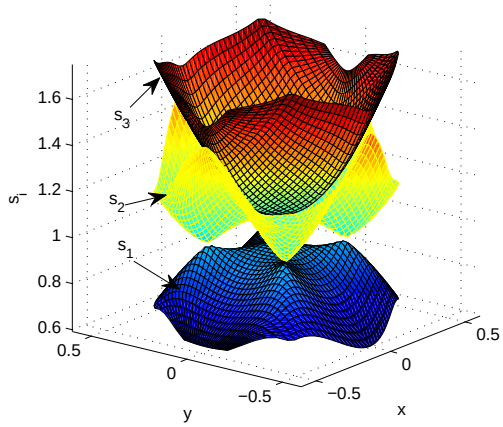

(b) $z = \pm 0.2$

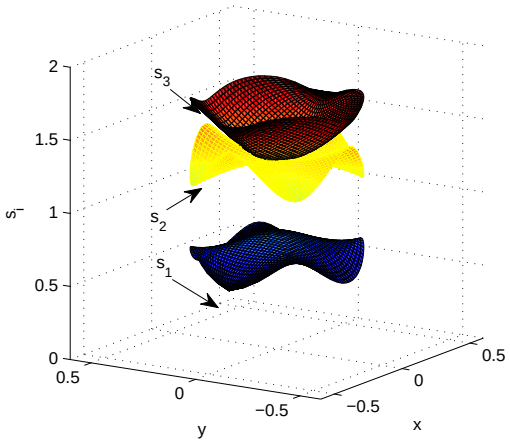

(c) $z = \pm 0.4$

Figure 6.9: The three natural frequencies of the spatial mechanism.

Chapter 7

Two-Degree-of-Freedom Decoupled Non-Redundant Cable-Loop-Driven Parallel Mechanism

A novel two-degree-of-freedom cable-loop slider-driven parallel mechanism is introduced in this chapter. The two degrees of freedom of the mechanism are uncoupled and only two actuators are needed to control the motion. There are two cable loops for each direction motion: one acts as the actuating loop while the other is the constraint loop. Due to the simple geometric design, the kinematic and static equations of the mechanism are very compact. The stiffness of the mechanism is analyzed. It can be observed that the mechanism's stiffness is much higher than the stiffness of the cables. The dynamic equations of the mechanism, including the compliance and the damping of the cables are also obtained. The proposed mechanism's workspace is essentially equal to its footprint and there are no singularities. The mechanism does not require the use of a rigid-link passive bridge and trolley (only cables are connected to the end-effector). Sliders located on the

edges of the workspace are used and actuation redundancy is eliminated while providing force closure everywhere in the workspace.

7.1 Introduction

In Chapters 3 and 4, planar and spatial spring-loaded cable-loop-driven parallel mechanisms were introduced. These mechanisms are non-redundant and avoid the use of cable-spool systems. However, they require the use of extension springs which limits their force capabilities. In [104], a Cartesian cable-driven mechanism is introduced, in which a long cable loop is circling on a rigid-link Cartesian translational mechanism, and three stationary actuators provide the 3-DOF motion. However, this mechanism requires the use of a rigid-link passive bridge and trolley. For parallel mechanisms, it is often difficult to decouple the motion. Nevertheless, there are notable examples, such as the fully-decoupled 3-DOF translational parallel mechanism proposed in [111].

In this chapter, a 2-DOF cable-loop driven parallel mechanism is presented. The mechanism does not require actuation redundancy and it does not include a rigid-link translational mechanism: only cables are connected to the end-effector. Therefore, it retains the advantages of cable-spool mechanisms while alleviating their drawbacks. Moreover, the two degrees of freedom are decoupled in the mechanism.

Generally speaking, the stiffness of cable-driven parallel mechanisms is not as good as that of link-driven mechanisms since cables are flexible elements, and critical vibrations might be induced when large accelerations are performed. With redundant actuation, the stiffness can be improved. The stiffness matrix and the natural frequency of general 6-DOF cable-driven parallel manipulators is obtained in [91] and it is also shown that the transversal vibration of cables is insignificant while the axial flexibility of cables is the most important. The stiffness of conventional cable-based robots is studied in [77], where an approach to obtain the total stiffness matrix and a set of sufficient conditions which ensure the manipulator stability are introduced. For most cable-driven mechanisms, the cable mass is negligible. However, for very large manipulators with a huge workspace, the cable mass cannot be neglected for the static and stiffness analysis [58, 78].

In the early stages of the dynamic analysis of cable-driven parallel mechanisms, the dynamic equations are compact since the cables are assumed to be massless and straight and the dynamical characteristics of cables themselves are neglected [39, 87]. However, the dynamic model for large cable-driven mechanisms considering the cable mass and the nonlinear dynamic equations of the mechanism with time-varying length cables is obtained in [93]. The preliminary study of the dynamics of a 6-DOF cable-driven parallel manipulator is presented in [84], where the inverse

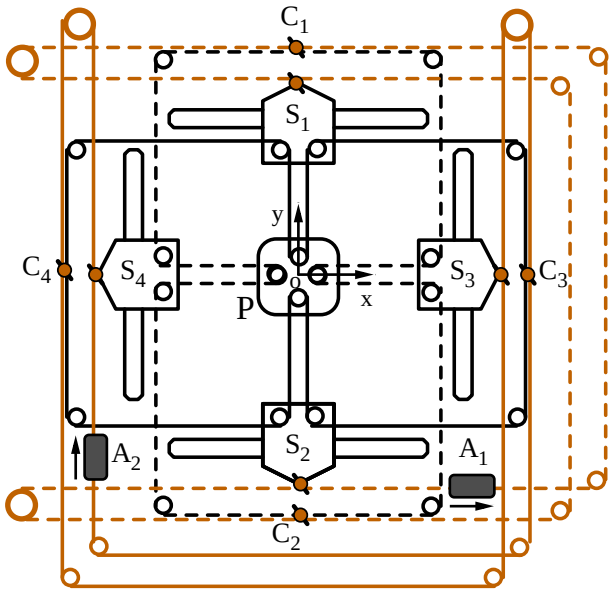

Figure 7.1: Schematic representation of the 2-DOF cable-loop slider driven parallel mechanism.

dynamics problem which is required for real-time control and the assessment of the rigidity characteristics due to the inevitable cable elasticity have been studied.

The dynamics and stiffness of the proposed planar decoupled cable-loop-driven parallel mechanism are analyzed here. This chapter is arranged as follows. First, the structure of the mechanism is described. Then, the kinematic and static equations are given. Since the geometry of the mechanism is simple, these equations are very compact. The effects of the cable compliance on the stiffness of the mechanism are studied after the static analysis. Finally, the dynamics of the mechanism are investigated. The dynamic model assuming that the cables are infinitely stiff and the model considering the stiffness and the damping of the cables are both obtained.

7.1.1 Description of the Mechanism

The routings of the 2-DOF decoupled non-redundant cable-loop-driven parallel mechanism are shown in Figure 7.1. Four sliders, $S_1, \ldots, S_4$, are located on the edges of a rectangle. The mechanism is symmetric and the origin of the fixed reference frame is located at the centre of the mechanism. Two cable loops are needed to control one DOF: the cable loop which is attached to the actuator is referred to as the drive-routing, while the other loop is referred to as the assist-routing. The mechanism has two such pairs of cable routings. The two cable loops represented

by the dashed gray curves and the dashed black curves, which are attached to one another by connectors C_1 and C_2, control the motion in the x direction. The cable loops represented with solid lines control the motion in the y direction and are attached to one another by connectors C_3 and C_4. The gray cable loops are attached to the slider actuators A_i, $i = 1, 2$, respectively. The motion of the actuators produces a displacement of the gray loops, which induces a motion of the black loops and sliders, thereby producing the motion of the end-effector.

It is now assumed that the distances between the sliders S_1 and S_2, S_3 and S_4 are $2s_y$ and $2s_x$ respectively while the reference position of the end-effector P_o is $\mathbf{p}_o = [0, 0]^T$, the reference position of the four sliding pulleys S_{io}, $i = 1, \ldots, 4$, is $\mathbf{s}_{1o} = [0, s_y]^T$, $\mathbf{s}_{2o} = [0, -s_y]^T$, $\mathbf{s}_{3o} = [s_x, 0]^T$ and $\mathbf{s}_{4o} = [-s_x, 0]^T$. Based on the geometry of the mechanism and on the routings described above, it can be readily observed that when the actuators A_j, $j = 1, 2$, are displaced by d_j, $j = 1, 2$, the position of S_i and the distance $|PS_i|$, $i = 1, \ldots, 4$, have the following relationships:

$$\mathbf{s}_1 = \begin{bmatrix} d_1 \\ s_y \end{bmatrix}, \quad \mathbf{s}_2 = \begin{bmatrix} d_1 \\ -s_y \end{bmatrix}, \quad \mathbf{s}_3 = \begin{bmatrix} s_x \\ d_2 \end{bmatrix}, \quad \mathbf{s}_4 = \begin{bmatrix} -s_x \\ d_2 \end{bmatrix},$$

and

$$|PS_1| - |P_oS_{1o}| = -d_2. \tag{7.1}$$

$$|PS_2| - |P_oS_{2o}| = d_2, \tag{7.2}$$

$$|PS_3| - |P_oS_{3o}| = -d_1, \tag{7.3}$$

$$|PS_4| - |P_oS_{4o}| = d_1, \tag{7.4}$$

Hence, the motion of the sliding actuators is directly reflected at the end-effector.

A demonstration model of the mechanism was built, as shown in Figure 7.2. Although the preload in the mechanism is not vary large, the model can be used to demonstrate the general principle of the mechanism.

7.1.2 Kinematic Analysis

According to the geometry of the mechanism and using Eqs.(7.1) — –(7.4), the kinematic equations can easily be found. Suppose the position of the end-effector $\mathbf{p} = [x, y]^T$ is known, then the

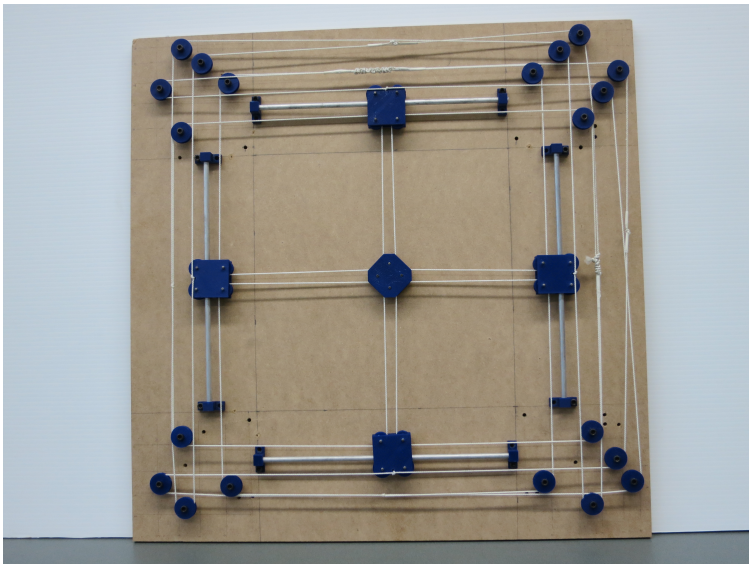

Figure 7.2: Photograph of the demonstration model of the decoupled non-redundant cable-loop-driven parallel mechanism.

displacements of the cable connectors l_{ci}, the displacements of the sliders l_{si}, $i = 1, \dots 4$, and the displacements of the actuators d_i, $i = 1, 2$, can be found as

$$d_1 = -l_{c1} = -l_{c2} = l_{s1} = l_{s2} = x, \tag{7.5}$$

$$d_2 = -l_{c3} = -l_{c4} = l_{s3} = l_{s4} = y. \tag{7.6}$$

Differentiating Eq. (7.5) and Eq. (7.6) with respect to time, we have the velocity relationships as

$$\dot{d}_1 = -\dot{l}_{c1} = -\dot{l}_{c2} = \dot{l}_{s1} = \dot{l}_{s2} = \dot{x}, \tag{7.7}$$

$$\dot{d}_2 = -\dot{l}_{c3} = -\dot{l}_{c4} = \dot{l}_{s3} = \dot{l}_{s4} = \dot{y}. \tag{7.8}$$

Then, differentiating Eq. (7.7) and Eq. (7.8) again, the acceleration can be found as

$$\ddot{d}_1 = -\ddot{l}_{c1} = -\ddot{l}_{c2} = \ddot{l}_{s1} = \ddot{l}_{s2} = \ddot{x}, \tag{7.9}$$

$$\ddot{d}_2 = -\ddot{l}_{c3} = -\ddot{l}_{c4} = \ddot{l}_{s3} = \ddot{l}_{s4} = \ddot{y}. \tag{7.10}$$

From Eq. (7.7) and Eq. (7.8), the Jacobian matrix can be found as a 2×2 identity matrix. That is to say

$$\dot{\mathbf{d}} = \mathbf{J}\dot{\mathbf{p}}. \tag{7.11}$$

where

$$\dot{\mathbf{d}} = \begin{bmatrix} \dot{d}_1 \\ \dot{d}_2 \end{bmatrix}, \qquad \dot{\mathbf{p}} = \begin{bmatrix} \dot{x} \\ \dot{y} \end{bmatrix}, \qquad \mathbf{J} = \begin{bmatrix} 1 & 0 \\ 0 & 1 \end{bmatrix}.$$

Clearly, the kinematics of this mechanism are very simple and the two degrees of freedom are completely decoupled. Also, the workspace of the mechanism is essentially equal to its footprint

and there are no singularities. Finally, the mechanism does not require a rigid-link passive bridge and trolley. Only cables are connected to the end-effector. Sliders located on the edges of the workspace are used and actuation redundancy is eliminated while providing force closure everywhere in the workspace.

7.1.3 Static Analysis

Consider the mechanism in which we neglect the friction in the sliders and in the pulleys. When the mechanism is in static equilibrium, if there is an external force $\mathbf{f}_e = [f_{ex}, f_{ey}]^T$ applied on the end-effector, by virtue of the principle of virtual work, the actuators' forces f_{ai}, $i = 1, 2$, should be

$$\mathbf{f}_a = -\mathbf{J}^T \mathbf{f}_e \tag{7.12}$$

where $\mathbf{f}_a = [f_{a1}, f_{a2}]^T$ and $\mathbf{f}_e = [f_{ex}, f_{ey}]^T$. Since the Jacobian matrix is equal to the identity matrix, one simply has

$$\mathbf{f}_a = -\mathbf{f}_e. \tag{7.13}$$

7.2 Stiffness analysis

Cables have a relatively low stiffness compared to rigid links, especially when a long span is used. Therefore, it is important to investigate the global stiffness of the mechanism.

The following assumptions are made:

1. There is no friction in the mechanism,
2. The position of the actuator is not changed when there is an external force applied on the end-effector,
3. The total cable length of each cable loop is assumed to be constant,
4. The cables between the sliders and the end-effector remain orthogonal.

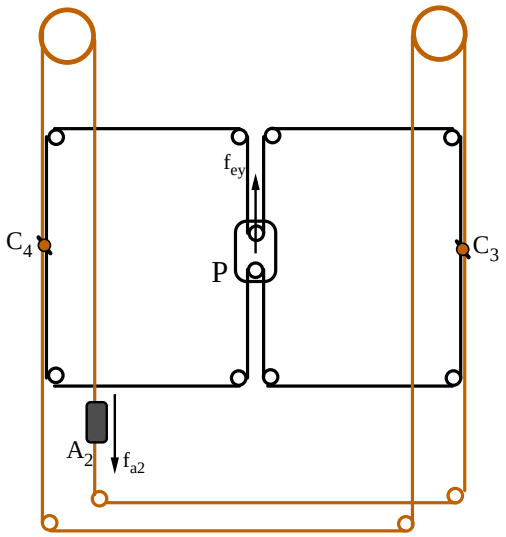

Figure 7.3: The forces on the cable-routing system for the y direction.

The second assumption arises from the fact that the stiffness of the cable transmission is investigated independently from the stiffness of the actuators, the third assumption is based on the condition that the cables do not become slack and the last assumption is proposed since the deformations of the end-effector are small compared to the workspace.

Suppose the end-effector of the mechanism undergoes a displacemnet of $\delta\mathbf{p} = [\delta x, \delta y]^T$ when there is an external force of $\mathbf{f}_e = [f_{ex}, f_{ey}]^T$ applied at the end-effector under static conditions, that is to say the stiffness relationship of the mechanism is

$$\mathbf{f}_e = \mathbf{K}\delta\mathbf{p}. \tag{7.14}$$

In other words, when there is an external force applied on the end-effector, a displacement $\delta\mathbf{p}$ will appear at the end-effector which is caused by the deformation of the cables.

As the motion of the two cable-routing systems are decoupled, they can be analyzed separately. For the y direction cable routing, the forces are shown in Figure 7.3.

It is assumed that the cable-routing system is symmetric. The lengths of the two segments of the assist-routing is the same which is noted l_2 and the stiffness of each segment is defined as k_2, the deformations of the cables are δy_1 and δy_2 respectively. For the drive-routing, the lengths of the cable segments in the drive-routing A_2C_4, C_4C_3 and C_3A_2 are l_{11}, l_{12} and l_{13} respectively. Because the stiffness of the cable is related to the cable length, the corresponding stiffness of the

cable segments can be defined as $\frac{k}{l_{11}}$, $\frac{k}{l_{12}}$ and $\frac{k}{l_{13}}$, where k is the stiffness of the cable per unit length.

In order to maintain the cables in tension, a preload is applied to the cable loops. Assume that the original deformation of the two segments of the assist-routing are δ_2, then the preload of the assist-routing is

$$f_{o2} = k_2\delta_2. \tag{7.15}$$

and the total length of the assist-routing is $2(l_2 + \delta_2)$. The original deformations for the three segments in the drive-routing are noted δ_{11}, δ_{12} and δ_{13} respectively, which produce a certain preload f_{o1}. Then, The preload of the drive-routing is

$$f_{o1} = \frac{k}{l_{11}}\delta_{11} = \frac{k}{l_{12}}\delta_{12} = \frac{k}{l_{13}}\delta_{13}.$$

The total length of the drive-routing is $l_1(1 + \frac{f_{o1}}{k})$, where $l_1 = l_{11} + l_{12} + l_{l3}$.

For the assist-routing, the cable length does not vary with an external force, therefore

$$\delta y_1 + \delta y_2 = 0 \tag{7.16}$$

where δy_1 and δy_2 are respectively the change of length for each half of the assist-routing. Using Eq. (7.15), the cable forces of each segments are then

$$f_{1p} = f_{o2} + k_2\delta y_1 = k_2\delta_2 + k_2\delta y_1 \tag{7.17}$$

$$f_{2p} = f_{o2} + k_2\delta y_2 = k_2\delta_2 - k_2\delta y_1 \tag{7.18}$$

where f_{1p} and f_{2p} are the cable forces between the slider S_i, $i = 1, 2$, and the end-effector P. Because the cables have to be maintained in tension, the relationships of $f_{1p} > 0$ and $f_{2p} > 0$ should be satisfied. Based on Eq. (7.16) to Eq. (7.18), it can be shown that

$$-\delta_2 < \delta y_1 < \delta_2 \tag{7.19}$$

It can be seen that the maximum cable force of the assist-routing (constraint-routing) is $2f_{o2} = 2k_2\delta_2$.

For the drive-routing, the cable segments undergo deformations δl_{11}, δl_{12} and δl_{13} respectively when there is an external force f_{ey} in the y direction. Because the length of the cable routing is constant, then we have

$$\delta l_{11} + \delta l_{12} + \delta l_{13} = 0 \tag{7.20}$$

The cable forces in the segments become

$$f_{y1} = f_{o1} + \frac{k}{l_{11}}\delta l_{11} = \frac{k}{l_{11}}(\delta_{11} + \delta l_{11}) \tag{7.21}$$

$$f_{y2} = f_{o1} + \frac{k}{l_{12}}\delta l_{12} = \frac{k}{l_{12}}(\delta_{12} + \delta l_{12}) \tag{7.22}$$

$$f_{y3} = f_{o1} + \frac{k}{l_{13}}\delta l_{13} = \frac{k}{l_{13}}(\delta_{13} + \delta l_{13}) \tag{7.23}$$

where f_{yi}, $i = 1, 2, 3$, are the cable forces in cable segments A_2C_4, C_4C_3 and C_3A_2 respectively.

When the mechanism is in static equilibrium, the free-body diagram of the end-effector leads to

$$2f_{1p} + f_{ey} = 2f_{2p} \tag{7.24}$$

which leads to

$$f_{ey} = 2(f_{2p} - f_{1p}) = 2(-k_2\delta y_1 + k_2\delta y_2) = -4k_2\delta y_1 \tag{7.25}$$

and the deformations are

$$\delta y_1 = -\delta y_2 = -\frac{f_{ey}}{4k_2}. \tag{7.26}$$

The static equilibrium of the connectors C_4 and C_3 leads to

$$C_4: \qquad f_{y1} + f_{1p} - f_{y2} - f_{2p} = 0 \tag{7.27}$$

$$C_3: \qquad f_{y2} + f_{1p} - f_{y3} - f_{2p} = 0 \tag{7.28}$$

Combining Eq. (7.27) and Eq. (7.28) with Eq. (7.20) and rearranging, one obtains

$$\mathbf{B}\boldsymbol{\delta}\mathbf{l_1} = \boldsymbol{\tau} \tag{7.29}$$

where $\delta\mathbf{l}_1 = \begin{bmatrix} \delta l_{11} & \delta l_{12} & \delta l_{13} \end{bmatrix}^t$, $\boldsymbol{\tau} = \begin{bmatrix} 0 & \frac{f_{ey}}{2k} & \frac{f_{ey}}{2k} \end{bmatrix}^T$ and

$$\mathbf{B} = \begin{bmatrix} 1 & 1 & 1 \\ \frac{1}{l_{11}} & -\frac{1}{l_{12}} & 0 \\ 0 & \frac{1}{l_{12}} & -\frac{1}{l_{13}} \end{bmatrix}.$$

Then, the deformations of the cable segments in the drive-routing caused by the external force can be expressed as

$$\delta\mathbf{l}_1 = \mathbf{C}\boldsymbol{\tau} = \frac{f_{ey}}{2l_1k}\begin{bmatrix} l_{11}(l_{12} + 2l_{13}) \\ l_{12}(l_{13} - l_{11}) \\ -l_{13}(2l_{11} + l_{12}) \end{bmatrix}, \tag{7.30}$$

where

$$\mathbf{C} = \frac{1}{l_1}\begin{bmatrix} l_{11} & l_{11}(l_{12} + l_{13}) & l_{11}l_{13} \\ l_{12} & -l_{11}l_{12} & l_{12}l_{13} \\ l_{13} & -l_{11}l_{13} & -l_{13}(l_{11} + l_{12}) \end{bmatrix}.$$

After finding all the deformations of the cable segments, the displacement of the end-effector in the y direction can be calculated as

$$\delta_y = \frac{1}{2}(\delta l_{11} - \delta l_{13}) - \frac{1}{2}\delta y_1 = -\frac{1}{2}\delta l_{12} - \frac{1}{2}\delta y_1 = \frac{f_{ey}}{4l_1 k} l_{12}(l_{11} + l_{13}) + \frac{f_{ey}}{8k_2}. \tag{7.31}$$

Then, the stiffness of the mechanism in the y direction is obtained as

$$k_y = \frac{f_{ey}}{\delta_y} = \frac{8k_2 l_1 k}{2l_{12}(l_{11} + l_{13})k_2 + l_1 k}. \tag{7.32}$$

As the cable segments have to be maintained in tension, the following relationships must be satisfied:

$$\delta_2 + \delta y_1 > 0, \quad \delta_2 + \delta y_2 > 0,$$
$$\delta_{11} + \delta l_{11} > 0, \quad \delta_{12} + \delta l_{12} > 0, \quad \delta_{13} + \delta l_{13} > 0.$$

Based on the solution for the deformations, the above inequalities can be modified as

$$-4f_{o2} < f_{ey} < 4f_{o2}, \tag{7.33}$$
$$-\frac{2f_{o1}(l_{11} + l_{12} + l_{13})}{l_{12} + 2l_{13}} < f_{ey} < \frac{2f_{o1}(l_{11} + l_{12} + l_{13})}{2l_{11} + l_{12}}. \tag{7.34}$$

From the geometry of the mechanism shown in Figure 7.3, it can be observed that the length of cable segment C_4C_3 is approximately the sum of the length of cable segments A_1C_4 and C_3A_2, i.e., $l_{12} = l_{11} + l_{13}$ and $l_1 = 2l_{12}$, then the deformation of the end-effector and the stiffness of the mechanism in the y direction can be simplified to

$$\delta_y = \frac{f_{ey}}{8}\left(\frac{l_{12}}{k} + \frac{1}{k_2}\right), \tag{7.35}$$
$$k_y = \frac{8k_2 k}{l_{12}k_2 + k}. \tag{7.36}$$

and if the geometry of the mechanism is symmetric, i.e., $l_{11} = l_{13}$, the relations between the preload forces of the two cable loops and the external force become

$$-2f_{o1} < f_{ey} < 2f_{o1}, \qquad -4f_{o2} < f_{ey} < 4f_{o2}.$$

That is to say, the preload of the drive-routing is twice that of the assist-routing.

Based on the analysis presented in this section, the actuating force can be found as

$$f_{a2} = f_{y3} - f_{y1} = k\left(\frac{\delta l_{13}}{l_{13}} - \frac{\delta l_{11}}{l_{11}}\right) = -f_{ey} \tag{7.37}$$

which is consistent with the result of the static analysis.

If the cables in the assist-routing and the drive-routing have the same stiffness per unit length, k, then the stiffness of one segment of the assist-routing can be written as

$$k_2 = \frac{k}{l_2}. \tag{7.38}$$

Substituting the latter relationship into Eqn. (7.36), one then obtains

$$k_y = \frac{8k}{l_{12} + l_2}. \tag{7.39}$$

Hence, the stiffness of mechanism is smaller with a larger workspace. However, the cable stiffness calculated using the lengths l_{12} and l_2 is amplified by a factor of 8 by the mechanism, which provides a very good global stiffness.

With the same method, the stiffness of the cable-routing that controls the motion along the x direction can also be found. The results are equivalent to those obtained for the y direction.

7.2.1 Dynamic Analysis

Depending on the application, the effects of the compliance of the cable on the dynamic model may be of interest. During the design process, the cables may be selected such that the stiffness of the mechanism is sufficiently large. In that case, the inclusion of the cable stiffness in the dynamic model will only increase the mathematical complexity and is not necessary. On the other hand, in high-speed applications, it might be required to include the stiffness of the cables in the dynamic model. In the following, the two situations will be studied separately. To obtain the dynamic model, it is assumed that cables are massless and that friction is negligible. Also, the cables are always under extension.

7.2.2 Dynamic Model Neglecting Cable Compliance

Using the Newton-Euler method, the dynamic equations of the connectors, the sliders, the actuators and the end-effector can be obtained. Suppose the masses of the end-effector, the sliders,

the connectors and the actuators are m_p, m_s, m_c and m_a respectively. The dynamic equations are written in the following.

For the end-effector, one has

$$m_p\ddot{x} = 2f_{3p} - 2f_{4p} + f_{ex}, \tag{7.40}$$

$$m_p\ddot{y} = 2f_{1p} - 2f_{2p} + f_{ey}, \tag{7.41}$$

where f_{ip}, $i = 1, \ldots, 4$, is the cable force between the slider S_i and the end-effector P, i.e., the cable forces in the assist loops. Referring to Figure 7.1, f_{1p} and f_{2p} are the forces in the solid black loop, while f_{3p} and f_{4p} are the forces in the dashed black loop.

For the connectors C_i, $i = 1, \ldots, 4$, one has

$$C_1: \quad -m_c\ddot{x} = f_{3p} + f_{c1A1} - f_{c1s1} - f_{4p}, \tag{7.42}$$

$$C_2: \quad -m_c\ddot{x} = f_{3p} + f_{c2s1} - f_{c2s2} - f_{4p}, \tag{7.43}$$

$$C_3: \quad -m_c\ddot{y} = f_{1p} + f_{c3s3} - f_{c3A2} - f_{2p}, \tag{7.44}$$

$$C_4: \quad -m_c\ddot{y} = f_{1p} + f_{c4s4} - f_{c4s3} - f_{2p}, \tag{7.45}$$

where f_{c2s1}, f_{c2s2}, f_{c1s1} and f_{c1A1} are respectively the cable forces on the dashed gray loop between the connector C_2 and the slider S_1, C_2 and S_2, C_1 and S_1, between C_1 and the actuator A_1. Similarly, f_{c4s4}, f_{c4s3}, f_{c3s3} and f_{c3A2} are the cable forces in the solid gray loop between the connector C_4 and the slider S_4, C_4 and S_3, C_3 and S_3, between the connector C_3 and the actuator A_2, respectively.

For the sliders S_i, $i = 1, \ldots, 4$, we have

$$S_1: \quad m_s\ddot{x} = f_{c2s1} - f_{c1s1}, \tag{7.46}$$

$$S_2: \quad m_s\ddot{x} = f_{A1s2} - f_{c2s2}, \tag{7.47}$$

$$S_3: \quad m_s\ddot{y} = f_{c3s3} - f_{c4s3}, \tag{7.48}$$

$$S_4: \quad m_s\ddot{y} = f_{c4s4} - f_{A2s4}, \tag{7.49}$$

where f_{A1s2} and f_{A2s4} are the cable forces in the gray dashed cable segment A_1S_2 and the gray solid cable segment A_2S_4 respectively.

For the actuators A_i, $i = 1, 2$, one has

$$A_1: \quad m_a\ddot{x} = f_{a1} + f_{c1A1} - f_{A1s2}, \tag{7.50}$$

$$A_2: \quad m_a\ddot{y} = f_{a2} + f_{A2s4} - f_{c3A2}, \tag{7.51}$$

Eq. (7.40) and Eq. (7.41) can be rewritten as

$$f_{3p} - f_{4p} = \frac{1}{2}(m_p\ddot{x} - f_{ex}), \tag{7.52}$$

$$f_{1p} - f_{2p} = \frac{1}{2}(m_p\ddot{y} - f_{ey}). \tag{7.53}$$

Substituting Eq. (7.52) into Eq. (7.44) and Eq. (7.45), substituting Eq. (7.53) into Eq. (7.42) and Eq. (7.43), one obtains

$$f_{c1A1} - f_{c1s1} = f_{c2s1} - f_{c2s2} = -(m_c + \frac{1}{2}m_p)\ddot{x} + \frac{1}{2}f_{ex}, \tag{7.54}$$

$$f_{c3s3} - f_{c3A2} = f_{c4s4} - f_{c4s3} = -(m_c + \frac{1}{2}m_p)\ddot{y} + \frac{1}{2}f_{ey}. \tag{7.55}$$

Adding Eq. (7.46) with Eq. (7.47), Eq. (7.48) with Eq. (7.49), and substituting Eq. (7.54) and Eq. (7.55) into them respectively, one has

$$f_{A1s2} - f_{c1A1} = (2m_s + 2m_c + m_p)\ddot{x} - f_{ex}, \tag{7.56}$$

$$f_{c3A2} - f_{A2s4} = (2m_s + 2m_c + m_p)\ddot{y} - f_{ey}. \tag{7.57}$$

Then, substituting Eq. (7.56) and Eq. (7.57) into Eq. (7.50) and Eq. (7.51) respectively, yields

$$f_{a1} = (m_a + 2m_s + 2m_c + m_p)\ddot{x} - f_{ex}, \tag{7.58}$$

$$f_{a2} = (m_a + 2m_s + 2m_c + m_p)\ddot{y} - f_{ey}. \tag{7.59}$$

The latter two equations can be combined as

$$\mathbf{M}\ddot{\mathbf{p}} = \mathbf{f}_a + \mathbf{f}_e, \tag{7.60}$$

where

$$\mathbf{M} = \begin{bmatrix} m_a + 2m_s + 2m_c + m_p & 0 \\ 0 & m_a + 2m_s + 2m_c + m_p \end{bmatrix}.$$

Since the structure of the mechanism is designed to be decoupled, the dynamic equations are also concise and decoupled.

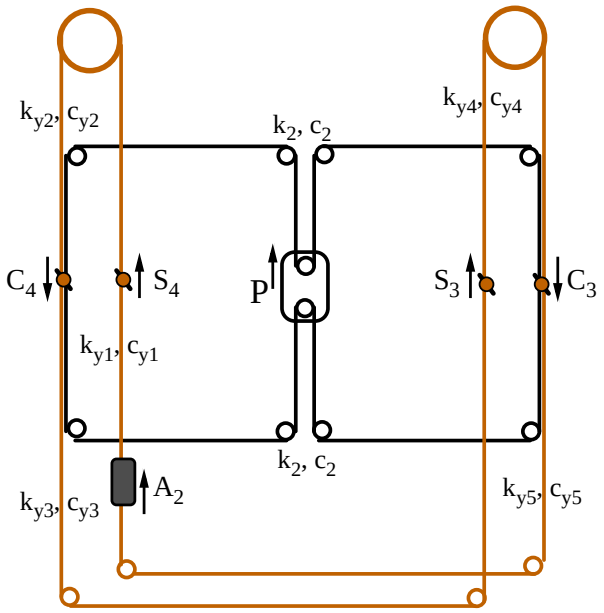

Figure 7.4: The positive directions and the stiffnesses, the dampings of the cable segments.

7.2.3 Dynamic Model Considering Cable Compliance

From the stiffness analysis, it can be observed that the motions in the x and y directions are decoupled. Therefore, the vibrations in the x and y directions can be analyzed separately. In the following, the y direction is used for the analysis.

Suppose the displacements of the connectors, sliders and actuator are y_{c4}, y_{c3}, y_{s4}, y_{s4}, y_{a2}, the velocities are $\dot{y}_{c4}$, $\dot{y}_{c3}$, $\dot{y}_{s4}$, $\dot{y}_{s3}$, $\dot{y}_{a2}$ and the accelerations are $\ddot{y}_{c4}$, $\ddot{y}_{c3}$, $\ddot{y}_{s4}$, $\ddot{y}_{s3}$, $\ddot{y}_{a2}$ when the end-effector undergoes a displacement, velocity and acceleration of y, $\dot{y}$ and $\ddot{y}$ in the y direction. The positive directions of motion are shown in Figure 7.4.

With the velocities and the displacements of the end-effector, the connectors, the sliders and

the actuator, the cable forces of each cable segments can be written as

$$f_{s1p} = f_{o2} + k_2(y_{c4} + y_{c3} - y) + c_2(\dot{y}_{c4} + \dot{y}_{c3} - \dot{y}), \tag{7.61}$$

$$f_{s2p} = f_{o2} - k_2(y_{c4} + y_{c3} - y) - c_2(\dot{y}_{c4} + \dot{y}_{c3} - \dot{y}), \tag{7.62}$$

$$f_{A2s4} = f_{o1} + k_{y1}(y_{s4} - y_{a2}) + c_{y1}(\dot{y}_{s4} - \dot{y}_{a2}), \tag{7.63}$$

$$f_{c4s4} = f_{o1} + k_{y2}(y_{c4} - y_{s4}) + c_{y2}(\dot{y}_{c4} - \dot{y}_{s4}), \tag{7.64}$$

$$f_{c4s3} = f_{o1} + k_{y3}(y_{s3} - y_{c4}) + c_{y3}(\dot{y}_{s3} - \dot{y}_{c4}), \tag{7.65}$$

$$f_{c3s3} = f_{o1} + k_{y4}(y_{c3} - y_{s3}) + c_{y4}(\dot{y}_{c3} - \dot{y}_{s3}), \tag{7.66}$$

$$f_{c3A2} = f_{o1} + k_{y5}(y_{a2} - y_{c3}) + c_{y5}(\dot{y}_{a2} - \dot{y}_{c3}). \tag{7.67}$$

where k_{yi}, k_2, c_{yi},and c_2, $i = 1, \ldots, 5$, are the stiffness and the dampings of the corresponding cable segments as shown in Figure 7.4.

The dynamic equations for the end-effector, the connectors, the sliders can be found as

$$P: \quad m_p\ddot{y} = 2f_{1p} - 2f_{2p}, \tag{7.68}$$

$$C_4: \quad m_c\ddot{y}_{c4} = f_{c4s3} + f_{2p} - f_{1p} - f_{c4s4}, \tag{7.69}$$

$$C_3: \quad m_c\ddot{y}_{c3} = f_{c3A2} + f_{2p} - f_{1p} - f_{c3s3}, \tag{7.70}$$

$$S_4: \quad m_s\ddot{y}_{s4} = f_{c4s4} - f_{A2s4}, \tag{7.71}$$

$$S_3: \quad m_s\ddot{y}_{s3} = f_{c3s3} - f_{c4s3}. \tag{7.72}$$

Substituting the cable forces into Eq. (7.68) to Eq. (7.72), we have

$$P: \quad 4k_2(y_{c4} + y_{c3} - y) + 4c_2(\dot{y}_{c4} + \dot{y}_{c3} - \dot{y}) - m_p\ddot{y} = 0, \tag{7.73}$$

$$C_4: \quad \begin{aligned}&(-k_{y3} - k_{y2} - 2k_2)y_{c4} + k_{y3}y_{s3} + k_{y2}y_{s4} - 2k_2y_{c3} + 2k_2y \\ &\quad - (c_{y3} + c_{y2} + 2c_2)\dot{y}_{c4} + c_{y3}\dot{y}_{s3} + c_{y2}\dot{y}_{s4} - 2c_2\dot{y}_{c3} + 2c_2\dot{y} - m_c\ddot{y}_{c4} = 0\end{aligned} \tag{7.74}$$

$$C_3: \quad \begin{aligned}&(-k_{y5} - k_{y4} - 2k_2)y_{c3} + k_{y5}y_{a2} + k_{y4}y_{s3} - 2k_2y_{c4} + 2k_2y \\ &- (c_{y5} + c_{y4} + 2c_2)\dot{y}_{c3} + c_{y5}\dot{y}_{a2} + c_{y4}\dot{y}_{s3} - 2c_2\dot{y}_{c4} + 2c_2\dot{y} - m_c\ddot{y}_{c3} = 0\end{aligned} \tag{7.75}$$

$$S_4: \quad \begin{aligned}&(-k_{y2} - k_{y1})y_{s4} + k_{y2}y_{c4} + k_{y1}y_{a2} \\ &+ (-c_{y2} - c_{y1})\dot{y}_{s4} + c_{y2}\dot{y}_{c4} + c_{y1}\dot{y}_{a2} - m_s\ddot{y}_{s4} = 0\end{aligned} \tag{7.76}$$

$$S_3: \quad \begin{aligned}&(-k_{y4} - k_{y3})y_{s3} + k_{y4}y_{c3} + k_{y3}y_{c4} \\ &+ (-c_{y4} - c_{y3})\dot{y}_{s3} + c_{y4}\dot{y}_{c3} + c_{y3}\dot{y}_{c4} - m_s\ddot{y}_{s3} = 0\end{aligned} \tag{7.77}$$

Then, the motions of the connectors, the sliders and the actuator can be determined using the latter equations. The actuating force f_{a2} can be calculated using the dynamic equation of the

actuator:

$$A_2: \qquad m_a\ddot{y}_{a2} = f_{a2} + f_{a2s4} - f_{c3a2} \tag{7.78}$$

That is to say, the actuating force is given by

$$f_{a2} = (-k_{y1} - k_{y5})y_{a2} + k_{y1}y_{s4} + k_{y5}y_{c3} + (-c_{y1} - c_{y5})\dot{y}_{a2} + c_{y1}\dot{y}_{s4} + c_{y5}\dot{y}_{c3} - m_a\ddot{y}_{a2}. \tag{7.79}$$

If the motion of the actuator and the actuating force are known, the motions of the end-effector, the connectors, the sliders can also be solved using the equations derived above.

7.2.4 Simulation

7.2.4.1 Cables with Compliance and without Damping

Neglecting the damping in the cables, it is assumed that the motion of the end-effector in the y direction is given by

$$y = y_{po}\sin(\omega t), \qquad \ddot{y} = -y_{po}\omega^2\sin(\omega t). \tag{7.80}$$

In the steady state, the motion of C_i, S_i, $i = 3, 4$, A_2 should also be a sine function without phase difference. Hence, we can write the following:

$$\begin{aligned}
y_{a2} &= y_{a2o}\sin(\omega t), & \ddot{y}_{a2} &= -\omega^2 y_{a2o}\sin(\omega t)\\
y_{c4} &= y_{c4o}\sin(\omega t), & \ddot{y}_{c4} &= -\omega^2 y_{c4o}\sin(\omega t)\\
y_{c3} &= y_{c3o}\sin(\omega t), & \ddot{y}_{c3} &= -\omega^2 y_{c3o}\sin(\omega t)\\
y_{s4} &= y_{s4o}\sin(\omega t), & \ddot{y}_{s4} &= -\omega^2 y_{s4o}\sin(\omega t)\\
y_{s3} &= y_{s3o}\sin(\omega t), & \ddot{y}_{s3} &= -\omega^2 y_{s3o}\sin(\omega t)
\end{aligned}$$

Then, Eq. (7.73) to Eq. (7.77) can be rewritten as

$$\mathbf{D}\mathbf{y} = \mathbf{y}_d \tag{7.81}$$

where

$$\mathbf{y} = \begin{bmatrix} y_{a2o}\\ y_{s4o}\\ y_{c4o}\\ y_{s3o}\\ y_{c3o} \end{bmatrix}, \qquad \mathbf{y}_d = y_{po}\begin{bmatrix} 4k_2 - m_p\omega^2\\ -2k_2\\ -2k_2\\ 0\\ 0 \end{bmatrix}, \qquad \mathbf{D} = \begin{bmatrix} \mathbf{d}_1^T\\ \mathbf{d}_2^T\\ \mathbf{d}_3^T\\ \mathbf{d}_4^T\\ \mathbf{d}_5^T \end{bmatrix},$$

and

$$\mathbf{d}_1 = \begin{bmatrix} 0 \\ 0 \\ 4k_2 \\ 0 \\ 4k_2 \end{bmatrix}, \qquad \mathbf{d}_2 = \begin{bmatrix} 0 \\ k_{y2} \\ -k_{y3} - k_{y2} - 2k_2 + m_c\omega^2 \\ k_{y3} \\ -2k_2 \end{bmatrix}, \qquad \mathbf{d}_3 = \begin{bmatrix} k_{y5} \\ 0 \\ -2k_2 \\ k_{y4} \\ -k_{y5} - k_{y4} - 2k_2 + m_c\omega^2 \end{bmatrix},$$

$$\mathbf{d}_4 = \begin{bmatrix} k_{y1} \\ -k_{y2} - k_{y1} + m_s\omega^2 \\ k_{y2} \\ 0 \\ 0 \end{bmatrix}, \qquad \mathbf{d}_5 = \begin{bmatrix} 0 \\ 0 \\ k_{y3} \\ -k_{y4} - k_{y3} + m_s\omega^2 \\ k_{y4} \end{bmatrix}.$$

The amplitude of motion of the actuator, the sliders and the connectors can be calculated as

$$\mathbf{y} = \mathbf{D}^{-1}\mathbf{y}_d. \tag{7.82}$$

The required actuating force should be

$$f_{a2} = \left[(-k_{y1} - k_{y5})y_{a2o} + k_{y1}y_{s4o} + k_{y5}y_{c3o} + m_a y_{a2o}\omega^2\right]\sin(\omega t). \tag{7.83}$$

If the stiffness of the springs is large enough, the motions of the actuator, the connectors and the sliders are almost the same for the given trajectory of the end-effector, as shown in Figure 7.5. In order to have an intuitive impression of the corresponding motions of the actuator, the connectors and the sliders, it is assumed that the stiffness of the cable segments is $k_2 = k_{y1} = k_{y5} = k_{y2} = k_{y4} = k_{y3} = 300\text{N/m}$, which is much lower than the stiffness that can be expected in practice. Then the plots for the displacements of C_i, S_i, $i = 3, 4$, A_2 are shown in Figure 7.6 and the required actuating force is shown in Figure 7.7.

7.2.4.2 Cables with Compliance and Damping

If besides the compliance, the cables have significant damping, the displacement of the actuator, the connectors and the sliders will include a phase shift. Suppose the motion of the end-effector is

$$\begin{aligned} y &= y_{po}\sin(\omega t), \\ \dot{y} &= y_{po}\omega\cos(\omega t), \\ \ddot{y} &= -y_{po}\omega^2\sin(\omega t). \end{aligned}$$

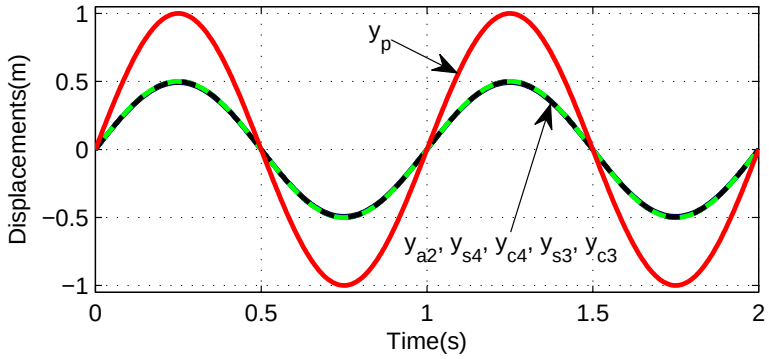

Figure 7.5: The motions of the masses in the mechanism ($y_p = \sin(2\omega t)$m, the stiffness of all the cable segments are 10^4N/m and the masses are $m_p = m_c = m_s = m_a = 1$Kg).

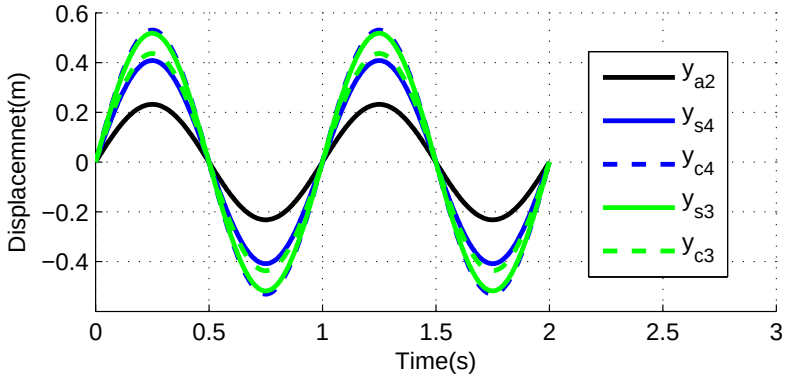

Figure 7.6: The motions of the masses in the mechanism.

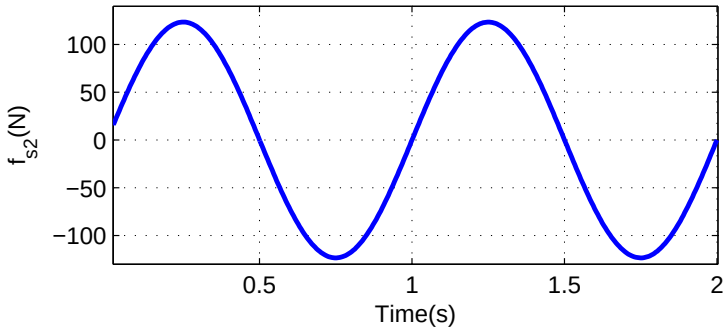

Figure 7.7: The required actuating force.

The corresponding displacements of A_2 and C_i, S_i, $i = 3, 4$, are

$$\begin{aligned} y_{a2} &= y_{a2o}\sin(\omega t + \phi_{a2}),\\ y_{s4} &= y_{s4o}\sin(\omega t + \phi_{s4}),\\ y_{c4} &= y_{c4o}\sin(\omega t + \phi_{c4}),\\ y_{s3} &= y_{s3o}\sin(\omega t + \phi_{s3}),\\ y_{c3} &= y_{c3o}\sin(\omega t + \phi_{c3}). \end{aligned}$$

where the five amplitudes and the five phases are the unknowns.

Substituting y_{c4} and y_{c3} into Eq. (7.73) and expanding the trigonometric functions, two equations are obtained for the coefficients for $\sin(\omega t)$ and $\cos(\omega t)$. That is to say

$$\begin{aligned} -4c_2\omega S_{c4} + 4k_2 C_{c4} - 4c_2\omega S_{c3} + 4k_2 C_{c3} &= 4k_2 y_{po} - m_p\omega^2 y_{po}\\ 4k_2 S_{c4} + 4c_2\omega C_{c4} + 4k_2 S_{c3} + 4c_2\omega C_{c3} &= 4c_2\omega y_{po} \end{aligned}$$

where $S_{c4} = y_{c4o}\sin\phi_{c4}$, $C_{c4} = y_{c4o}\cos\phi_{c4}$, $S_{c3} = y_{c3o}\sin\phi_{c3}$ and $C_{c3} = y_{c3o}\cos\phi_{c3}$. Using the same approach, eight other equations can be built. Assembling these ten equations, one obtains

$$\left[\begin{array}{cc} \mathbf{M}_s & \mathbf{M}_c \end{array}\right] \left[\begin{array}{c} \mathbf{v}_s \\ \mathbf{v}_c \end{array}\right] = \left[\begin{array}{c} \mathbf{u}_s \\ \mathbf{u}_c \end{array}\right], \tag{7.84}$$

where

$$\mathbf{v}_s = \left[\begin{array}{c} y_{a2o}\sin\phi_{a2} \\ y_{c4o}\sin\phi_{c4} \\ y_{c3o}\sin\phi_{c3} \\ y_{s4o}\sin\phi_{s4} \\ y_{s3o}\sin\phi_{s3} \end{array}\right], \qquad \mathbf{v}_c = \left[\begin{array}{c} y_{a2o}\cos\phi_{a2} \\ y_{c4o}\cos\phi_{c4} \\ y_{c3o}\cos\phi_{c3} \\ y_{s4o}\cos\phi_{s4} \\ y_{s3o}\cos\phi_{s3} \end{array}\right],$$

$$\mathbf{u}_s = \left[\begin{array}{c} -m_p y_{po}\omega^2 + 4k_2 y_{po} \\ -2k_2 y_{po} \\ -2k_2 y_{po} \\ 0 \\ 0 \end{array}\right], \qquad \mathbf{u}_c = \left[\begin{array}{c} 4c_2\omega y_{po} \\ -2c_2\omega y_{po} \\ -2c_2\omega y_{po} \\ 0 \\ 0 \end{array}\right],$$

$$\mathbf{M}_s = \left[\begin{array}{c} \mathbf{m}_{s1}^T \\ \mathbf{m}_{s2}^T \\ \vdots \\ \mathbf{m}_{s10}^T, \end{array}\right], \qquad \mathbf{M}_c = \left[\begin{array}{c} \mathbf{m}_{c1}^T \\ \mathbf{m}_{c2}^T \\ \vdots \\ \mathbf{m}_{c10}^T, \end{array}\right],$$

and

$$\mathbf{m}_{s1} = -\mathbf{m}_{c2} = \omega \begin{bmatrix} 0 \\ -4c_2 \\ -4c_2 \\ 0 \\ 0 \end{bmatrix}, \qquad \mathbf{m}_{s2} = \mathbf{m}_{c1} = \begin{bmatrix} 0 \\ 4k_2 \\ 4k_2 \\ 0 \\ 0 \end{bmatrix},$$

$$\mathbf{m}_{s3} = -\mathbf{m}_{c4} = \omega \begin{bmatrix} 0 \\ (c_{y3} + c_{y2} + 2c_2) \\ 2c_2 \\ -c_{y2} \\ -c_{y3} \end{bmatrix}, \qquad \mathbf{m}_{s4} = \mathbf{m}_{c3} = \begin{bmatrix} 0 \\ -(k_{y3} + k_{y2} + 2k_2) + m_c\omega^2 \\ -2k_2 \\ k_{y2} \\ k_{y3} \end{bmatrix},$$

$$\mathbf{m}_{s5} = -\mathbf{m}_{c6} = \omega \begin{bmatrix} -c_{y5} \\ 2c_2 \\ (c_{y5} + c_{y4} + 2c_2) \\ 0 \\ -c_{y4} \end{bmatrix}, \qquad \mathbf{m}_{s6} = \mathbf{m}_{c5} = \begin{bmatrix} k_{y5} \\ -2k_2 \\ -(k_{y5} + k_{y4} + 2k_2) + m_c\omega^2 \\ 0 \\ k_{y4} \end{bmatrix},$$

$$\mathbf{m}_{s7} = -\mathbf{m}_{c8} = \omega \begin{bmatrix} -c_{y1} \\ -c_{y2} \\ 0 \\ (c_{y2} + c_{y1}) \\ 0 \end{bmatrix}, \qquad \mathbf{m}_{s8} = \mathbf{m}_{c7} = \begin{bmatrix} k_{y1} \\ k_{y2} \\ 0 \\ -(k_{y2} + k_{y1}) + m_s\omega^2 \\ 0 \end{bmatrix},$$

$$\mathbf{m}_{s9} = -\mathbf{m}_{c10} = \omega \begin{bmatrix} 0 \\ -c_{y3} \\ -c_{y4} \\ 0 \\ (c_{y4} + c_{y3}) \end{bmatrix}, \qquad \mathbf{m}_{s10} = \mathbf{m}_{c9} = \begin{bmatrix} 0 \\ k_{y3} \\ k_{y4} \\ 0 \\ -(k_{y4} + k_{y3}) + m_s\omega^2 \end{bmatrix}.$$

Then, the ten unknowns can be solved for. From Eq. (7.84), vectors $\mathbf{v}_s$ and $\mathbf{v}_c$ can be obtained and the amplitude and the phase for the actuator, the connectors and the sliders can be found. Taking A_2 as an example, one has

$$y_{a2o} = \sqrt{v_{s1}^2 + v_{c1}^2}, \qquad \phi_{s2} = \arctan(v_{s1}, v_{c1}),$$

where v_{s1} and v_{c1} are the first element of vector $\mathbf{v}_s$ and $\mathbf{v}_c$ respectively. With y_{a2}, y_{s4} and y_{c3}, the required actuating force can be obtained using Eq. (7.79).

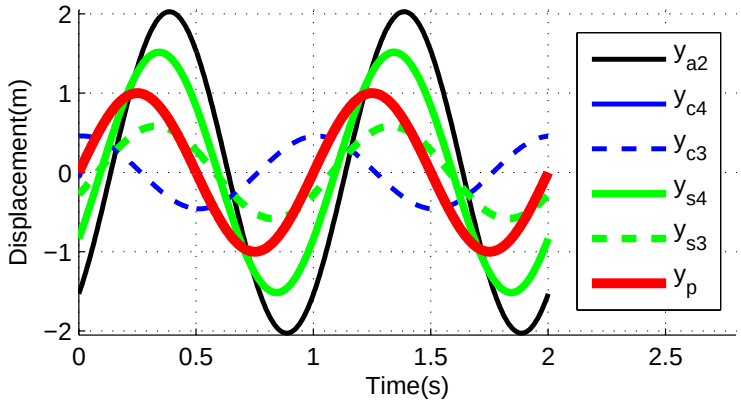

Figure 7.8: The motions of the masses in the mechanism when cables have compliance and damping.

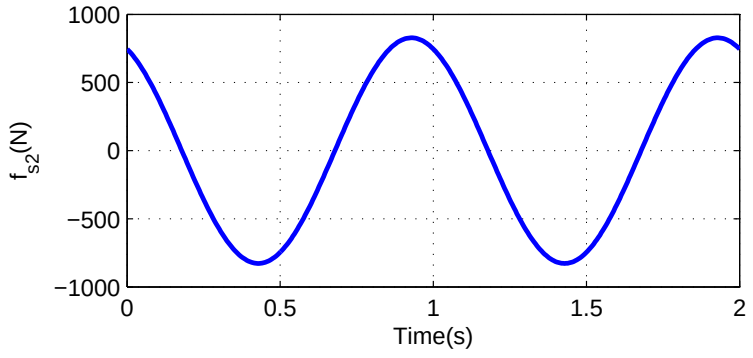

Figure 7.9: The required actuating force.

In order to see the influence of the damping and compared with Figure 7.6, it is assumed that the trajectory of the end-effector in the y direction is $y_p = \sin(2\pi t)$m, the stiffness of the cable segments is $k_2 = k_{yi} = 300$N/m, the damping of the cable segments is $c_2 = c_{yi} = 1$Ns/m, $i = 1, \ldots, 5$, and the masses are $m_p = m_c = m_s = m_a = 1$kg. Then the plots for the displacements of C_i, S_i, $i = 3, 4$, and A_2 are shown in Figure 7.8. The required actuating force is shown in Figure 7.9.

7.3 Conclusion

A novel structure of 2-DOF decoupled cable-loop slider-driven parallel mechanism is introduced in this chapter. The displacement in two directions can be controlled separately by the combined cable-routings. The kinematic and static equations of this mechanism are very simple because of the decoupling. The stiffness of the mechanism is analyzed: it can be observed that the mechanism has a excellent stiffness. If the cable compliance is neglected in the dynamic analysis, the dynamic equations are also simple. Considering the compliance and the damping of the cables, though the dynamic equations are complex, the motion of the actuator, the sliders and the connectors and the required actuating force can be found.

Chapter 8

Conclusions

8.1 Summary and Contributions of the Thesis

In order to avoid the cable-spool system and eliminate actuation redundancy in cable-driven parallel mechanisms, the concept of using cable loops in the cable-driven parallel mechanisms has been proposed in this thesis. Several architectures of cable-loop mechanisms are developed and the basic studies for these mechanisms are given. Variations that improve the properties of the mechanisms are proposed gradually. First, the cable-spool system is replaced with a cable-loop slider-driven system: the motion of the end-effector can be controlled by the displacement of the slider. However, the mechanism is redundantly actuated. Then, springs are introduced in the cable loops. The mechanisms eliminate actuation redundancy since the force closure conditions can be established by the compliance of the springs. The characteristics of the mechanisms, for example the workspace and the force capabilities, are influenced by the parameters of the springs. Finally, the planar decoupled non-redundant cable-loop-driven parallel mechanism is presented. The two degrees of freedom of the mechanism are decoupled and only two actuators are needed

to control the motion. The mechanism does not require actuation redundancy and it does not include a rigid-link translational mechanism or the compliance provided by springs. Therefore, it retains the advantages of cable-spool mechanisms while alleviating their drawbacks.

The redundantly actuated planar cable-loop driven mechanisms proposed in Chapter 2 is intended to avoid the cable-spool system. By replacing the cable and spool arrangement with closed cable loops which are free to move around a set of pulleys, the difficulties of measuring the extension of the cables are alleviated. The inverse kinematics, the Jacobian matrices and the static equations for these mechanisms are obtained. The workspace of the mechanisms are also studied. Since the position of the end-effector is the intersection of several ellipses, the boundary of the force-closed workspace is determined from geometric reasoning. Compared with the surface of the polygon determined by the fixed pulleys, the workspace of the mechanism is quite large. It is shown that the concept of cable loop can be used in cable-driven parallel mechanisms.

Planar and spatial spring-loaded cable-loop-driven parallel mechanisms are proposed subsequently. By attaching springs to the cable loops, the cable-loop-driven mechanisms require only N actuators to control N-DOF motion. The spring-loaded cable-loop models are first applied to planar mechanisms. From the workspace analysis, it can be observed that the mechanism in which the compliance is symmetric on both sides of the actuator has better characterics than the non-symmetric mechanism in which the compliance is just on one side of the actuator. Therefore, the mechanism with symmetric compliance is extended to a spatial mechanism. The inverse kinematic equations and the static equations for these mechanisms are given. It is shown that the mechanisms have significantly large workspaces with proper springs. It is observed that the spring-loaded mechanisms have force capabilities that are not as good as those of the conventional cable-driven mechanisms with the same geometries since there are fewer actuators. Nevertheless, the analysis of the force capabilities of the mechanisms show that the spring-loaded cable-loop-driven parallel mechanisms can provide very good force capabilities while being more efficient and cost-effective. It should be noticed that the minimum cable force has a significant impact on the spring-loaded mechanisms due to the coupled compliance on each side of the actuators. Then, it is essential to minimise the friction in the practical design. The natural frequencies and the corresponding ratio of the amplitudes for these two mechanisms are also found. They can provide an estimation of the acceleration boundary which guarantees that the mechanisms do not undergo undesirable vibrations and that the cables do not become slack.

The actuation redundancy is replaced with passive redundancy realized by springs in spring-

loaded mechanisms. However, the requirement of using extension springs limits their force capabilities. Therefore, a planar decoupled non-redundant cable-loop-driven parallel mechanism is proposed. The mechanism does not require the use of a bridge and trolley structure: only cables are connected to the end-effector. The displacements in two directions can be controlled separately by combined cable-routings. The kinematic and static equations of this mechanism are very simple due to the simple geometric design. The workspace is essentially equal to the footprint of the mechanism and there are not singularities. The mechanism has an excellent stiffness. If the cable compliance is neglected in the dynamic analysis, the dynamic equations are very simple. Considering the compliance and the damping of the cables, a more complex model is obtained.

The mechanisms proposed in this thesis have many kinds of architectures. However, for all of them, motion is realized with cable loops. The objectives of avoiding the cable-spool systems and eliminating actuation redundancy are achieved.

8.2 Directions for Future Work

Many cable-loop-driven parallel mechanisms are proposed in this thesis. It can be seen that the mechanisms can complete the tasks of displacing the end-effector in a planar or spatial space. However, it is difficult to find mechanisms which can produce torques at the end-effector. It was intended to find a 6-DOF spring-loaded cable-loop-driven mechanism and a 3-DOF decoupled non-redundant cable-loop-driven parallel mechanism. However, such architectures could not be found. Perhaps such mechanisms can be developed in the future.

Due to the geometry of the mechanisms, almost all the equations contain many different square roots which have the variables associated with the end-effectors' position as their denominators. The analysis for such equations is difficult, since derivations using polar coordinates or spherical coordinates makes the expressions become even more complex. Alternative mathematical frameworks could be investigated in order to reduce the mathematical complexity and provide insight.

Simplifying assumptions are used for the analysis. Therefore, the dynamic equations for the planar and spatial spring-loaded cable-loop-driven mechanisms are simplified models which only

consider the mass of the actuators and the end-effector. More complete and accurate models could be established in the future. Also, the introduction of friction terms in the models could be important for some applications.

The architectures proposed in this thesis avoid the cable-spool system and may lead to better accuracy. In the future, the spring-loaded cable-loop-driven mechanisms can be used in situations for which the force capabilities are not an important and the mechanisms need to be more economically viable.

Bibliography

[1] J. Albus, R. Bostelman and N. Dagalakis, 1993, "The NIST robocrane", *Journal of Robotics Systems*, Vol. 10, No. 5, pp. 709–724.

[2] L. L. Cone, 1985, "Skycam, an aerial robotic camera system", *Byte*, Vol. 10, pp. 122–132.

[3] R. G. Roberts, T. Graham and T. Lippitt, 1998, "On the inverse kinematics, statics, and fault tolerance of cable-suspended robots", *Journal of Robotic Systems*, Vol. 15, No. 10, pp. 581-597.

[4] M. Yamamoto, N. Yanai and A. Mohri, 1999, "Inverse dynamics and control of crane-type manipulator", *in Proceedings of IEEE/RSJ International Conference on Intelligent Robots and Systems*, pp. 1228-1233.

[5] M. Yamamoto and A. Mohri, 2000, "Inverse kinematics analysis for incompletely restrained parallel wire mechanisms", *in proceedings of IEEE/RSJ International Conference on Intelligent Robots and Systems*, pp. 504-509.

[6] J. J. Gorman, K. W. Jablokow and D. J. Cannon, 2001, "The cable array robot: theory and experiment", *in Proceedings of IEEE International Conference on Robotics & Automation*, Seoul, Korea, pp. 2804-2810.

[7] A. B. Alp and S. K. Agrawal, 2002, "Cable suspended robots: design, planning and control", *in Proceedings of IEEE International Conference on Robotics & Automation*, Washington, DC, pp. 4275-4280.

[8] J. Pusey, A. Fattah, S. Agrawal and E. Messina, 2004, "Design and workspace analysis of a 6-6 cable-suspended parallel robot", *Mechanism and Machine Theory*, Vol. 39, pp. 761-778.

[9] S. Bouchard and C. M. Gosselin, 2006, "Kinematic sensitivity of a very large cable-driven parallel mechanism", *in Proceedings of ASME International Design Engineering Technical Conferences & Computers and Information in Engineering Conference*, Philadelphia, Pennsylvania, USA, DETC2006-99222.

[10] S. Tadokoro, R. Verhoeven, M. Hiller and T. Takamori, 1999, "A portable parallel manipulator for search and rescue at large-scale urban earthquakes and an identification algorithm for the installation in unstructured environments", *in proceedings of the IEEE/RSJ International Conference on Intelligent Robots and Systems*, pp. 1222-1227.

[11] P. Gallina, 2004, "23 wire driven robots for rehabilitation", *Advances in Rehabilitation Robotics*, Vol. 306, pp. 365-375.

[12] S. Fang, D. Franitza, M. Torlo, F. Bekes and M. Hiller, 2004, "Motion control of a tendon-based parallel manipulator using optimal tension Distribution", *in IEEE/ASME Transactions on Mechatronics*, Vol. 9, No. 3, pp. 561-568.

[13] R. L. Williams II, J. S. Albus and R. V. Bostelman, 2004, "3D cable-based Cartesian metrology system", *Journal of Robotic Systems*, Vol. 21, No. 5, pp. 237-257.

[14] J. Du, H. Bao, X. Duan and C. Cui, 2010, "Jacobian analysis of a long-span cable-driven manipulator and its application to forward solution", *Mechanism and Machine Theory*, Vol. 45, pp. 1227-1238.

[15] A. Alikhani, S. Behzadipour, A. Alasty and S. A. S. Vanini, 2011, "Design of a large-scale cable-driven robot with translational motion", *Robotics and Computer-Integrated Manufacturing*, Vol. 27, pp. 357-366.

[16] S. Kawamura, W. Choe, S. Tanaka and S. Pandian, 1995, "Development of an ultrahigh speed robot FALCON using wire drive system", *in Proceedings of the IEEE International Conference on Robotics and Automation*, Nagoya, Japan, Vol. 1, pp. 215–220.

[17] T. Morizono, K. Kurahashi and S Kawamura, 1997, "Realization of a virtual sports training system with parallel wire mechanism", *in proceedings of the IEEE International Conference on Robotics and Automation*, Albuquerque, New Mexico, pp. 3025-3030.

[18] S. Kawamura, H. Kino and C. Won, 2000, "High-speed manipulator by using parallel wire-driven robots", *Robotica*, Vol. 18, pp. 13-21.

[19] S. Tadokoro and T. Matsushima, 2001, "A parallel cable-driven motion base for virtual acceleration", *in Proceedings of the IEEE/RSJ International Conference on Intelligent Robots and Systems*, Maui, Hawaii, USA, pp. 1700-1705.

[20] E. Ottaviano, M. Ceccarelli and F. Palmucci, 2009, "An application of CaTraSys, a cable-based parallel measuring system for an experimental characterization of human walking", *Robotica*, Cambridge University Press, pp. 1-15.

[21] S. Behzadipour and A. Khajepour, 2005, "A new cable-based parallel robot with three degrees of freedom", *Multibody System Dynamics*, Vol. 13, pp. 371-383.

[22] S.-R. Oh and S. K. Agrawal, 2005, "A reference governor-based controller for a cable robot under input constraints", *IEEE Transactions on Control Systems Technology*, Vol. 13, No. 4, pp. 639-645.

[23] E. Ottaviano, 2008, "Analysis and design of a four-cable-driven parallel manipulator for planar and spatial tasks", *Journal of Mechanical Engineering Science*, Vol. 222, Part C, pp. 1583-1592.

[24] R. L. Williams II and P. Gallina, 2001, "Planar cable-driven robots, part I: kinematics and statics", *in Proceedings of ASME Design Engineering Technical Conferences*, Pittsburgh, PA, DETC2001/DAC-21145.

[25] P. Gallina, A. Rossi and R. L. Williams II, 2001, "Planar cable-driven robots, part II: dynamics and control ", *in Proceedings of ASME Design Engineering Technical Conferences*, Pittsburgh, PA, DETC2001/DAC-21146.

[26] R. L. Williams II and J. Vadia, 2003, "Planar translational cable-direct-driven robots: hardware implementation", *in Proceedings of ASME Design Engineering Technical Conferences*, Chicago, IL, DETC2003/DAC-48823.

[27] M. S. Varziri and L. Notash, 2007, "Kinematic calibration of a wire-actuated parallel robot", *Mechanism and Machine Theory*, Vol. 42, pp. 960-976.

[28] M. Hiller, S. Fang, S. Mielczarak, R. Verhoeven and D. Franitza, 2005, "Design, analysis and realization of tendon-based parallel manipulators", *Mechanism and Machine Theory*, Vol. 40, pp. 429-445.

[29] A. M. Hay and J. A. Snyman, 2005, "Optimization of a planar tendon-driven parallel manipulator for a maximal dexterous workspace", *Engineering Optimization*, Vol. 37, No. 3, pp. 217-236.

[30] E. Ottaviano, M. Ceccarelli and M. De Ciantis, 2007, "A 4-4 cable-based parallel manipulator for an application in hospital environment", *Mediterranean Conference on Control and Automation*, Athens, Greece, T30-018.

[31] P. Bosscher, R. L. Williams II and M. Tummino, 2005, "A concept for rapidly-deployable cable robot search and rescue systems", *in proceedings of ASME International Design Engineering Technical Conferences and Computers and Information in Engineering Conference*, Long Beach, California, USA, DETC2005-84324.

[32] D. Mayhew, B. Bachrach, W. Z. Rymer and R. F. Beer, 2005, "Development of the MACARM - a novel cable robot for upper limb neurorehabilitation", *in Proceedings of IEEE 9th International Conference on Rehabilitation Robotics*, Chicago, IL, USA, pp. 299-302.

[33] P. Bosscher, R. L. Williams II, L. Sebastian Bryson and D. Castro-Lacouture, 2007, "Cable-suspended robotic contour crafting system", *Automation in Construction*, Vol. 17, pp. 45–55.

[34] P. Gallina, G. Rosati and A. Rossi, 2001, "3-d.o.f. wire driven planar haptic interface", *Journal of Intelligent and Robotic Systems*, Vol. 32, pp. 23-36.

[35] K. Maeda, S. Tadokoro, T. Takamori, M. Hiller and R. Verhoeven, 1999, "On design of a redundant wire-driven parallel robot WARP manipulator", *in proceedings of the IEEE international conference on robotics & automation*, Detroit, Michigan, pp. 895-900.

[36] C. Gosselin, R. Poulin and D. Laurendeau, 2008, "A planar parallel 3-dof cable-driven haptic interface", *in Proceedings of the 12th World Multi-Conference on Systemics, Cybernetics and Informatics: WM-SCI '08*, Orlando, Florida, USA, Vol. 3, pp. 266-271.

[37] R. Verhoeven and M. Hiller, 2001, "Estimating the controllable workspace of tendon-based Stewart platforms", *Advances in Robot Kinematics*, pp. 277-284.

[38] P. Bosscher and I. Ebert-Uphoff, 2004, "A stability measure for underconstrained cable-driven robots", *in Proceedings of IEEE International Conference on Robotics & Automation*, New Orleans, LA, pp. 4943-4949.

[39] A. Trevisani, P. Gallina and R. L. Williams II, 2006, "Cable-Direct-Driven Robot (CDDR) with passive SCARA support: theory and simulation", *Journal of Intelligent and Robotic Systems*, Vol. 46, pp. 73-94.

[40] A. Ghasemi, M. Eghtesad and M. Farid, 2008, "Workspace analysis of planar and spatial redundant cable robots", *in Proceedings of American Control Conference*, Seattle, Washington, USA, pp. 2389-2394.

[41] C. B. Pham, S. H. Yeo, G. Yang and I-M. Chen, 2009 "Workspace analysis of fully restrained cable-driven manipulators", *Robotics and Autonomous Systems*, Vol. 57, pp. 901-912.

[42] A. Pott, 2008, "Forward kinematics and workspace determination of a wire robot for industrial applications", *Advances in Robot Kinematics: Analysis and Design*, pp. 451-458.

[43] E. Stump and V. Kumar, 2006, "Workspaces of cable-actuated parallel manipulators", *Journal of Mechanical Design*, Vol. 126, pp. 159-167.

[44] G. Yang, C. B. Pham and S. H. Yeo, 2006, "Workspace performance optimization of fully restrained cable-driven parallel manipulators", *in Proceedings IEEE/RSJ International Conference on Intelligent Robots and Systems*, Beijing, China, pp. 85-90.

[45] S. Bouchard and C. M. Gosselin, 2007, "Workspace optimization of a very large cable-driven parallel mechanism for a radiotelescope application", *in Proceedings of ASME International Design Engineering Technical Conference & Computers and Information in Engineering Conference*, Las Vegas, Nevada, USA, DETC2007-34286.

[46] C. Gosselin and S. Bouchard, 2010, "A gravity-powered mechanism for extending the workspace of a cable-driven parallel mechanism: Application to the appearance modeling of objects", *International Journal of Automation Technology*, Vol. 4, No. 4, July, pp. 372-379.

[47] A. Trevisani, 2010, "Underconstrained planar cable-direct-driven: a trajectory planning method ensuring positive and bounded cable tensions", *Mechatronics*, Vol. 20, pp. 113-127.

[48] P. Gallina and G. Rosati, 2002, "Manipulability of a planar wire driven haptic device", *Mechanism and Machine Theory*, Vol. 37, pp. 215-228.

[49] A. Alikhani, S. Behzadipour, S.A. Sadough Vanini and A. Alasty, 2009, "Workspace analysis of a three DOF cable-driven mechanism", *ASME Journal of Mechanisms and Robotics*, Vol. 1, No. 4, paper No. 041005.

[50] S. Perreault and C. M. Gosselin, 2008, "Cable-driven parallel mechanisms: application to a locomotion interface", *Journal of Mechanical Design*, Vol. 130, 102301.

[51] J. Sefrioui and C. M. Gosselin, 1992, "Singularity analysis and representation of planar parallel manipulators", *Robotics and Autonomous Systems*, Vol. 10, pp. 209-224.

[52] J. Sefrioui and C. M. Gosselin, 1995, "On the quadratic nature of the singularity curves of planar three-degree-of-freedom parallel manipulators", *Mechanism and Machine Theory*, Vol. 30, No. 4, pp. 533-551.

[53] B. M. St-Onge and C. M. Gosselin, "Singularity analysis and representation of the general Gough-Stewart Platform", *The International Journal of Robotics Research*, Vol. 19, No. 3, pp. 271-288.

[54] E. Ottaviano and M. Ceccarelli, 2007, "Numerical and experimental characterization of singularities of a six-wire parallel architecture", *Robotica*, Vol. 25, pp. 315-324.

[55] X. Diao, O. Ma and Q. Lu, 2008, "Singularity analysis of planar cable-driven parallel robots", *in Proceedings of IEEE Conference on Robotics, Automation and Mechatronics*, Chengdu, China, pp. 272-277.

[56] X. Diao and O. Ma, 2007, "A method of verifying force-closure condition for general cable manipulators with seven cables", *Mechanism and Machine Theory*, Vol. 42, pp. 1563-1576.

[57] X. Diao and O. Ma, 2008, "Force-closure analysis of 6-DOF cable manipulators with seven or more cables", *Robotica*, Vol. 27, pp. 209-215.

[58] K. Kozak, Q. Zhou and J. Wang, 2006, "Static analysis of cable-driven manipulators with non-negligible cable mass", *IEEE Transactions on Robotics*, Vol. 22, No. 3, pp. 425-433.

[59] T. Bruckmann, A. Pott and M. Hiller, 2006, "Calculating force distributions for redundantly actuated tendon-dased Stewart platforms", *Advances in Robot Kinematics*, pp. 403-412.

[60] I. Ebert-Uphoff and P. A. Voglewede, 2004, "On the connections between cable-driven robots, parallel manipulators and grasping", *proceedings of the IEEE International Conference on Robotics & Automation*, New Orleans, LA, pp. 4512-4526.

[61] A. T. Riechel and I. Ebert-Uphoff, 2004, "Force-feasible workspace analysis for underconstrained point-mass cable robots", *in Proceedings of IEEE International Conference on Robotics & Automation*, New Orleans, LA, pp. 4956-4962.

[62] C. B. Pham, S. H. Yeo and G. Yang, 2005, "Tension analysis of cable-driven parallel mechanisms", *proceedings of IEEE/RSJ International Conference on Intelligent Robots and Systems*, Edmonton, Alberta, Canada, pp. 2601-2606.

[63] L. Mikelsons, T. Bruckmann, M. Hiller and D. Schramm, 2008, "A real-time capable force calculation algorithm for redundant tendon-based parallel manipulators", *in Proceedings of the IEEE International Conference on Robotics and Automation*, Pasadena, CA, USA, pp. 3869-3874.

[64] M. Gouttefarde, J-P. Merlet and D. Daney, 2006, "Determination of the wrench-closure workspace of 6-DOF parallel cable-driven mechanisms", *Advances in Robot Kinematics*, pp. 315-322.

[65] M. Gouttefarde, J-P. Merlet and D. Daney, 2007, "Wrench-feasible workspace of parallel cable-driven mechanisms", *in Proceedings of IEEE International Conference on Robotics and Automation*, Rome, Italy, pp. 1492-1497.

[66] C. B. Pham, S. H. Yeo, G. Yang, M. S. Kurbanhusen and I-M. Chen, 2006, "Force-closure workspace analysis of cable-driven parallel mechanisms", *Mechanism and Machine Theory*, Vol. 41, pp. 53-69.

[67] W.B. Lim, G. Yang, S.H. Yeo, S.K. Mustafa and I.-M. Chen, 2009, "A generic tension-closure analysis method for fully-constrained cable-driven parallel manipulators", *in Proceedings of IEEE International Conference on Robotics and Automation*, Kobe, Japan, pp. 2187-2192.

[68] J. Park, W.-K. Chung and W. Moon, 2005, "Wire-suspended dynamical system: stability analysis by tension-closure", *IEEE Transactions on Robotics*, Vol. 21, No. 3, pp. 298-308.

[69] W.B. Lim, G. Yang, S.H. Yeo and S.K. Mustafa, 2011, "A generic force-closure analysis algorithm for cable-driven parallel manipulators", *Mechanism and Machine Theory*, Vol. 46, pp. 1265-1275.

[70] M. Gouttefarde and C. M. Gosselin, 2006, "Analysis of the wrench-closure workspace of planar parallel cable-driven mechanisms", *IEEE transactions on Robotics*, Vol. 22, No. 3, pp. 434-445.

[71] M. Gouttefarde and C. M. Gosselin, 2005, "Wrench-closure workspace of six-DOF parallel mechanisms driven by 7 cables", *Transactions of the Canadian Society for Mechanical Engineering*, Vol. 29, No. 4, pp. 541-552.

[72] M. Gouttefarde, 2008, "Characterizations of fully constrained poses of parallel cable-driven robots: a review", *in Proceedings of the ASME International Design Engineering Technical Conferences & Computers and Information in Engineering Conference*, Brooklyn, New York, USA, DETC2008-49467.

[73] P. Bossecher, A. T. Riechel and I. Ebert-Uphoff, 2006, "Wrench-feasible workspace generation for cable-driven robots", *IEEE Transactions on Robotics*, Vol. 22, No. 5, pp. 890-902.

[74] S. Bouchard, C. M. Gosselin and B. Moore, 2008, "On the ability of a cable-driven robot to generate a prescribed set of wrenches", *in Proceedings of ASME International Design Engineering Technical Conference & Computers and Information in Engineering Conference*, Brooklyn, New York, USA, DETC2008-49518.

[75] M. Gouttefarde and S. Krut, 2010, "Characterization of parallel manipulator available wrench set facets", *Advances in Robot Kinematics: Motion in Man and Machine*, pp. 475-482.

[76] M. Gouttefarde, D. Daney and J.-P. Merlet, 2011, "Interval-analysis-based determination of the wrench-feasible workspace of parallel cable-driven robots", *IEEE Transactions on Robotics*, Vol. 27, No. 1, pp. 1-13.

[77] S. Behzadipour and A. Khajepour, 2006, "Stiffness of cable-based parallel manipulators with application to stability analysis", *Journal of Mechanical Design*, Vol. 128, pp. 303-310.

[78] R. Yao, X. Tang, J. Wang and P. Huang, 2010, "Dimensional optimization design of the four-cable-driven parallel manipulator in FAST", *IEEE/ASME Transactions on Mechatronics*, Vo. 15, No. 6, pp. 932-941.

[79] W.-J. Shiang, D. Cannon and J. Gorman, 1999, "Dynamic analysis of the cable array robotic crane", *in Proceedings of IEEE International Conference on Robotics & Automation*, Detroit, Michigan, pp. 2495-2500.

[80] C. B. Pham, G. Yang and S. H. Yeo, 2005, "Dynamic analysis of cable-driven parallel mechanisms", *in Proceedings of IEEE/ASME International Conference on Advanced Intelligent Mechatronics*, Monterey, California, USA, pp. 612-617.

[81] S.-R. Oh, J.-C. Ryu and S. K. Agrawal, 2006, "Dynamics and control of a helicopter carrying a payload using a cable-suspended robot", *Journal of Mechanical Design*, Vol. 128, pp. 1113-1121.

[82] S.-R. Oh, K. Mankala, S. K. Agrawal and J. S. Albus, 2005, "Dynamic modeling and robost controller design of a two-stage parallel cable robot", *Multibody System Dynamics*, Vol. 13, pp. 385-399.

[83] G. Barrette and C. M. Gosselin, 2005, "Determination of the dynamic workspace of cable-driven planar parallel mechanisms", *Journal of Mechanical Design*, Vol. 127, pp. 242-248.

[84] O. Ma and X. Diao, 2005, "Dynamics analysis of a cable-driven parallel manipulator for hardware-in-the-loop dynamic simulation", *in Proceedings of IEEE/ASME International Conference on Advanced Intelligent Mechatronics*, Monterey, California, USA, pp. 837-842.

[85] H. D. Taghirad and M. A. Nahon, 2008, "Dynamic analysis of a Macro-Micro redundantly actuated parallel manipulator", *Advanced Robotics*, Vol. 22, pp. 949-981.

[86] S.-R. Oh, K. Mankala, S. K. Agrawal and J. S. Albus, 2005, "A dual-stage planar cable robot: dynamic modeling and design of a robust controller with positive inputs", *Journal of Mechanical Design*, Vol. 127, pp. 612-620.

[87] M. M. Aref, P. Gholami and H. D. Taghirad, 2008, "Dynamic and sensitivity analysis of KNTU CDRPM: a cable driven redundant parallel manipulator", *IEEE/ASME International Conference on Mechtronic and Embedded Systems and Applications*, Beijing, P. R. China, pp. 528-533.

[88] Y. B. Bedoustani, H. D. Taghirad and M. M. Aref, 2008, "Dynamics analysis of a redundant parallel manipulator driven by elastic cables", *in Proceedings of 10th International Conference on Control, Automation, Robotics and Vision*, Hanoi, Vietnam, pp. 536-542.

[89] A. Berlioz and C-H. Lamarque, 2005, "Nonlinear vibrations of an inclined cable", *Journal of Vibration and Acoustics*, Vol. 127, pp. 315-323.

[90] T. Heyden and C. Woernle, 2006, "Dynamics and flatness-based control of a kinematically undetermined cable suspension manipulator", *Multibody System Dynamics*, Vol. 16, pp. 155-177.

[91] X. Diao and O. Ma, 2009, "Vibration analysis of cable-driven parallel manipulators", *Multibody System Dynamics*, Vol. 21, pp. 347-360.

[92] M. H. Korayem, M. Bamdad, H. Tourajizadeh, A. H. Korayem and S. Bayat, 2011, "Analytical design of optimal trajectory with dynamic load-carrying for cable-suspended manipulator", *International Journal of Advanced Manufacturing Technology*, DIO 10.1007/s00170-011-3579-9.

[93] J. Du, H. Bao, C. Cui and D. Yang, 2012, "Dynamic analysis of cable-driven parallel manipulators with time-varying cable lengths", *Finite Elements in Analysis and Design*, Vol. 48, pp. 1392-1399.

[94] N. M. Kircanski, A. A. Goldenberg and S. K. Dickie, 1995, "An autonomous cable winding and pay-out system for mobile robots",*Autonomous Robots*, Vol. 2, pp. 237-253.

[95] M. Aria and S. Hirose, 2007, "Improved reel mechanism to wind a cable uniformly in spherical trailer", *in Proceedings of IEEE International Workspace on Safety, Security and Rescue Robotics*, Rome, Italy, 978-1-4244-1569-4.

[96] F. Takemura, M. Enomoto, T. Tanaka, K. Denou, Y. Kobayashi and S. Tadokoro, 2005, "Development of the balloon-cable driven robot for information collection from sky and proposal of the strategy at a major disaster", *in Proceedings of IEEE/ASME International Conference on Advanced Intelligent Mechatronics*, Monterey, California, USA, pp. 658-663.

[97] D. W. Hong and R. J. Cipra, 2003, "A method for representing the configuration and analyzing the motion of complex cable-pulley systems", *Journal of Mechanical Design*, Vol. 125, pp. 332-341.

[98] P. H. Borgstrom, B. L. Jordan, B. J. Borgstrom, M. J. Stealey, G. S. Sukhatme, M. A. Batalin and W. J. Kaiser, 2009, "NIMS-PL: a cable-driven robot with self-calibration capabilities", *IEEE Transactions on Robotics*, Vol. 25, No. 5, pp. 1005-1015.

[99] Y. Wischnitzer, N. Shvalb and M. Shoham, 2008, "Wire-driven parallel robot: permitting collisions between wires", *The International Journal of Robotics Research*, Vol. 27, pp. 1007-1026.

[100] J. P. Merlet, 2008, "Kinematics of the wire-driven parallel robot MARIONET using linear actuators", *in proceedings of the IEEE International Conference on Robotics and Automation*, Pasadena, CA, USA, pp. 3857-3862.

[101] J. P. Merlet, 2010, "MARIONET, a family of modular wire-driven parallel robots", *Advances in Robot Kinematics: Motion in Man and Machine*, pp. 53-61.

[102] J. Rodnunsky, 2009, "Safety system and method for objects moved by a driving cabling system", *United States Patent Application Publication*, US2009/0301814 A1.

[103] C. Gosselin, S. Lefrançois and N. Zoso, 2010, "Underactuated cable-driven robots: machine, control and suspended bodies", *Brain, Body and Machine*, Vol. 83, pp. 311-323.

[104] S. Behzadipour, 2009, "Kinematics and dynamics of a self-stressed Cartesian cable-driven mechanism", *Journal of Mechanical Design*, Vol. 131, 061005.

[105] T. Laliberté, C. Gosselin and D. Gao, 2010, "Closed-loop transmission routings for Cartesian SCARA-type manipulators", *in Proceedings of ASME International Design Engineering Technical Conferences & Computers and Information in Engineering Conference*, DETC2010-28718.

[106] B. Gao, J. Zhao, N. Xi and J. Xu, 2011, "Combined kinematic and static analysis of a cable-driven manipulator with a spring spine", *in Proceedings of IEEE International Conference on Robotics and Automation*, Shanghai, China, pp. 2725-2730.

[107] R. A. Russell, 1994, "A robotic system for performing sub-millimeter grasping and manipulation tasks", *Robotics and autonomous systems*, Vol. 13, pp. 209-218.

[108] L. Kashdan, C. Seepersad, M. Haberman, P. S. Wilson, "Design, fabrication and evaluation of negative stiffness elements", http://www.me.utexas.edu/∼ppmdlab/files/Kashdan_Paper11 _FINAL.pdf

[109] Y. C. Wang and R. S. Lakes, 2004, "Extreme stiffness systems due to negative stiffness elements", *American Journal of Physics*, Vol. 72, No. 1, pp. 40-50.

[110] C.-M. Lee, V.N. Goverdovskiy and A.I. Temnikov, 2007, "Design of springs with "negative" stiffness to improve vehicle driver vibration isolation", *Journal of Sound and Vibration*, Vol. 302, pp. 865-874.

[111] C. Gosselin, X. Kong, S. Foucault, I.A. Bonev, 2004, "A fully-decoupled 3-dof translational parallel mechanism", *Parallel Kinematic Machines in Research and Practice, The 4th Chemnitz Parallel Kinematics Seminar*, pp. 595–610.

Appendix A

Inequalities for all Cable Forces of the Planar Mechanism Considering the External Force

Since the cable forces f_{ai}, f_{bi}, $i = 1, 2$, should be positive within the workspace, using the cable force equations, the following inequalities can be found

$$(y_{sb2} - y_{sa2})f_{ex} - (x_{sb2} - x_{sa2})f_{ey} < f_{B1}, \tag{A.1}$$

$$-(y_{sb1} - y_{sa1})f_{ex} + (x_{sb1} - x_{sa1})f_{ey} < f_{B2}, \tag{A.2}$$

$$(y_{sa2} - y_{sb2})f_{ex} - (x_{sa2} - x_{sb2})f_{ey} < f_{A1}, \tag{A.3}$$

$$-(y_{sa1} - y_{sb1})f_{ex} + (x_{sa1} - x_{sb1})f_{ey} < f_{A2}, \tag{A.4}$$

where x_{sai}, y_{sai}, x_{sbi}, y_{sbi} are the corresponding components of vectors $\mathbf{s}_{ai}$, $\mathbf{s}_{bi}$, $i = 1, 2$, and

$$f_{B1} = \left\{ \frac{k}{8} \left[x_{sa1}(n_{a1} + n_{b1}) + x_{sa2}(n_{a2} + n_{b2}) \right] + \frac{f_o}{2}(x_{sa1} + x_{sa2}) \right\} (y_{sb2} - y_{sa2})$$
$$- \left\{ \frac{k}{8} \left[y_{sa1}(n_{a1} + n_{b1}) + y_{sa2}(n_{a2} + n_{b2}) \right] + \frac{f_o}{2}(y_{sa1} + y_{sa2}) \right\} (x_{sb2} - x_{sa2}),$$

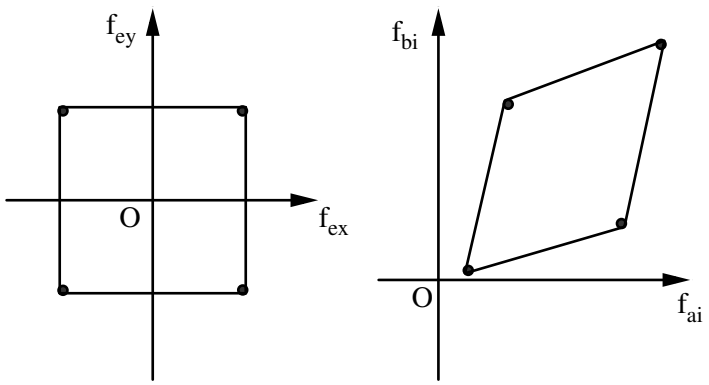

Figure A.1: Linear relationships between external force and cable forces.

$$f_{B2} = -\left\{\frac{k}{8}\left[x_{sa1}(n_{a1}+n_{b1}) + x_{sa2}(n_{a2}+n_{b2})\right] + \frac{f_o}{2}(x_{sa1}+x_{sa2})\right\}(y_{sb1}-y_{sa1}) + \left\{\frac{k}{8}\left[y_{sa1}(n_{a1}+n_{b1}) + y_{sa2}(n_{a2}+n_{b2})\right] + \frac{f_o}{2}(y_{sa1}+y_{sa2})\right\}(x_{sb1}-x_{sa1}),$$

$$f_{A1} = \left\{\frac{k}{8}\left[x_{sb1}(n_{a1}+n_{b1}) + x_{sb2}(n_{a2}+n_{b2})\right] + \frac{f_o}{2}(x_{sb1}+x_{sb2})\right\}(y_{sa2}-y_{sb2}) - \left\{\frac{k}{8}\left[y_{sb1}(n_{a1}+n_{b1}) + y_{sb2}(n_{a2}+n_{b2})\right] + \frac{f_o}{2}(y_{sb1}+y_{sb2})\right\}(x_{sa2}-x_{sb2}),$$

$$f_{A2} = -\left\{\frac{k}{8}\left[x_{sb1}(n_{a1}+n_{b1}) + x_{sb2}(n_{a2}+n_{b2})\right] + \frac{f_o}{2}(x_{sb1}+x_{sb2})\right\}(y_{sa1}-y_{sb1}) + \left\{\frac{k}{8}\left[y_{sb1}(n_{a1}+n_{b1}) + y_{sb2}(n_{a2}+n_{b2})\right] + \frac{f_o}{2}(y_{sb1}+y_{sb2})\right\}(x_{sa1}-x_{sb1}).$$

Suppose that the external force applied on the end-effector is $|f_{ex}| \leq a$, $|f_{ey}| \leq b (a > 0, b > 0)$. For a given position of the end-effector, the external force and the cable forces have a linear relationship shown in Figure A.1. All the vertices of the intersection of f_{bi} and f_{ai} should be in the first quadrant if the end-effector is within the workspace. So the workspace can be found by checking the four following conditions (1) $f_{ex} = a$ and $f_{ey} = b$, (2) $f_{ex} = -a$ and $f_{ey} = b$, (3) $f_{ex} = -a$ and $f_{ey} = -b$, (4) $f_{ex} = a$ and $f_{ey} = -b$.

A.1 $f_o \neq 0$, $k = 0$ and $\mathbf{f}_e \neq \mathbf{0}$

When the springs are constant force springs, the four cable force equations can be written as

$$\begin{aligned}\Delta \cdot f_{a1} &= f_{ax}(y_{sa2} - y_{sb2}) - f_{ay}(x_{sa2} - x_{sb2}) \\ &= f_{ex}(y_{sa2} - y_{sb2}) - f_{ey}(x_{sa2} - x_{sb2}) \\ &- \frac{1}{2} f_o(x_{sb1}y_{sa2} - x_{sb1}y_{sb2} + x_{sb2}y_{sa2} - x_{sa2}y_{sb1} + x_{sb2}y_{sb1} - x_{sa2}y_{sb2})\end{aligned} \tag{A.5}$$

$$\begin{aligned}\Delta \cdot f_{b1} &= f_{bx}(y_{sb2} - y_{sa2}) - f_{by}(x_{sb2} - x_{sa2}) \\ &= f_{ex}(y_{sb2} - y_{sa2}) - f_{ey}(x_{sb2} - x_{sa2}) \\ &- \frac{1}{2} f_o(x_{sa1}y_{sb2} - x_{sa1}y_{sa2} + x_{sa2}y_{sb2} - x_{sb2}y_{sa1} + x_{sa2}y_{sa1} - x_{sb2}y_{sa2})\end{aligned} \tag{A.6}$$

$$\begin{aligned}\Delta \cdot f_{a2} &= -f_{ax}(y_{sa1} - y_{sb1}) + f_{ay}(x_{sa1} - x_{sb1}) \\ &= f_{ex}(y_{sb1} - y_{sa1}) + f_{ey}(x_{sa1} - x_{sb1}) \\ &- \frac{1}{2} f_o(x_{sb2}y_{sb1} - x_{sb1}y_{sa1} - x_{sb2}y_{sa1} + x_{sa1}y_{sb1} + x_{sa1}y_{sb2} - x_{sb1}y_{sb2})\end{aligned} \tag{A.7}$$

$$\begin{aligned}\Delta \cdot f_{b2} &= -f_{bx}(y_{sb1} - y_{sa1}) + f_{by}(x_{sb1} - x_{sa1}) \\ &= f_{ex}(y_{sa1} - y_{sb1}) + f_{ey}(x_{sb1} - x_{sa1}) \\ &- \frac{1}{2} f_o(x_{sa2}y_{sa1} - x_{sa1}y_{sb1} - x_{sa2}y_{sb1} + x_{sb1}y_{sa1} + x_{sb1}y_{sa2} - x_{sa1}y_{sa2})\end{aligned} \tag{A.8}$$

As stated in Chapter 3, Δ is always negative within the rectangle formed by $A_1A_2B_1B_2$. Since the four cable forces should be positive, the workspace is the region within which Eqs. (A.5) to (A.8) are negative.

- For f_{a1}, since $y_{sa2} - y_{sb2}$ is negative and $-(x_{sa22} - x_{sb22})$ is positive, it can be seen that the worst situation is $f_{ex} < 0$ and $f_{ey} > 0$ from Eq. (A.5);
- For f_{b1}, since $y_{sb22} - y_{sa22}$ is positive and $-(x_{sb22} - x_{sa22})$ is negative, it can be seen that the worst situation is $f_{ex} > 0$ and $f_{ey} < 0$ from Eq. (A.6);
- For f_{a2}, since $y_{sb1} - y_{sa12}$ and $x_{sa12} - x_{sb12}$ are positive, it can be seen that the worst situation is $f_{ex} > 0$ and $f_{ey} > 0$ from Eq. (A.7);

- For f_{b2}, since $y_{sa12}-y_{sb12}$ and $x_{sb12}-x_{sa12}$ are negative, it can be seen that the worst situation is $f_{ex}<0$ and $f_{ey}<0$ from Eq. (A.8).

Assuming the external force space is $|f_{ex}| \leq k_{fe}f_o$, $|f_{ey}| \leq k_{fe}f_o$, then the four inequalities should be satisfied within the workspace:

$$\begin{aligned} f_{a1}: \quad & k_{fe}\Big[(x+y)\sqrt{B_{12}}(\sqrt{B_{22}}-\sqrt{A_{22}})+(x_{b22}+y_{b22})\sqrt{B_{12}}(\sqrt{B_{22}}+\sqrt{A_{22}})\Big] \\ & -y_{b22}(x+x_{b22})\sqrt{B_{22}}+(-y_{b22}x+x_{b22}y)\sqrt{B_{12}}+x_{b22}(y-y_{b22})\sqrt{A_{22}} \leq 0 \end{aligned} \tag{A.9}$$

$$\begin{aligned} f_{a2}: \quad & k_{fe}\Big[(x-y)\sqrt{B_{22}}(\sqrt{A_{12}}-\sqrt{B_{12}})+(x_{b22}+y_{b22})\sqrt{B_{22}}(\sqrt{A_{12}}+\sqrt{B_{12}})\Big] \\ & +x_{b22}(y-y_{b22})\sqrt{A_{12}}+(y_{b22}x+x_{b22}y)\sqrt{B_{22}}+y_{b22}(x-x_{b22})\sqrt{B_{12}} \leq 0 \end{aligned} \tag{A.10}$$

$$\begin{aligned} f_{b1}: \quad & k_{fe}\Big[(x+y)\sqrt{A_{12}}(\sqrt{B_{22}}-\sqrt{A_{22}})+(x_{b22}+y_{b22})\sqrt{A_{12}}(\sqrt{A_{22}}+\sqrt{B_{22}})\Big] \\ & +y_{b22}(x-x_{b22})\sqrt{A_{22}}+(y_{b22}x-x_{b22}y)\sqrt{A_{12}}-x_{b22}(y+y_{b22})\sqrt{B_{22}} \leq 0 \end{aligned} \tag{A.11}$$

$$\begin{aligned} f_{b2}: \quad & k_{fe}\Big[(x-y)\sqrt{A_{22}}(\sqrt{A_{12}}-\sqrt{B_{12}})+(x_{b22}+y_{b22})\sqrt{A_{22}}(\sqrt{A_{12}}+\sqrt{B_{12}})\Big] \\ & -x_{b22}(y+y_{b22})\sqrt{B_{12}}-(y_{b22}x+x_{b22}y)\sqrt{A_{22}}-y_{b22}(x+x_{b22})\sqrt{A_{12}} \leq 0 \end{aligned} \tag{A.12}$$

where $A_{i2}=(x_{ai2}-x)^2+(y_{ai2}-y)^2$, $B_{i2}=(x_{bi2}-x)^2+(y_{bi2}-y)^2$, $i=1,2$.

In order to find the boundary point on the diagonals, assume that the quadrilateral formed by the four fixed pulleys is a square, that is to say $x_{b2}=y_{b2}$. From the simulation presented in Chapter 3, it can be seen that f_{a2} and f_{b2} determine the workspace boundary on the diagonal $x=y$ and f_{a1} and f_{b1} determine the workspace boundary on the opposite diagonal $x=-y$. Substituting $y=x$, $y=-x$ into Eqs. (A.10) and (A.11) respectively, they can be written as

$$2\sqrt{2}k_{fe}\sqrt{x^2+x_{b22}^2}-\sqrt{x^2+x_{b22}^2}+x=0. \tag{A.13}$$

Substituting $y=x$, $y=-x$ into Eqs. (A.12) and (A.9) respectively, they can be written as

$$2\sqrt{2}k_{fe}\sqrt{x^2+x_{b22}^2}-\sqrt{x^2+x_{b22}^2}-x=0 \tag{A.14}$$

A.2 $f_o \neq 0$, $k \neq 0$ and $\mathbf{f}_e \neq \mathbf{0}$

If the springs in the mechanism have non zero stiffness, the cable force equations become very complicated. In order to simplify the analysis, suppose the rectangle is square with the half side length a unit.

1. For f_{a1}, let $y = -x$, $f_{ex} = -k_{fe}f_0$ and $f_{ey} = k_{fe}f_0$, we obtain

$$f_0\left(\frac{2\sqrt{2}k_{fe}}{\sqrt{x^2+1}} - \frac{1}{\sqrt{x^2+1}} - \frac{x}{1+x^2}\right) - \frac{\sqrt{2}}{2}k\frac{x(\sqrt{x^2+1}-1)}{x^2+1} \leq 0. \tag{A.15}$$

2. For f_{a2}, let $y = x$, $f_{ex} = k_{fe}f_0$ and $f_{ey} = k_{fe}f_0$, we obtain

$$f_0\left(\frac{2\sqrt{2}k_{fe}}{\sqrt{x^2+1}} - \frac{1}{\sqrt{x^2+1}} + \frac{x}{1+x^2}\right) + \frac{\sqrt{2}}{2}k\frac{x(\sqrt{x^2+1}-1)}{x^2+1} \leq 0. \tag{A.16}$$

3. For f_{b1}, let $y = -x$, $f_{ex} = k_{fe}f_0$ and $f_{ey} = -k_{fe}f_0$, we get the same inequality as Eq. (A.16).
4. For f_{b2}, let $y = x$, $f_{ex} = -k_{fe}f_0$ and $f_{ey} = -k_{fe}f_0$, we get the same inequality as Eq. (A.15).

Appendix B

Determinants of the Matrices $\mathbf{A}_i$ and $\mathbf{B}_i$ for the Spatial Mechanism

B.1 $f_o \neq 0$, $k = 0$ and $\mathbf{f}_e = 0$

$$\mathbf{f}_{be} = \frac{1}{2} f_o \begin{bmatrix} \dfrac{a+x}{X_a} + \dfrac{x}{Y_a} + \dfrac{x}{Z_a} \\ \dfrac{y}{X_a} + \dfrac{a+y}{Y_a} + \dfrac{y}{Z_a} \\ \dfrac{z}{X_a} + \dfrac{z}{Y_a} + \dfrac{a+z}{Z_a} \end{bmatrix}, \tag{B.1}$$

where

$$\begin{aligned} X_a &= |PA_1| = \sqrt{(a+x)^2 + y^2 + z^2}, & X_b &= |PB_1| = \sqrt{(a-x)^2 + y^2 + z^2}, \\ Y_a &= |PA_2| = \sqrt{x^2 + (a+y)^2 + z^2}, & Y_b &= |PB_2| = \sqrt{x^2 + (a-y)^2 + z^2}, \\ Z_a &= |PA_3| = \sqrt{x^2 + y^2 + (a+z)^2}, & Z_b &= |PB_3| = \sqrt{x^2 + y^2 + (a-z)^2}. \end{aligned}$$

Then, the determinants of $\mathbf{B}_i$, $i = 1, 2, 3$, are

$$\begin{aligned}\det(\mathbf{B}_1)_{f_o} &= \frac{f_o a^2}{2X_aY_aY_bZ_aZ_b}\left[(x+a)(Y_a+Y_b)(Z_a+Z_b) - y(Y_a-Y_b)(Z_a+Z_b)\right. \\ &\quad \left. -z(Y_a+Y_b)(Z_a-Z_b) + 2xX_a(Y_a+Y_b+Z_a+Z_b)\right],\end{aligned} \tag{B.2}$$

$$\begin{aligned}\det(\mathbf{B}_2)_{f_o} &= \frac{f_o a^2}{2X_aX_bY_aZ_aZ_b}\left[(y+a)(X_a+X_b)(Z_a+Z_b) - x(X_a-X_b)(Z_a+Z_b)\right. \\ &\quad \left. -z(X_a+X_b)(Z_a-Z_b) + 2yY_a(X_a+X_b+Z_a+Z_b)\right],\end{aligned} \tag{B.3}$$

$$\begin{aligned}\det(\mathbf{B}_3)_{f_o} &= \frac{f_o a^2}{2X_aX_bY_aY_bZ_a}\left[(z+a)(X_a+X_b)(Y_a+Y_b) - x(X_a-X_b)(Y_a+Y_b)\right. \\ &\quad \left. -y(X_a+X_b)(Y_a-Y_b) + 2zZ_a(X_a+X_b+Y_a+Y_b)\right].\end{aligned} \tag{B.4}$$

$$\mathbf{f}_{ae} = \frac{1}{2}f_o\begin{bmatrix} \dfrac{x-a}{X_b} + \dfrac{x}{Y_b} + \dfrac{x}{Z_b} \\ \dfrac{y}{X_b} + \dfrac{y-a}{Y_b} + \dfrac{y}{Z_b} \\ \dfrac{z}{X_b} + \dfrac{z}{Y_b} + \dfrac{z-a}{Z_b} \end{bmatrix}. \tag{B.5}$$

The determinants of matrices $\mathbf{A}_i$, $i = 1, 2, 3$, are

$$\begin{aligned}\det(\mathbf{A}_1)_{f_o} &= -\frac{f_o a^2}{2X_bY_aY_bZ_aZ_b}\left[(a-x)(Y_a+Y_b)(Z_a+Z_b) - y(Y_a-Y_b)(Z_a+Z_b)\right. \\ &\quad \left. -z(Y_a+Y_b)(Z_a-Z_b) - 2xX_b(Y_a+Y_b+Z_a+Z_b)\right],\end{aligned} \tag{B.6}$$

$$\begin{aligned}\det(\mathbf{A}_2)_{f_o} &= -\frac{f_o a^2}{2X_aX_bY_bZ_aZ_b}\left[(a-y)(X_a+X_b)(Z_a+Z_b) - x(X_a-X_b)(Z_a+Z_b)\right. \\ &\quad \left. -z(X_a+X_b)(Z_a-Z_b) - 2yY_b(X_a+X_b+Z_a+Z_b)\right],\end{aligned} \tag{B.7}$$

$$\begin{aligned}\det(\mathbf{A}_3)_{f_o} &= -\frac{f_o a^2}{2X_aX_bY_aY_bZ_b}\left[(a-z)(X_a+X_b)(Y_a+Y_b) - x(X_a-X_b)(Y_a+Y_b)\right. \\ &\quad \left. -y(X_a+X_b)(Y_a-Y_b) - 2zZ_b(X_a+X_b+Y_a+Y_b)\right].\end{aligned} \tag{B.8}$$

Using the spherical coordinates (α, β, r), the position of the end-effector is

$$x = r\sin\beta\cos\alpha, \quad y = r\sin\beta\sin\alpha, \quad z = r\cos\beta. \tag{B.9}$$

For a certain direction, the workspace boundary defined by r can been found by the cable force equations. The workspace boundary for different ranges of α and β can be determined by the corresponding cable force which is listed in the following:

$$\begin{aligned}
f_{a1}: &\quad \alpha \in \left[0, \frac{\pi}{4}\right] \bigcup \left[\frac{7\pi}{4}, 2\pi\right], \quad \beta \in \left[\frac{\pi}{4}, \frac{3\pi}{4}\right], \\
f_{a2}: &\quad \alpha \in \left[\frac{\pi}{4}, \frac{3\pi}{4}\right], \quad \beta \in \left[\frac{\pi}{4}, \frac{3\pi}{4}\right], \\
f_{a3}: &\quad \alpha \in [0, 2\pi], \quad \beta \in \left[0, \frac{\pi}{4}\right] \\
f_{b1}: &\quad \alpha \in \left[\frac{3\pi}{4}, \frac{5\pi}{4}\right], \quad \beta \in \left[\frac{\pi}{4}, \frac{3\pi}{4}\right], \\
f_{b2}: &\quad \alpha \in \left[\frac{5\pi}{4}, \frac{7\pi}{4}\right], \quad \beta \in \left[\frac{\pi}{4}, \frac{3\pi}{4}\right], \\
f_{b3}: &\quad \alpha \in [0, 2\pi], \quad \beta \in \left[\frac{3\pi}{4}, \pi\right].
\end{aligned}$$

B.2 $f_o = 0$, $k \neq 0$ and $\mathbf{f}_e = \mathbf{0}$

When $f_o = 0$, $k \neq 0$ and $\mathbf{f}_e = \mathbf{0}$, $\mathbf{f}_{be}$ and $\mathbf{f}_{ae}$ are

$$\mathbf{f}_{be} = \frac{k}{8} \begin{bmatrix} a + 3x + \dfrac{a+x}{X_a}(X_b - 2a) + \dfrac{x}{Y_a}(Y_b - 2a) + \dfrac{x}{Z_a}(Z_b - 2a) \\ a + 3y + \dfrac{y}{X_a}(X_b - 2a) + \dfrac{a+y}{Y_a}(Y_b - 2a) + \dfrac{y}{Z_a}(Z_b - 2a) \\ a + 3z + \dfrac{z}{X_a}(X_b - 2a) + \dfrac{z}{Y_a}(Y_b - 2a) + \dfrac{a+z}{Z_a}(Z_b - 2a) \end{bmatrix}, \tag{B.10}$$

$$\mathbf{f}_{ae} = \frac{k}{8} \begin{bmatrix} 3x - a + \dfrac{x-a}{X_b}(X_a - 2a) + \dfrac{x}{Y_b}(Y_a - 2a) + \dfrac{x}{Z_b}(Z_a - 2a) \\ 3y - a + \dfrac{y}{X_b}(X_a - 2a) + \dfrac{y-a}{Y_b}(Y_a - 2a) + \dfrac{y}{Z_b}(Z_a - 2a) \\ 3z - a + \dfrac{z}{X_b}(X_a - 2a) + \dfrac{z}{Y_b}(Y_a - 2a) + \dfrac{z-a}{Z_b}(Z_a - 2a) \end{bmatrix}. \tag{B.11}$$

In this situation, the determinant of matrices $\mathbf{B}_i$ and $\mathbf{A}_i$, $i = 1, 2, 3$, are

$$\begin{aligned}
\det(\mathbf{B}_1)_k = \frac{ka^2}{8X_aY_aY_bZ_aZ_b} \big[& a(X_a + X_b)(Y_a + Y_b)(Z_a + Z_b) + x(5X_a + X_b)(Y_a + Y_b) \\
& (Z_a + Z_b) - y(X_a + X_b)(Y_a - Y_b)(Z_a + Z_b) - z(X_a + X_b)(Y_a + Y_b)(Z_a - Z_b) \\
& - 2a(x + a)(Y_a + Y_b)(Z_a + Z_b) + 2ay(Y_a - Y_b)(Z_a + Z_b) \\
& + 2az(Y_a + Y_b)(Z_a - Z_b) - 4axX_a(Y_a + Y_b + Z_a + Z_b)\big],
\end{aligned} \tag{B.12}$$

$$\begin{aligned}\det(\mathbf{B}_2)_k = \frac{ka^2}{8X_aX_bY_aZ_aZ_b}\,[&a(X_a+X_b)(Y_a+Y_b)(Z_a+Z_b) - x(X_a-X_b)(Y_a+Y_b)\\ &(Z_a+Z_b) + y(X_a+X_b)(5Y_a+Y_b)(Z_a+Z_b) - z(X_a+X_b)(Y_a+Y_b)(Z_a-Z_b)\\ &+ 2ax(X_a-X_b)(Z_a+Z_b) - 2a(y+a)(X_a+X_b)(Z_a+Z_b)\\ &+2az(X_a+X_b)(Z_a-Z_b) - 4ayY_a(X_a+X_b+Z_a+Z_b)]\,,\end{aligned} \tag{B.13}$$

$$\begin{aligned}\det(\mathbf{B}_3)_k = \frac{ka^2}{8X_aX_bY_aY_bZ_a}\,[&a(X_a+X_b)(Y_a+Y_b)(Z_a+Z_b) - x(X_a-X_b)(Y_a+Y_b)\\ &(Z_a+Z_b) - y(X_a+X_b)(Y_a-Y_b)(Z_a+Z_b) + z(X_a+X_b)(Y_a+Y_b)(5Z_a+Z_b)\\ &+ 2ax(X_a-X_b)(Y_a+Y_b) + 2ay(X_a+X_b)(Y_a-Y_b)\\ &-2a(z+a)(X_a+X_b)(Y_a+Y_b) - 4azZ_a(X_a+X_b+Y_a+Y_b)]\,,\end{aligned} \tag{B.14}$$

$$\begin{aligned}\det(\mathbf{A}_1)_k = -\frac{ka^2}{8X_bY_aY_bZ_aZ_b}\,[&a(X_a+X_b)(Y_a+Y_b)(Z_a+Z_b) - x(X_a+5X_b)(Y_a+Y_b)\\ &(Z_a+Z_b) - y(X_a+X_b)(Y_a-Y_b)(Z_a+Z_b) - z(X_a+X_b)(Y_a+Y_b)(Z_a-Z_b)\\ &- 2a(a-x)(Y_a+Y_b)(Z_a+Z_b) + 2ay(Y_a-Y_b)(Z_a+Z_b)\\ &+2az(Y_a+Y_b)(Z_a-Z_b) + 4axX_b(Y_a+Y_b+Z_a+Z_b)]\,,\end{aligned} \tag{B.15}$$

$$\begin{aligned}\det(\mathbf{A}_2)_k = -\frac{ka^2}{8X_aX_bY_aZ_aZ_b}\,[&a(X_a+X_b)(Y_a+Y_b)(Z_a+Z_b) - x(X_a-X_b)(Y_a+Y_b)\\ &(Z_a+Z_b) - y(X_a+X_b)(Y_a+5Y_b)(Z_a+Z_b) - z(X_a+X_b)(Y_a+Y_b)(Z_a-Z_b)\\ &+ 2ax(X_a-X_b)(Z_a+Z_b) - 2a(a-y)(X_a+X_b)(Z_a+Z_b)\\ &+2az(X_a+X_b)(Z_a-Z_b) + 4ayY_a(X_a+X_b+Z_a+Z_b)]\,,\end{aligned} \tag{B.16}$$

$$\begin{aligned}\det(\mathbf{A}_3)_k = -\frac{ka^2}{8X_aX_bY_aY_bZ_b}\,[&a(X_a+X_b)(Y_a+Y_b)(Z_a+Z_b) - x(X_a-X_b)(Y_a+Y_b)\\ &(Z_a+Z_b) - y(X_a+X_b)(Y_a-Y_b)(Z_a+Z_b) - z(X_a+X_b)(Y_a+Y_b)(Z_a+5Z_b)\\ &+ 2ay(X_a+X_b)(Y_a-Y_b) + 2ax(X_a-X_b)(Y_a+Y_b)\\ &-2a(a-z)(X_a+X_b)(Y_a+Y_b) + 4azZ_b(X_a+X_b+Y_a+Y_b)]\,.\end{aligned} \tag{B.17}$$

B.3 $f_o = 0$, $k = 0$ and $\mathbf{f}_e \neq \mathbf{0}$

When $f_o = 0$, $k = 0$ and $\mathbf{f}_e \neq \mathbf{0}$, we have $\mathbf{f}_{be} = \mathbf{f}_{ae} = \mathbf{f}_e$. The determinants of $\mathbf{B}_i$ and $\mathbf{A}_i$, $i = 1, 2, 3$, are

$$\begin{aligned}\det(\mathbf{B}_1)_{\mathbf{f}_e} =& \frac{a}{Y_a Y_b Z_a Z_b} \left[f_x a (Y_a + Y_b)(Z_a + Z_b) \right. \\ & \left. + (f_y x - f_x y)(Y_a - Y_b)(Z_a + Z_b) + (f_z x - f_x z)(Y_a + Y_b)(Z_a - Z_b) \right],\end{aligned} \tag{B.18}$$

$$\begin{aligned}\det(\mathbf{B}_2)_{\mathbf{f}_e} =& \frac{a}{X_a X_b Z_a Z_b} \left[f_y a (X_a + X_b)(Z_a + Z_b) \right. \\ & \left. + (f_x y - f_y x)(X_a - X_b)(Z_a + Z_b) + (f_z y - f_y z)(X_a + X_b)(Z_a - Z_b) \right],\end{aligned} \tag{B.19}$$

$$\begin{aligned}\det(\mathbf{B}_3)_{\mathbf{f}_e} =& \frac{a}{X_a X_b Y_a Y_b} \left[f_z a (X_a + X_b)(Y_a + Y_b) \right. \\ & \left. + (f_x z - f_z x)(X_a - X_b)(Y_a + Y_b) + (f_y z - f_z y)(X_a + X_b)(Y_a - Y_b) \right],\end{aligned} \tag{B.20}$$

and

$$\det(\mathbf{A}_i)_{\mathbf{f}_e} = \det(\mathbf{B}_i)_{\mathbf{f}_e}, \qquad i = 1, 2, 3. \tag{B.21}$$